Alkaline Earth and Rare Earth Complexes for the Ring Opening Polymerisation of Cyclic Esters

Lawrence Clark MChem AMRSC

Thesis submitted to the University of Oxford for the degree of Doctor of Philosophy, April 2012.

The work described in this Thesis was carried out in the Chemistry Research Laboratory, University of Oxford from October 2008 to April 2012 under the supervision of Professor Philip Mountford. All work is my own unless stated to the contrary, and has not previously been submitted for any degree at this or any other university.

Lawrence Clark

April 2012

Abstract

Lawrence Clark
Trinity College

Hilary Term 2012
DPhil Thesis

This Thesis describes the use of alkaline earth and rare earth complexes bearing phenolate ligands as catalysts in the amine-initiated, immortal ring opening polymerisation (ROP) of cyclic esters. Mechanistic elucidation was performed and two propagation pathways are presented.

Chapter One introduces cyclic esters and catalytic routes to polyesters by ROP. Common techniques for polymer characterisation are described and an overview of relevant phenolate-supported ROP catalysts is given. Reversible chain transfer in ROP is also discussed.

Chapter Two describes the synthesis and characterisation of zwitterionic Group 3 complexes bearing bis(phenolate)-amino ligands and the development of the amine-initiated, immortal ROP methodology using this class of catalyst. Detailed studies into the ROP of *rac*-lactide using amines and a zwitterionic yttrium complex are presented and the mechanism of amine-initiated, immortal ROP was derived.

Chapter Three documents further amine-initiated, immortal ROP studies using a zwitterionic yttrium complex as the catalyst. The preparation of multiarm polymers is described and further investigations using the cyclic esters, ε-caprolactone and *rac*-β-butyrolactone are presented.

Chapter Four describes the use of Group 2 and lanthanide phenolate complexes in the amine-initiated ROP of *rac*-lactide. Bulk polymerisation studies revealed the generality of the amine-initiated, immortal ROP methodology and an alternative propagation pathway was derived from mechanistic studies.

Chapter Five details the synthesis and characterisation of Group 3 amide complexes supported by phenolate-amino ligands. Each complex was screened for ROP capability and amine co-initiators were employed.

Chapter Six contains experimental details and characterisation data for the new complexes and polymer products described in this Thesis.

CD Appendix contains crystallography .cif files, supporting information for each Chapter and spreadsheets containing polymerisation data.

Contents

Acknowledgements

I am extremely grateful to my supervisor, Professor Philip Mountford for his help, support and guidance throughout the course of my studies. I thank him for providing me with a thoroughly engaging project, which has been challenging but extremely rewarding. I would also like to express my appreciation for all the hard work that Philip does for the research group and wish him continued success in his career.

I would like to thank my predecessor, Dr. Hellen E. Dyer, from whom I inherited this project and continued to nurture. Thanks for teaching me how to use the GPC and all your help when I was new to ROP. Dr. Andrew D. Schwarz also deserves a special mention for all his help when I was starting out. I must also thank Prof. Glen B. Deacon, Prof. Peter C. Junk, and Dr. Joshua P. Townley, our collaborators at Monash University, Melbourne, Australia for the extra supplies of compounds when we thought of more reactions to do!

Thanks to all Mountford group members past and present for making the group such a fantastic place to work. I would especially like to thank Jon Selby, Andy Schwarz, Alex Heath and Michael Cushion for being so welcoming on my return from my Part II year, as well as my contemporary, Dan Schofield for being a good friend inside and outside of the lab. I am grateful to Matt Blake for all his proof reading over the past few months and George Hilton for being an excellent and conscientious Part II. I extend my best wishes for the future to all current members of the group.

I must express my gratitude to Dr. Nick Rees and Colin Sparrow for help with NMR and running MALDI-ToF MS samples for me. Drs. David Watkin and Amber Thompson also deserve a special mention for all the hard work they do in crystallography. Thanks again to Philip, Matt and Andy for their assistance with data collection, structure refinement and graphics.

It has been a privilege to study at Oxford for nearly eight years, over which time I have made countless friendships that will last a lifetime. I would especially like to thank Nick, Fred, Alex and Matt for being great housemates in Jeune Street over the past couple of years and everyone else still at Trinity who started in 2008. I reserve my greatest thanks to my parents and my sisters for their continued support throughout my time at Oxford.

Abbreviations

General

Å	Ångstrom
ca.	*circa*, about
calcd	calculated
cf.	*confer*, compare to
°C	degrees Celsius
Conv.	conversion
°	degrees
DFT	Density Functional Theory
equiv(s).	equivalent(s)
g	gram(s)
GPC	Gel Permeation Chromatography
h	hour(s)
η	initrinsic viscosity
J	Joule(s)
k	kilo
K	Kelvin
k_{app}	apparent rate constant of propagation
k_i	rate constant of initiation
k_p	rate constant of propagation
k_{CT}	rate constant of chain transfer
L	litre(s)
mg	milligram(s)
min(s)	minute(s)
mL	millilitre(s)
μL	microlitre(s)
R_p	rate law for propagation
rt	room temperature
SEC	Size Exclusion Chromatography
T	temperature

T_m	melting temperature
vs.	*versus*

Chemical

Ar	aryl
BBL	β-butyrolactone
BDI	β-diiminate
BHT	2,6-di-*tert*-butyl-4-methylphenol
Bn	benzyl
^{n}Bu	*n*-butyl
^{t}Bu	*tert*-butyl
Cp	cyclopentadienyl
Cp*	pentamethylcyclopentadienyl
Cy	cyclohexyl
ε-CL	ε-caprolactone
DMAP	4-dimethylaminopyridine
D-LA	(*R,R*)-*cis*-3,6-dimethyl-1,4-dioxane-2,5-dione
DME	1,2-di-methoxyethane
Et	ethyl
GL	glycolide
HMPA	hexamethylphosphoramide
i	*iso*
L	generic ligand
LA	lactide
L-LA	(*S,S*)-*cis*-3,6-dimethyl-1,4-dioxane-2,5-dione
lact	lactate
Ln	Group 3 or lanthanide element
m	*meso*
M	metal or mol L^{-1}
MALLS	Multiangle Laser Light Scattering
Me	methyl
Mes	2,4,6-$C_6H_2Me_3$

meso-LA	(*R,S*)-*cis*-3,6-dimethyl-1,4-dioxane-2,5-dione
(m/μ)mol	millimole(s), micromole(s) or mole(s)
M_n	number average molecular weight
M_w	weight average molecular weight
M_p	peak molecular weight
M_R	relative molecular weight
MW	molecular weight
NHC	*N*-heterocyclic carbene
OAc	acetate
Oct	octanoate
O_xN^L	phenolate-amino or bis(phenolate)-amino ligand
OTf	CF_3SO_3
P	polymer chain
P_m	probability of *meso*-linkages
P_r	probability of *racemic*-linkages
PCL	poly(ε-caprolactone)
PDI	polydispersity index
PDLA	poly(*D*-LA)
PET(E)	polyethylene terephthalate
PHA	poly(hydroxyalkonate)
PHB	poly(3-hydroxybutanaote)
PLA	poly(lactide)
PLLA	poly(*L*-LA)
Ph	phenyl
^{i}Pr	*iso*-propyl
^{n}Pr	*n*-propyl
py	pyridine
r	*racemic*
R	generic alkyl group or hydrogen atom, or polymer chain
rac	racemic
RI	Refractive Index
ROP	Ring Opening Polymerisation

s	*syndio*
TEA	triethanolamine
TMC	trimethylene carbonate
THF	tetrahydrofuran
tren	tris(2-aminoethyl)amine
X	initiating group

Nuclear Magnetic Resonance Spectroscopy

app	apparent
br	broad
^{1}H-{^{1}H}	proton-decoupled ^{1}H
^{13}C-{^{1}H}	proton-decoupled ^{13}C
d	doublet
δ	chemical shift in ppm
HETCOR	hetereonuclear correlation
Hz	Hertz
J	coupling constant
m	multiplet
MHz	Megahertz
NMR	Nuclear Magnetic Resonance
ppm	parts per million
q	quartet or quaternary
s	singlet
sept	septet
t	triplet
VT	variable temperature

Mass Spectrometry

EI	Electron Impact
m/z	mass to charge ratio
MALDI-ToF	Matrix Assisted Laser Desorption Ionisation, Time of Flight
MS	Mass Spectrometry

Infrared Spectroscopy

cm^{-1}	wavenumbers
IR	Infrared
m	medium
s	strong
w	weak

Notes

Literature compounds described in this Thesis are numbered **1.x**, **2.x**, **3.x**, **4.x** or **5.x** according to the Chapter in which they are first presented. Some literature compounds detailed in Chapter One and Two are mentioned in later Chapters but retain the **1.x** or **2.x** prefix. Novel compounds are labelled **1**–**19**, but it should be noted that Dr. Hellen E. Dyer (University of Oxford) originally prepared compounds **1** and **2** and Dr. Joshua P. Townley (Monash University, Melbourne, Australia) originally prepared **10**–**14**.

X-ray crystallography data collection was performed by the author, but final structure refinements, .cif preparation and molecular drawings were produced by Professor Philip Mountford.

MALDI-ToF MS and EI-MS were performed by Colin Sparrow and the departmental service. Elemental Analysis was performed by the service at London Metropolitan University.

Chapter One

Introduction

1.1 Overview

This Chapter provides an introduction to the ring opening polymerisation (ROP) of cyclic esters. A brief account of the development of polyesters is given and cyclic ester monomers are introduced. Common techniques for polymer characterisation are summarised and catalytic ROP pathways are discussed alongside a general literature review. Rare earth complexes supported by phenolate ligands are emphasised in this review and are the focus of work reported in this Thesis, along with investigations involving alkaline earth phenolate compounds.

1.2 General introduction

Polyesters have been widely exploited in the production of clothing and furnishing materials. Carothers reported the first example of a polyester fibre material prepared by the ring opening polymerisation of lactide and other cyclic esters in 1932 but owing to the interest in polyamides (Nylon) at that particular time, the next major development in polyester technology was not realised was until Whinfield and Dickson patented polyethylene terephthalate (PET or PETE) in 1941.[1, 2] The worldwide production of plastic materials soared in the post-war era as oil prices fell and research efforts intensified, and plastic materials became viable and superior alternatives to traditional materials (textiles, wood, paper and metals) in a plethora of applications.[2] In more recent times, socio-economic and political pressures on fossil fuel resources, as well as the desire to produce plastic materials which degrade over a relatively short timescale has led to renewed interest in polyester development.[3, 4]

1.2.1 Biodegradable and biorenewable polyesters

Polyesters that are derived from biorenewable sources or polyesters that are biodegradable have received considerable attention over the past 30–40 years and two of the most prominent examples in this class are poly(lactide) (PLA) and poly(ε-caprolactone) (PCL).[3-7] These materials have been used to produce sutures and stents, used in medical procedures and PLA structures have been shown to be suitable hosts for drug molecule encapsulation and delivery.[8-11] PLA is also a suitable packaging and food storage material and NatureWorks LLC is just one of several manufactures producing PLA on an industrial scale.[12]

The most efficient route to PLA or PCL is *via* ROP of the cyclic ester monomers, lactide, LA, or ε-caprolactone, ε-CL (or CL). ROP is a chain-growth process, which

offers a greater degree of control over molecular weight and molecular weight distribution than step-growth pathways, such as the polycondensation of α-hydroxy acids.[3, 8, 13, 14] LA and ε-CL are shown in Figure 1.1 along with other relevant cyclic monomers, including glycolide (GL), β-butyrolactone (BBL) and trimethylene carbonate (TMC).

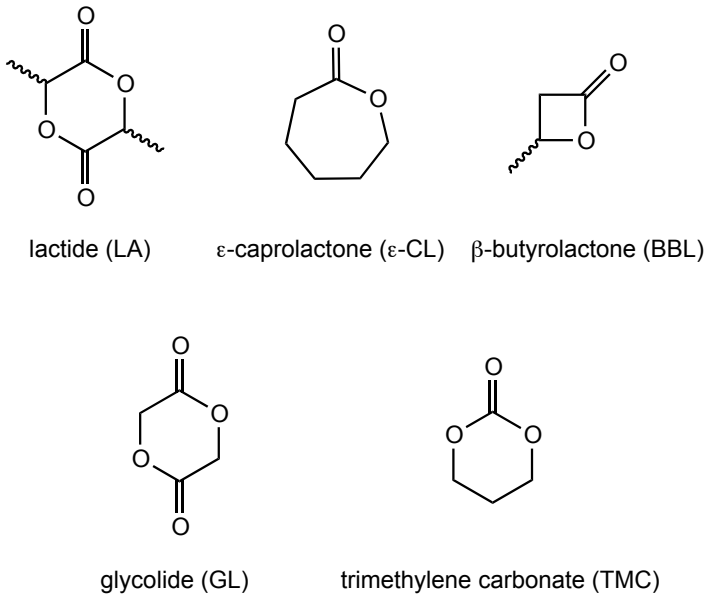

Figure 1.1. Examples of cyclic monomers used to produce biodegradable polymers.

The production of LA begins with *D*-glucose, which can be obtained from biomass such as corn or sugar beet. Fermentation of *D*-glucose using bacteria of the genera *Lactobacillus*, *Streptococcus* and *Pediococcus* generates optically pure *L*-lactic acid.[15] Low molecular weight (MW = 1000–5000) oligomers can be achieved from direct condensation of *L*-lactic acid. The cyclic dimer is then obtained *via* depolymerisation of the pre-polymer with loss of optical purity.[5, 12, 15] ROP of lactide using a metal-based catalyst under homogenous conditions generates high molecular weight PLA and is the process in the PLA cycle of most interest to the synthetic chemist. PLA degrades by both physical and biological pathways involving microorganisms or enzymes, but the rate of degradation, as well as the mechanical and rheological properties of PLA at a given molecular weight are heavily dependent on the microstructure.[5, 7, 11, 15-17] In principle, PLA is a biorenewable polymer, since the final degradation products are carbon dioxide and water. However, the processes involved in lactide production and ROP are not carbon neutral. PCL is also a biodegradable polymer but the cyclic monomer, ε-CL, is not derived from biorenewable sources. A

Baeyer-Villiger oxidation of cyclohexanone leads to formation of the seven-membered lactone.[18] BBL is another petrochemical based monomer, although the ring opened polymer product, poly(3-hydroxybutanonate) and other poly(3-hydroxyalkonates), are naturally occurring polymeric products.[4, 6, 7]

1.3 ROP: thermodynamic and kinetic considerations

The widely accepted driving force for the polymerisation of cyclic compounds is the alleviation of ring strain, which encompasses deviations from ideal bond angles, bond stretching and/or compression, repulsion between eclipsed hydrogen atoms and non-bonding interactions between substituents.[19] The enthalpy of polymerisation is an approximate measure of ring strain in systems where specific monomer, polymer and solvent interactions can be neglected. Most cyclic ester polymerisations are disfavoured entropically, due to the loss of translational degrees of freedom. As a consequence, the enthaplic contribution to ΔG_p must prevail in order for polymerisation to be allowed thermodynamically.

Duda and Penczek determined $\Delta H_p = -22.9$ kJ mol^{-1} and $\Delta S_p = -41.1$ J mol^{-1} K^{-1} for *L*-LA polymerisations conducted in 1,4-dioxane solution using $Sn(Oct)_2$ as the catalyst,[19, 20] whilst $\Delta H_p = -28.8$ kJ mol^{-1} and $\Delta S_p = -53.9$ J mol^{-1} K^{-1} were calculated for the seven-membered lactone, ε-CL (neat, liquid phase).[19] The majority of six-membered rings cannot be polymerised because of relatively low ring strain and theoretical polymerisation parameters for cyclohexane, which adopts a more stable chair conformation, were determined as $\Delta H_p = 2.9$ kJ mol^{-1} and $\Delta S_p = -10.5$ J mol^{-1} K^{-1}.[21] However, the presence of ester functional groups increases ring strain in lactide, which adopts a skewed-boat conformation in the solid state and is presumed to adopt a boat conformation in solution.[20, 22] Four and five-membered rings are also much more strained and enthalpy prevails.[19] Equilibrium concentrations ($\Delta G_p = 0$ kJ mol^{-1}, standard conditions) of monomer, $[\text{monomer}]_{eq}$, when polymerisation is complete have also been determined, according to the equation, $\ln[\text{monomer}]_{eq} = \Delta H_p/RT - \Delta S_p/R$, and $[LA]_{eq} = 0.012$ M (1,4-dioxane solution, room temperature) and $[\varepsilon\text{-CL}]_{eq} = 0.051$ M (neat, room temperature).[19, 20]

Thermodynamic parameters cannot be used alone when comparing monomer reactivity. Propagation rate constants, k_p, may not be reflective of relative ring strain, as noted with the four-membered lactone, BBL. Thermodynamic polymerisation

parameters have not been determined for this monomer but enthalpy and entropy of polymerisation for the related four-membered lactone, β-propiolactone (neat), were $\Delta H_p = -82.3$ kJ mol^{-1} and $\Delta S_p = -74.0$ J mol^{-1} K^{-1}.[19] Despite significant ring strain in β-butyrolactone, the monomer is generally less reactive than *rac*-LA or ε-CL under comparable conditions.[23]

Initiation and propagation processes in chain-growth ROP have been described using elementary kinetic models that have also recognised reversible chain transfer processes or temporary deactivation and reactivation pathways.[19, 24] Kinetic data from polymerisation reactions are obtained by monitoring the consumption of monomer against time, t, with propagation rate constants calculated from first-order models. Living ROP of *rac*-LA generally proceeds with a first-order dependence in $[rac\text{-LA}]_0$ and it has been suggested that rigorous first-order models should incorporate equilibrium monomer concentrations, $[\text{monomer}]_{eq}$.[19, 25, 26] Initiation processes and any associated induction periods have also been modelled in order to gain a more in-depth understanding of polymerisation mechanisms.[27-29] However, elementary kinetic models are usually sufficient for the determination of relative propagation rate constants.

1.4 Polymer characterisation

Polymer products rarely consist of one uniform length species so are described by average molecular weights, calculated as number average or weight average. The number average (arithmetic mean) molecular weight, M_n, is described by Equation 1.1 (where N_i is the number of molecules having a molar mass M_i). The weight average molecular weight, M_w, is given by Equation 1.2 (where W_i is the total mass of polymer ($N_i \times M_i$ having molar mass M_i). The polydispersity index (PDI), calculated from the ratio, M_w/M_n, provides a measure of the distribution of molecular weights.[30]

$$M_n = \frac{\sum N_i \times M_i}{\sum N_i} \qquad \textbf{Equation 1.1}$$

$$M_w = \frac{\sum W_i \times M_i}{\sum W_i} \qquad \textbf{Equation 1.2}$$

The weight average molecular weight, M_w, is biased towards polymer chains of higher molecular weights and since polymers contain a distribution of chain lengths, M_w is greater than M_n and PDIs are greater than 1.0. In living polymerisations, only

initiation and propagation processes occur, leading to the formation of polymer chains with a predictable molecular weight based on the initial stoichiometry of monomer to catalyst (assuming a finite supply of monomer). A PDI = 1.0 would be expected if a polymer sample consisted of chains of the same length, but in practice, even extremely well-controlled polymerisation reactions that may be described as living, yield polymer products with PDIs greater than 1.0. This deviation from unity arises because of chain termination and irreversible transfer processes, as well as transesterification and slow initiation pathways with respect to propagation. Undesired polymer products, arising from transesterification or chain termination reactions skew M_w and M_n, leading to a broadening of the molecular weight distribution. With regard to polyesters produced by ROP, polymers are described as having a narrow molecular weight distribution if PDI < 1.2. PDIs between 1.2 and 1.8 are moderate, whilst PDIs > 1.8 are broad.

1.4.1 GPC analysis

Gel Permeation Chromatography (GPC) or Size Exclusion Chromatography (SEC), is used to determine polymer molecular weight and molecular weight distribution and separates polymers on the basis of their size in solution, not molecular weight. Typically, polymer samples are dissolved in a compatible solvent and eluted through a column packed with porous beads of a styrene divinyl-benzene co-polymer. Separation occurs through the partitioning of polymer molecules into the pore structure, with smaller polymer chains having a longer retention time than larger polymers.

Polymer detection is often performed using refractive index (RI) methods and molecular weights are calculated with reference to known standards, typically polystyrenes with known M_w, M_n and M_p (distribution maximum point) values. However, even if a polystyrene sample and a polyester sample have the same molecular weight, they will have different sizes (hydrodynamic volumes) in solution under the same conditions. Viscometry has been used to establish a universal calibration method, based on the hydrodynamic volume of a polymer in solution.[31]

Viscometry is primarily used to determine intrinsic viscosity, [η], and relies on the principle that all polymers increase the viscosity of solutions by increasing the resistance to flow. The intrinsic viscosity of a polymer solution is dependent on

interactions between the solute and the solvent and at any given molecular weight, a high intrinsic viscosity indicates that the sample is a large diffuse molecule, whereas a small intrinsic viscosity is reflective of a small, compact molecule. In practice, solution specific viscosities, η_{sp}, are measured and the ratio of the solution specific viscosity to the concentration of the solute (η_{sp}/c) is extrapolated to zero concentration (or infinite dilution) to determine $[\eta]$.[30] The hydrodynamic volume of a polymer in a given solution is equal to $[\eta]M$, where M is the molecular weight of the polymer chain and a universal plot of $\log[\eta]M$ against retention time holds true for all polymer types. The Mark-Houwink relationship relates $[\eta]$ and M according to Equation 1.3.

$$[\eta] = KM^{\alpha} \qquad \textbf{Equation 1.3}$$

K and α are referred to as the Mark-Houwink constants or corrections and can be determined experimentally from a linear plot of $\log[\eta]$ against logM. K is determined from the vertical-axis intercept and α represents the gradient. K and α values are specific to the polymer they describe and are dependent on solvent and temperature. Values of α typically range from 0.0 to 2.0 and reflect the nature of the polymer in solution. A value of 2.0 is indicative of a rigid rod and 0.0 a hard sphere, whilst values of $\alpha = 1.0$ represent coils or helical structures.

Mark-Houwink corrections have been determined for PCL and PLA chains in THF solution at 30 °C and were used to calculate the molecular weights of PLA described in this Thesis.[31, 32] Polystyrenes were used as the primary calibration standard but it should be noted that these correction factors apply to linear polymer chains and do not accurately describe cyclic polymer side products that can be produced during polymerisation reactions. Approximate correction factors have been used for mixtures of linear and cyclic products, given that the Mark-Houwink correction factors translate approximately to M_n(polystyrene) ≈ 0.58 × M_n(PLA). Absolute molecular weights can be measured using Multiangle Laser Light Scattering (MALLS) techniques and the most sophisticated GPC instruments incorporate three methods of detection: RI, viscometry and MALLS.

1.4.2 MALDI-ToF MS

Matrix Assisted Laser Desorption Ionisation – Time of Flight mass spectrometry (MALDI-ToF MS) is a non-destructive technique that can be applied to

macromolecules. Polymer chains are embedded in a protective matrix such as *trans*-2-[3-(4-*tert*-butylphenyl)-2-methyl-2-propenylidene]malononitrile (DCTB) or 4-hydroxy-3-methoxy-cinnamic acid before an ionising laser source is then focused on the matrix.[33] Through this process, the polymer is energetically excited but shielding of the polymer by the matrix prevents unwanted fragmentation of the polymer. A cationic dopant e.g. K^+ (as potassium trifluoroacetate) binds to the polymer molecules, forming [polymer-K]$^+$ *pseudo*-complexes. These ions are accelerated through a time-of-flight spectrometer where they are resolved by their mass-to-charge (*m/z*) ratio. MALDI-ToF MS is used in polymer analysis as traditional vaporisation techniques used in mass spectrometry lead to unwanted ionisation and fragmentation of the polymer. An example MALDI-ToF MS spectrum of benzyl amine-capped PLA is shown in Figure 1.2 by way of example. The peak separation, $\Delta(m/z) = 144$ g mol^{-1} reflects the molecular weight of PLA units but each chain also contains BnNH– and HOCH(Me)– end-groups as well as the bound K^+ ion.[34]

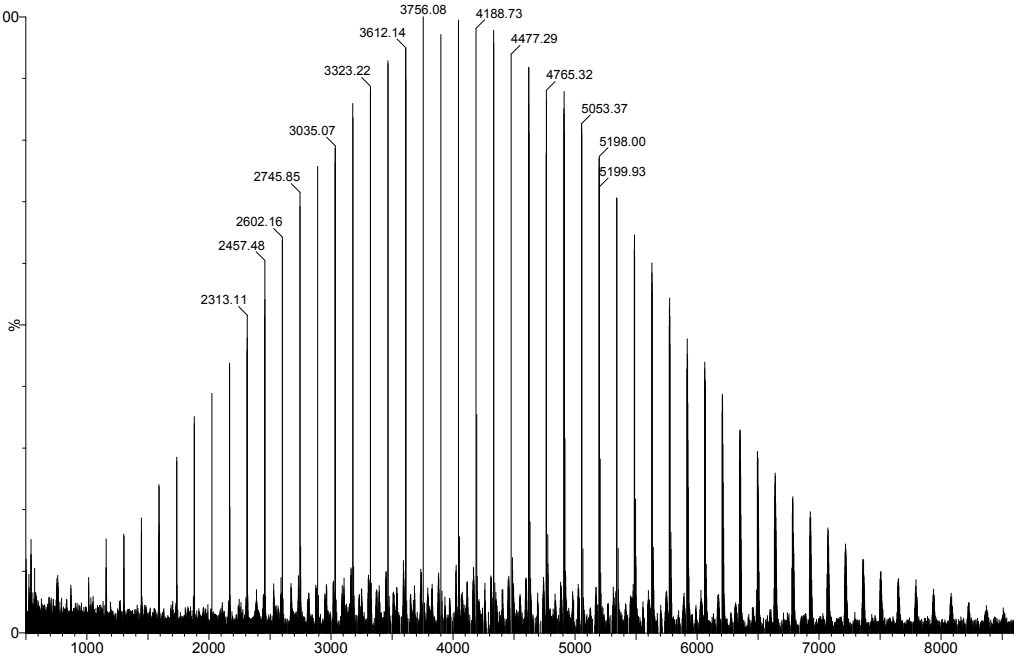

Figure 1.2. Full MALDI-ToF mass spectrum of benzyl amine-capped PLA. K^+ dopant, $\Delta(m/z) = 144$ g mol^{-1}.[34]

1.4.3 NMR spectroscopy

^{1}H NMR spectroscopy is a used to monitor polymerisation reactions for kinetic analysis as well as to characterise isolated polymer products. Integration of polymer peaks against residual or unreacted monomer environments can be used to calculate

the percentage conversion of monomer to polymer or the remaining concentration of monomer at a given time, *t*. The resultant kinetic profiles can be very informative with regard to the polymerisation mechanism and plots of molecular weights against % conversion are used to determine if M_n grows in a linear fashion, a key characteristic of living polymerisation.

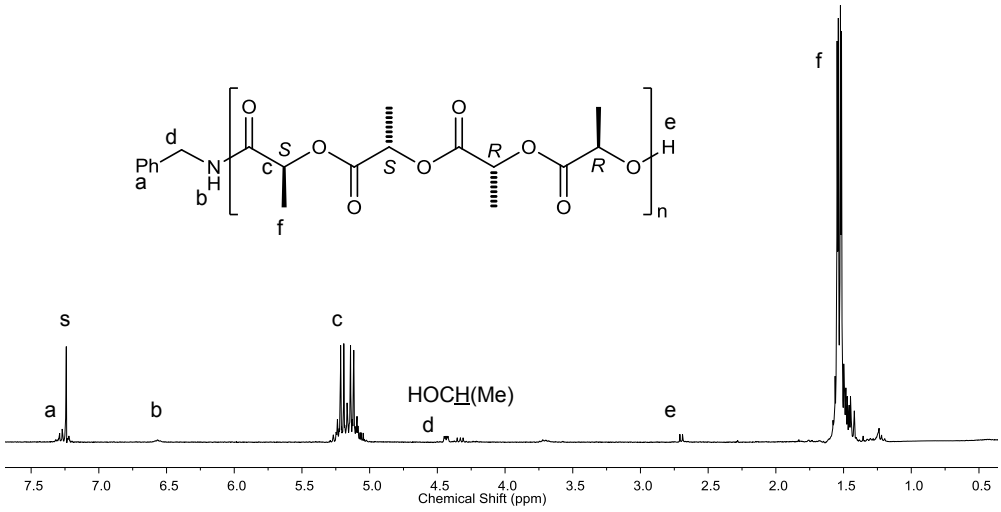

Figure 1.3. ^{1}H NMR spectrum of a benzyl amine-capped, highly heterotactic PLA, with assignments.[34]

The internal resonances of polymer products are the dominant features in the ^{1}H NMR spectra of isolated polymer products, but if a sufficiently low loading of monomer is used and a relatively low molecular weight polymer is formed, then end-group environments can be resolved. The ^{1}H NMR spectrum of a benzyl amine-capped PLA with assignment is shown in Figure 1.3.[34] Integration of the internal C<u>H</u>Me resonances against unique end-group protons can be used to calculate M_n by NMR and is often used in support of M_n(GPC), especially if reliable Mark-Houwink corrections have not been determined for a particular polymer. In the example shown (Figure 1.3), M_n(GPC) = 2,600 g mol^{-1} and M_n(NMR) = 2,410 g mol^{-1}.

1.4.4 Stereocontrol and tacticity in PLA

Lactide contains two stereocentres, leading to three possible stereoisomers. The two enantiomers, *L*-LA and *D*-LA contain two *S*-stereocentres or two *R*-stereocentres respectively. The third stereoisomer, *meso*-LA contains both *R*- and *S*-stereocentres. The racemic mixture of *L*- and *D*-LA, *rac*-LA, or enantiopure *L*-LA are readily available from commercial sources and are the most commonly studied LA

monomers. The stereochemistry of the polymer microstructure has a dramatic influence on macromolecular properties and it is often desirable to ensure a high degree of stereo-regularity in the polymer chain in order to optimise the mechanical properties. Random enchainment of *D*- and *L*-LA units when *rac*-LA (or *meso*-LA) is polymerised results in the formation of atactic PLA, which is amorphous and has a glass transition temperature (T_g) of around 55–60 °C.[11] These polymers also have a low tensile strength and degrade relatively quickly by hydrolysis.[16] Assuming that no epimerisation processes occur during polymerisation, ROP of *L*-LA or *D*-LA yields isotactic PLLA or PDLA, which are crystalline materials with melting temperatures (T_m) around 180 °C and greater tensile strength.[7, 16, 17, 35, 36] Interestingly, isotactic PLA chains of opposing stereochemistry have been mixed and co-crystallised and the resultant stereocomplex has been shown to have greatly enhanced properties, including a melting temperature up to 230 °C, which is 50 °C higher than PLLA or PDLA alone.[35]

Stereoselective ROP of *rac*-LA has broadened the range of available stereochemical microstructures. Alternating enchainment of *L*- and *D*-LA units present in *rac*-LA produces heterotactic PLA (Figure 1.4) and has been achieved using achiral catalytic systems *via* a chain-end control mechanism.[34, 37-63] In the chain-end control mechanism, the stereochemistry of the latest enchained polymer unit influences which enantiomer will be enchained next. Whilst the catalyst is achiral, the coordination geometry of the supporting ligand(s) and solvent are crucial to establishing this selectivity. Owing to the amorphous nature of heterotactically enriched PLA, melting points have been difficult to distinguish, but $T_m \approx 130$ °C have been reported, along with $T_g < 45$ °C.[62, 64, 65] It should also be noted that isotactically enriched stereoblock PLA have been prepared when *rac*-LA has been polymerised using achiral catalysts.[37, 57, 61, 66-74]

Enantiomorphic site control relies on the retention of catalyst chirality during monomer enchainment. Since *L*- and *D*-LA are chiral monomers, chiral catalysts display a consistent preference for either the *L*- or *D*-LA monomer. Under enantiomorphic site control conditions, it is possible to synthesise isotactically enriched, stereoblock or stereogradient PLA from *rac*-LA and a racemic[75-78] or resolved[77-79] catalyst, as well as syndiotactic PLA from *meso*-LA (Figure 1.4).[76, 80] Reported melting points of isotactic stereoblock polymers have ranged between 180

and 190 °C, which are greater than the melting points of enantiopure PLLA or PDLA (170–180 °C), but not as high as those of stereocomplexes, prepared post-polymerisation (T_m = 230 °C). In cases where isotactic stereoblock poly(*rac*-LA) have been formed from racemic catalysts, it has been proposed that growing isotactic PLA chains transfer between catalysts of opposing stereochemistry and when polymerisation resumes, the opposite enantiomer is preferentially enchained, before further exchange processes occur.[75, 76] Stereo-gradients form when chiral catalysts enchain the preferred enantiomer present in *rac*-LA is polymerised at a much greater rate than the opposite enantiomer.[79] With regard to *meso*-LA polymerisation, resolved catalysts may display a preference for the *R*- or *S*-stereocentre, and *RSRSRS* syndiotactic stereosequences form.[76, 80] Interestingly, heterotactic PLA can be produced from *meso*-LA if the system alternates between which stereocentre is ring-opened, and *RSSRRS* stereosequences form.[76]

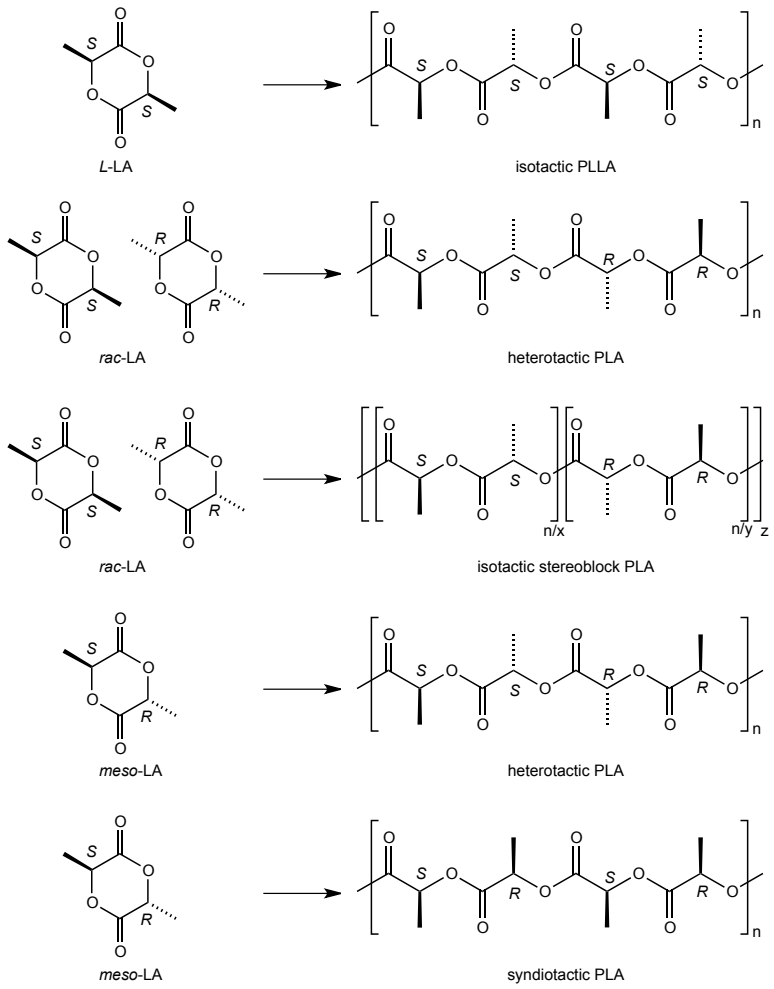

Figure 1.4. LA stereoisomers and a selection of PLA stereochemical microstructures.[76]

1.4.5 Assignment of PLA stereosequences using NMR spectroscopy

Whilst physical analysis provides an indication of the stereochemical properties of PLA, spectroscopic techniques have been shown to provide the most reliable evidence for tacticity in PLA chains. Polymer tacticity is determined by analysis of homonuclear and heteronuclear decoupled ^{1}H-{^{1}H} and ^{13}C-{^{1}H} NMR spectra. The first stereochemical assignments were made by Lillie and Schulz,[81] and Schindler and Harper[82] in the mid 1970s and were derived from Bernoullian statistical models for single and pair wise enchainment of lactide repeating units, assuming that epimerisation of stereocentres did not take place.

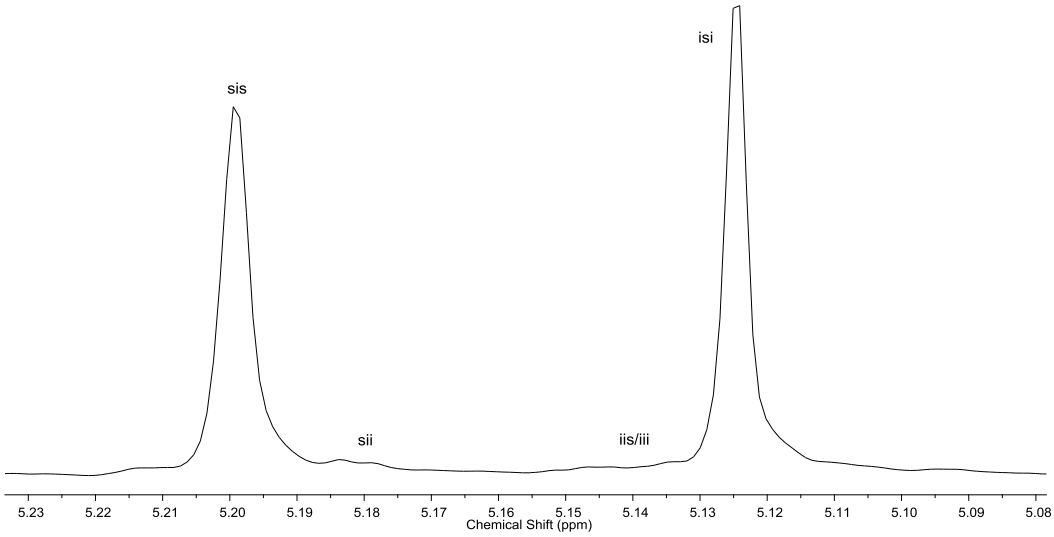

Figure 1.5. ^{1}H-{^{1}H} NMR spectrum of the methine region of heterotactically enriched PLA with tetrad assignments.[34, 50, 51, 83]

The notation, *i* (or *m*), refers to an isotactic (or *meso*) linkage (two adjacent stereocentres of the same configuration, i.e. *SS* or *RR*), and the notation, *s* (or *r*), refers to syndiotactic (or *racemic*) linkages (two adjacent stereocentres of opposite configuration, i.e. *SR* or *RS*). A typical ^{1}H-{^{1}H} NMR spectrum of the methine region of PLA displaying a high degree of heterotactic enrichment is shown in Figure 1.5, with assignments at the tetrad level (4 stereocentres, 2 LA units).[34, 50, 51, 83] HETCOR NMR studies (^{1}H-{^{1}H} and ^{13}C-{^{1}H} correlation) have been used to confirm these assignments and high-resolution hexad assignments have also been made.[83-91]

In heterotactic PLA, the dominant resonances are the *sis* and *isi* tetrads, which correspond to *RRSSRR* or *SSRRSS* stereosequences. Heterotactic enrichment is usually quoted as a probability, P_r (from the *m*/*r* stereochemical notation), where P_r is the

probability of forming racemic linkages (enchainment of opposite enantiomers). P_r can be calculated by integration of the *sis* and *isi* peaks against the total peak area, but P_r may also be calculated by integration of the *sis* peak against the *sii* tetrad.[53, 76] The *sii* and *iis* tetrads correspond to atactic stereosequences whereas the *iii* sequence represents isotactic linkages. Isotactic enrichment is expressed as P_m, where P_m is the probability of forming *meso* linkages. In isotactic PLA, the *iii* peak is the dominant stereosequence. According to the Bernoullian pair wise model, there are some sequences that are not possible in the polymerisation of *rac*-LA such as *sss* (*RSRSRS*), since *rac*-LA consists of *SS* and *RR* enantiomers. However, such as sequence can arise when *meso*-LA is polymerised and PLA with syndiotactic enrichment is produced.[76, 80] The *sss* stereosequence can arise in *rac*-LA polymerisations if transesterification or epimerisation processes are occurring, but in practice, peaks corresponding to *sss* sequences are likely to be obscured and MALDI-ToF MS is a more reliable indicator of transesterification products.

1.5 Ionic and metal free ROP mechanisms

Owing to the polarity of cyclic esters, there are many suitable reactive nucleophiles or electrophiles that can initiate ROP.[19] Both cationic and anionic pathways are known, as well as metal free mediated pathways, which typically involve organic carbenes or enzymes.[92, 93] Metal catalysed ROP reactions are the focus of this Thesis and usually proceed *via* activated-monomer or coordination-insertion pathways.

1.5.1 Anionic ROP

Initiation of ROP by nucleophilic reagents is broadly categorised as anionic ROP. Simple organometallic species such as alkyllithiums and Grignards or metal alkoxide species may initiate ROP and a mechanism for the anionic ROP of ε-CL is shown in Figure 1.6.[19, 94] In this example, the alkoxide initiator reacts with the lactone at the carbonyl, and the process of ring opening leads to the generation of an alkoxide at the propagating chain-end, which subsequently reacts with another lactone molecule.[11] With smaller lactones or lactide, these anionic pathways are prone to alkyl-oxygen scission, rather than the preferred, acyl-oxygen cleavage. Alkyl-oxygen scission is disfavoured and can lead to the epimerisation of stereocentres in the case of LA ROP. Polymerisations of enantiopure monomers are often performed to establish, or dismiss, propagation *via* anionic pathways. Anionic ROP of ε-CL typically proceeds

via acyl-oxygen cleavage, but linear chain growth is often accompanied by intramolecular back-biting by the terminal alkoxide into an ester linkage. These back-biting reactions generate macrocyclic PLA molecules and the process is generally termed, transesterification.

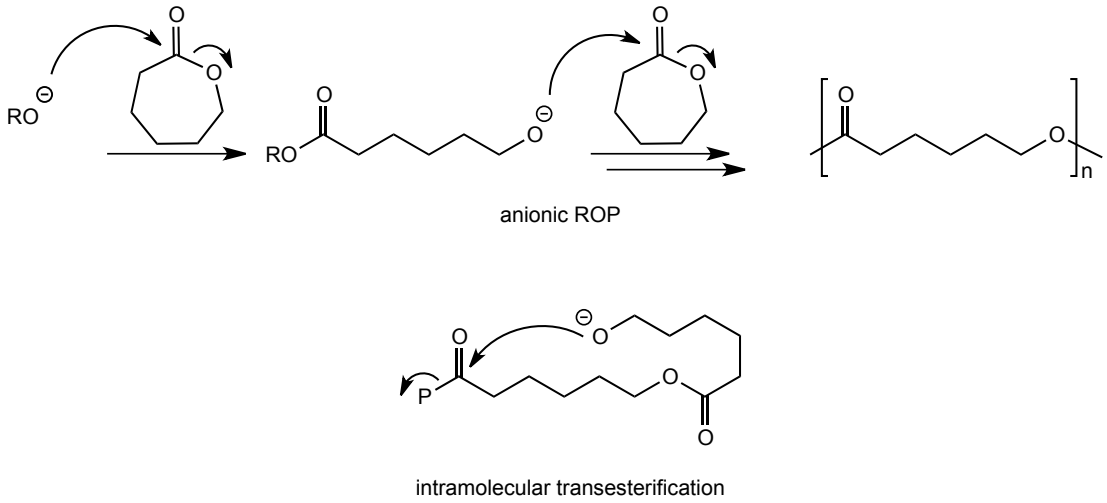

Figure 1.6. Anionic ROP *via* acyl-oxygen cleavage and intramolecular tranesterification. R = alkyl, P = polymer chain.[11, 19, 94]

1.5.2 Cationic ROP

Cationic mechanisms may operate when electrophilic initiators including Brønsted and Lewis acids are used to ring open epoxides or cyclic ethers.[19, 94-96] Such an example is the cationic chain-end polymerisation of ethylene oxide, which can be prone to intramolecular back-biting (Figure 1.7). Kricheldorf transferred this methodology to the ROP of *L*-LA, using trifluoromethanesulfonic acid (TfOH) as the protic source, but initiation *via* alkyl-oxygen bond cleavage was shown to operate.[97, 98] Figure 1.7 also shows cationic ROP by an activated-monomer process. In this activated-monomer pathway, a proton combines with the epoxide and attack by an exogenous alcohol initiator or macromonomer ring opens the activated monomer.[19, 96] The proton is transferred to the next monomer, which is subsequently attacked by the alcoholic end-group of the macromonomer. Bourissou polymerised LA in the presence of primary and secondary alcohols (ROH, Figure 1.7), as well as TfOH and showed that the exogenous alcohol formed the chain-end of the resultant PLA.[99, 100] Furthermore, good agreement was seen between the expected and observed M_n and transesterification side products were absent from PLA mass spectra. Studies with *L*-

LA showed that no epimerisation of stereocentres occurred, which confirmed that ring opening proceeded *via* acyl-oxygen cleavage.

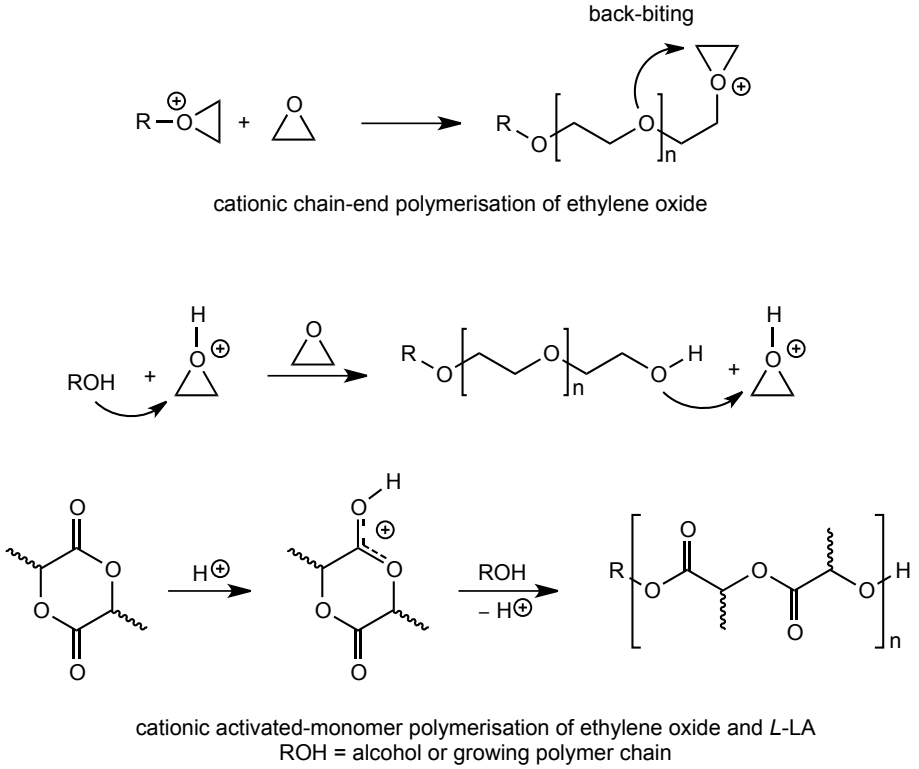

Figure 1.7. Cationic ROP by chain-end and activated-monomer pathways.[19, 94-96, 99]

1.5.3 Organocatalysis

Pyridines, such as 4-dimethylaminopyridine (DMAP) and *N*-heterocyclic carbenes (NHCs) are just two examples of the numerous organic substrates that have proved to be efficient initiators for the ROP of lactide.[19, 66] Most of these polymerisations require a protic initiator, ROH, although ambiguity over the precise mechanism remains. Polymerisations most probably occur through nucleophilic activation of the monomer and/or base catalysed processes (Figure 1.8).[101] Hedrick and Waymouth have also used NHCs in the absence of a protic initiator and proposed that the active propagating species is zwitterionic (Figure 1.9).[102, 103] The carbene inserted across the acyl-oxygen bond and macrocyclic PLA were ultimately formed.

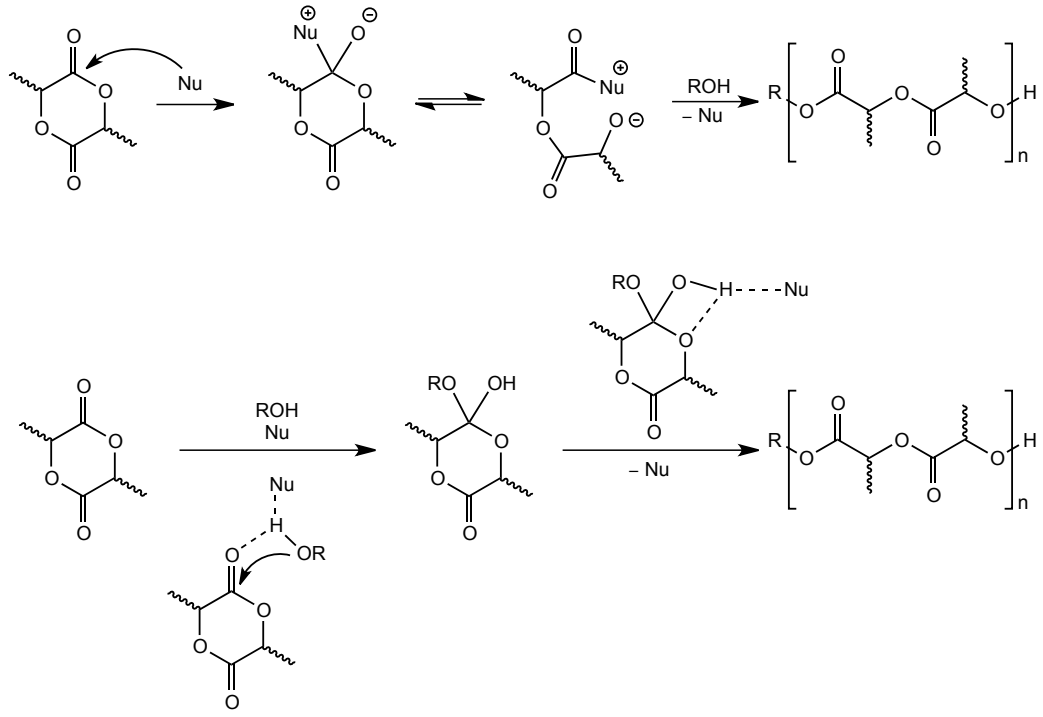

Figure 1.8. Organocatalytic ROP *via* nucleophilic or basic pathways. Nu = DMAP or *N*-heterocyclic carbene, ROH = alcohol initiator or growing polymer chain.[92, 93]

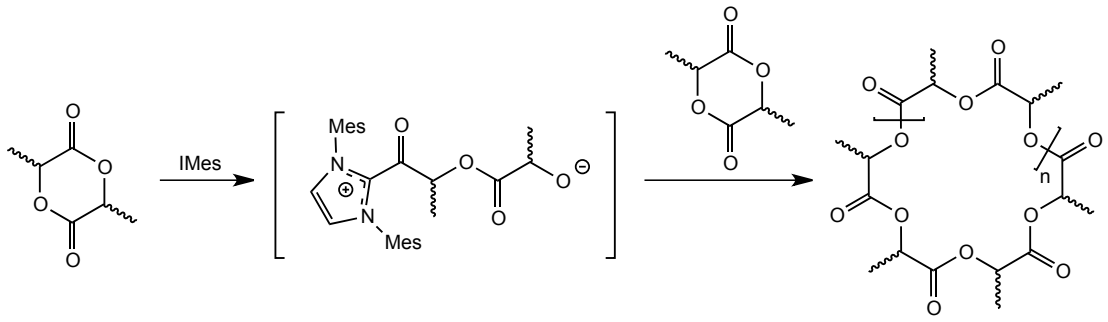

Figure 1.9. Production of cyclic PLA with a zwitterionic active species.[102, 103]

1.6 ROP using metal based catalysts

Metal-based catalysts for ROP of cyclic esters usually feature Lewis acidic, closed shell metals[13, 14, 104, 105] and include magnesium, calcium and zinc,[47-53, 106-114] aluminium,[13, 14, 37, 104, 105, 115, 116] yttrium and the lanthanides,[13, 34, 40, 45, 46, 56, 104, 117-126] the Group 4 elements[13, 14, 104, 127, 128] and tin.[11, 13, 14, 104, 105] Germanium,[58] indium,[59, 60, 129-133] bismuth[134, 135] and iron[136, 137] based catalysts are also known but are less prevalent. The relative ROP activities of metal-based initiators generally follows the order: rare earth and yttrium ≈ calcium > magnesium > zinc > tin ≈ zirconium and hafnium > titanium > aluminium.[19, 138]

Since many biodegradable polyesters are used in food packaging and biomedical applications, non-toxic elements are preferred although a tin dicarboxylate catalyst, $Sn(Oct)_2$ (Figure 1.10), is used in industry.[5] Tin(II) octonoate is also a convenient catalyst for laboratory scale ROP reactions owing to its ease of handling and solubility in organic solvents.[14] Industrial scale ROP of LA processes using $Sn(Oct)_2$ and alcohol co-initiators are performed under melt conditions at 140–180 °C and polymer products with molecular weights of 10^5–10^6 g mol^{-1} are produced within minutes or hours. Despite Sn(IV) residues being toxic, use of $Sn(II)(Oct)_2$ to polymerise LA is approved for non-biomedical applications.[139-141]

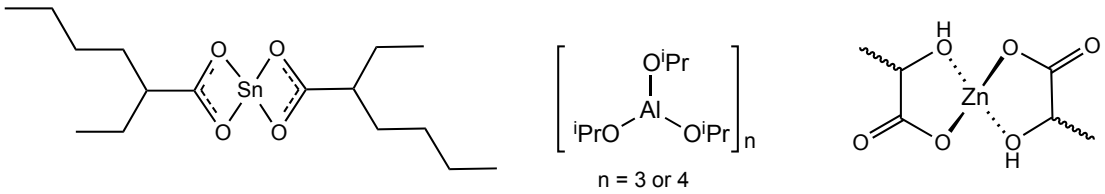

Figure 1.10. $Sn(Oct)_2$, $Al(O^iPr)_3$ and $Zn(lact)_2$.[19]

Initiation in $Sn(Oct)_2$ based systems has been proposed to occur *via* an activated-monomer process, where LA is activated by coordination to the tin centre.[11] In this process an exogenous alcohol molecule attacks the activated carbonyl and ring opens the lactide unit. However, further studies by Krichelforf, Duda and Penczek, and Albertsson have concluded that $Sn(Oct)_2$ and exogenous alcohols form equilibrium mixtures of tin alkoxides under mild conditions (T < 100 °C).[11, 142-147] Initiation and propagation are most likely to ensue *via* a coordination-insertion mechanism, where the active chain-end remains coordinated to the tin centre and enchainment occurs by insertion of coordinated lactide units into the metal-alkoxide bond. The activated-monomer and coordination-insertion mechanisms are discussed further in Sections 1.6.1 and 1.7.

Zinc based catalysts including zinc metal, zinc lactate and other zinc carboxylate derivatives are typically used to prepare PLA for use in biomedical applications, owing to the biocompatibility of zinc residues present in PLA.[14, 140, 148-150] Industrial scale ROP of LA using zinc based catalysts (Figure 1.10) are also performed in the melt at 140 °C. Aluminium catalysts generally show poor activities, due to the small radius of Al^{3+}, but simple aluminum alkoxides, e.g. $[Al(O^iPr)_3]_n$ (n = 3 or 4) (Figure 1.10), have been used extensively in mechanistic investigations.[14, 138, 151-154]

1.6.1 Activated-monomer ROP

The activated-monomer mechanism is mostly observed when simple Lewis acidic metal salts or complexes with non-labile ligands are used as ROP catalysts.[155, 156] An excess of exogenous alcohol e.g. *iso*-propyl alcohol or benzyl alcohol over the metal catalyst may be employed as a nucleophilic initiator, which attacks monomer units that have been activated by the metal centre. If initiation is efficient, all of the alcohol molecules are consumed at the beginning of the reaction, enabling the generation of multiple polymer chains per metal (or one chain per alcohol). As shown in Figure 1.11, no formal bond between the alcoholic polymer chain-end and the metal centre forms; propagation is reliant on the activation of monomer units at the metal centre with subsequent attack by terminal alcohol group of the polymer chains. In well-controlled, activated-monomer ROP, the molecular weight of the polymer formed is dependent on the initial ratio of $[rac\text{-LA}]_0$:$[\text{alcohol}]_0$. There are relatively few reports of ROP systems where propagation proceeds *via* an activated-monomer pathway, but kinetic analysis has usually reported dependencies in $[\text{monomer}]_0$, $[\text{metal}]_0$ and $[\text{alcohol}]_0$, where $[\text{alcohol}]_0$:$[\text{metal}]_0$ determines the number of propagating chains.[157, 158]

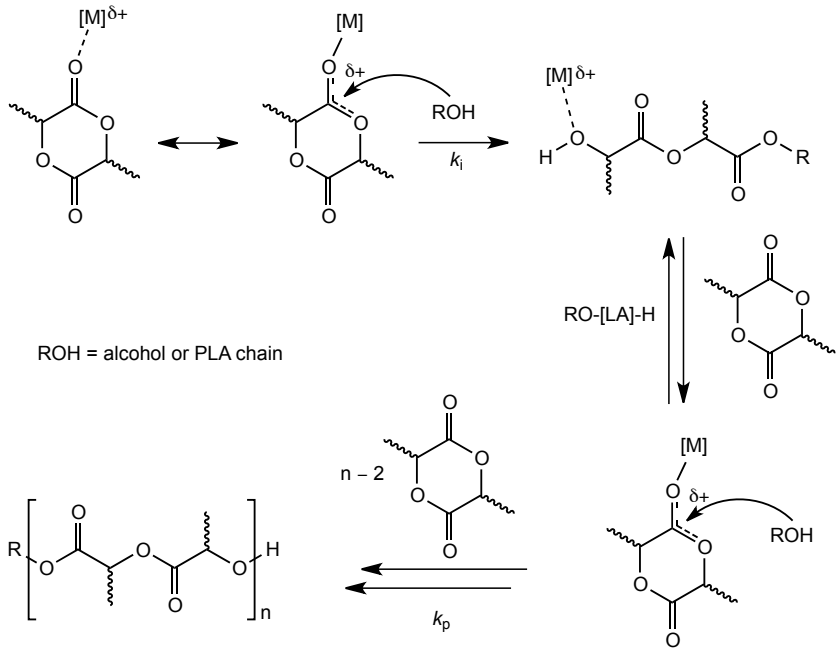

Figure 1.11. Activated-monomer ROP in the presence of a metal catalyst and protic initiator.[158]

In two separate reports, Nomura and Hedrick have reported the activated-monomer ROP of lactones using $Sc(OTf)_3$ and alcohols.[155, 156] Nomura demonstrated that 50 equivs of ε-CL could be polymerised in the presence of varying equivalents of benzyl alcohol and $Sc(OTf)_3$. In a run, $[\varepsilon\text{-CL}]_0:[BnOH]_0:[Sc(OTf)_3]_0 = 50:5:1$ in toluene at room temperature, complete conversion was achieved within 2 h and M_n(GPC) = 2,400 g mol^{-1} (treated as a polystyrene) and PDI = 1.17. The narrow molecular weight distribution was suggestive of a well-controlled polymerisation process, but M_n(GPC) was higher than expected (M_n(calcd) = 1,100 g mol^{-1}) for one chain forming per BnOH. Despite this attractive approach to metal-mediated ROP, activated-monomer polymerisation reactions are more likely to display poor control over molecular weight and PDI, and the nature of the catalyst under polymerisation conditions may be difficult to elucidate. Over the past 20 years, ROP catalyst development has focused on the incorporation of robust, ancillary ligand frameworks as well as metal bound initiators, rather than exogenous nucleophiles. These types of systems were designed specifically to achieve ROP *via* the coordination-insertion mechanism, where the active chain-end remains bound to the metal centre.

1.7 Coordination-insertion ROP

The coordination-insertion or active chain-end mechanism is a *pseudo* anionic polymerisation pathway that has been exploited successfully for the ROP of cyclic esters. Initiators that efficiently polymerise cyclic esters *via* a coordination-insertion generally feature a labile metal-alkoxide bond in addition to a robust, polydentate ancillary ligand. Initiation involves coordination of the carbonyl functional group of the monomer to the metal centre, followed by insertion of the metal alkoxide into the activated electrophilic centre and subsequent scission of the acyl-oxygen bond.[13, 14, 19, 138, 159] The original alkoxide initiating group forms the polymer end-group and propagation ensues through a newly formed metal-macroinitiator moiety (Figure 1.12).

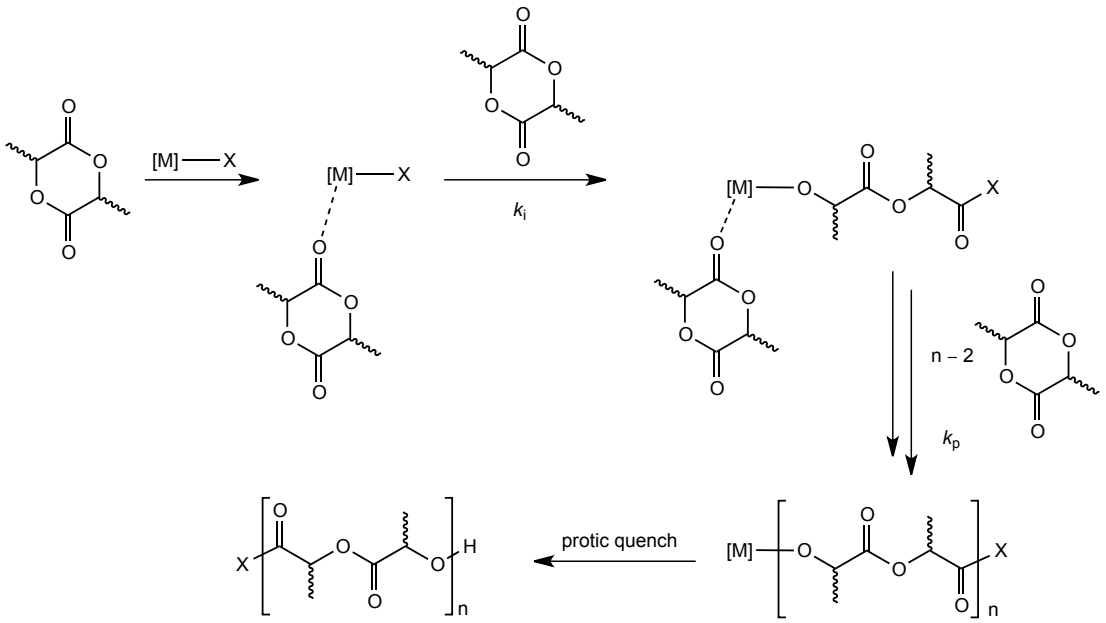

Figure 1.12. Coordination-insertion mechanism. X = OR or NR_2.[13, 14, 19]

In a coordination-insertion regime, propagation is limited by $[monomer]_0$ and $[catalyst]_0$ (assuming complete transformation of the pre-catalyst) and polymerisations are reliant on fast initiation with respect to propagation. In this scenario, all of the initiator is consumed in ring opening processes before bulk propagation begins, which leads to the formation of polymers with predictable molecular weights, based on the monomer to initiator ratio. If propagation is competitive with initiation, then insertion of a monomer unit into a metal-macroinitiator bond may be favoured kinetically over ring opening events by metal-alkoxide initiators. Consequently, polymer molecular weights may be greater than expected and initiation appears incomplete. Furthermore, the molecular weight distribution may be broadened as chains of widely varying length are formed. These observations have consistently been made when metal amide or alkyl complexes have been used as ROP initiators.[45, 48, 51, 53, 120, 127, 160, 161] Amides and alkyls are inefficient initiators for ROP by coordination-insertion and may act as bases, rather than nucleophiles. For this reason, metal-alkoxides have received the most attention with a view towards ROP by coordination-insertion.

1.7.1 Transesterification

Living ROP can be achieved if the initiation step is fast with respect to propagation and the polymerisation is free from irreversible chain transfer or permanent deactivation pathways. The most common deactivation processes in ROP are intermolecular and intramolecular transesterification side reactions (Figure 1.13).[14]

Intramolecular tranesterification or back-biting during propagation involves insertion of the active metal-alkoxide bond into an internal ester unit of the growing polymer chain, leading to elimination of an inert macrocyclic ester. These cyclic products appear alongside linear polymer chains in MALDI-ToF MS and contain no apparent end-group. In the case of *rac*-LA, a diester, peak envelopes in MALDI-ToF MS separated by $\Delta(m/z)$ = 72.0 g mol^{-1} or half lactide units, are consistent with transesterification products forming.[138, 162] Intermolecular transesterification involves redistribution of polymer chains between active propagating species.[24, 162] The active metal-alkoxide may insert into an ester linkage of another propagating species, leading to a broadening of the molecular weight distribution. In both instances, chain growth may resume through the new metal alkoxides formed.

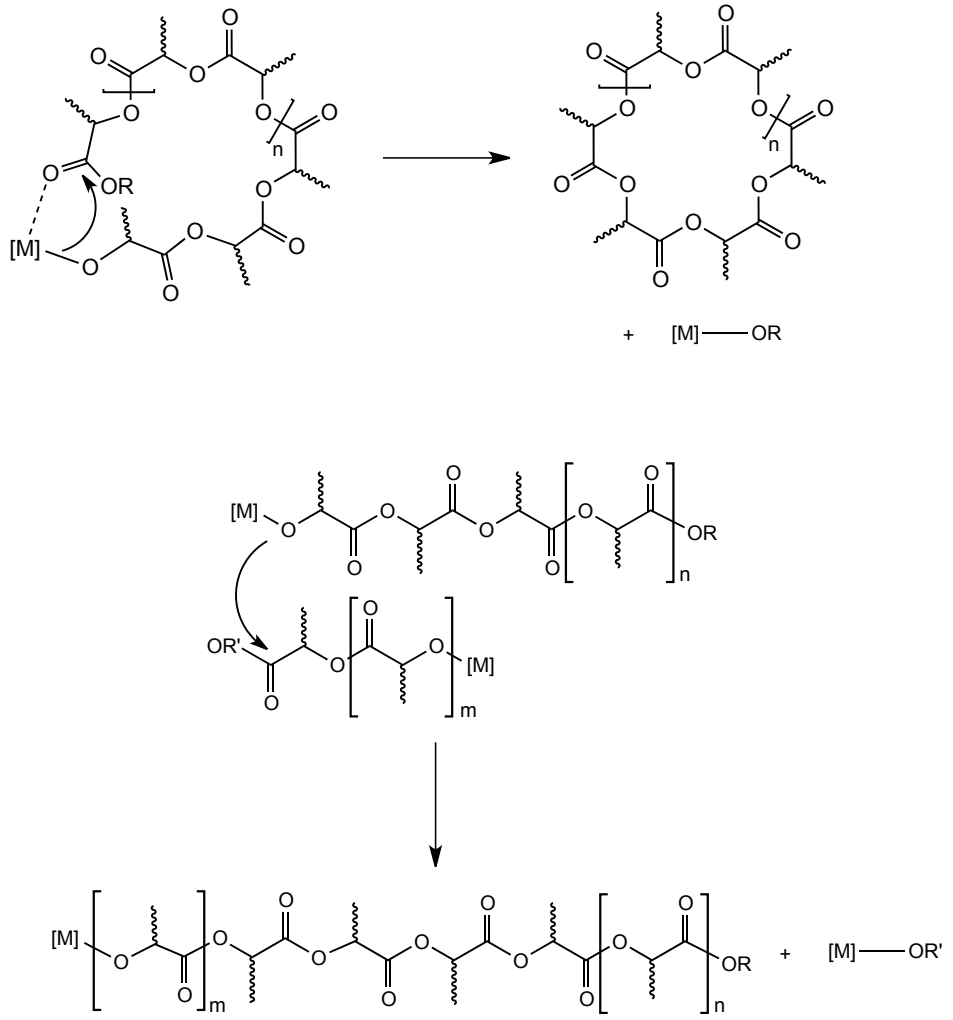

Figure 1.13. Intramolecular and intermolecular transesterification processes in ROP. R or R′ = PLA chain.[14, 24, 138, 162]

The transesterification mechanisms shown in Figure 1.13 are applicable to ROP systems that propagate *via* the coordination-insertion mechanism, where a formal bond exists between the metal centre and the active chain-end. Transesterification occurs in activated-monomer systems, although the mechanism is less well understood, but is likely to involve attack of activated internal ester linkages by alcoholic chain-ends. Post-polymerisation tranesterification may also occur and is associated with the gradual decrease in M_n and broadening of molecular weight distributions over prolonged reaction times.[45] Optimisation of reaction conditions can minimise detrimental post-polymerisation transesterification, as well as prompt isolation of polymer products after the termination of polymerisation reactions. Non-linear M_n *vs*. Conversion and M_n *vs*. $[monomer]_0$:$[initiator]_0$ relationships may arise from detrimental transesterification processes, but MALDI-ToF MS data provide the most conclusive evidence for transesterification.

1.7.2 Classical organometallic ROP initiators

Homoleptic, trivalent lanthocenes such as Cp^*_3Sm have been tested for ROP capability. It was shown that Cp^*_3Sm could activate THF molecules but a new stoichiometric, alkoxide species was formed ($Cp^*_2Sm\{O(CH_2)_4C_5Me_5\}(THF)$).[163] ε-CL was polymerised by Cp^*_3Sm with possible initiation by a reactive η^1-C_5Me_5 group that slipped from a η^5 coordination mode in the presence of a competitive ε-CL donor. (η^5-$C_5H_4R)_3Ln$ (R = Me or H, Ln = Y, Sm or Er) compounds were also capable of initiating ROP of ε-CL and *rac*-LA in the bulk or in toluene solution at elevated or ambient temperatures.[164] Polymers with $M_n \approx 10^4$ g mol^{-1} were produced but control over molecular weight was modest and molecular weight distributions were broad. Suitable initiating groups including hydrides, alkyls and alkoxides have been incorporated into lanthocene complexes, with several examples shown in Figure 1.14.

A dimeric, hydride complex, $[Cp^*_2Sm(\mu\text{-}H)]_2$ (**1.1**) and mononuclear lanthanide methyl complexes, such as $Cp^*_2Sm(Me)(THF)$ (**1.2**), were prepared by Yasuda and co-workers (Figure 1.14).[165] The mononuclear complex, **1.2**, had a superior activity to **1.1** when the polymerisation of ε-CL was performed in toluene at room temperature, presumably on account of the tendency of the hydride complex to promote non-polymerisation lactone reduction reactions. Nevertheless, PCL with M_n > 75,000 g

mol^{-1} with PDI < 1.08 were produced. A linear increase M_n with conversion was observed when **1.2** was employed, despite molecular weights being approximately twice that expected for one chain forming per initiator.

The alkoxide complexes, $[Cp_2Y(\mu\text{-}OMe)]_2$ (**1.3**) and $Cp^*_2Ln(OR)(L)$ (Ln = Sm, R = Et, L = OEt_2 (**1.4**) and Ln = Y, R = Me, L = THF (**1.5**)) (Figure 1.14) were also reported by Yasuda.[165] Each complex was screened for the ROP of ε-CL in toluene at 0 °C and monomer to PCL conversions > 90% were achieved after 10 h. $M_n \approx 95{,}000$ g mol^{-1} were approximately twice that expected for one PCL chain forming per alkoxide initiating group but PDIs were narrow (≈ 1.1) and M_n grew linearly with conversion. This work was later reviewed by Agarwal and Greiner and it was noted that whilst ROP with **1.3**–**1.5** initiated *via* a coordination-insertion mechanism, non-ring opened acetals were formed in the presence of the alkyl complex, **1.2**, prior to ROP.[121-123, 166, 167] Okuda also prepared achiral or chiral, heterobimetallic lanthocene complexes with pendant silyl-amido donors and the ROP of ε-CL and *L*-LA was achieved under ambient conditions and at elevated temperatures.[168, 169] Good agreement between expected and theoretical molecular weights was achieved and narrow PDIs were also recorded under certain conditions.

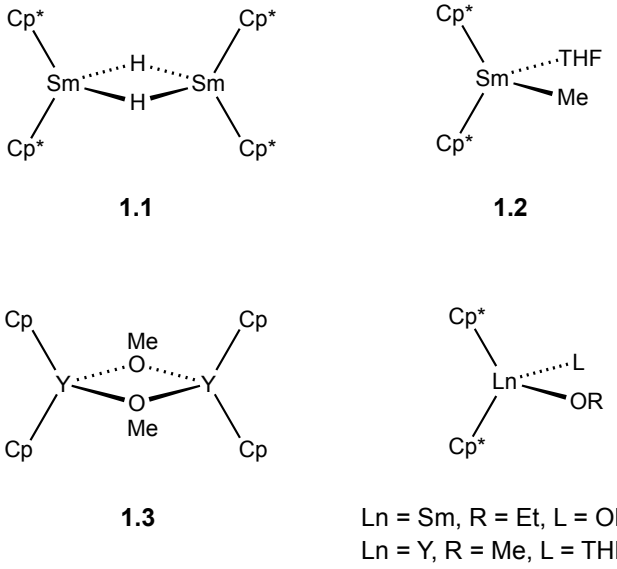

1.1 **1.2**

1.3

Ln = Sm, R = Et, L = OEt_2 (**1.4**)
Ln = Y, R = Me, L = THF (**1.5**)

Figure 1.14. Lanthocene complexes used for the ROP of lactones.[165]

1.7.3 Phenolate supported initiators

Ligand progression in single-site ring opening polymerisation catalysts has closely followed the development of post-metallocene olefin polymerisation catalysts.

Phenolate ligands have received significant attention owing to their compatibility with early transition metal and rare earth elements.[170-173] A bis(phenolate) ligand framework, with linked phenolate rings has proven to be a robust and successful ligand architecture. Owing to the commercial availability of many phenol derivatives and the ease of incorporating aryl functionality, a wide variety of bis(phenolate) ligands have been developed. Figure 1.15 shows examples of metal complexes bearing bis(phenolate) ligands with aliphatic linking bridges, as well as an example of a homoleptic yttrium phenolate complex, Y(O-2,6-$C_6H_3{}^tBu_2)_3$ (**1.6**).

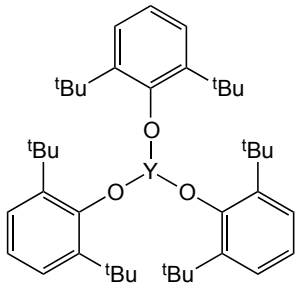

1.6

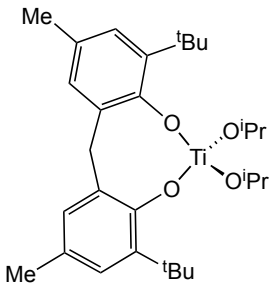

1.7

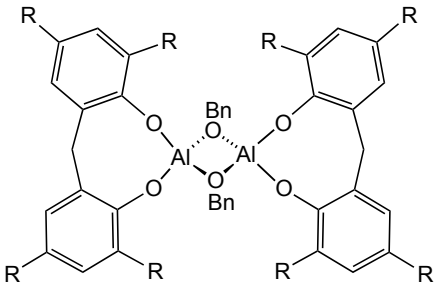

1.8 R = $CPhMe_2$

Figure 1.15. Mono and bis(phenolate) complexes utilised in ROP.[174-178]

Feijen utilised **1.6** (Figure 1.15) for the polymerisation of *L*-LA (and ε-CL) in the presence of three equivalents of *iso*-propyl alcohol in dichloromethane at room temperature.[174-176] The phenolate ligands were eliminated in the presence of ^iPrOH and the active species was derived from the *in situ* formed tris(alkoxide) complex. 150 equivs. of *L*-LA per **1.6** were polymerised to 98% conversion within 2 mins. M_n(calcd) = 7,200 g mol^{-1}, based on one PLA forming per equivalent of ^iPrOH and M_n(GPC) = 10,800 g mol^{-1}. M_n(NMR) = 7,100 g mol^{-1}, calculated from PLA end-group integration was close to that expected based on the monomer to PLA conversion and one chain forming per ^iPrOH. The PDI = 1.14 was narrow and consistent with a living polymerisation but ambiguity over the polymerisation

mechanism remained. A first-order dependence in $[L\text{-LA}]_0$ was determined but dependencies in initiator could not be determined, and it was also unclear whether or not there was more than one type of active species present under polymerisation conditions.

The bis(phenolate) alkoxide complexes, **1.7** and **1.8** (Figure 1.15) and related examples have been screened for ROP capability. Aida employed the titanium bis(alkoxide) initiator, **1.7**, to polymerise 100 equivs. of ε-CL in dichloromethane at ambient temperature.[177] Complete conversion of monomer to PCL was achieved within hours and M_n(GPC) ≈ 6,500 g mol^{-1} suggested that two PCL chains formed per equivalent of **1.7** (i.e. one chain per alkoxide initiating group). The PDI = 1.15 was narrow, consistent with a well-controlled process but no LA polymerisation was reported. Liu prepared and utilised the dimeric bis(phenolate) aluminum initiator, **1.8**, for the ROP of *L*-LA.[178] The complex displayed low activity, and 50 equivs. of *L*-LA were polymerised to 81% completion after 48 h in toluene solution at 110 °C. The observed molecular weight, M_n(GPC) = 13,000 g mol^{-1} was more than twice that expected, M_n(calcd) = 5,900 g mol^{-1}, but the PDI = 1.09 was narrow.

1.7.4 Aluminum [ONNO] salen and salan complexes

Salen and salan ligands have received considerable attention and numerous trivalent alkoxide and amide species are known, and examples are shown in Figure 1.16.[37, 179] Aluminium initiators generally display low activities with reactions requiring heating over several days before high conversions of monomer to polymer are observed.[13, 14, 104] Low monomer loadings typically feature when aluminum initiators are used in ROP of LA studies on account of their low activity, but ROP reactions including the initiators shown in Figure 1.16 have displayed excellent control between observed and expected molecular weights and narrow distributions have formed (PDI < 1.2). Furthermore, excellent stereocontrol has typically been observed with these initiators and chiral initiators have been prepared to probe stereoselectivity in the ROP of LA stereoisomers.

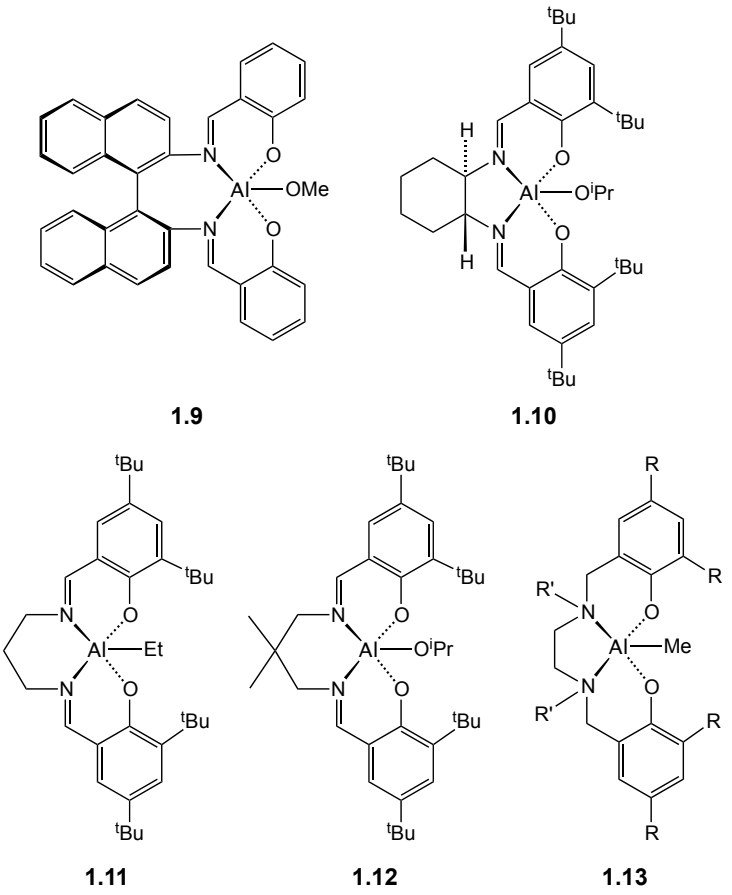

Figure 1.16. Examples of salan and salen aluminium and complexes.[37, 57, 67-69, 75-80, 180, 181]

Spassky provided the earliest evidence for stereoselective ROP of *rac*-LA using homogeneous catalysts.[79] The (*R*)-enantiomer of the bis(naphthyl) aluminum salen complex, (*R*)-**1.9**, preferentially polymerised the *D*-enantiomer of LA in a polymerisation reaction performed in toluene at 70 °C. *D*-LA was polymerised approximately 20 times faster than *L*-LA, and at conversions less than 50%, the PLA microstructure was predominantly isotactic poly(*D*-LA). At 60% conversion, only *L*-LA remained in solution but complete conversion (90%) of 75 equivs. of *rac*-LA was not achieved until 113 h had elapsed. The resultant PLA had a tapered stereoblock microstructure, where isotactic sequences of *D*-LA units were followed by sequences of *L*-LA units, until *L*-LA was predominantly enchained at high conversion. The polymer product had a melting temperature, T_m, of 187 °C, which was higher than that of enantiopure, isotactic poly(*D*-LA) or poly(*L*-LA) (T_m = 170–180 °C). Stereoblock PLA, consisting of alternating sequences of *D*-LA, followed by *L*-LA, was formed when Coates used the *iso*-propoxide analogue of (*rac*)-**1.9** under the same

conditions as Spassky's experiment, and a T_m = 179 °C was recorded.[75, 76] Baker and Smith also used a racemic mixture of **1.9** and its enantiomer to polymerise *rac*-LA, and suggested that enantiopure, isotactic poly(*D*-LA) and poly(*L*-LA) chains were formed in parallel, leading to the formation of a stereocomplex.[180] The reported melting temperature, T_m = 191 °C, was greater than that expected of stereoblock PLA, but not as high as that recorded for stereocomplexes formed by mixing of poly(*D*-LA) and poly(*L*-LA) chains prepared in isolation (T_m = 230 °C).[35] Stereoerrors (or polymer exchange, *vide infra*) may have accounted for the reduced melting temperature, and it was debated in the literature whether a true stereocomplex was formed or not. Coates suggested that stereoblock PLA formed based on the presence of minor *sii*, *iis* and *isi* tetrad sequences of equal intensity in the PLA methine region in homonuclear-decoupled ^{1}H-{^{1}H} NMR spectra.[76]

Coates also used the *iso*-propoxide analogue of (*R*)-**1.9** to polymerise *meso*-LA. The catalyst showed a preference for ring opening at the carbonyl adjacent to the *R*-stereocentre of *meso*-LA and PLA with high syndiotactic enrichment was produced (P_m = 0.96 and T_m = 153 °C).[76] When (*rac*)-**1.9** was used to polymerise *meso*-LA, PLA with a high degree of heterotactic enrichment was obtained (P_r = 0.80), rather than syndiotactic PLA.[76, 80] To account for this novel production of heterotactically enriched PLA, a polymer exchange mechanism was postulated, whereby each individual polymer chain switched between enantiomorphic aluminum centres prior to insertion of the next monomer unit.

Duda exploited the stereobias exhibited by **1.9** and the slowing of the reaction after 50% conversion to prepare isotactic stereoblock poly(*rac*-LA) with T_m = 210 °C.[181] Enantiopure (*S*)-**1.9** selectively polymerised *L*-LA up to 50% conversion before an equimolar quantity of the protio-(*R*)-bis(napthyl)salen ligand was added to the polymerisation mixture. The protio-(*R*)-bis(napthly)salen ligand exchanged with the (*S*)-bis(napthyl)salen ligand bound to the aluminum centre of **1.9** and polymerisation resumed, with the enchainment of *D*-LA units. The optical rotation exhibited by the polymer peaked prior to the addition of the protio-(*R*)-bis(napthyl)salen ligand but reduced as the *D*-LA enantiomer was enchained. This novel approach produced a much more pronounced switchover between *L*- and *D*-LA units along the chain, with little tapering, and a high T_m = 210 °C was recorded.

Feijen utilised Jacobsen's ligand and prepared enantiopure (*R*,*R*) and racemic aluminum alkoxide complexes, **1.10** (Figure 1.16).[77, 78] (*R*,*R*)-**1.10** was used to polymerise *rac*-LA and the catalyst showed a kinetic preference for *L*-LA, which was enchained fourteen times faster than *D*-LA. The racemic complex, (*rac*)-**1.10** was used to polymerise *rac*-LA and isotactic stereoblock PLA (P_m = 0.93) were produced with narrow molecular weight distributions (PDI < 1.10) and predictable molecular weights. Chisholm has recently examined the polymerisation of *rac*-LA using (*R*,*R*)-**1.10** and revealed that a combination of factors account for the stereoselectivity shown by the complex, including the chirality of the complex, the identity of initiating group, the stereochemistry of the latest enchained monomer units and the reaction solvent.[182, 183] It is therefore unclear if stereoselective ROP of *rac*-LA is governed exclusively by enantiomorphic site control or whether chain-end control processes influence stereoselectivity in this system.

Nomura prepared the achiral aluminum salen complex, **1.11**, which was likely to have been converted to an alkoxide initiator under polymerisation conditions, as one equivalent of benzyl alcohol was included in the polymerisation mixture.[67] Poly(*rac*-LA) with a high isotactic bias (P_m = 0.91) was produced by **1.11** and a chain-end control mechanism was proposed, but the selectivity was less pronounced when a C_2 ethylene-bridge between the imine donors was present. Computational experiments suggested that the C_3-propylene diimine bridge was more flexible, which allowed the complex to form a favourable coordination mode for a specific lactide enantiomer. Chen's achiral complex, **1.12**,[68, 69] also generated isotactic stereoblock PLA (P_m = 0.90, T_m = 193 °C) from *rac*-LA and a derivative of **1.12**, where the phenolate ^{t}Bu groups were replaced by a ^{t}BuMe$_2$Si substituent at the *ortho*-position and a hydrogen atom at the *para*-position was produced. The PLA produced by this achiral complex (**1.12**-^{t}BuMe$_2$Si) had a melting point, T_m = 210 °C and P_m = 0.98.[71]

Gibson and others investigated various derivatives of **1.13** (including salen analogues) and showed that heterotactic or isotactic poly(*rac*-LA) could be produced from *rac*-LA depending on the choice of substituents.[57] Gibson undertook *rac*-LA polymerisation studies with **1.13** in toluene at 70 °C and converted the aluminum alkyl to a benzyl alkoxide *in situ*. When **1.13** (R′ = Bn and R = Cl) was employed, heterotactic PLA (P_r = 0.96) was produced, but the selectivity switched to isotactic enrichment (P_m = 0.79) when R′ = Bn and R = H.

1.7.5 Tetradentate bis(phenolate) supported initiators

Bis(phenolate)-amino ligands are another class of tetradentate, [ONNO]-type ligand that have been employed in Group 4 post-metallocene α-olefin polymerisation catalysts as well as in trivalent and tetravalent ROP catalysts. Kol[184-192] and Mountford[46, 125, 193-195] originally developed and utilised these ligands and a comprehensive library of ligand derivatives and complexes has been prepared.[170, 196-204] Figure 1.17 shows a selection of rare earth bis(phenolate)-amino complexes that were successfully prepared by Carpentier,[38, 39, 205] Mountford,[45, 124, 206] and Cui.[44] Okuda also exploited the 1,ω-dithiaalkanediyl-bridged bis(phenolate) class of ligands that are shown in Figure 1.17 to prepare Group 3 ROP initiators.[54, 55, 207] Although ^{t}Bu substituents are shown on the phenolate rings, cumyl, adamantyl or less bulky methyl groups or combinations of, are amongst several other substituents that have been employed in structure-activity investigations. There is also scope for variation in the identity of the pendant arm functional group. Ethereal, amino and pyridyl donors are shown in Figure 1.17, but thioether and furan examples are known.[189, 190] A "dummy arm" ligand (L = Me) is also known, and studies with the resultant complexes formed using this ligand have highlighted the necessity of the pendant arm to the formation of active catalysts.[45, 185-187, 206]

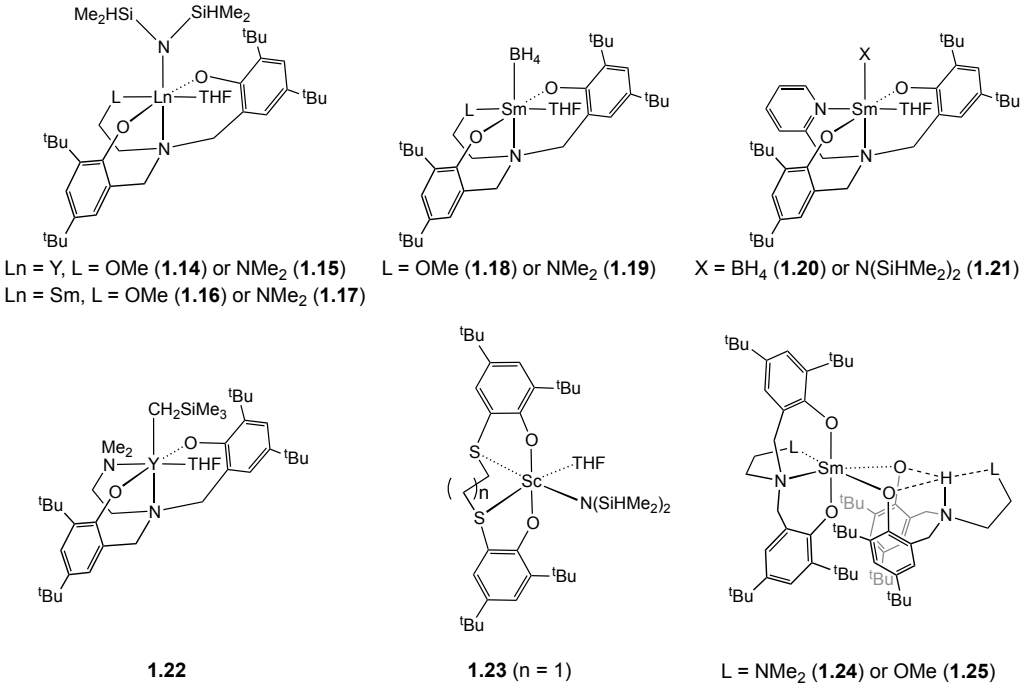

Figure 1.17. Examples of bis(phenolate)-amino and 1,ω-dithiaalkanediyl-bridged bis(phenolate) rare earth complexes.[38, 39, 44, 45, 54, 55, 124, 205-207]

Carpentier reported the yttrium silyl-amide complexes, **1.14** and **1.15**, which were achieved when $Y\{N(SiHMe_2)_2\}_3(THF)_2$ was treated with one equivalent of the appropriate protio-ligand in hydrocarbon solvent.[39, 205] The samarium amide analogues, $Sm(O_2N^L)\{N(SiHMe_2)_2\}(THF)$ (L = OMe (**1.16**) and NMe_2 (**1.17**)), were also synthesised by protonolysis routes by Dr. Hellen E. Dyer, a previous student in the Mountford group.[45, 206] **1.14** and **1.15** were viable initiators for ROP and each initiator was treated with 100 equivs. of *rac*-LA in THF at room temperature.[38, 39] Complete conversion was achieved within 5 mins (M_n(calcd) = 14,400 g mol^{-1}) and M_n(GPC) = 15,500 g mol^{-1} and PDI = 1.33 for **1.14** and M_n(GPC) = 20,900 g mol^{-1} and PDI = 1.17 for **1.15** were suggestive of reasonably well-controlled ROP reactions. The PDI was broader with **1.14**, but a high degree of heterotactic enrichment was observed (P_r = 0.80), which increased to P_r = 0.90 when the ^{t}Bu groups of **1.14** were replaced by cumyl substituents. Further investigations concluded that the steric bulk of the *ortho*-substituents largely dictated the level of heterotactic enrichment. Electron-withdrawing groups had negligible influence but the fluorinated substituents used in this study were relatively remote.[43] **1.14** has featured heavily for immortal ROP studies, where alcohol chain transfer agents were included in polymerisation mixtures (Section 1.8).[40, 41, 208]

The borohydride complexes, $Sm(O_2N^L)(BH_4)(THF)$ (L = OMe (**1.18**) , NMe_2 (**1.19**) or py (**1.20**)) were also prepared in the Mountford group and were achieved by metathesis reactions between $Sm(BH_4)_3(THF)_3$ and sodiated bis(phenolate)-amino ligands.[45, 46, 206] Borohydrides are of interest because the borohydride initiating group reduces the primary enchained ester to an aldehyde or alcohol upon ring opening. Reduction of LA esters to alcohols was predominant when **1.18** and **1.20** were employed and α,ω-telechelic PLA formed (both end-groups are alcohols). With **1.19**, which contained the NMe_2 pendant donor arm, a mixture of aldehyde and alcohol terminated polymers were formed (as well as cyclic products), according to MALDI-ToF MS. A two-stage initiation mechanism was modelled using DFT, and whilst double reduction of the ester to an alcohol was energetically favourable in most cases, "reduction" may stop at the aldehyde, which led to the presence of both alcohol and aldehyde polymer end groups when **1.19** was used as the initiator.

The ROP of *rac*-LA (and ε-CL) was undertaken with **1.18**–**1.20** and their amide counterparts, **1.16**, **1.17** and **1.21**.[45, 206] Each complex was treated with 200 equivs. of

rac-LA ([*rac*-LA]$_0$:[Sm]$_0$ = 200:1) in THF at room temperature and the conversion of monomer to polymer was recorded after both 5 and 30 mins. With **1.18**–**1.20**, 80–90% conversion rates were recorded after 30 mins but the highest activity was observed with **1.19**, with 80% and 92% conversion recorded after 5 and 30 mins. The observed molecular weights were consistently lower than expected with these borohydride initiators. For example, with **1.19**, M_n(calcd) = 23,100 g mol^{-1} and M_n(GPC) = 20,600 g mol^{-1} after 5 mins and M_n(calcd) = 26,500 g mol^{-1} and M_n(GPC) = 21,700 g mol^{-1} after 30 mins The narrowest molecular weight distributions were observed with **1.19** and PDI = 1.41 (5 mins) and 1.48 (30 mins). Transesterification products, including cyclic PLA were present in MALDI-ToF mass spectra and the consistently lower than expected molecular weights and broadening of the molecular weight distribution over a prolonged reaction time were consistent with adverse post-polymerisation transesterification. The PLA products formed by **1.18**–**1.20** showed a relatively high degree of heterotactic enrichment ($P_r \approx 0.8$ after 5 mins), which was consistent with Carpentier's observations with **1.14** and proposal of a metal-mediated, chain-end control mechanism. In line with the broadening of the molecular weight distributions, P_r consistently reduced by 0.01–0.06 when ROP reactions with **1.18**–**1.20** were run over 30 mins. Tranesterification or chain length modification processes may have led to some scrambling of heterotactic *isi* or *sis* tetrads, but the insubstantial reduction in the level of enrichment is suggestive that a degree of stereoselectivity may exist in back-biting processes.

Selected reactions were also undertaken with the silyl-amide complexes, **1.16**, **1.17** and **1.21**, to compare with the borohydride initiators, **1.18**–**1.20**.[45, 206] Whilst the amides were more active than the borohydrides, observed polymer molecular weights were much greater than expected after 5 mins. For example, with **1.16**, 95% conversion of *rac*-LA to PLA was recorded after 5 mins and M_n(calcd) = 27,510 g mol^{-1}, M_n(GPC) = 58,200 g mol^{-1} and PDI = 1.43. However, prolonging the reaction time to 30 mins (97% conversion) led to a reduction in M_n and a broadening of the PDI, M_n(calcd) = 28,100 g mol^{-1}, M_n(GPC) = 33,800 g mol^{-1} and PDI = 1.94 (P_r reduced from 0.81 to 0.79). The higher than expected molecular weights were reflective of fast initiation with respect to propagation but the reduction in M_n and broadening of PDI over an extended period were indicative of post-polymerisation chain shortening by tranesterification pathways. As in the case of the borohydride

initiators, **1.18**–**1.20**, heterotactic enrichment was observed when the silyl-amides (**1.16**, **1.17** and **1.21**) were used for ROP of *rac*-LA and demonstrated that stereoselectivity was governed by the bis(phenolate)-amino framework.

$Sm(O_2N^{Me})(BH_4)(THF)_2$ (**1.26**) was also prepared and was found to be inactive for the ROP of *rac*-LA.[45, 206] The complex was shown to lose THF and dimerise *in vacuo* or after prolonged handling in solution. Kol prepared $Zr(O_2N^{NMe2})(Bn)_2$ (**1.27**) and $Zr(O_2N^{Me})(Bn)_2$ (**1.28**) for 1-hexene polymerisation studies and noted that **1.27** formed an active catalyst after activation by $B(C_6F_5)_3$ whereas **1.28** was inactive.[186] These studies established that the presence of a pendant arm donor was crucial to the formation of an active polymerisation catalyst. Dyer's investigations with the borohydride initiators, **1.18**–**1.20**, suggested that the NMe_2 donor produced a more active catalyst and gave better control over molecular weight distribution, whereas Kol noted that the OMe donor produced superior activity in 1-hexene polymerisation studies using $Zr(O_2N^{L})(Bn)_2$-type catalysts.[189]

Cui investigated the potential of $Y(O_2N^{NMe2})(CH_2SiMe_3)(THF)$ (**1.22**) for the ROP of *rac*-LA and treated **1.22** with 100 equivs. of *rac*-LA ($[rac\text{-LA}]_0$:$[\mathbf{1.22}]_0$ = 100:1) in THF at room temperature.[44] Complete conversion of *rac*-LA to LA was achieved after 1 h and M_n(GPC) = 19,300 g mol^{-1} (uncorrected, polymer treated as a polystyrene) agreed favourably with M_n(calcd) = 14,400 g mol^{-1}. The PDI = 1.25 was also narrow and a Me_3SiCH_2– end-group was observed in the ^{1}H NMR spectrum of a PLA product, but no MALDI-ToF mass spectra were described.

Okuda has utilised 1,ω-dithiaalkanediyl-bridged bis(phenolate) ligands to prepare complexes of the type, $Sc(O^{tBu2}\text{-S-}C_2\text{-S-}O^{tBu2})\{N(SiHMe_2)_2\}(THF)$ (**1.23**). In the example shown in Figure 1.17 (*vide supra*), ^{t}Bu groups are present on the phenolate rings and a simple alkyl bridge links both phenolate rings.[207] A library of compounds of this type was prepared through systematic variation of the phenolate ring substituents and length of the alkyl bridge. Phenylene and cyclcohexylene linkers were also included, which permitted the incorporation of stereogenic centres into the ligand architecture.[54, 55]

A derivative of **1.23**, $Sc(O^{tBu,Me}\text{-S-}C_3\text{-S-}O^{tBu,Me})\{N(SiHMe_2)_2\}(THF)$ (**1.29**), with methyl groups in the *para*-positions and a C_3-propylene linking group was characterised in the solid state, along with an yttrium complex, $Y(O^{tBu2}\text{-S-}C_3\text{-S-}$

O^{tBu2}){N(SiHMe$_2$)$_2$}(THF) (**1.30**).[207] In the molecular structure of **1.29**, the phenolate oxygen donors were in *trans* arrangement, whereas in **1.30**, the phenolate groups were *cis*. Each complex was fluxional in solution over a range of temperatures, which was attributed to the apparent flexibility of C_3-linked phenolate ligands. **1.29** was treated with 300 equivs. of *rac*-LA in THF at room temperature and 81% conversion was recorded after 8 h.[54] M_n(GPC) = 126,000 g mol^{-1} was much higher than expected (M_n(calcd) = 35,000 g mol^{-1}) and the molecular weight distribution was broad (PDI = 1.85). These molecular weight data were consistent with competitive propagation with respect to initiation and the long reaction time was expected for smaller metal. Despite the low activity of **1.29**, P_r = 0.95 was consistent with a high degree of heterotactic enrichment and the C_3-propylene linking group was a key contributor to this level of selectivity. Compound **1.29** was reacted with one equivalent of *R*-*tert*-butyl lactate and a dimeric scandium *R*-*tert*-butoxy-lactate alkoxide complex was formed.[54] This model complex had a single [OSSO]-ligand confirmation (Λ), induced by the chiral *R*-lactate alkoxide and highlighted the potential for ligand interconversion as a mechanism for lactide enantiomer recognition.[55, 209] This is at odds with a pure chain-end control mechanism where the stereochemistry of the latest enchained lactide unit dictates which enantiomer is enchained next. Okuda has also shown that **1.29** and related achiral complexes can produce syndiotactic PLA from *meso*-LA.[209]

Y(O^{tBu2}-S-C_3-S-O^{tBu2}){N(SiHMe$_2$)$_2$}(THF) (**1.30**) was used to polymerise *L*-LA and 300 equivs. were polymerised to 97% completion over 24 h.[160] M_n(calcd) = 41,900 g mol^{-1} and M_n(GPC) = 29,300 g mol^{-1} were in relatively good agreement for one chain forming per amide initiator and the PDI = 1.28 was suggestive of a relatively well-controlled polymerisation process, although the prolonged reaction time may have promoted post-polymerisation chain modification processes. Kinetics experiments with **1.30** established a first-order dependence in *L*-LA and a fractional order of 0.5 in catalyst, which possibly arose because of catalyst aggregation. In addition to this fractional order in catalyst, polymer molecular weights did not grow evenly with conversion. Higher than expected molecular weight PLLA was observed in the early stages of polymerisation, but the molecular continued to increase with conversion, albeit at a rate below that expected. The final M_n was less than expected, probably due to post-polymerisation chain shortening by transesterification. Fast propagation with

respect to initiation was proposed in light of the higher than expected molecular weights in the early stages of the reaction.

Bis and tris(phenolate)-amino ligands have been heavily utilised in Group 4 and main group complexes. Bochmann,[210] Kol[192, 211] and Davidson[212-214] have exploited these ligands in both olefin and cyclic ester polymerisation studies and many main group complexes bearing bis(phenolate)-amino (and 1,ω-dithiaalkanediyl-bridged bis(phenolate)) ligands are also known.[215-220] Zwitterionic complexes, **1.24** and **1.25**, were prepared in the Mountford group and have been used in immortal ROP studies both by Dr. Hellen E. Dyer and the author (Chapters Two and Three).[34, 45, 124, 206]

1.8 Reversible chain transfer in ROP

ROP with single site initiators with has enabled the generation of PLA with molecular weights that are reflective of the initial monomer to initiator ratio. Whilst this degree of control is consistent with living behaviour, the coordination-insertion approach to ROP is inefficient with respect to the metal initiator since only one polymer chain is generated. In α-olefin polymerisation, multiple chains of high molecular weight are generated and despite the propensity of propagating polyolefins to undergo irreversible chain termination, additives or chain transfer agents (CTA) such as H_2 or $ZnEt_2$ may be included in polymerisation mixtures to deliberately shorten polymer chains and reduce molecular weights. In well-controlled systems, polymer molecular weights are linearly dependent on the initial monomer to CTA ratio.

Reversible chain transfer in ROP is becoming an increasingly attractive strategy for the generation of polymer products with predictable molecular weights and narrow molecular weight distributions. The formation of stereoblock PLA from *rac*-LA and racemic catalysts demonstrated that propagating polymer chains can exchange between the metal centres of well-defined, single site catalysts and alcohols have been included in polymerisation mixtures as chain transfer agents. The deliberate introduction of chain transfer agents in polymerisation mixtures has been described as immortal polymerisation. In living polymerisation, only initiation and propagation processes occur, but under immortal ROP conditions, chains terminate but can be reactivated through reversible exchange. Inoue first demonstrated immortal ROP when epoxides or lactones were polymerised in the presence of aluminum porphyrin-based catalysts and a suitable protic compound.[221-224] Carpentier and Okuda have also

used alcohol chain transfer agents alongside bis(phenolate)-amino rare earth complexes. Carpentier included *iso*-propyl alcohol in polymerisation mixtures of $Y(O_2N^{OMe})\{N(SiHMe_2)_2\}(THF)$ (**1.14**) and *rac*-LA.[40, 41, 208] The presence of the alcohol forced elimination of $HN(SiHMe_2)_2$ (which is inert under polymerisation conditions) from **1.14**, generating a new metal-alkoxide species, "$Y(O_2N^{OMe})(O^iPr)(THF)_n$", which behaved as a coordination-insertion initiator. However, the remaining alcohol molecules that were present in solution could exchange with the newly formed $M–[LA]_x–O^iPr$ macroinitiator, given the comparable pK_as of ^{i}PrOH and the secondary alcohol chain-end. Thus, $H–[LA]_x–O^iPr$ was eliminated, $M–O^iPr$ formed, and a new chain initiated (Figure 1.18). In practice, ^{i}PrOH is consumed rapidly by exchange at the metal centre and multiple ^{i}PrOH-capped PLA macromonomers are generated. Under coordination-insertion conditions, only the chain bound to the metal centre can propagate and non-bound polylactide chains are dormant in solution. However, the alcoholic end-groups of the dormant chains are chain transfer agents, and are reactivated through fast exchange with the active chain bound to the metal centre.

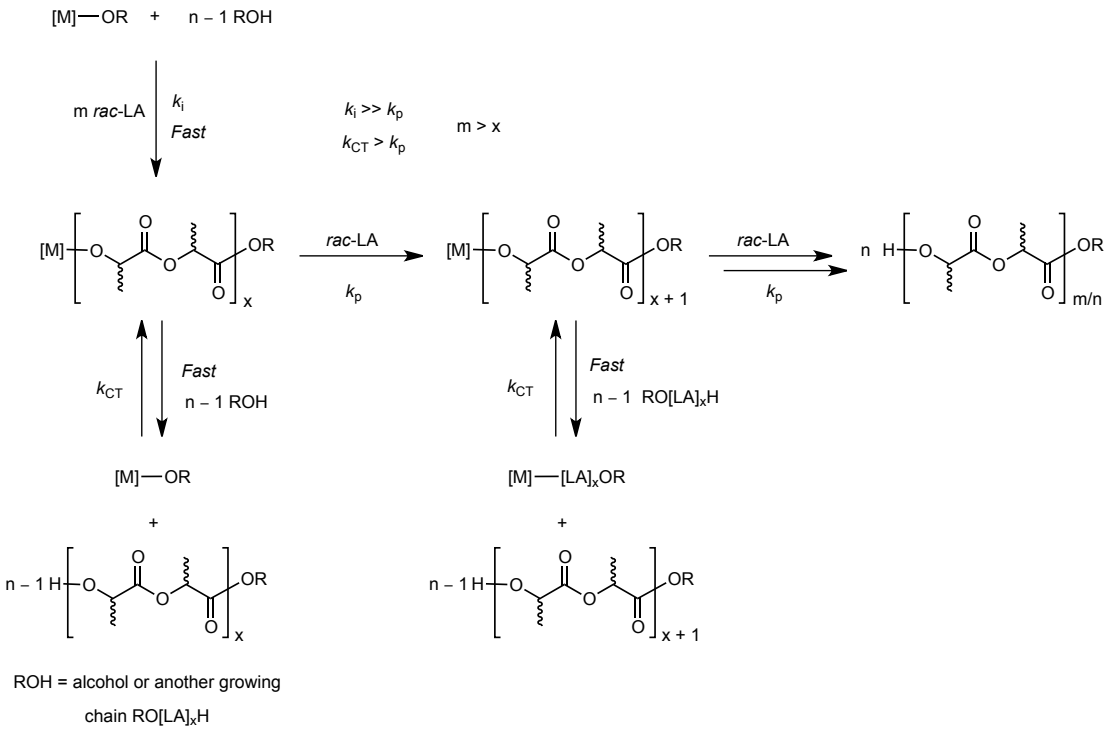

Figure 1.18. Immortal ROP of *rac*-LA using alcohol chain transfer agents.[40, 41, 208]

A key feature of living polymerisation is the predictability of molecular weights and narrow PDIs, based on the initial monomer to alcohol ratio. This control over

molecular weight is transferred to immortal ROP, where M_n is determined by the [*rac*-LA]$_0$:[alcohol]$_0$ ratio. In a ROP reaction performed by Carpentier using **1.14**, 1000 equivs. of *rac*-LA were polymerised to complete conversion in 40 mins in THF at room temperature in the presence of 4 equivs. of *iso*-propyl alcohol ([*rac*-LA]$_0$:[^{i}PrOH]$_0$:[**1.14**]$_0$ = 1000:4:1).[40, 41, 208] M_n(calcd) = 36,000 g mol^{-1}, based on one PLA forming per ^{i}PrOH (or 4 chains forming per **1.14**), and M_n(GPC) = 37,900 g mol^{-1}. The PDI = 1.13 was consistent with a well-controlled polymerisation reaction and heterotactic enrichment was retained (P_r = 0.80). Furthermore, MALDI-ToF mass spectra confirmed that PLA chains were ^{i}PrOH-capped and the $\Delta(m/z)$ = 144 g mol^{-1} indicated that tranesterification side reactions were minimal. A linear dependence between M_n and [*rac*-LA]$_0$:[^{i}PrOH]$_0$ was established, meaning that molecular weight could be accurately tuned through systematic variation of the initial [*rac*-LA]$_0$:[^{i}PrOH]$_0$ ratio. The excellent control over molecular weight and PDI was achieved because reversible chain transfer was fast with respect to propagation. If propagation is too competitive with chain transfer then the active chain may remain bound to the metal for too long and a broader distribution of molecular weights form.

Okuda observed similar behaviour when Y(O^{tBu2}-S-C$_3$-S-O^{tBu2}){N(SiHMe$_2$)$_2$}(THF) (**1.30**) was used to polymerise *L*-LA in the presence of *iso*-propyl alcohol.[160] In a typical run, [*L*-LA]$_0$:[^{i}PrOH]$_0$:[**1.30**]$_0$ = 300:3:1 in toluene at room temperature, 95% conversion was achieved within 5 mins (in the absence of a alcohol, the reaction took 24 h to reach completion) and M_n(calcd) = 13,800 g mol^{-1}, M_n(GPC) = 15,600 g mol^{-1} and PDI = 1.03. However, transesterification products were noted in MALDI-ToF mass spectra, given the $\Delta(m/z)$ = 72.0 g mol^{-1} between peak envelopes. Kinetic analysis revealed first order dependencies in [*L*-LA]$_0$ and [**1.30**]$_0$ when [^{i}PrOH]$_0$:[**1.30**]$_0$ = 2:1, which contrasted reactions where no exogenous alcohol was used. A first-order dependence in [*L*-LA]$_0$ was noted in this case, but the order in [**1.30**]$_0$ was 0.5 and catalyst aggregation was proposed as the cause of deactivation.

When the reaction, [*L*-LA]$_0$:[^{i}PrOH]$_0$:[**1.30**]$_0$ = 300:3:1, was repeated using one equivalent of ^{i}PrOH ([*L*-LA]$_0$:[^{i}PrOH]$_0$:[**1.30**]$_0$ = 300:1:1), the reaction time extended to 19 h and a broader PDI = 1.11 was noted.[160] Addition of 1 equiv. ^{i}PrOH to **1.30** resulted in elimination of HN(SiHMe$_2$)$_2$, and an alkoxide dimer formed in toluene solution. This dimeric structure was likely to have been cleaved in the presence of excess ^{i}PrOH, as in the case of the [*L*-LA]$_0$:[^{i}PrOH]$_0$:[**1.30**]$_0$ = 300:3:1 run, where fast

polymerisation ensued. However, cleavage of the dimer by LA is much slower, hence the prolonged reaction time in the [*L*-LA]$_0$:[^{i}PrOH]$_0$:[**1.30**]$_0$ = 300:1:1 run. The rate of propagation may also have been competitive with initiation in this run, leading to the broader PDI observed.

The introduction of alcoholic chain transfer agents for a given catalytic system generally leads to better control over molecular weights. This is primarily due to more efficient initiation, associated with the introduction of an excess of nucleophilic alcohol molecules. However, as in the case of living polymerisation, polymer products should have molecular weights that are consistent with the initial monomer to alcohol and molecular weights should be narrow. Furthermore, irreversible chain termination processes such as back-biting transesterification should be minimal. Immortal ROP is not limited to simple primary and secondary amines. Complex molecules with alcohol substrates have been included in the polymerisation mixture and are incorporated as the polymer end-group. This methodology has allowed for polymer synthesis and end-group functionalisation in "one-pot" processes.[225, 226]

1.9 Zwitterionic rare earth complexes and immortal ROP

Dyer and Mountford discovered that when amines e.g. benzyl amine ($BnNH_2$) were included in polymerisation mixtures alongside *rac*-LA and zwitterionic rare earth complexes e.g. $Sm(O_2N^{NMe2})(HO_2N^{NMe2})$ (**1.24**), polymer molecular weights were reflective of the [*rac*-LA]$_0$:[$BnNH_2$]$_0$ ratio and benzyl amine formed the polymer chain-ends (Figure 1.19).[34, 206] A summary of these results, including structure-activity investigations is provided in Chapter Two. Metal amides are relatively poor initiators for ROP but the amide is expected to form the polymer end-group under coordination-insertion conditions. However, the polymer products formed in these reactions tend to have molecular weights that are much greater than expected and broad PDIs (Section 1.7, *vide supra*). In a run, [*rac*-LA]$_0$:[$BnNH_2$]$_0$:[**1.24**]$_0$ = 100:5:1 in THF at room temperature, 92% conversion of LA to PLA was achieved within 5 mins and M_n(GPC) = 2,700 g mol^{-1} and PDI = 1.15, were reflective of one PLA chain forming per $BnNH_2$, M_n(calcd) = 2,760 g mol^{-1}. It was proposed that initiation proceeds by an activated-monomer process, where the amine attacks a pre-coordinated LA unit at the metal centre, but ambiguity remained over the nature of the active species and the propagation mechanism.

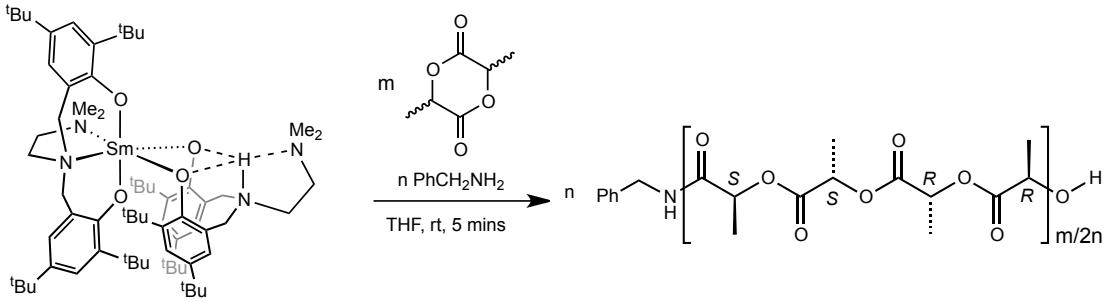

1.24

Figure 1.19. ROP of *rac*-LA using zwitterionic bis(phenolate)-amino rare earth complexes and primary amines.[34, 206]

1.10 Project outline

The initial discovery by Dyer that amines can be incorporated into PLA chains in immortal ROP warranted further investigation. These preliminary investigations and studies by Carpentier using alcohol chain transfer agents and related bis(phenolate)-amino rare earth amide complexes, were limited by a lack of conclusive mechanistic investigation and kinetic analysis. With alcoholic chain transfer agents, it is presumed that alcohols eliminate a suitable leaving group from the pre-catalyst, and a conventional alkoxide initiator is formed. Amines are unlikely to effect a similar transformation and investigations into the amine-initiated, immortal ROP of *rac*-LA mechanism are discussed in Chapter Two. Chapters Three, Four and Five cover the scope of the amine-initiated, immortal ROP methodology with regard to the range of suitable amines and monomers, as well as the design of the catalyst. Chapter Three details investigations into the preparation of multiarm PLA using polyamines as well as the preparation of amine-capped, poly(3-hydroxybutanoate). Chapter Four describes the results of polymerisation reactions with alkaline earth and rare earth complexes bearing phenolate ligands, whilst Chapter Five details the synthesis, characterisation and polymerisation capability of new rare earth complexes bearing phenolate-amino ligands.

1.11 References for Chapter One

1. W. H. Carothers, G. L. Dorough and F. J. v. Natta, *J. Am. Chem. Soc.*, 1932, **54**, 761.
2. A. J. East, *Encyclopedia of Polymer Science and Technology*, John Wiley & Sons, Inc., 2002.

3. M. Okada, *Prog. Polym. Sci.*, 2002, **27**, 87.
4. E. Chiellini and R. Solaro, *Adv. Mater.*, 1996, **8**, 305.
5. R. E. Drumright, P. R. Gruber and D. E. Henton, *Adv. Mater.*, 2000, **12**, 1841.
6. S. Mecking, *Angew. Chem. Int. Ed.*, 2004, **43**, 1078.
7. W. Amass, A. Amass and B. Tighe, *Polym. Int.*, 1998, **47**, 89.
8. D. K. Gilding and A. M. Reed, *Polymer*, 1979, **20**, 1459.
9. K. E. Uhrich, S. M. Cannizzaro, R. S. Langer and K. M. Shakesheff, *Chem. Rev.*, 1999, **99**, 3181.
10. Y. Ikada and H. Tsuji, *Macromol. Rapid Commun.*, 2000, **21**, 117.
11. A.-C. Albertsson and I. K. Varma, *Biomacromolecules*, 2003, **4**, 1466.
12. E. T. H. Vink, K. R. Rábago, D. A. Glassner and P. R. Gruber, *Polym. Deg. Stab.*, 2003, **80**, 403.
13. R. H. Platel, L. M. Hodgson and C. K. Williams, *Polym. Rev.*, 2008, **48**, 11.
14. O. Dechy-Cabaret, B. Martin-Vaca and D. Bourissou, *Chem. Rev.*, 2004, **104**, 6147.
15. A. N. Vaidya, R. A. Pandey, S. Mudliar, M. S. Kumar, T. Chakrabarti and S. Devotta, *Crit. Rev. Environ. Sci. Technol.*, 2005, **35**, 429.
16. A. Södergård and M. Stolt, *Prog. Polym. Sci.*, 2002, **27**, 1123.
17. J. Lunt, *Polym. Deg. Stab.*, 1998, **59**, 145.
18. R. Raja and J. M. Thomas, *Z. Anorg. Allg. Chem.*, 2005, **631**, 2942.
19. P. Dubois, O. Coulembier and J.-M. Raquez, *Handbook of Ring-Opening Polymerization*, Wiley-VCH, 2009.
20. A. Duda and S. Penczek, *Macromolecules*, 1990, **23**, 1636.
21. F. S. Dainton and K. J. Ivin, *Q. Rev. Chem. Soc.*, 1958, **12**, 61.
22. G. J. van Hummel, S. Harkema, F. E. Kohn and J. Feijen, *Acta Crystallogr.*, 1982, **B38**, 1679.
23. J.-F. Carpentier, *Macromol. Rapid Commun.*, 2010, **31**, 1696.
24. J. Baran, A. Duda, A. Kowalski, R. Szymanski and S. Penczek, *Macromol. Rapid Commun.*, 1997, **18**, 325.
25. S. Penczek and K. Matyjaszewski, *J. Polym. Sci., Polym. Symp.*, 1976, **56**, 255.
26. M. Save, M. Schappacher and A. Soum, *Macromol. Chem. Phys.*, 2002, **203**, 889.
27. Z. Liu, E. Somsook and C. R. Landis, *J. Am. Chem. Soc.*, 2001, **123**, 2915.

28. Z. Liu, E. Somsook, C. B. White, K. A. Rosaaen and C. R. Landis, *J. Am. Chem. Soc.*, 2001, **123**, 11193.
29. F. Song, R. D. Cannon and M. Bochmann, *J. Am. Chem. Soc.*, 2003, **125**, 7641.
30. D. Walton and P. Lorimer, *Polymers, Oxford Chemistry Primers*, Oxford University Press, 2000.
31. A. Rudin and H. L. W. Hoegy, *J. Polym. Sci., Part A: Polym. Chem.*, 1972, **10**, 217.
32. J. R. Dorgan, J. Janzen, D. M. Knauss, S. B. Hait, B. R. Limoges and M. H. Hutchinson, *J. Polym. Sci., Part B: Polym. Phys.*, 2005, **43**, 3100.
33. R. C. Beavis, B. T. Chait and K. G. Standing, *Rapid Commun. Mass Spec.*, 1989, **3**, 436.
34. L. Clark, M. G. Cushion, H. E. Dyer, A. D. Schwarz, R. Duchateau and P. Mountford, *Chem. Commun.*, 2010, **46**, 273.
35. Y. Ikada, K. Jamshidi, H. Tsuji and S. H. Hyon, *Macromolecules*, 1987, **20**, 904.
36. N. Nomura, J. Hasegawa and R. Ishii, *Macromolecules*, 2009, **42**, 4907.
37. P. J. Dijkstra, H. Du and J. Feijen, *Polym. Chem.*, 2011, **2**, 520.
38. C.-X. Cai, A. Amgoune, C. W. Lehmann and J.-F. Carpentier, *Chem. Commun.*, 2004, 330.
39. A. Amgoune, C. M. Thomas, T. Roisnel and J.-F. Carpentier, *Chem. Eur. J.*, 2006, **12**, 169.
40. A. Amgoune, C. M. Thomas and J.-F. Carpentier, *Pure Appl. Chem.*, 2007, **79**, 2013.
41. A. Amgoune, C. M. Thomas and J.-F. Carpentier, *Macromol. Rapid Commun.*, 2007, **28**, 693.
42. J.-F. Carpentier, *Angew. Chem. Int. Ed.*, 2010, **49**, 2662.
43. M. Bouyahyi, N. Ajellal, E. Kirillov, C. M. Thomas and J.-F. Carpentier, *Chem. Eur. J.*, 2011, **17**, 1872.
44. X. Liu, X. Shang, T. Tang, N. Hu, F. Pei, D. Cui, X. Chen and X. Jing, *Organometallics*, 2007, **26**, 2747.
45. H. E. Dyer, S. Huijser, N. Susperregui, F. Bonnet, A. D. Schwarz, R. Duchateau, L. Maron and P. Mountford, *Organometallics*, 2010, **29**, 3602.
46. F. Bonnet, A. R. Cowley and P. Mountford, *Inorg. Chem.*, 2005, **44**, 9046.

47. M. H. Chisholm, N. W. Eilerts, J. C. Huffman, S. S. Iyer, M. Pacold and K. Phomphrai, *J. Am. Chem. Soc.*, 2000, **122**, 11845.
48. M. H. Chisholm, J. Gallucci and K. Phomphrai, *Inorg. Chem.*, 2002, **41**, 2785.
49. M. H. Chisholm, J. Gallucci and K. Phomphrai, *Chem. Commun.*, 2003, 48.
50. M. H. Chisholm, J. C. Gallucci and K. Phomphrai, *Inorg. Chem.*, 2004, **43**, 6717.
51. M. H. Chisholm, J. C. Gallucci and K. Phomphrai, *Inorg. Chem.*, 2005, **44**, 8004.
52. M. Cheng, A. B. Attygalle, E. B. Lobkovsky and G. W. Coates, *J. Am. Chem. Soc.*, 1999, **121**, 11583.
53. B. M. Chamberlain, M. Cheng, D. R. Moore, T. M. Ovitt, E. B. Lobkovsky and G. W. Coates, *J. Am. Chem. Soc.*, 2001, **123**, 3229.
54. H. Ma, T. P. Spaniol and J. Okuda, *Angew. Chem. Int. Ed.*, 2006, **45**, 7818.
55. H. Ma, T. P. Spaniol and J. Okuda, *Inorg. Chem.*, 2008, **47**, 3328.
56. T.-P.-A. Cao, A. Buchard, X. F. Le Goff, A. Auffrant and C. K. Williams, *Inorg. Chem.*, 2012, **51**, 2157.
57. P. Hormnirun, E. L. Marshall, V. C. Gibson, A. J. P. White and D. J. Williams, *J. Am. Chem. Soc.*, 2004, **126**, 2688.
58. A. J. Chmura, C. J. Chuck, M. G. Davidson, M. D. Jones, M. D. Lunn, S. D. Bull and M. F. Mahon, *Angew. Chem. Int. Ed.*, 2007, **46**, 2280.
59. A. Pietrangelo, M. A. Hillmyer and W. B. Tolman, *Chem. Commun.*, 2009, 2736.
60. A. Pietrangelo, S. C. Knight, A. K. Gupta, L. J. Yao, M. A. Hillmyer and W. B. Tolman, *J. Am. Chem. Soc.*, 2010, **132**, 11649.
61. T. R. Jensen, L. E. Breyfogle, M. A. Hillmyer and W. B. Tolman, *Chem. Commun.*, 2004, 2504.
62. C. Romain, B. Heinrich, S. B. Laponnaz and S. Dagorne, *Chem. Commun.*, 2012, **48**, 2213.
63. Z. Zhang and D. Cui, *Chem. Eur. J.*, 2011, **17**, 11520.
64. A. P. Dove, *Chem. Commun.*, 2008, 6446.
65. J. M. Becker, R. J. Pounder and A. P. Dove, *Macromol. Rapid Commun.*, 2010, **31**, 1923.
66. A. P. Dove, H. Li, R. C. Pratt, B. G. G. Lohmeijer, D. A. Culkin, R. M. Waymouth and J. L. Hedrick, *Chem. Commun.*, 2006, 2881.

67. N. Nomura, R. Ishii, M. Akakura and K. Aoi, *J. Am. Chem. Soc.*, 2002, **124**, 5938.
68. Z. Tang, X. Chen, X. Pang, Y. Yang, X. Zhang and X. Jing, *Biomacromolecules*, 2004, **5**, 965.
69. Z. Tang, X. Chen, Y. Yang, X. Pang, J. Sun, X. Zhang and X. Jing, *J. Polym. Sci., Part A: Polym. Chem.*, 2004, **42**, 5974.
70. Z. Tang, Y. Yang, X. Pang, J. Hu, X. Chen, N. Hu and X. Jing, *J. Appl. Polym. Sci.*, 2005, **98**, 102.
71. N. Nomura, R. Ishii, Y. Yamamoto and T. Kondo, *Chem. Eur. J.*, 2007, **13**, 4433.
72. M. Wisniewski, A. L. Borgne and N. Spassky, *Macromol. Chem. Phys.*, 1997, **198**, 1227.
73. A. Bhaw-Luximon, D. Jhurry and N. Spassky, *Polym. Bull.*, 2000, **44**, 31.
74. D. Jhurry, A. Bhaw-Luximon and N. Spassky, *Macromol. Symp.*, 2001, **175**, 67.
75. T. M. Ovitt and G. W. Coates, *J. Polym. Sci., Part A: Polym. Chem.*, 2000, **38**, 4686.
76. T. M. Ovitt and G. W. Coates, *J. Am. Chem. Soc.*, 2002, **124**, 1316.
77. Z. Zhong, P. J. Dijkstra and J. Feijen, *Angew. Chem. Int. Ed.*, 2002, **41**, 4510.
78. Z. Zhong, P. J. Dijkstra and J. Feijen, *J. Am. Chem. Soc.*, 2003, **125**, 11291.
79. N. Spassky, M. Wisniewski, C. Pluta and A. Le Borgne, *Macromol. Chem. Phys.*, 1996, **197**, 2627.
80. T. M. Ovitt and G. W. Coates, *J. Am. Chem. Soc.*, 1999, **121**, 4072.
81. E. Lillie and R. C. Schulz, *Makromol. Chem.*, 1975, **176**, 1901.
82. A. Schindler and D. Harper, *J. Polym. Sci.: Polym. Lett. Ed.*, 1976, **14**, 729.
83. M. T. Zell, B. E. Padden, A. J. Paterick, K. A. M. Thakur, R. T. Kean, M. A. Hillmyer and E. J. Munson, *Macromolecules*, 2002, **35**, 7700.
84. H. R. Kricheldorf, C. Boettcher and K.-U. Tonnes, *Polymer*, 1992, **33**, 2817.
85. J. E. Kasperczyk, *Macromolecules*, 1995, **28**, 3937.
86. J. E. Kasperczyk, *Polymer*, 1999, **40**, 5455.
87. K. A. M. Thakur, R. T. Kean, E. S. Hall, J. J. Kolstad, T. A. Lindgren, M. A. Doscotch, J. I. Siepmann and E. J. Munson, *Macromolecules*, 1997, **30**, 2422.
88. K. A. M. Thakur, R. T. Kean, M. T. Zell, B. E. Padden and E. J. Munson, *Chem. Commun.*, 1998, 1913.

89. J. L. Espartero, I. Rashkov, S. M. Li, N. Manolova and M. Vert, *Macromolecules*, 1996, **29**, 3535.
90. M. H. Chisholm, S. S. Iyer, M. E. Matison, D. G. McCollum and M. Pagel, *Chem. Commun.*, 1997, 1999.
91. M. H. Chisholm, S. S. Iyer, D. G. McCollum, M. Pagel and U. Werner-Zwanziger, *Macromolecules*, 1999, **32**, 963.
92. N. E. Kamber, W. Jeong, R. M. Waymouth, R. C. Pratt, B. G. G. Lohmeijer and J. L. Hedrick, *Chem. Rev.*, 2007, **107**, 5813.
93. M. K. Kiesewetter, E. J. Shin, J. L. Hedrick and R. M. Waymouth, *Macromolecules*, 2010, **43**, 2093.
94. S. Penczek, M. Cypryk, A. Duda, P. Kubisa and S. Słomkowski, *Prog. Polym. Sci.*, 2007, **32**, 247.
95. S. Penczek, *J. Polym. Sci., Part A: Polym. Chem.*, 2000, **38**, 1919.
96. M. Baśko and P. Kubisa, *J. Polym. Sci., Part A: Polym. Chem.*, 2006, **44**, 7071.
97. H. R. Kricheldorf and R. Dunsing, *Makromol. Chem.*, 1986, **187**, 1611.
98. H. R. Kricheldorf and I. Kreiser, *Makromol. Chem.*, 1987, **188**, 1861.
99. D. Bourissou, B. Martin-Vaca, A. Dumitrescu, M. Graullier and F. Lacombe, *Macromolecules*, 2005, **38**, 9993.
100. Y. Shibasaki, H. Sanada, M. Yokoi, F. Sanda and T. Endo, *Macromolecules*, 2000, **33**, 4316.
101. N. E. Kamber, W. Jeong, S. Gonzalez, J. L. Hedrick and R. M. Waymouth, *Macromolecules*, 2009, **42**, 1634.
102. D. A. Culkin, W. Jeong, S. Csihony, E. D. Gomez, N. P. Balsara, J. L. Hedrick and R. M. Waymouth, *Angew. Chem. Int. Ed.*, 2007, **46**, 2627.
103. W. Jeong, E. J. Shin, D. A. Culkin, J. L. Hedrick and R. M. Waymouth, *J. Am. Chem. Soc.*, 2009, **131**, 4884.
104. B. J. O'Keefe, M. A. Hillmyer and W. B. Tolman, *J. Chem. Soc., Dalton Trans.*, 2001, 2215.
105. J. Wu, T.-L. Yu, C.-T. Chen and C.-C. Lin, *Coord. Chem. Rev.*, 2006, **250**, 602.
106. M. H. Chisholm and N. W. Eilerts, *Chem. Commun.*, 1996, 853.
107. M. H. Chisholm, J. C. Huffman and K. Phomphrai, *J. Chem. Soc., Dalton Trans.*, 2001, 222.

108. V. Poirier, T. Roisnel, J.-F. Carpentier and Y. Sarazin, *Dalton Trans.*, 2009, 9820.
109. Z. Zhong, P. J. Dijkstra, C. Birg, M. Westerhausen and J. Feijen, *Macromolecules*, 2001, **34**, 3863.
110. C. A. Wheaton, P. G. Hayes and B. J. Ireland, *Dalton Trans.*, 2009, 4832.
111. C. K. Williams, N. R. Brooks, M. A. Hillmyer and W. B. Tolman, *Chem. Commun.*, 2002, 2132.
112. C. K. Williams, L. E. Breyfogle, S. K. Choi, W. Nam, V. G. Young, M. A. Hillmyer and W. B. Tolman, *J. Am. Chem. Soc.*, 2003, **125**, 11350.
113. M. G. Cushion and P. Mountford, *Chem. Commun.*, 2011, **47**, 2276.
114. M. S. Hill and P. B. Hitchcock, *Chem. Commun.*, 2003, 1758.
115. A. D. Schwarz, Z. Chu and P. Mountford, *Organometallics*, 2010, **29**, 1246.
116. I. Taden, H.-C. Kang, W. Massa and J. Okuda, *J. Organomet. Chem.*, 1997, **540**, 189.
117. L. M. Hodgson, A. J. P. White and C. K. Williams, *J. Polym. Sci., Part A: Polym. Chem.*, 2006, **44**, 6646.
118. R. H. Platel, L. M. Hodgson, A. J. P. White and C. K. Williams, *Organometallics*, 2007, **26**, 4955.
119. L. M. Hodgson, R. H. Platel, A. J. P. White and C. K. Williams, *Macromolecules*, 2008, **41**, 8603.
120. R. H. Platel, A. J. P. White and C. K. Williams, *Inorg. Chem.*, 2008, **47**, 6840.
121. Z. Hou and Y. Wakatsuki, *Coord. Chem. Rev.*, 2002, **231**, 1.
122. H. Yasuda and E. Ihara, *Bull. Chem. Soc. Jpn.*, 1997, **70**, 1745.
123. H. Yasuda, *J. Organomet. Chem.*, 2002, **647**, 128.
124. H. E. Dyer, S. Huijser, A. D. Schwarz, C. Wang, R. Duchateau and P. Mountford, *Dalton Trans.*, 2008, 32.
125. F. Bonnet, A. C. Hillier, A. Collins, S. R. Dubberley and P. Mountford, *Dalton Trans.*, 2005, 421.
126. P. L. Arnold, J.-C. Buffet, R. P. Blaudeck, S. Sujecki, A. J. Blake and C. Wilson, *Angew. Chem. Int. Ed.*, 2008, **47**, 6033.
127. A. D. Schwarz, A. L. Thompson and P. Mountford, *Inorg. Chem.*, 2009, **48**, 10442.
128. A. D. Schwarz, K. R. Herbert, C. Paniagua and P. Mountford, *Organometallics*, 2010, **29**, 4171.

129. I. P. Hsieh, C.-H. Huang, H. M. Lee, P.-C. Kuo, J.-H. Huang, H.-I. Lee, J.-T. Cheng and G.-H. Lee, *Inorg. Chim. Acta*, 2006, **359**, 497.
130. A. F. Douglas, B. O. Patrick and P. Mehrkhodavandi, *Angew. Chem. Int. Ed.*, 2008, **47**, 2290.
131. I. Peckermann, A. Kapelski, T. P. Spaniol and J. Okuda, *Inorg. Chem.*, 2009, **48**, 5526.
132. J.-C. Buffet, J. Okuda and P. L. Arnold, *Inorg. Chem.*, 2010, **49**, 419.
133. M. P. Blake, A. D. Schwarz and P. Mountford, *Organometallics*, 2011, **30**, 1202.
134. H. R. Kricheldorf, G. Behnken, G. Schwarz and J. Kopf, *Macromolecules*, 2008, **41**, 4102.
135. H. R. Kricheldorf, G. Behnken, G. Schwarz and J. A. Brockaert, *Macromol. Chem. Phys.*, 2008, **209**, 1586.
136. B. J. O'Keefe, S. M. Monnier, M. A. Hillmyer and W. B. Tolman, *J. Am. Chem. Soc.*, 2001, **123**, 339.
137. B. J. O'Keefe, L. E. Breyfogle, M. A. Hillmyer and W. B. Tolman, *J. Am. Chem. Soc.*, 2002, **124**, 4384.
138. H. R. Kricheldorf, M. Berl and N. Scharnagl, *Macromolecules*, 1988, **21**, 286.
139. U. S. Government, *Code of Federal Regulations*, 2008, **3**, 154.
140. G. Schwach, J. Coudane, R. Engel and M. Vert, *Polym. Int.*, 1998, **46**, 177.
141. A. Stjerndahl, A. F. Wistrand and A.-C. Albertsson, *Biomacromolecules*, 2007, **8**, 937.
142. M. Ryner, K. Stridsberg, A.-C. Albertsson, H. von Schenck and M. Svensson, *Macromolecules*, 2001, **34**, 3877.
143. A. J. Nijenhuis, D. W. Grijpma and A. J. Pennings, *Macromolecules*, 1992, **25**, 6419.
144. H. R. Kricheldorf, I. Kreiser-Saunders and A. Stricker, *Macromolecules*, 2000, **33**, 702.
145. H. R. Kricheldorf, *Macromol. Symp.*, 2000, **153**, 55.
146. A. Kowalski, A. Duda and S. Penczek, *Macromolecules*, 2000, **33**, 7359.
147. J. Libiszowski, A. Kowalski, A. Duda and S. Penczek, *Macromol. Chem. Phys.*, 2002, **203**, 1694.
148. G. Schwach, J. Coudane, R. Engel and M. Vert, *Polym. Bull.*, 1996, **37**, 771.
149. G. Schwach, J. Coudane, R. Engel and M. Vert, *Polym. Bull.*, 1994, **32**, 617.

150. G. Schwach and M. Vert, *Int. J. Biol. Macromol.*, 1999, **25**, 283.
151. A. Kowalski, A. Duda and S. Penczek, *Macromolecules*, 1998, **31**, 2114.
152. P. Vanhoorne, P. Dubois, R. Jerome and P. Teyssie, *Macromolecules*, 1992, **25**, 37.
153. A. Duda and S. Penczek, *Macromolecules*, 1995, **28**, 5981.
154. C. Miola-Delaite, T. Hamaide and R. Spitz, *Macromol. Chem. Phys.*, 1999, **200**, 1771.
155. M. Möller, R. Kånge and J. L. Hedrick, *J. Polym. Sci., Part A: Polym. Chem.*, 2000, **38**, 2067.
156. N. Nomura, A. Taira, T. Tomioka and M. Okada, *Macromolecules*, 2000, **33**, 1497.
157. W. Zhao, D. Cui, X. Liu and X. Chen, *Macromolecules*, 2010, **43**, 6678.
158. Y. Sarazin, B. Liu, T. Roisnel, L. Maron and J.-F. Carpentier, *J. Am. Chem. Soc.*, 2011, **133**, 9069.
159. P. Dubois, C. Jacobs, R. Jerome and P. Teyssie, *Macromolecules*, 1991, **24**, 2266.
160. H. Ma and J. Okuda, *Macromolecules*, 2005, **38**, 2665.
161. Z. Zhang, X. Xu, W. Li, Y. Yao, Y. Zhang, Q. Shen and Y. Luo, *Inorg. Chem.*, 2009, **48**, 5715.
162. N. Spassky, V. Simic, M. S. Montaudo and L. Hubert-Pfalzgraf, *Macromol. Chem. Phys.*, 2000, **201**, 2432.
163. W. J. Evans, K. J. Forrestal and J. W. Ziller, *J. Am. Chem. Soc.*, 1998, **120**, 9273.
164. X. Deng, M. Yuan, X. Li and C. Xiong, *Eur. Polym. J.*, 2000, **36**, 1151.
165. M. Yamashita, Y. Takemoto, E. Ihara and H. Yasuda, *Macromolecules*, 1996, **29**, 1798.
166. S. Agarwal, C. Mast, K. Dehnicke and A. Greiner, *Macromol. Rapid Commun.*, 2000, **21**, 195.
167. H. Sun, S. Chen, Y. Yao, Q. Shen and K. Yu, *Appl. Organometal. Chem.*, 2006, **20**, 310.
168. K. C. Hultzsch, T. P. Spaniol and J. Okuda, *Organometallics*, 1997, **16**, 4845.
169. K. Beckerle, K. C. Hultzsch and J. Okuda, *Macromol. Chem. Phys.*, 1999, **200**, 1702.
170. H. Kawaguchi and T. Matsuo, *J. Organomet. Chem.*, 2004, **689**, 4228.

171. M. H. Chisholm, D. Navarro-Llobet and W. J. Simonsick, *Macromolecules*, 2001, **34**, 8851.
172. M. H. Chisholm, C.-C. Lin, J. C. Gallucci and B.-T. Ko, *Dalton Trans.*, 2003, 406.
173. B.-T. Ko, C.-C. Wu and C.-C. Lin, *Organometallics*, 2000, **19**, 1864.
174. W. M. Stevels, M. J. K. Ankone, P. J. Dijkstra and J. Feijen, *Macromolecules*, 1996, **29**, 3332.
175. W. M. Stevels, M. J. K. Ankone, P. J. Dijkstra and J. Feijen, *Macromolecules*, 1996, **29**, 6132.
176. W. M. Stevels, M. J. K. Ankone, P. J. Dijkstra and J. Feijen, *Macromolecules*, 1996, **29**, 8296.
177. D. Takeuchi, T. Nakamura and T. Aida, *Macromolecules*, 2000, **33**, 725.
178. Y.-C. Liu, B.-T. Ko and C.-C. Lin, *Macromolecules*, 2001, **34**, 6196.
179. A. W. Kleij, *Eur. J. Inorg. Chem.*, **2009**, 193.
180. C. P. Radano, G. L. Baker and M. R. Smith, *J. Am. Chem. Soc.*, 2000, **122**, 1552.
181. K. Majerska and A. Duda, *J. Am. Chem. Soc.*, 2004, **126**, 1026.
182. M. H. Chisholm, N. J. Patmore and Z. Zhou, *Chem. Commun.*, 2005, 127.
183. M. H. Chisholm, J. C. Gallucci, K. T. Quisenberry and Z. Zhou, *Inorg. Chem.*, 2008, **47**, 2613.
184. E. Y. Tshuva, I. Goldberg and M. Kol, *J. Am. Chem. Soc.*, 2000, **122**, 10706.
185. E. Y. Tshuva, I. Goldberg, M. Kol and Z. Goldschmidt, *Inorg. Chem. Commun.*, 2000, **3**, 611.
186. E. Y. Tshuva, I. Goldberg, M. Kol, H. Weitman and Z. Goldschmidt, *Chem. Commun.*, 2000, 379.
187. E. Y. Tshuva, I. Goldberg, M. Kol and Z. Goldschmidt, *Organometallics*, 2001, **20**, 3017.
188. E. Y. Tshuva, I. Goldberg, M. Kol and Z. Goldschmidt, *Inorg. Chem.*, 2001, **40**, 4263.
189. E. Y. Tshuva, S. Groysman, I. Goldberg, M. Kol and Z. Goldschmidt, *Organometallics*, 2002, **21**, 662.
190. S. Groysman, I. Goldberg, M. Kol, E. Genizi and Z. Goldschmidt, *Organometallics*, 2003, **22**, 3013.
191. S. Segal, I. Goldberg and M. Kol, *Organometallics*, 2005, **24**, 200.

192. S. Gendler, S. Segal, I. Goldberg, Z. Goldschmidt and M. Kol, *Inorg. Chem.*, 2006, **45**, 4783.
193. M. E. G. Skinner, B. R. Tyrrell, B. D. Ward and P. Mountford, *J. Organomet. Chem.*, 2002, **647**, 145.
194. T. Toupance, S. R. Dubberley, N. H. Rees, B. R. Tyrrell and P. Mountford, *Organometallics*, 2002, **21**, 1367.
195. C. L. Boyd, T. Toupance, B. R. Tyrrell, B. D. Ward, C. R. Wilson, A. R. Cowley and P. Mountford, *Organometallics*, 2005, **24**, 309.
196. O. Wichmann, R. Sillanpää and A. Lehtonen, *Coord. Chem. Rev.*, 2012, **256**, 371.
197. A. J. Chmura, M. G. Davidson, M. D. Jones, M. D. Lunn and M. F. Mahon, *Dalton Trans.*, 2006, 887.
198. A. J. Chmura, M. G. Davidson, M. D. Jones, M. D. Lunn, M. F. Mahon, A. F. Johnson, P. Khunkamchoo, S. L. Roberts and S. S. F. Wong, *Macromolecules*, 2006, **39**, 7250.
199. M. G. Davidson, C. T. O'Hara, M. D. Jones, C. G. Keir, M. F. Mahon and G. Kociok-Koehn, *Inorg. Chem.*, 2007, **46**, 7686.
200. F. M. Kerton, A. C. Whitwood and C. E. Willans, *Dalton Trans.*, 2004, 2237.
201. C. E. Willans, M. A. Sinenkov, G. K. Fukin, K. Sheridan, J. M. Lynam, A. A. Trifonov and F. M. Kerton, *Dalton Trans.*, 2008, 3592.
202. H. Guo, H. Zhou, Y. Yao, Y. Zhang and Q. Shen, *Dalton Trans.*, 2007, 3555.
203. K. Nie, X. Gu, Y. Yao, Y. Zhang and Q. Shen, *Dalton Trans.*, 2010, **39**, 6832.
204. S. Barroso, J. Cui, J. M. Carretas, A. Cruz, I. C. Santos, M. T. Duarte, J. P. Telo, N. Marques and A. M. Martins, *Organometallics*, 2009, **28**, 3449.
205. C.-X. Cai, L. Toupet, C. W. Lehmann and J.-F. Carpentier, *J. Organomet. Chem.*, 2003, **683**, 131.
206. H. E. Dyer, D.Phil Thesis, University of Oxford, 2009.
207. H. Ma, T. P. Spaniol and J. Okuda, *Dalton Trans.*, 2003, 4770.
208. N. Ajellal, J.-F. Carpentier, C. Guillaume, S. M. Guillaume, M. Helou, V. Poirier, Y. Sarazin and A. Trifonov, *Dalton Trans.*, 2010, **39**, 8363.
209. J.-C. Buffet, A. Kapelski and J. Okuda, *Macromolecules*, 2010, **43**, 10201.
210. Y. Sarazin, R. H. Howard, D. L. Hughes, S. M. Humphrey and M. Bochmann, *Dalton Trans.*, 2006, 340.

211. M. Kol, M. Shamis, I. Goldberg, Z. Goldschmidt, S. Alfi and E. Hayut-Salant, *Inorg. Chem. Commun.*, 2001, **4**, 177.
212. M. G. Davidson, C. L. Doherty, A. L. Johnson and M. F. Mahon, *Chem. Commun.*, 2003, 1832.
213. A. J. Chmura, M. G. Davidson, C. J. Frankis, M. D. Jones and M. D. Lunn, *Chem. Commun.*, 2008, 1293.
214. E. L. Whitelaw, M. D. Jones, M. F. Mahon and G. Kociok-Kohn, *Dalton Trans.*, 2009, 9020.
215. C. M. Silvernail, L. J. Yao, L. M. R. Hill, M. A. Hillmyer and W. B. Tolman, *Inorg. Chem.*, 2007, **46**, 6565.
216. L. M. Alcazar-Roman, B. J. O'Keefe, M. A. Hillmyer and W. B. Tolman, *Dalton Trans.*, 2003, 3082.
217. C.-T. Chen, C.-A. Huang and B.-H. Huang, *Dalton Trans.*, 2003, 3799.
218. Z. Tang and V. C. Gibson, *Eur. Polym. J.*, 2007, **43**, 150.
219. L. Wang and H. Ma, *Macromolecules*, 2010, **43**, 6535.
220. H. Ma, G. Melillo, L. Oliva, T. P. Spaniol, U. Englert and J. Okuda, *Dalton Trans.*, 2005, 721.
221. T. Aida, Y. Maekawa, S. Asano and S. Inoue, *Macromolecules*, 1988, **21**, 1195.
222. S. Inoue, *J. Macromol. Sci.: Part A - Chem*, 1988, **25**, 571.
223. T. Aida, *Prog. Polym. Sci.*, 1994, **19**, 469.
224. T. Aida and S. Inoue, *Acc. Chem. Res.*, 1996, **29**, 39.
225. C. K. Williams, *Chem. Soc. Rev.*, 2007, **36**, 1573.
226. I. Barakat, P. Dubois, R. Jérôme and P. Teyssié, *J. Polym. Sci., Part A: Polym. Chem.*, 1993, **31**, 505.

Chapter Two

Zwitterionic rare earth complexes supported by bis(phenolate)-amino ligands and amine-initiated, immortal ROP of *rac*-LA

2.1 Overview

This Chapter describes detailed investigations into the amine-initiated ROP of *rac*-LA using a zwitterionic yttrium catalyst bearing a bis(phenolate)-amino ligand. Dr. Hellen E. Dyer, a previous member of the Mountford group, originally developed a range of these Ln(III) complexes with systematic variation of the O_2N^L (L = OMe, NMe_2 or Me) bis(phenolate)-amino ligand and performed initial polymerisation studies. A summary of these results is provided, in addition to details of further studies undertaken by the author. These investigations include the scope of amine-initiated, immortal ROP in terms of the range of amines that can be used for this process, as well as in-depth mechanistic evaluation. Comparative studies with an appropriate literature catalyst are also described, as well as attempts to extend the family of known zwitterionic bis(phenolate)-amino complexes to scandium. Five new yttrium and scandium complexes are presented as well as two X-ray structures. Some of this work has been published.[1-4]

2.2 Introduction: Group 3 and lanthanide ROP initiators

The Lewis acidic nature of the rare earth elements and low toxicity make them ideal candidates as ROP catalysts. Despite the synthetic challenges regarding sensitivity to air and moisture, the range of ionic radii permits comprehensive structure-activity relationships to be developed. However, the strong paramagnetism of most Ln(III) complexes is not conducive to study by NMR, which can be very helpful in ROP studies. For this reason, lanthanum, ytterbium(II), yttrium and scandium have received the most attention, although successful studies have been undertaken with neodymium and samarium(III) complexes.[5, 6] As described in Chapter One, there are several leading reviews documenting work using lanthanide based initiators and following on from earlier work undertaken in the Mountford group, there was sufficient scope to pursue further work on the lanthanide elements.[7, 8]

2.2.1 Bis(phenolate)-amino supported samarium initiators

The ionic radius of samarium(III) (1.04 Å) lies midway between lanthanum (1.15 Å) and yttrium (0.93 Å), thus is suitable as an intermediary between some of the most active and less active trivalent lanthanide ROP catalysts.[9] Although Sm(III) is paramagnetic ($4f^5$), use of the appropriate ligands has led to effective solution phase NMR studies. Dianionic bis(phenolate)-amino and related ligands have been

developed by a number of a research groups including Carpentier, Kol and Mountford amongst others and stem from developments in the post-metallocene era.[2, 4, 7, 8, 10-46] They form dianionic chelates and the ease of preparation of the protio-ligands *via* a Mannich condensation allows for selective variation of the pendant arm functionality and the steric bulk on the aryl ring. The hard donor atoms are ideally suited to the rare earth elements, whilst the coordination mode provides a balance between the exposure and steric protection of the active site in polymerisation reactions.

2.2.2 Synthesis of samarium amide initiators

The most widely used lanthanide amide initiators feature Ln-N(SiMe$_3$)$_2$ moieties or the less bulky "Anwander-type" Ln-N(SiHMe$_2$)$_2$ analogues. Samarium amides supported by bis(phenolate)-amino ligands were prepared (Scheme 2.1, Section 2.3) by Dyer in order to provide direct comparison with borohydride analogues and to make comparisons with complexes prepared by Carpentier, notably Ln(O$_2$N^{OMe}){N(SiHMe$_2$)$_2$}(THF) (Ln = Y (**1.14**) and La (**2.1**)).[10, 13] Sm(O$_2$N^{L})-{N(SiHMe$_2$)$_2$}(THF) (L = OMe (**1.16**), NMe$_2$ (**1.17**) or py (**1.21**)) complexes were obtained by protonolysis routes where Sm{N(SiHMe$_2$)$_2$}$_3$(THF)$_2$ was treated with the appropriate protio-ligand in hydrocarbon solvent. Isolated complexes possessed the expected C_s-symmetry and the solid state structures were retained in solution, where meaningful ^{1}H NMR spectra could be obtained.[2, 4]

Attempts were also made to prepare base-free bis(phenolate)-amino samarium amide complexes, using the bulkier Sm{N(SiMe$_3$)$_2$}$_3$ precursor. However, zwitterionic complexes of the type, Sm(O$_2$N^{L})(HO$_2$N^{L}) (L = NMe$_2$ (**1.24**), OMe (**1.25**) or Me (**2.2**)) were formed exclusively, irrespective of the reaction stoichiometry.[2-4] These complexes may have been observed by other research groups but were never isolated or prepared rationally. For example, Carpentier (and Cui) noted side products in the reaction between Y{N(SiHMe$_2$)$_2$}$_3$(THF)$_2$ (or Y(CH$_2$SiMe$_3$)$_3$(THF)$_2$) and H$_2$O$_2$N^{NMe2}.[13, 44] The five-coordinate complex, Sm(O$_2$N^{NMe2}){N(SiMe$_3$)$_2$} (**2.3**), was obtained when Sm(O$_2$N^{NMe2})(BH$_4$)(THF) (**1.19**) was treated with KN(SiMe$_3$)$_2$. A summary of selected reactivity is presented in Scheme 2.1 (Section 2.3) and further details can be found in the appropriate references.[2, 4]

2.3 Preparation of zwitterionic complexes

Yttrium, lanthanum and samarium zwitterionic complexes, $Ln(O_2N^L)(HO_2N^L)$ (**1.24**, **1.25**, **2.2**, **2.4**, **1** and **2**) were prepared rationally by the addition of two equivalents of the protio-ligand to either base-stabilised or base-free amide precursors (Scheme 2.1).[1-4] All complexes were obtained in good yields and were shown to be structurally analogous. As illustrated in Scheme 2.1, each complex was monomeric with *pseudo*-octahedral geometry around the metal centre. One bis(phenolate)-amino ligand is doubly deprotonated and binds in the usual tetradentate arrangement with the two phenolate oxygen atoms in a *trans* configuration. The second mono-deprotonated (phenolate)-amino ligand is bidentate, with only the oxygen atoms coordinating to the metal centre. The central nitrogen atom of this ligand is protonated and there is hydrogen bonding between the proton and the two-phenolate oxygen atoms as well as the N or O donor-arm. Ammonium hydrogen atoms were located in Fourier difference maps and positionally and isotropically refined in all examples. A five-coordinate trigonal-bipyramidal complex, **2.2**, was obtained when the protio-ligand, $H_2O_2N^{Me}$, with a "dummy" pendant arm was reacted with the samarium precursor. Variation of the bond lengths and angles was consistent with the increasing metal ion radius from Y to La, although a detailed discussion is not provided in this Thesis.[2, 4]

Zwitterionic complexes could also be prepared sequentially from the amides, $Sm(O_2N^L)\{N(SiHMe_2)_2\}_3(THF)$ (L = OMe (**1.16**) or NMe_2 (**1.17**)). This methodology permitted the preparation of complexes with mixed donor arms. Of particular note is $Sm(O_2N^{OMe})(HO_2N^{NMe2})$ (**2.5**), which was prepared by treating $Sm(O_2N^{NMe2})\{N(SiHMe_2)_2\}(THF)$ (**1.17**) with one equivalent of $H_2O_2N^{OMe}$. Ligand rearrangement was shown to occur so that the O_2N^{OMe} ligand became tetradentate, thus maximising the number of oxygen donor atoms at the oxophilic samarium centre. Catalytic studies with $Sm(O_2N^{NMe2})(HO_2N^{Me})$ (**2.6**) established that the identity of the bidentate mono-deprotonated HO_2N^L ligand had no influence on polymerisation performance (*vide infra*).

The retained ammonium proton could also be substituted for a Li^+ or Na^+ ion. For example, treating $Sm(O_2N^{NMe2})(HO_2N^{NMe2})$ (**1.24**) with $LiN(SiMe_3)_2$ or $NaN(SiMe_3)_2$ led to the formation of bimetallic complexes, $Sm(O_2N^{NMe2})(MO_2N^{NMe2})$ (M = Li (**2.8**) or Na (**2.9**)), with the Li^+ or Na^+ ion occupying the O_2N_2 pocket of the bidentate O_2N^L ligand. The proton could not be substituted for a potassium ion owing to the greater

ionic radius of K^+ *cf*. Li^+ or Na^+. A summary of this reactivity is described in Scheme 2.1 and the reader is directed to the appropriate reference for further details.[2]

These zwitterionic complexes have distinctive ^{1}H NMR spectra. The eight ^{t}Bu and eight aryl-H environments are chemically inequivalent, providing a characteristic fingerprint. The ^{1}H NMR spectrum of $Y(O_2N^{NMe2})(HO_2N^{NMe2})$ (**1**) is shown in Figure 2.1 by way of example. Other noteworthy features include the broad signal at 8.75 ppm corresponding to the retained proton at the ammonium centre and multiple diastereotopic methylene protons. Unfortunately, diagnostic N–H stretches could not be detected in the IR spectra, presumably on account of weakening of the N–H bond through hydrogen bonding.

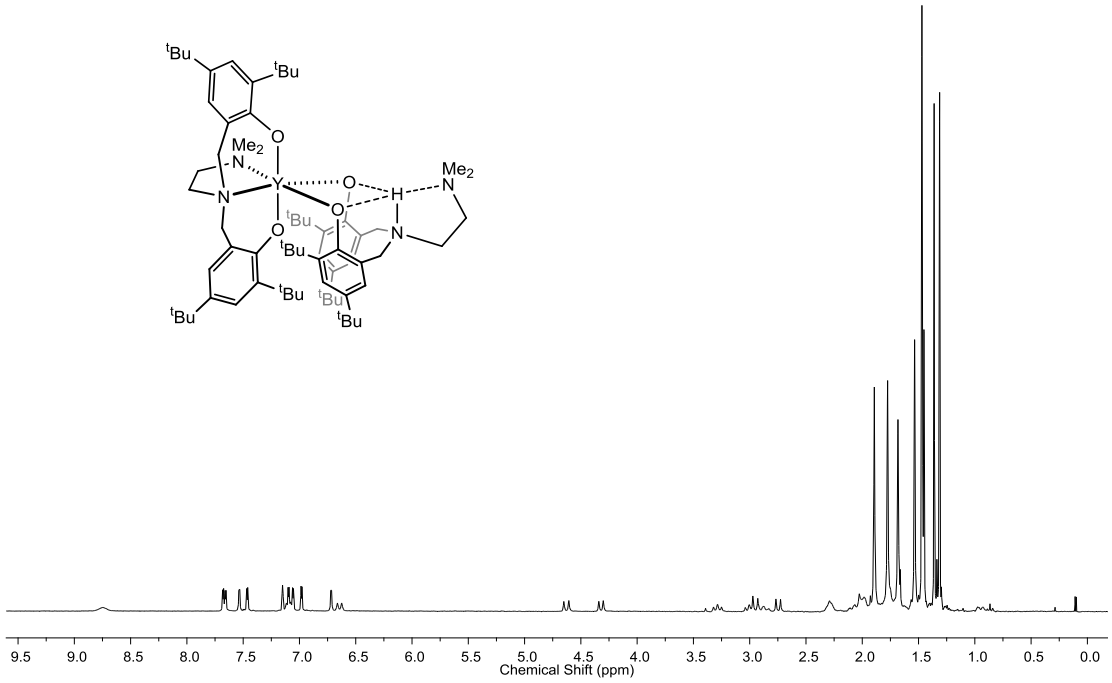

Figure 2.1. ^{1}H NMR (299.9 MHz, C_6D_6, 298 K) spectrum of **1**.[1, 2] Residual protio-solvent, δ = 7.15 ppm.

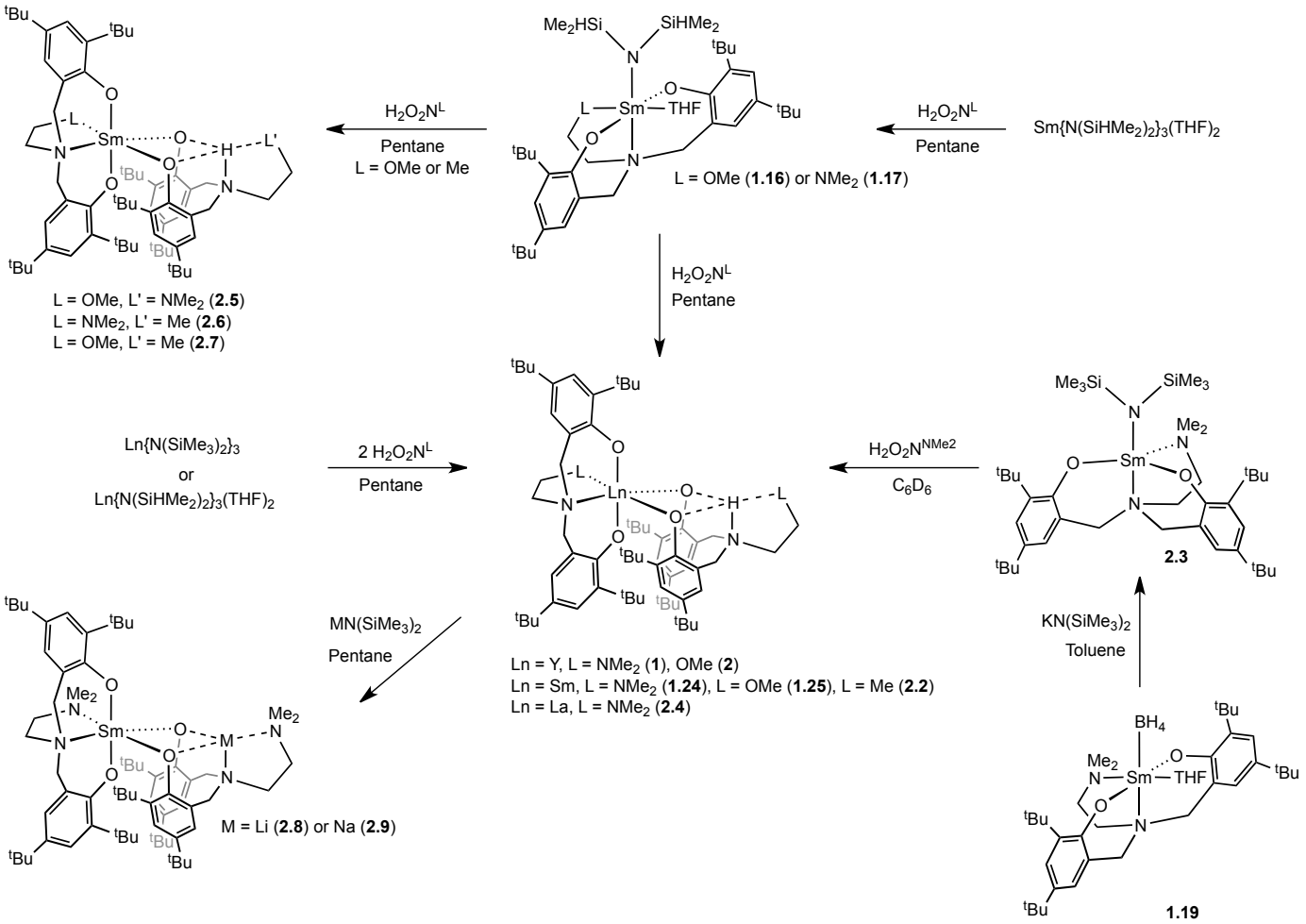

Scheme 2.1. Summary of rare earth amide and zwitterion syntheses. Note that complex **2.2** is five-coordinate and the HO_2N^{Me} bidentate ligands in **2.6** and **2.7** do not form hydrogen bonds between the pendant arm and the ammonium centre.[1-4]

2.4 Rare earth zwitterionic complexes for the ROP of *rac*-LA

Despite the lack of an initiating group, rare earth bis(phenolate)-amino zwitterionic complexes were shown to be active initiators for the ROP of *rac*-LA at room temperature.[1-3] In a representative procedure, 100 equivs. of *rac*-LA were added to each complex in THF solution at room temperature. The aim of this initial study was to highlight the influence of the pendant arm donor substituents and importance of the cationic centre (H^+, Li^+ or Na^+) on the ROP of *rac*-LA. The data are summarised in Table 2.1.

Table 2.1. ROP of *rac*-LA using zwitterionic initiators.[a]

Zwitterion	Conv. (%)[b]	M_n(calcd) (g mol^{-1})[c]	M_n(GPC) (g mol^{-1})[d]	M_w/M_n[d]
$Sm(O_2N^{NMe2})(HO_2N^{NMe2})$ (**1.24**)	80	11,530	25,210	1.54
$Sm(O_2N^{NMe2})(LiO_2N^{NMe2})$ (**2.8**)	0	-	-	-
$Sm(O_2N^{NMe2})(NaO_2N^{NMe2})$ (**2.9**)	36	5,250	19,730	1.32
$Sm(O_2N^{OMe})(HO_2N^{OMe})$ (**1.25**)	89	12,660	25,240	2.23
$Sm(O_2N^{NMe2})(HO_2N^{Me})$ (**2.6**)	65	9,350	20,380	1.98
$Sm(O_2N^{Me})(HO_2N^{Me})$ (**2.2**)	0	-	-	-
$Y(O_2N^{NMe2})(HO_2N^{NMe2})$ (**1**)	89	12,500	33,800	1.50

[a] [*rac*-LA]$_0$:[Ln]$_0$ = 100:1, 2 mL THF, [*rac*-LA]$_0$ = 0.69 M, rt, 5 mins (20 mins for **1**). [b] Measured by ^{1}H NMR in $CDCl_3$. [c] M_n(calcd) = (Conv. (%) × 144.1) assuming one chain per metal. [d] Measured by GPC against polystyrene standards using the appropriate Mark-Houwink corrections for poly(*rac*-LA) in THF at 30 °C.

The most active catalysts were $Sm(O_2N^{NMe2})(HO_2N^{NMe2})$ (**1.24**) and $Sm(O_2N^{OMe})(HO_2N^{OMe})$ (**1.25**), with polymerisations proceeding to high conversion within 5 mins. The bimetallic complexes, **2.8** and **2.9**, and complexes bearing ligands without pendant arm donors, **2.2** and **2.6**, showed no or moderate activity over this time period. $Y(O_2N^{NMe2})(HO_2N^{NMe2})$ (**1**) was not as active either, reaching high conversion within 20 mins. Regarding molecular weight data, all measured M_n(GPC) figures were reflective of fast chain propagation reactions with respect to initiation, assuming one chain per metal. In this kinetic regime, once chain growth is initiated, the rate of propagation, k_p, is greater than other initiating processes, hence initiation

appears incomplete with respect to expected M_n. These polymerisation reactions were likely to have been initiated by trace water or lactic acid, given the lack of evidence for bis(phenol)-amine-capped poly(*rac*-LA) chains in MALDI-ToF mass spectra. In fact, only cyclic transesterification products ($\Delta(m/z)$ = 72.0 g mol^{-1} (half a lactide unit)) with no apparent end-group could be assigned. The broad polydispersity indices also reflected uncontrolled polymerisation reactions, where transesterification and chain termination processes were competing with linear chain growth. However, it was apparent that the structure of the zwitterionic complex and the identity of the pendant arm did significantly affect the activity of the Sm based catalysts. The absence of a pendant arm donor (**2.2**) or the presence of a metal ion, rather than a proton (**2.8** and **2.9**) was detrimental to catalyst activity. The previously reported borohydride complex, $Sm(O_2N^{Me})(BH_4)(THF)_2$ (**1.26**), was also shown to be inactive for ROP of *rac*-LA.[2, 4] The ethereal donor (**1.25** *vs*. **1.24**) increased activity marginally and the larger metal (**1.24** *vs*. **1**) also appeared advantageous. These trends resembled observations made by Kol, when bis(phenolate)-amino supported Group 4 complexes were utilised for olefin polymerisation. The presence and nature of the pendant arm was shown to have a profound effect on polymerisation.[17, 19, 20, 22, 23]

2.5 Introduction of co-initiators

It was clear that the zwitterionic complexes were active initiators or co-initiators for the ROP of *rac*-LA, despite the inherent lack of control. During the development of this work, Carpentier and others, began to focus strongly on using chain transfer agents or co-initiators alongside highly developed coordination-insertion type initiators. As described in Chapter One, alcohol chain transfer reagents were included in polymerisation feeds to improve catalyst efficiency through the preparation of multiple poly(*rac*-LA) chains (Figure 2.2).[14, 15, 30] These operate by firstly generating a metal alkoxide species *in situ*, which can act as a conventional initiator for ROP. Early in the polymeriation reaction, the remaining equivalents of alcohol are consumed through facile exchange with the initially formed PLA chain bound at the metal centre, before ring opening lactide units in a coordination-insertion type process.

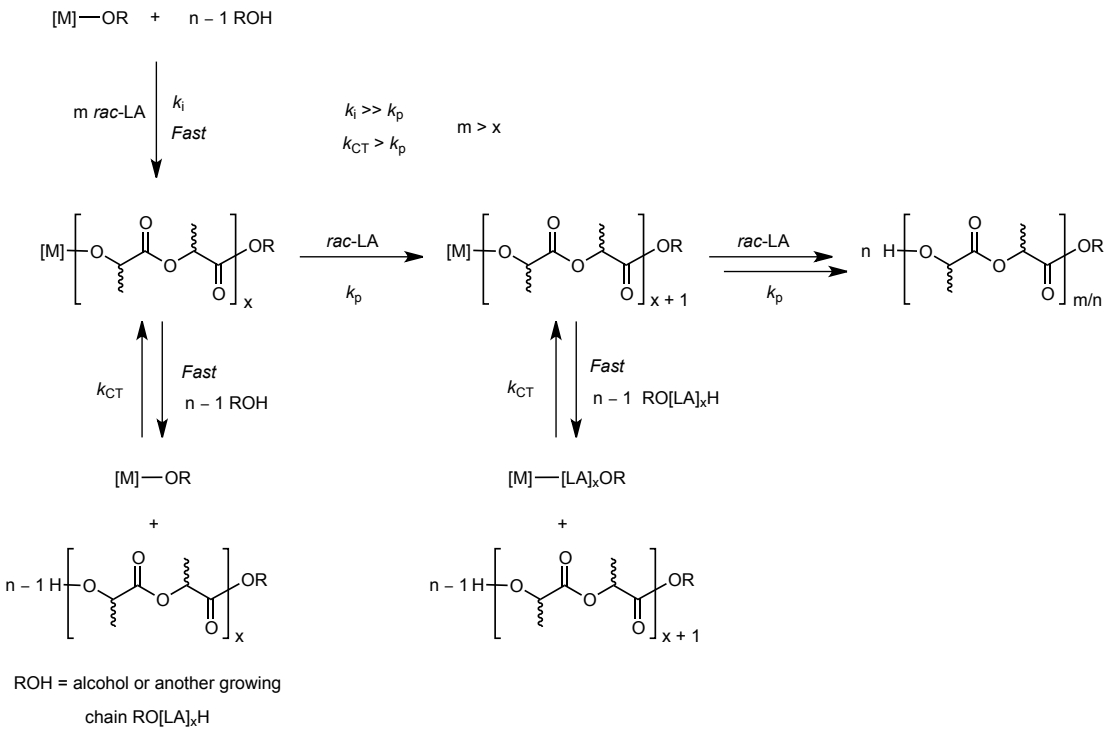

Figure 2.2. Propagation and chain transfer processes in immortal ROP.

Fast chain transfer during propagation ensures that the number averaged molecular weight, M_n, is proportional to [*rac*-LA]$_0$:[alcohol]$_0$ and polydispersity indices are narrow. These breakthroughs were made using the bis(phenolate)-amino supported yttrium amide catalysts, $Y(O_2N^L)\{N(SiHMe_2)_2\}(THF)$ (L = OMe (**1.14**) or NMe_2 (**1.15**)), and since the rare-earth zwitterions (**1.24**, **1.25**, **2.2**, **2.4**–**2.9**, **1** and **2**) also bear these ligands, it was felt that these complexes were suitable candidates for ROP in the presence of co-initiators.

Amines have been used as co-initiators in ROP, often in conjunction with the industrial ROP catalyst, $Sn(Oct)_2$. Duda and Penczek were able to prepare well-defined PLA, when *rac*-LA was polymerised in the presence of $^nBuNH_2$.[47, 48] Polymerisations in the presence of $^nBuNH_2$ proceeded at almost the same rate as those co-initiated by ^{n}BuOH and it was proposed that the amine was incorporated as the end-group at the beginning of the reaction, in an activated-monomer type process. No metal-amide bond is formed in this associative process; instead the nucleophilic amine attacks the activated lactide unit. Other reports have described attempts to prepare amine-capped PLA in the presence of simple Lewis acidic metal salts or by organocatalytic approaches, often with a focus on growing multi-arm polymers from polyamine cores.[49-58] Based on the paucity of reports on ROP in the presence of

amines and well-defined organometallic promoters, the zwitterions were investigated for ROP in the presence of amine co-initiators with a view to establishing their capability for immortal type polymerisation and the mechanism of initiation and propagation.

2.5.1 Amine-initiated, immortal ROP

Eight zwitterionic complexes were used to polymerise 100 equivs. of *rac*-LA in the presence of 5 equivs. of $BnNH_2$. The reactions were quenched after 5 mins with THF (as supplied) and aliquots were taken for ^{1}H NMR, GPC and MALDI-ToF MS analysis. Based on post-polymerisation analysis (Table 2.2), the introduction of amines led to well-controlled ROP reactions, particularly for the samarium and yttrium zwitterions, **1.24** and **1**, and M_n(GPC) values of 2,700 and 2,460 g mol^{-1} were in very good agreement with those expected for one poly(*rac*-LA) chain per added $BnNH_2$ (2,760 and 2,440 g mol^{-1}). Furthermore, the narrow PDIs of 1.15 and 1.12 were consistent with well-controlled polymerisation reactions. Previous studies employing organocatalytic methods have shown that primary amines can behave as bifunctional initiators, generating two chains per initiating amine.[54, 58] Only one chain per amine appeared to have been generated in this metal mediated process, based on M_n(GPC) values and the presence of a BnN<u>H</u>– resonance in the ^{1}H NMR spectra of isolated poly(*rac*-LA).

It should be noted that in reactions where no co-initiator was employed (Table 2.1), poly(*rac*-LA) products displayed a high degree of hetereotactic enrichment, based on tetrad assignments in homonuclear decoupled ^{1}H-{^{1}H} NMR spectra.[5, 11, 13, 15, 59-72] Similarly, poly(*rac*-LA) products from reactions including amine co-initiators displayed a high degree of heterotactic enrichment, with a P_r value up to 0.94 recorded for poly(*rac*-LA) produced by **1**. This enrichment is believed to arise through a selective chain-end control mechanism, where the stereochemistry of the latest enchained unit dictates which enantiomer is the next to be enchained. In the case of heterotactic enrichment, alternating *D*- and *L*-lactide units are enchained. The coordination geometry of the bis(phenolate)-amino ligand is crucial to this selectivity and Carpentier and Okuda have shown that P_r can be maximised when the steric bulk at the *ortho*-position of the bis(phenolate)-amino ligand is increased and when polymerisations are performed in THF.[11, 15, 31, 32, 73]

La(O_2N^{NMe2})(HO_2N^{NMe2}) (**2.4**) was also able to polymerise 100. equivs of *rac*-LA to completion within 5 mins with good agreement between M_n(calcd) = 2,850 g mol^{-1} and M_n(GPC) = 2,950 g mol^{-1}. However, the slightly broader PDI = 1.22 and P_r = 0.76 was indicative of a less well-controlled polymerisation process. These differences are attributed to the larger metal radius of La and possible influence on the conformation of the ancillary bis(phenolate)-amino ligand, despite **1**, **1.24** and **2.4** being structurally analogous.[2, 11] The MALDI-ToF mass spectra of the poly(*rac*-LA) produced by **1.24** and **1** showed one major distribution with a separation between peak envelopes, Δ(*m/z*), of 144 g mol^{-1}. There was minimal transesterification and $BnNH_2$ was calculated as the PLA end-group. With La(O_2N^{NMe2})(HO_2N^{NMe2}) (**2.4**), there was much more transesterification, which has been noted for the larger metal based catalysts.[74] The La centre is more likely to facilitate back-biting and intermolecular processes that are less accessible with smaller and more sterically crowded metal centres. These factors may also account for the slightly broader molecular weight distribution (PDI = 1.22) observed for PLA produced using **2.4**.

Table 2.2. ROP of *rac*-LA using zwitterionic initiators in the presence of $BnNH_2$.[a]

Zwitterion	Conv. (%)[b]	M_n(calcd) (g mol^{-1})[c]	M_n(GPC) (g mol^{-1})[d]	M_w/M_n[d]	P_r[e]
Sm(O_2N^{NMe2})(HO_2N^{NMe2}) (**1.24**)	92	2,760	2,700	1.15	0.87
Sm(O_2N^{NMe2})(LiO_2N^{NMe2}) (**2.8**)	62	1,890	1,930	1.13	0.81
Sm(O_2N^{NMe2})(NaO_2N^{NMe2}) (**2.9**)	100	2,990	5,880	2.00	0.42
Sm(O_2N^{OMe})(HO_2N^{OMe}) (**1.25**)	64	1,950	2,110	1.13	0.73
Sm(O_2N^{NMe2})(HO_2N^{Me}) (**2.6**)	89	2,670	2,570	1.15	0.91
Sm(O_2N^{Me})(HO_2N^{Me}) (**2.2**)	0	-	-	-	-
La(O_2N^{NMe2})(HO_2N^{NMe2}) (**2.4**)	95	2,850	2,950	1.22	0.76
Y(O_2N^{NMe2})(HO_2N^{NMe2}) (**1**)	81	2,440	2,460	1.12	0.94

[a] [*rac*-LA]$_0$:[$BnNH_2$]$_0$:[Ln]$_0$ = 100:5:1, 2 mL THF, [*rac*-LA]$_0$ = 0.69 M, rt, 5 mins. [b] Measured by ^{1}H NMR in $CDCl_3$. [c] M_n(calcd) = (Conv. (%) × 144.1/5 + 107.2) assuming one chain per $BnNH_2$. [d] Measured by GPC against polystyrene standards using the appropriate Mark-Houwink corrections for poly(*rac*-LA) in THF at 30 °C. [e] Determined from integration of appropriate tetrads in ^{1}H-{^{1}H} NMR spectra.

The bimetallic complexes, **2.8** and **2.9**, were more active in these experiments compared to when no $BnNH_2$ was employed (Table 2.1) but control over molecular weight was poor, especially for **2.9**. Despite the encouraging figures for M_n(calcd), M_n(GPC), PDI and P_r for **2.8**, MALDI-ToF MS indicated extensive transesterification, in contrast to benzyl amine-capped PLA prepared using $Sm(O_2N^{NMe2})(HO_2N^{NMe2})$ (**1.24**). The results for $Sm(O_2N^{NMe2})(HO_2N^{Me})$ (**2.6**) showed that the identity of the remote bidentate (mono-deprotonated) ligand was unimportant, whereas the inactive $Sm(O_2N^{Me})(HO_2N^{Me})$ (**2.2**) highlighted that the employment of a tetradentate bis(phenolate)-amino ligand with a pendant arm donor was key to the formation of an active catalyst. Kol noted the poor performance of the pentacoordinate pre-catalyst when Group 4 systems were used for 1-hexene polymerisation. Five-coordinate $Ti(O_2N^{Me})(Bn)_2$ (**2.10**) was more active than six-coordinate $Ti(O_2N^{NMe2})(Bn)_2$ (**2.11**) but **2.10** produced only oligomers, whilst six-coordinate **2.11** displayed living type behaviour. With heavier Zr analogues, good activity was observed with $Zr(O_2N^{NMe2})(Bn)_2$ (**1.27**), but five-coordinate $Zr(O_2N^{Me})(Bn)_2$ (**1.28**) was inactive.[17, 19, 20] $Sm(O_2N^{Me})(BH_4)(THF)_2$ (**1.26**) was also inactive for ROP.[2, 4] In light of these observations perhaps the unsaturated metal centres of **1.26**, **1.28** and **2.2** are more prone to deactivation through aggregation or potential PLA chelation.

$Sm(O_2N^{NMe2})(HO_2N^{NMe2})$ (**1.24**), a mid-range lanthanide provided the balance between activity and control *cf*. **2.4** and **1**. The experimental evidence for these three superior complexes presented in Table 2.2, in conjunction with MALDI-ToF mass spectra was consistent with an activated-monomer type initiation process, resulting in the formation of benzyl amine-capped poly(*rac*-LA), BnNH-[PLA]-H.[48] Based on work by Carpentier, M_n(GPC) were reflective of the $[rac\text{-LA}]_0$:$[BnNH_2]_0$ ratio of 100:5, and facile chain transfer processes with respect to propagation led to the narrow molecular weight distributions. Heterotactically-enriched poly(*rac*-LA) have been consistently documented when bis(phenolate)-amino ligands have been utilised as ancillary ligands. The replication of this observation indicated that polymerisations in this case were mediated by the metal-centre.[14, 15] In order to probe the nature of the active species and the mechanism of initiation and propagation, an in-depth reactivity and mechanistic study was undertaken by the author using $Y(O_2N^{NMe2})(HO_2N^{NMe2})$

(**1**). The lower activity of this catalyst and diamagnetic metal centre facilitated these studies.

2.5.2 Development of further zwitterions

The initial focus was to expand the yttrium zwitterion library to include the pyridyl donor ligand HO_2N^{py} and the "dummy arm" ligand HO_2N^{Me} to compliment $Y(O_2N^{NMe2})(HO_2N^{NMe2})$ (**1**) and $Y(O_2N^{OMe})(HO_2N^{OMe})$ (**2**), as well as to develop a scandium family. This allowed for an evaluation of structure-activity relationships akin to those determined for samarium and since Y(III) and Sc(III) are diamagnetic, mechanistic investigations using ^{1}H NMR spectroscopy were possible. Scheme 2.2 describes the reactions of $Y\{N(SiHMe_2)_2\}_3(THF)_2$ or $Sc(CH_2SiMe_3)_3(THF)_2$ with two equivalents of $HO_2^{tBu2}N^L$. From NMR tube scale experiments, it was clear that successful zwitterion formation was only achieved when $Y\{N(SiHMe_2)_2\}_3(THF)_2$ was treated with $HO_2^{tBu2}N^{Me}$ (forming **3**) and when $Sc(CH_2SiMe_3)_3(THF)_2$ was treated with $HO_2^{tBu2}N^{py}$ (forming **4**). Three more scandium zwitterions, **5**–**7**, were prepared utilising less bulky $HO_2^{Me2}N^L$ ligands (L = py, NMe_2 or OMe) and were obtained in 35–50% yield. This lack of comparability between the metal centre and the bis(phenolate)-amino ligands prevented a comprehensive structure-activity study but the scandium-centred zwitterions (**4**–**7**) and $Y(O_2N^{Me})(HO_2N^{Me})$ (**3**) were found to be poor catalysts for the ROP of *rac*-LA in the presence of an amine co-initiator (*vide infra*).

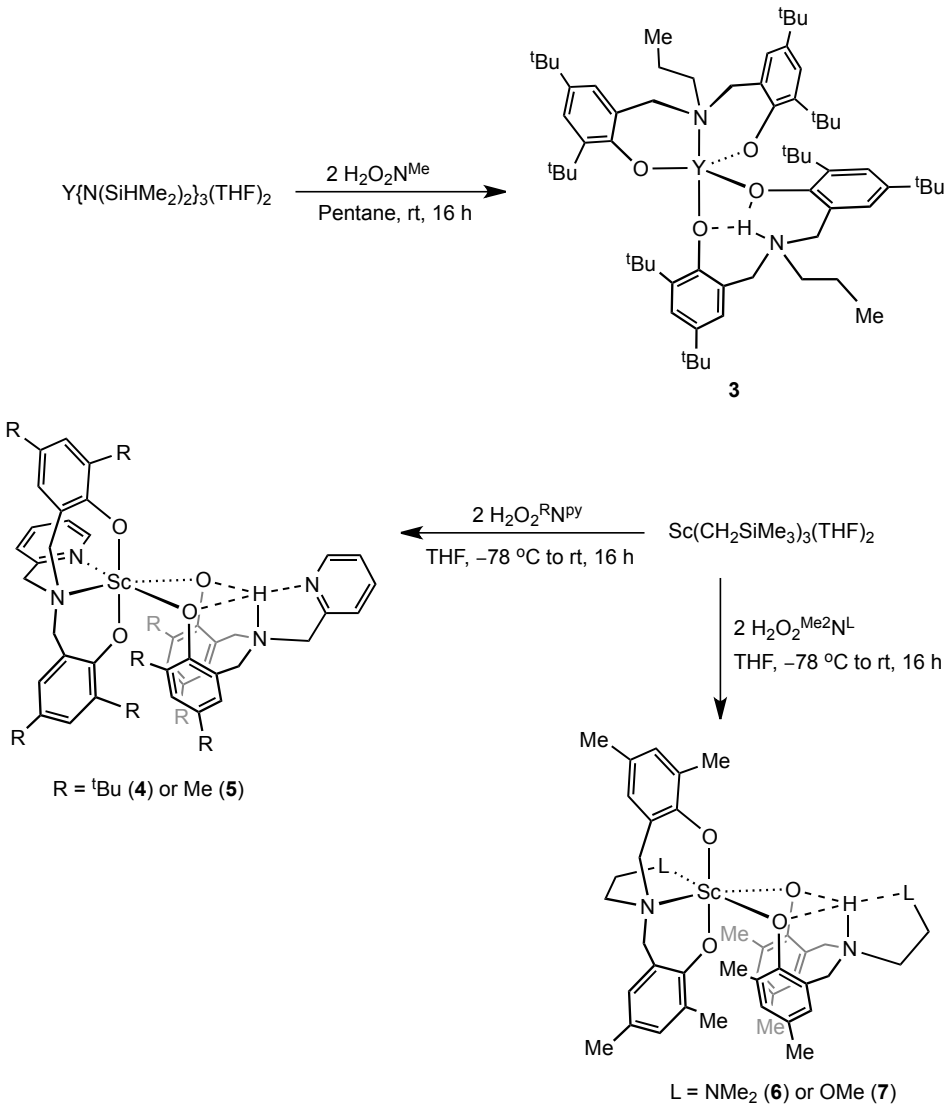

Scheme 2.2. Syntheses of **3** and scandium centred zwitterions **4**–**7**.

Unlike their heavier congeners, the scandium zwitterions had poor solubility in aliphatic hydrocarbons and had greater sensitivity to air and moisture. Solution phase NMR studies were undertaken and a representative ^{1}H NMR spectrum is presented in Figure 2.3. Each spectrum featured the distinctive eight *tert*-butyl or methyl resonances along with eight aryl protons, with two pyridyl rings further complicating the ^{1}H NMR spectra of **4** and **5**. In contrast, **3** was shown to be fluxional in solution and was characterised by ^{1}H NMR over a range of temperatures, but the most meaningful data were obtained at room temperature.

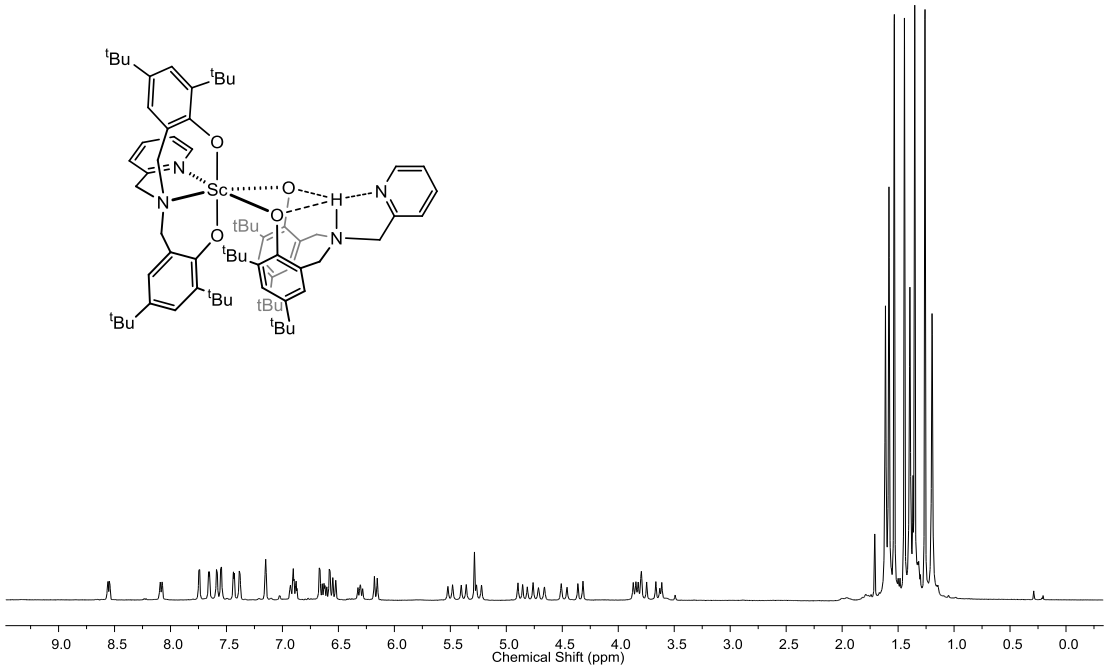

Figure 2.3. ^{1}H NMR (299.9 MHz, C_6D_6, 298 K) spectrum of **4**. Residual protio-solvent, δ = 7.15 ppm.

Sc($O_2{}^{Me2}N^{py}$)($HO_2{}^{Me2}N^{py}$) (**5**) was characterised by single crystal X-ray diffraction, along with Y(O_2N^{Me})(HO_2N^{Me}) (**3**) and their molecular structures are presented in Figures 2.5 and 2.4. The Y–O bond lengths were expectedly longer than Sc–O bond distances, despite **3** and **5** not being directly comparable structures. The solid state structure of **3** is analogous to its samarium counterpart, **2.2**, and the Y(1)–O(1) and Y(1)–O(2) bond lengths in **3** of 2.140(3) and 2.102(3) Å were shorter than the comparable distances in **1** (2.170(2) and 2.267(2) Å) and in **2** (2.160(3) and 2.234(3) Å). This is a likely reflection of the lower coordination number of the yttrium centre in **3** and less strain in the bis(phenolate)-amino ligand. These trends were also observed in the corresponding samarium complexes, **1.24**, **1.25** and **2.2**.[2, 4, 40]

Regarding **5**, the Sc(1)–O(1) (2.0113(19) Å) and Sc(1)–O(2) (2.0759(17) Å) bond lengths were comparable to those observed in Mountford's Sc(O_2N^{py})(Cl)(py) (**2.12**) complex[28] (2.002(4) and 1.968(4) Å) and Okuda's 1,ω-dithiaalkanediyl species, Sc($O^{tBu,Me}$-S-C_3-S-$O^{tBu,Me}$){$N(SiHMe_2)_2$}(THF) (**1.29**) (2.004(4) and 2.007(4) Å).[29] Shorter Sc–O distances of 1.889(5), 1.854(5) and 1.865(5) Å were observed in Lappert's three coordinate scandium tris(phenolate), Sc(O-2,4,6-$C_6H_2{}^tBu_2Me)_3$ (**2.13**), where the ligands were non-chelating.[75] Despite the pyridyl donor arm, the N(1)–

Sc(1)–N(2) bite angle of 72.19(8)° was greater than that observed in **1** but similar to that seen in **2.12** (73.2(2)°).

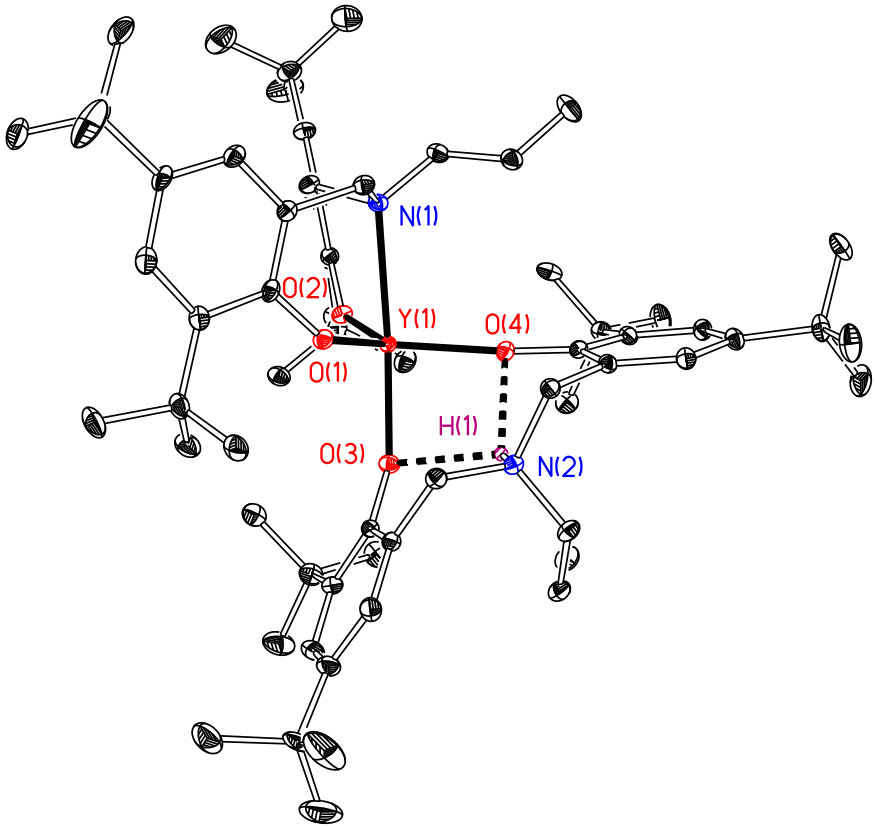

Figure 2.4. Molecular structure of $Y(O_2N^{Me})(HO_2N^{Me})$ (**3**), drawn at the 20% probability level. C-bound H atoms and pentane of crystallisation omitted. Selected bond lengths (Å) and angles (°): Y(1)–O(1) 2.140(3), Y(1)–O(2) 2.102(3), Y(1)–O(3) 2.161(3), Y(1)–O(4) 2.135(3), Y(1)–N(1) 2.567(3), N(1)–H(1) 0.865(10), O(3)•••H(1) 2.33(4), O(4)•••H(1) 2.21(3); O(1)–Y(1)–O(2) 120.99(12), O(1)–Y(1)–O(4) 119.64(12), O(2)–Y(1)–O(4) 117.26(12), O(1)–Y(1)–O(3) 89.60(11), O(2)–Y(1)–O(3) 108.89(11), O(3)–Y(1)–O(4) 85.87(11), O(1)–Y(1)–N(1) 78.35(11), O(2)–Y(1)–N(1) 80.77(11), O(4)–Y(1)–N(1) 96.93(11).

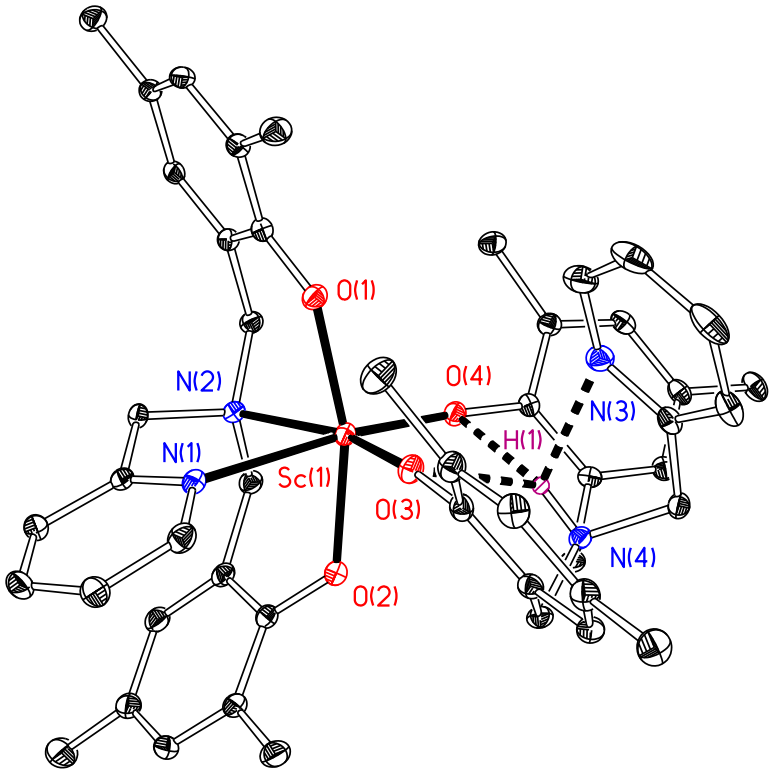

Figure 2.5. Molecular structures of $Sc(O_2N^{py})(HO_2N^{py})$ (**5**), drawn at the 20% probability level. C-bound H atoms omitted. Selected bond lengths (Å) and angles (°): Sc(1)–O(1) 2.0113(19), Sc(1)–O(2) 2.0759(17), Sc(1)–O(3) 1.9896(19), Sc(1)–O(4) 2.0028(18), Sc(1)–N(1) 2.370(2), Sc(1)–N(2) 2.369(2), N(4)–H(1) 0.92(3), N(3)•••H(1) 2.14(3), O(3)•••H(1) 2.33(3), O(4)•••H(1) 2.15(3); O(1)–Sc(1)–O(2) 163.12, O(3)–Sc(1)–O(4) 92.09(8), O(4)–Sc(1)–N(2) 96.88(8), O(3)–Sc(1)–N(1) 90.13(8), N(1)–Sc(1)–N(2) 72.19(8).

2.6 Further ROP studies with zwitterions

Not having direct scandium and yttrium zwitterion analogues limited the conclusions that could be drawn from structure-activity investigations. Nevertheless, the scandium zwitterions **4**–**7** were tested as catalysts for the ROP of *rac*-LA under the conditions described in Table 2.2 ([*rac*-LA]$_0$:[BnNH$_2$]$_0$:[Sc]$_0$ = 100:5:1). Compounds **5**–**7** appeared to be inactive, even after a period of several hours. Compound **4,** on the other hand, showed some activity, with 35% conversion achieved after 1 h and 59% conversion achieved after 4 h (the reduced activity is attributed to the smaller metal centres and was noted by Okuda[31]). There was excellent agreement between experimental and theoretical M_n, 1,830 g mol^{-1} and 1,700 g mol^{-1} respectively, based on one chain per amine. The polydispersity was narrow (PDI = 1.11) and there was little evidence of transesterification according to the MALDI-ToF mass spectrum of the isolated PLA. However, heterotactic enrichment was not evident (P_r = 0.65), so **4** could not replicate the Y(O$_2$N^{NMe2})(HO$_2$N^{NMe2}) (**1**) system fully. The lower activity of Sc(O$_2$N^{py})(HO$_2$N^{py}) (**4**) was not ideal for high-throughput type study in this instance and no further studies were undertaken.

Y(O$_2$N^{OMe})(HO$_2$N^{OMe}) (**2**) and Y(O$_2$N^{Me})(HO$_2$N^{Me}) (**3**) were also tested under the conditions, [*rac*-LA]$_0$:[BnNH$_2$]$_0$:[Y]$_0$ = 100:5:1, and the results are summarised in Table 2.3. The M_n(GPC) of poly(*rac*-LA) produced by **2** (3,340 g mol^{-1}) was higher than that expected, M_n(calcd) = 2,790 g mol^{-1} and in a duplicate run with **1**, good agreement was observed once more (M_n(GPC) = 2,600 g mol^{-1}, M_n(calcd) = 2,730 g mol^{-1}). Furthermore, the level of heterotactic enrichment was not as high with **2** (P_r = 0.83) and the MALDI-ToF mass spectrum of isolated poly(*rac*-LA) showed a significant distribution of tranesesterification products. Better agreement between M_n(GPC) = 2,790 g mol^{-1} and M_n(calcd) = 2,730 g mol^{-1} and a narrow PDI = 1.12 was observed with **2** when the reaction time was reduced to 10 mins. However, transesterification products were present in the MALDI-ToF mass spectrum of this PLA. The P_r value of 0.83 was consistent with that reported by Carpentier for Y(O$_2$N^{OMe}){N(SiHMe$_2$)$_2$}(THF) (**1.14**), which was described as a "non-optimal system".[14, 15] Compound **3** behaved like its samarium analogue **2.2** and Sm(O$_2$N^{Me})(BH$_4$)(THF)$_2$ (**1.26**) in that the activity of the catalyst was severely diminished by the absence of a pendant arm donor. Monitoring the reaction over time,

54% conversion was achieved after 3.5 h at which point the catalyst was no longer active.

Table 2.3. Comparative ROP data between yttrium zwitterions using $BnNH_2$.[a]

Zwitterion	Conv. (%)[b]	M_n(calcd)[c] (g mol^{-1})	M_n(GPC)[d] (g mol^{-1})	M_w/M_n[d]	P_r[e]
$Y(O_2N^{NMe2})(HO_2N^{NMe2})$ (**1**)	91	2,730	2,600	1.14	0.92
$Y(O_2N^{OMe})(HO_2N^{OMe})$ (**2**)	93	2,790	3,340	1.17	0.83
$Y(O_2N^{OMe})(HO_2N^{OMe})$ (**2**)	91[f]	2,730	2,790	1.12	[g]
$Y(O_2N^{Me})(HO_2N^{Me})$ (**3**)	0	-	-	-	-
$Y(O_2N^{Me})(HO_2N^{Me})$ (**3**)	54[h]	[g]	[g]	[g]	[g]

[a] [*rac*-LA]$_0$:[$BnNH_2$]$_0$:[Y]$_0$ = 100:5:1, 2 mL THF, [*rac*-LA]$_0$ = 0.69 M, rt, 20 mins. [b] Measured by ^{1}H NMR in $CDCl_3$. [c] M_n(calcd) = (Conv. (%) × 144.1/5 + 107.2) assuming one chain per $BnNH_2$. [d] Measured by GPC against polystyrene standards using the appropriate Mark-Houwink corrections for poly(*rac*-LA) in THF at 30 °C. [e] Determined from integration of appropriate tetrads in ^{1}H-{^{1}H} NMR spectra. [f] 10 min run. [g] Not measured. [h] Conversion recorded after 3.5 h.

2.6.1 Loading experiments

Given the superiority of **1** compared to related yttrium zwitterions and the heavier lanthanide analogues, the remainder of the results described in this Chapter and Chapter Three detail ROP studies undertaken using **1** as the catalyst. A standard polymerisation reaction involving addition of a *rac*-LA solution to a mixture of $BnNH_2$ and **1** at room temperature is described by Equation 2.1.

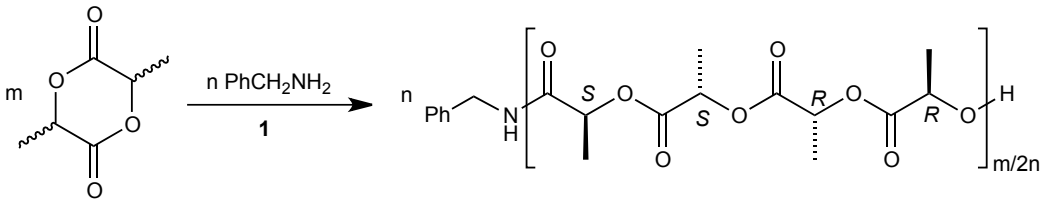

Equation 2.1

In light of the high control over polymer growth in this system, variation of the reaction stoichiometry has been shown to directly affect observed M_n(GPC). In a series of individual polymerisation experiments, the initial molar equivs. of $BnNH_2$ were varied from 1–5, with [*rac*-LA]$_0$:[Y]$_0$ kept constant at 100:1. Each reaction was run to high conversion (≈ 90% after 20 min) and quenched with THF (as supplied).

Data from these experiments are presented graphically in Figure 2.6, where each point represents a unique test run.

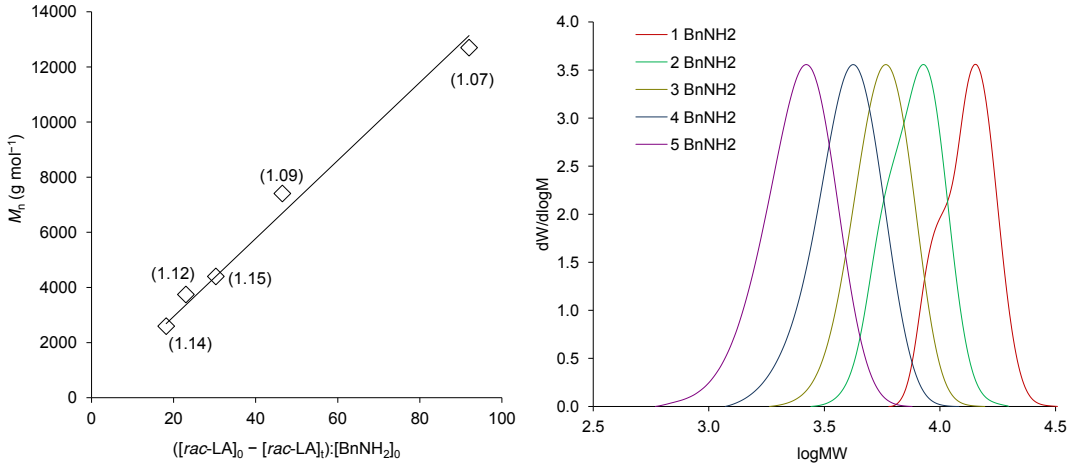

Figure 2.6. Representations of M_n(GPC) as a function of [*rac*-LA]$_0$:[BnNH$_2$]$_0$. The PDIs are given in parentheses. Vertical-axis intercept of M_n *vs*. ([*rac*-LA]$_0$ – [*rac*-LA]$_t$):[BnNH$_2$]$_0$ plot set to 107.2 g mol^{-1} (M_R BnNH$_2$).

There was excellent agreement between the expected and observed polymer M_n, and the PDIs were narrow in each instance. For example, when [*rac*-LA]$_0$:[BnNH$_2$]$_0$:[**1**]$_0$ = 100:3:1, M_n(GPC) = 4,400 g mol^{-1} and M_n(calcd) = 4,470 g mol^{-1}, with a PDI of 1.15. The gradient of least-squares fit, 142(8) g mol^{-1} (R^2 = 0.991), was representative of the relative molecular mass of a lactide unit and elegantly demonstrated the linear relationship between M_n(GPC) and [*rac*-LA]$_0$:[BnNH$_2$]$_0$. There was a shoulder on the distribution plot representing [*rac*-LA]$_0$:[BnNH$_2$]$_0$:[**1**]$_0$ = 100:1:1 (Figure 2.6, right), indicating the possible presence of a secondary distribution. Since **1** is an active catalyst without the addition of BnNH$_2$, and there was a low concentration of BnNH$_2$ in this run, polymerisation may have been initiated by another competing pathway hence the appearance of a shoulder. An excess of BnNH$_2$ is likely to be required in order to suppress competing initiating pathways or to ensure that the rate of amine-initiation is more competitive than propagation in these reactions.

In a complimentary series of runs, M_n control was demonstrated by holding [BnNH$_2$]$_0$:[**1**]$_0$ constant at 3:1 but [*rac*-LA]$_0$:[**1**]$_0$ was varied between 50, 100, 150, 200 and 250 equivs., with the concentration of [*rac*-LA]$_0$ kept constant throughout at 0.69 M or 0.10 g mL^{-1}. Data from these experiments are presented graphically in Figure 2.7. Since M_n(GPC) was plotted against [*rac*-LA]$_0$:[**1**]$_0$, the gradient of least-squares fit based on the fitted line was 49(4) g mol^{-1} (R^2 = 0.982), approximately

equal to 144.1/3. Higher loading experiments where $[rac\text{-LA}]_0:[BnNH_2]_0:[\mathbf{1}]_0$ = 1000:5:1 and 2000:5:1 were performed to demonstrate catalyst tolerance. With the 1000:5:1 run, 86% conversion was achieved after 1 h, with M_n(GPC) = 21,750 g mol^{-1} and PDI = 1.06 (M_n(calcd) = 24,900 g mol^{-1}). A conversion of 83% was reached after 2 h during the 2000:5:1 run and the calculated and observed M_n were 47,960 and 39,100 g mol^{-1}, with PDI = 1.06. This conversion rate represents 1,660 monomer turnovers and was comparable to that recorded by Carpentier using bis(phenolate)-amino yttrium catalysts.[14, 15]

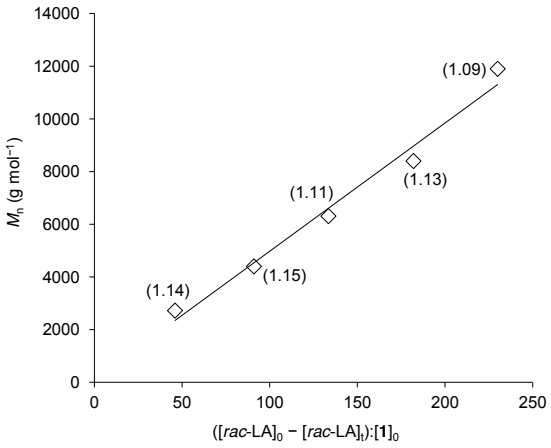

Figure 2.7. M_n(GPC) as a function of ($[rac\text{-LA}]_0 - [rac\text{-LA}]_t$):$[\mathbf{1}]_0$. The PDIs are given in parentheses. Vertical-axis intercept set to 107.2 g mol^{-1} (M_R $BnNH_2$).

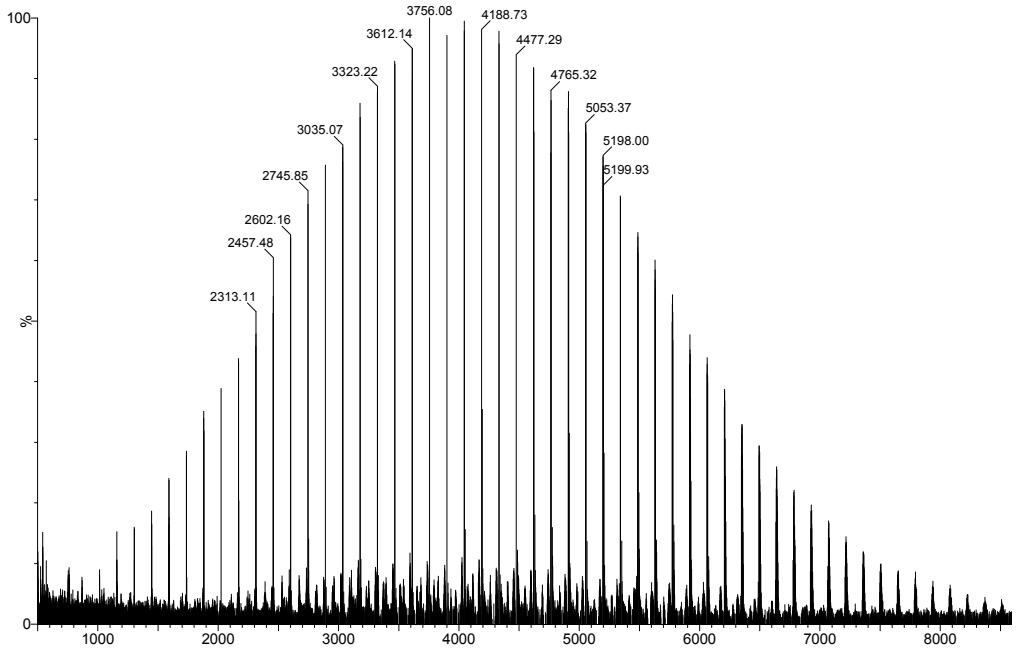

Figure 2.8. Full MALDI-ToF mass spectrum of isolated poly(*rac*-LA) for the run $[rac\text{-LA}]_0:[BnNH_2]_0:[\mathbf{1}]_0$ = 100:3:1. K^+ dopant, $\Delta(m/z)$ = 144 g mol^{-1}.

MALDI-ToF mass spectra also confirmed the incremental increase of M_n and a spectrum for the 100:3:1 run is presented in Figure 2.8. Poly(*rac*-LA) products were consistent with benzyl amine derived end-groups and heterotactic enrichment remained above 90% ($P_r > 0.9$).

2.6.2 Scope of functional end-group incorporation

There has been considerable interest in incorporating end-group functionality into PLA chains. A range of terminating groups from simple organics such as amides or esters, to highly functional natural products have been investigated.[76] The aim of these studies is to improve PLA compatibility for specific functions such as vehicles for drug delivery or the grafting of PLA onto surfaces.[77] Multi-step preparations to generate functionalised PLA can be successfully performed with pre-prepared PLA, but an attractive strategy for polymer chemists is to simultaneously generate PLA with end-group incorporation in a "one-pot" method.[78]

Table 2.4. Scope of end-group functionalisation in amine-initiated, immortal ROP.[a]

Co-initiator	Conv. (%)[b]	M_n(calcd) (g mol^{-1})[c]	M_n(GPC) (g mol^{-1})[d]	M_w/M_n[d]	P_r[b]
-	87	12,500	33,800	1.50	0.91
$BnNH_2$	91	2,770	2,600	1.14	0.95
$^{n}PrNH_2$	91	2,680	3,030	1.17	0.89
Piperidine	90	2,680	2,810	1.19	0.90
$^{t}BuNH_2$	92	2,730	14,800	1.56	0.92
$^{t}BuNH_2$[e]	50	361	7,600	1.41	0.91
$^{t}BuNH_2$[f]	36	1,110	6,260	1.25	0.92
BnOH	90	2,700	2,620	1.19	0.92
$^{i}PrOH$	89	2,630	4,160	1.35	0.95

[a] [*rac*-LA]$_0$:[Co-initiator]$_0$:[**1**]$_0$ = 100:5:1, 2 mL THF, [*rac*-LA]$_0$ = 0.69 M, rt, 20 mins. [b] Conversion and P_r (by integration of appropriate tetrads) measured by ^{1}H and ^{1}H-{^{1}H} NMR ($CDCl_3$). [c] M_n(calcd) = (Conv. (%) × [*rac*-LA]$_0$:[Co-initiator]$_0$ × 144.1 + M_R Co-initiator). [d] Measured by GPC against polystyrene standards using the appropriate Mark-Houwink corrections for poly(*rac*-LA) in THF at 30 °C. [e] [*rac*-LA]$_0$:[Co-initiator]$_0$:[**1**]$_0$ = 20:5:1. [f] [*rac*-LA]$_0$:[Co-initiator]$_0$:[**1**]$_0$ = 20:1:1.

In light of the $[rac\text{-LA}]_0:[BnNH_2]_0:[\mathbf{1}]_0$ system reliably producing benzyl amine-capped PLA, different primary and secondary amines and alcohols were included in the polymerisation mixture. Under the conditions specified in Table 2.4, benzyl amine was replaced by *n*-propyl amine, *tert*-butyl amine, piperidine ($C_5H_{10}NH$), benzyl alcohol and *iso*-propyl alcohol. Initial analysis showed that systems incorporating *n*-propyl amine, the secondary amine piperidine and benzyl alcohol, a widely used chain transfer agent in immortal ROP, behaved like the benzyl amine system. M_n(GPC) ≈ 2,800 g mol^{-1} were generally reflective of one PLA chain forming per equivalent of co-initiator and PDIs were narrow (PDI = 1.14–1.19). These polymers were isolated and characterised by ^{1}H and ^{13}C-{^{1}H} NMR, GPC and MALDI-ToF MS methods.

There was some evidence of transesterification side reactions in the polymerisation reaction involving piperidine and the MALDI-ToF mass spectrum of piperidine-capped poly(*rac*-LA) is shown in Figure 2.9. Although the major distribution is representative of this polymer product, there is a distribution representing transterification products, which were not seen in benzyl amine, benzyl alcohol or *n*-propyl amine-capped poly(*rac*-LA). The origin of the transesterification remains unclear, but this observation represents a limitation of the bulkier secondary amine.

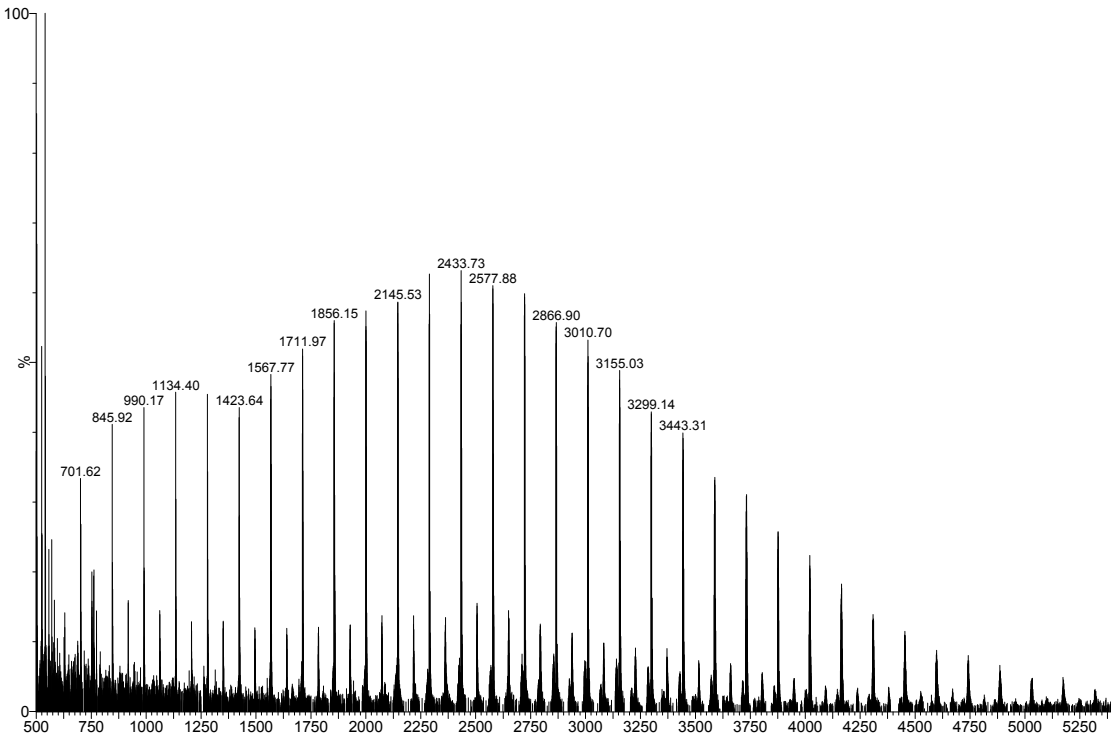

Figure 2.9. Full MALDI-ToF mass spectrum of piperidine-capped poly(*rac*-LA) ($[rac\text{-LA}]_0:[\text{piperidine}]_0:[\mathbf{1}]_0$ = 100:5:1). K^+ dopant, Δ(*m/z*) = 144 g mol^{-1}.

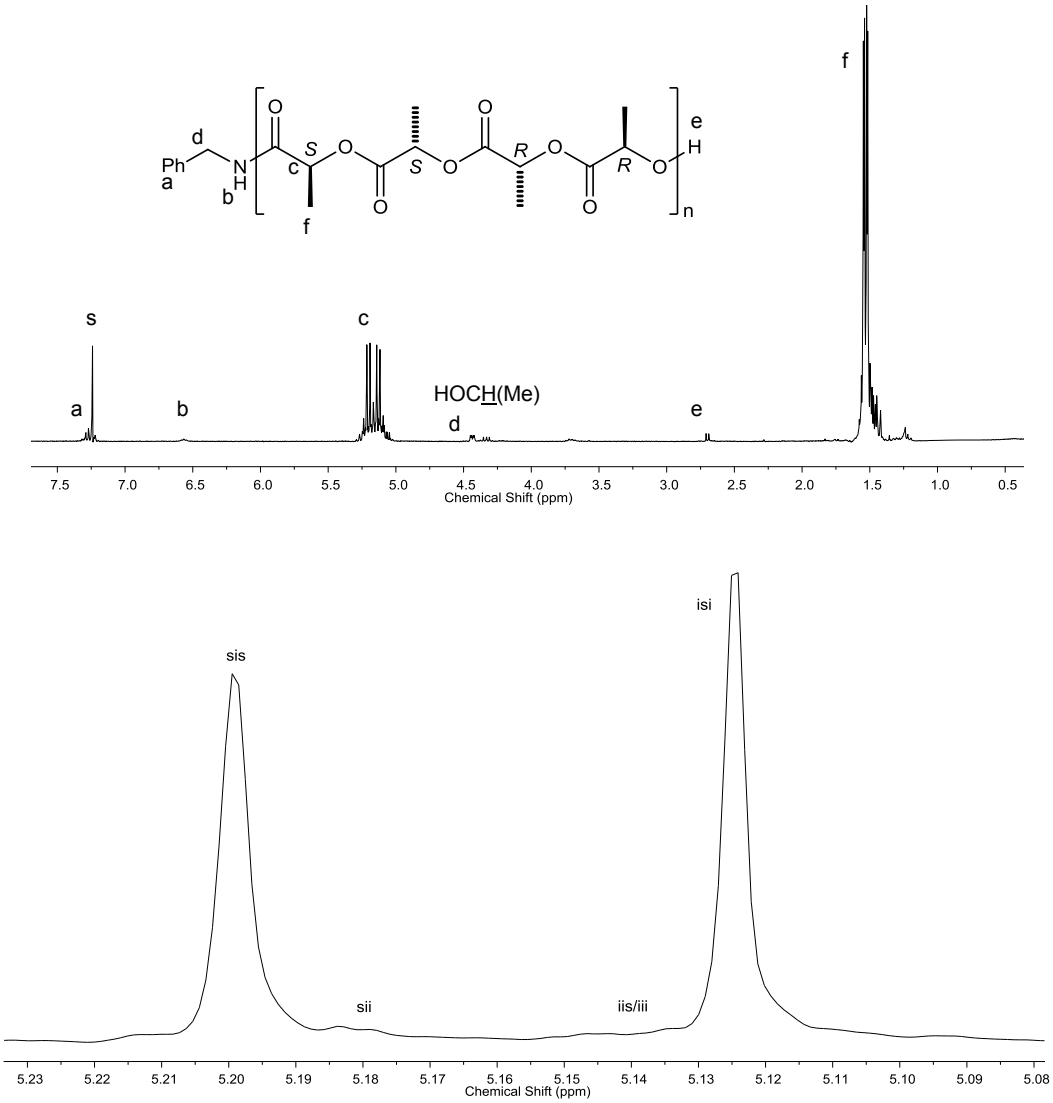

Figure 2.10. ^{1}H NMR (299.9 MHz, $CDCl_3$, 298 K) spectrum (top) of benzyl amine-capped poly(*rac*-LA), BnNH-[PLA]-H and a typical ^{1}H-{^{1}H} NMR spectrum (299.9 MHz, $CDCl_3$, 298 K) (bottom) of the methine region of poly(*rac*-LA) featuring high heterotactic enrichment. Residual protio-solvent, δ = 7.24 ppm.

The ^{1}H NMR spectrum of BnNH-[PLA]-H is shown in Figure 2.10 along with a typical homonuclear decoupled ^{1}H-{^{1}H} NMR spectrum of poly(*rac*-LA) displaying heterotactic enrichment. The internal poly(*rac*-LA) resonances were clearly visible in the ^{1}H NMR spectrum (Figure 2.10, top), with overlapping methyl doublets at *ca.* 1.5 ppm and overlapping methine quartets at *ca.* 5.2 ppm. This pattern is indicative of poly(*rac*-LA) with heterotactic enrichment. In atactic poly(*rac*-LA), which has random stereosequences, the methyl and methine regions appear as scrambled multiplets. When the methyl and methine protons are decoupled (Figure 2.10,

bottom), the overlapping methine quartets resolve as singlets, corresponding to the *sis* and *isi* tetrads.[11, 13, 15, 59-70] ^{13}C-{^{1}H} NMR spectra of poly(*rac*-LA) samples were also consistent with a high degree of heterotactic enrichment.[71, 72, 79] The benzyl amine end-group was also resolved, with phenyl resonances at *ca*. 7.2 ppm, a NH peak at *ca*. 6.6 ppm and the PhC$\underline{H}_2$NH– methylene protons at *ca*. 4.4 ppm. The HOC$\underline{H}$(Me)– environment, adjacent to the hydroxyl terminus appeared upfield from the PhC$\underline{H}_2$NH– methylene group at *ca*. 4.3 ppm. These signals integrated against each other in the expected 2:1 ratio. The doublet present at *ca*. 2.7 ppm was assigned to the terminating hydroxyl proton.

Addition of *tert*-butyl amine had the effect of reducing polymer M_n compared to the polymerisation of *rac*-LA without the inclusion of a co-initiator (Table 2.4). The observed M_n(GPC) = 14,800 g mol^{-1} for the [*rac*-LA]$_0$:[^{t}BuNH$_2$]$_0$[**1**]$_0$ = 100:5:1 run resembled one PLA chain per metal forming and broader polydispersities (1.25–1.56) indicated the poorer performance of these systems. M_n(GPC) = 4,160 g mol^{-1} was also higher than expected (M_n(calcd) = 2,630 g mol^{-1}, PDI = 1.35) when ^{i}PrOH was employed as the co-initiator despite the MALDI-ToF mass spectra of respective crude samples showing the presence of *tert*-butyl amine and ^{i}PrOH capped-poly(*rac*-LA) chains. The lack of M_n control could be attributed to slow initiation with respect to propagation, hence the higher than expected molecular weights and broader PDIs, arising through incomplete initiation or competing initiation pathways. Carpentier and Okuda have shown that ^{i}PrOH is an effective co-initiator so its lack of success in this case is disappointing.[14, 15, 30] The results in Table 2.4 demonstrated that amine-initiated, immortal ROP could be extended to other co-initiators albeit with some limitations, i.e. the bulkier *tert*-butyl amine.

2.7 Kinetic and mechanistic studies with $Y(O_2N^{NMe2})(HO_2N^{NMe2})$ (1)

The loading experiments (Figures 2.6 and 2.7) have demonstrated that M_n can be tuned by both variation of [*rac*-LA]$_0$:[$BnNH_2$]$_0$ and [*rac*-LA]$_0$:[**1**]$_0$, as described in many previous works, utilising alcohol co-initiators. Many of the literature catalysts used for immortal ring-opening polymerisation feature a bound M–OR moiety as well as an additional excess of ROH and propose that initiation occurs *via* a coordination-insertion mechanism. According to this model, Figure 2.2 (*vide supra*), the remaining ROH is consumed rapidly by exchanging with M-[LA]$_x$-OR to form M–OR which, in turn, ring-open lactide units. Propagation is mediated by the metal with facile chain transfer processes between active M-[LA]$_x$-OR and dormant H-[PLA]-OR. Despite many of these studies demonstrating immortal behaviour, full kinetic investigations are often lacking.[14, 15] In a study with $Y(O^{tBu2}\text{-S-}C_3\text{-S-}O^{tBu2})\{N(SiHMe_2)_2\}(THF)$ (**1.30**) and ^{i}PrOH, Okuda determined first-order dependencies in metal and *L*-LA but did not determine the order in alcohol.[30] Initial studies with **1**, focused on the [*rac*-LA]$_0$:[$BnNH_2$]$_0$:[**1**]$_0$ system and were supported by investigations with BnOH and piperidine co-initiators. Typical ROP studies follow LA polymerisation by taking aliquots from the reaction at regular time intervals and ^{1}H NMR spectroscopy is used to measure LA consumption. These methods were used in this study and aliquots were quenched with THF (as supplied). $Y(O_2N^{NMe2})\{N(SiHMe_2)_2\}(THF)$ (**1.15**) was also studied as an established literature initiator and NMR tube scale studies probed mechanistic details further.

2.7.1 $BnNH_2$ dependence

Initial kinetic studies were performed using the polymerisation mixture, [*rac*-LA]$_0$:[$BnNH_2$]$_0$:[**1**]$_0$ = 200:3:1 (Figure 2.11). The reaction was performed on a 0.40 g LA scale in a total THF volume of 4 mL ([*rac*-LA]$_0$ = 0.69 M) at room temperature, and monitored by ^{1}H NMR ($CDCl_3$). The Conversion *vs*. Time plot (Figure 2.11, left) shows that the polymerisation reaction proceeded very quickly and approached 80% conversion after 7 mins. After this time, the rate predictably slowed as the monomer was consumed. Plots of l/[*rac*-LA]$_t$ against time (Figure 2.12, left), taken from the integrated second-order rate law, $R_{app} = k_{app}[rac\text{-LA}]^2$, suggested a second-order dependence in [*rac*-LA]$_0$. A *pseudo* first-order plot is shown in Figure 2.11 (right) as a representative example. Up to 6 mins (70% conversion) the plot was linear but then

began to deviate as the rate of monomer consumption slowed and the second-order dependency became apparent.

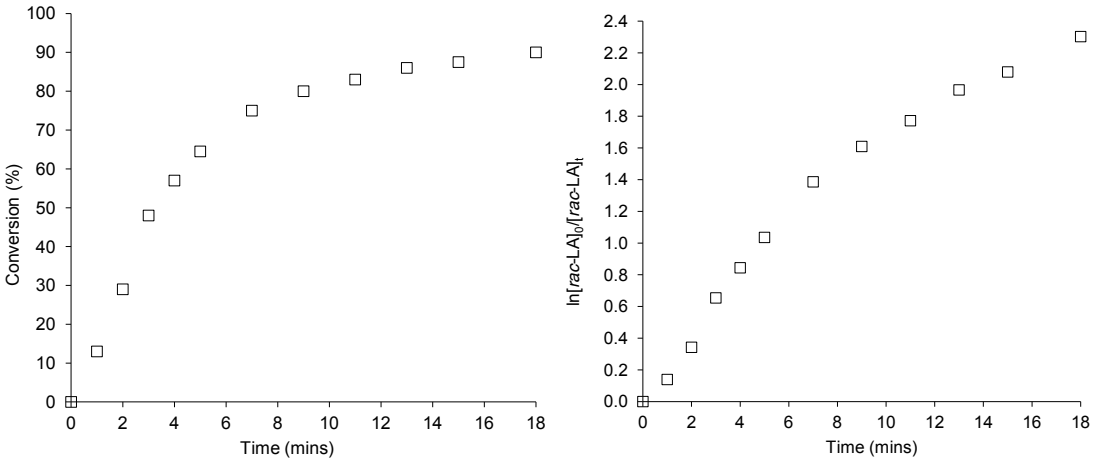

Figure 2.11. Conversion *vs*. Time (left) and semi-logarithmic plot (right) for *rac*-LA consumption for the run, $[rac\text{-LA}]_0$:$[BnNH_2]_0$:$[\mathbf{1}]_0$ = 200:3:1.

In further runs, the $[rac\text{-LA}]_0$:$[\mathbf{1}]_0$ ratio was kept constant at 200:1 ($[\mathbf{1}]_0$ = 0.003 M), but $[BnNH_2]_0$ was increased between 2 (0.007 M), 4 (0.014 M) and 6 (0.021 M) molar equivs. Based on the plots in Figure 2.12 (left), there was no systematic variation in the apparent rate constants, which were determined as k_{app} = 0.783(24) (R^2 = 0.991), 0.712(18) (R^2 = 0.994), 0.816(25) (R^2 = 0.992) and 0.824(24) (R^2 = 0.992) M^{-1} min^{-1} for $[rac\text{-LA}]_0$:$[BnNH_2]_0$ = 200:2, 200:3, 200:4 and 200:6. Each line of least-squares fit intercepted the vertical axis at *ca*. 0.8–0.9 M^{-1}, which was indicative of a minor induction period, given that the fitted lines of least-squares fit should intercept the vertical axis at 1.44 M^{-1} ($1/[rac\text{-LA}]_0$). However, this induction period was included in the propagation model in light of the appreciable conversion rates in the first minute of the reaction. No dependence in $[BnNH_2]_0$ indicated that consumption of $BnNH_2$ to generate the initially formed macromonomers was a fast step and that propagation was limited by the metal. M_n *vs*. Conversion plots (Figure 2.12, right and Table 2.5 (*vide infra*)) demonstrated that polymer chain growth occurred in a linear fashion and that $BnNH_2$ did not serve to scramble or average polymer chains in a post-polymerisation process. As determined in the loading studies, M_n(GPC) were reflective of $[rac\text{-LA}]_0$:$[BnNH_2]_0$ and polydispersity indices were narrow for all points measured (1.05–1.15).

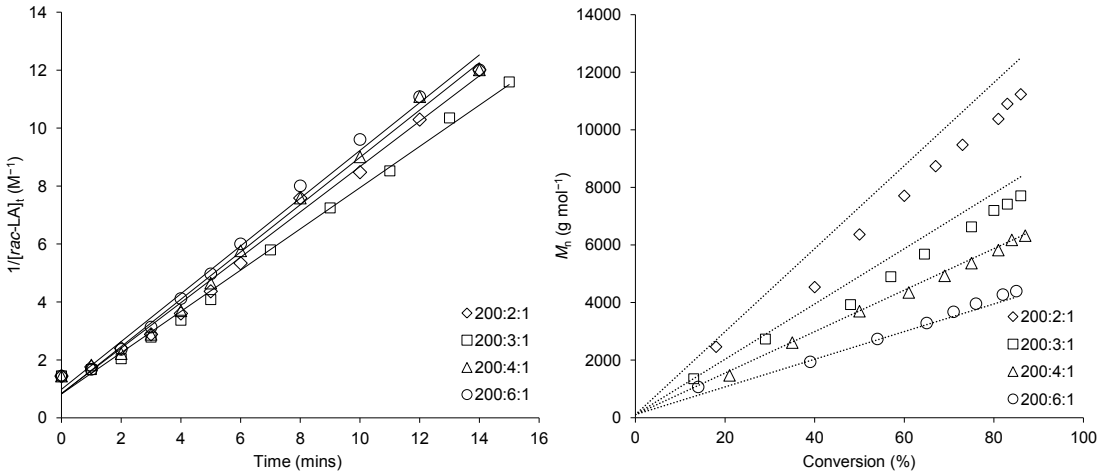

Figure 2.12. Left, second-order rate plots for the runs $[rac\text{-LA}]_0$:$[BnNH_2]_0$:$[\mathbf{1}]_0$ = 200:2, 3, 4 and 6:1, with k_{app} = 0.783(24) (R^2 = 0.991), 0.712(18) (R^2 = 0.994), 0.816(25) (R^2 = 0.992) and 0.824(24) (R^2 = 0.992) M^{-1} min^{-1}. The vertical-axis intercepts of the plots are 0.843(178), 0.826(145), 0.829(183) and 0.986(176) M^{-1}, with the expected intercept $1/[rac\text{-LA}]_0$ = 1.44 M^{-1}. Right, measured M_n(GPC) plotted against Conversion. The dashed lines represent M_n(calcd) and PDIs = 1.05–1.15.

2.7.2 Metal dependence

Appropriate runs were performed to determine the dependence of the metal on the overall rate law for propagation. Given that $k_{app} = k_p[\mathbf{1}]^x$, $[rac\text{-LA}]_0$:$[BnNH_2]_0$ was held at 200:6 and $[\mathbf{1}]_0$ was increased through 1–4 molar equivs. ($[\mathbf{1}]_0$ = 0.003 M, 0.007 M, 0.010 M and 0.014 M). It was important to ensure an excess of $BnNH_2$ throughout, as **1** is active without $BnNH_2$. For example, when 200 equivs. of *rac*-LA were added to **1** in the absence of a co-initiator, 70% conversion of monomer to poly(*rac*-LA) was achieved within 18 mins but an induction period of *ca*. 7 mins, with no apparent conversion was recorded.

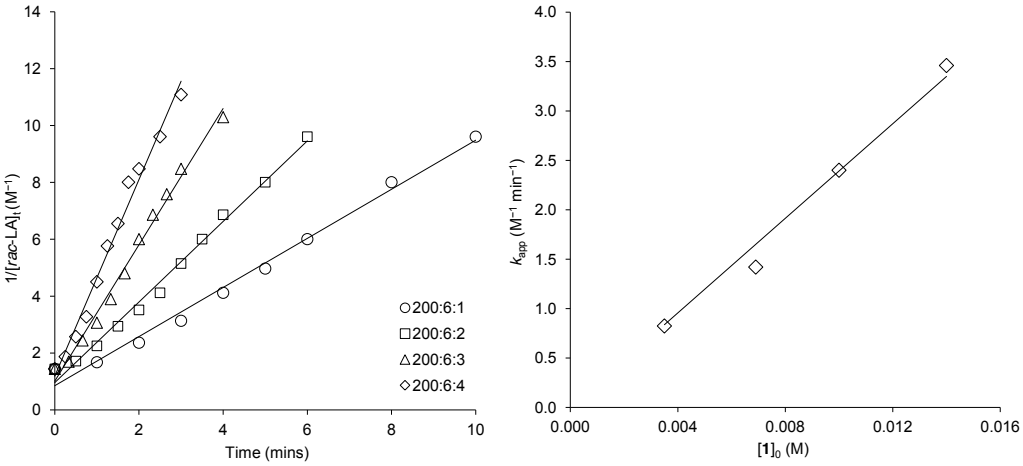

Figure 2.13. Left, second-order rate plots for the runs [*rac*-LA]$_0$:[BnNH$_2$]$_0$:[**1**]$_0$ = 200:6:1, 2, 3 and 4, with k_{app} = 0.824(24) (R^2 = 0.992), 1.417(43) (R^2 = 0.992), 2.398(76) (R^2 = 0.991) and 3.459(141) (R^2 = 0.985) M^{-1} min^{-1}. The vertical-axis intercepts of the plots are 0.986(176), 0.956(136), 1.008(159) and 1.183(225) M^{-1}, with the expected intercept, 1/[*rac*-LA]$_0$ = 1.44 M^{-1}. Right, linear plot of k_{app} against [**1**]$_0$, k_p = 239(8) (R^2 = 0.984) M^{-2} min^{-1}.

As expected, reaction times were shortened as the metal concentration was increased. Second-order rate plots are shown in Figure 2.13 (left) along with plots of apparent rate constants against [**1**]$_0$ (Figure 2.13, right), confirming the first-order dependence in **1**. The overall propagation rate law was determined as $R_p = k_p$[*rac*-LA]^2[**1**], with k_p = 239(8) M^{-2} min^{-1}. It should be noted that **1** is a pre-catalyst and is likely to transform into an active species, **1*** and it could be more appropriate to express the propagation rate law as $R_p = k_p$[*rac*-LA]^2[**1***], with [**1***] = [**1** − *x*]. Attempts have been made to model pre-catalyst activation during initiation for olefin polymerisation catalysts, as well as the formation of latent sites or permanent deactivation during propagation.[80-83] In light of the linear relationship between k_{app} and [**1**]$_0$ (Figure 2.13), the proportion of [**1**]$_0$ transformed into an active species and any subsequent deactivation appears consistent. Inconsistences may appear at higher *rac*-LA loadings as the concentration of intrinsic impurities, relative to [**1**]$_0$ increases.

Interestingly, observed polymer molecular weights were consistent with [*rac*-LA]$_0$:[BnNH$_2$]$_0$ = 200:6 and independent of [**1**]$_0$ (Figure 2.14 and Table 2.5). In light of the observed dependencies on the overall propagation rate law it is proposed that initiation is a fast with respect to propagation and all of the BnNH$_2$ is consumed in this process to generate an equivalent number of growing macromonomers.

Consistent with a coordination-insertion mechanism, propagation occurs at the metal centre, with growing and dormant chains in fast exchange to ensure molecular weight and PDIs are controlled. This also demonstrated that a higher catalyst loading may be used if necessary to overcome any detrimental catalyst deactivation.

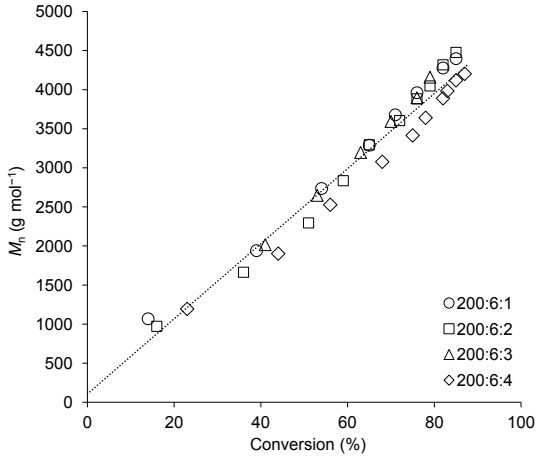

Figure 2.14. Plots of M_n(GPC) *vs*. Conversion demonstrating the independence of M_n(GPC) with respect to [**1**]$_0$. The dashed line represents M_n(calcd) based on [*rac*-LA]$_0$:[$BnNH_2$]$_0$ = 200:6 and PDIs ranged from 1.09–1.12.

Table 2.5. Summary of kinetic and molecular weight data from ROP experiments co-initiated by $BnNH_2$ and **1**.[a]

Entry	$[rac\text{-LA}]_0$:$[BnNH_2]_0$:$[\mathbf{1}]_0$	k_{app} (M^{-1} min^{-1})[b]	R^2 [b]	Conv. (%)[c]	M_n(calcd) (g mol^{-1})[c]	M_n(GPC) (g mol^{-1})[d]	M_w/M_n [d]
1	200:2:1	0.783(24)	0.991	88	12,790	11,430	1.05
2	200:3:1	0.712(18)	0.994	88	8,520	7,910	1.10
3	200:4:1	0.816(25)	0.992	88	6,450	6,460	1.10
4	200:6:1	0.824(24)	0.992	85	4,190	4,400	1.10
5	200:6:2	1.417(43)	0.992	85	4,240	4,480	1.11
6	200:6:3	2.398(76)	0.991	79	3,900	4,160	1.10
7	200:6:4	3.459(141)	0.985	87	4,290	4,200	1.12

[a] $[rac\text{-LA}]_0$ = 0.69 M, 4 mL THF, rt. [b] Apparent second-order rate constants for consumption of *rac*-LA with standard error and R^2 determined by linear regression analysis. [c] Reactions monitored by ^1H NMR ($CDCl_3$). All quoted conversions refer to the last point where M_n(GPC) was determined. M_n(calcd) = (Conv. (%) × $[rac\text{-LA}]_0$:$[BnNH_2]_0$ × 144.1 + 107.2). [d] Measured by GPC against polystyrene standards using the appropriate Mark-Houwink corrections for poly(*rac*-LA) in THF at 30 °C.

2.7.3 Second-order dependence in [*rac*-LA]$_0$

The second-order dependence in [*rac*-LA]$_0$ is unusual but not unprecedented, with previous reports suggesting that two-lactide units must come together in the transition state or that non-innocent ligands play a role in propagation.[7, 84-86] Catalyst aggregation has also been suggested as a possible reason for second-order dependencies in [*rac*-LA]$_0$.[86] In α-olefin polymerisation studies, reaction orders in monomer concentration have been shown to vary between 0 and 2. In first-order processes the widely accepted enantiomorphic site control mechanism for stereoselective propylene polymerisation relies on the flipping of the growing polymer chain between coordination sites, which is possible if the monomer coordination site is vacant immediately after enchainment.[87-94]

Where the order in monomer concentration has exceeded 1, Ystenes has alluded to a possible trigger mechanism based on the interaction of two monomers in the transition state.[95] In this mechanism, the monomer coordination site is always occupied but a second monomer is required to force enchainment. In cases where syndiotactic poly(propylene) has resulted from propylene polymerisation in the presence of an achiral homogenous catalyst, Ystenes has proposed that the selectivity arises from the lowest energy transition state involving two propene monomers. However, this lowest energy state is based on lowest energy steric interactions and is likely to be overcome at moderate temperatures.

Regarding ROP of *rac*-LA and the proposed trigger mechanism, if the second-order dependence in [*rac*-LA]$_0$ and the heterotactic enrichment are inherently linked, two lactide monomers of opposing chirality may form a co-operative transition state that is rate-limiting with respect to facile chain transfer. However, where kinetic analysis has been performed on systems displaying heterotactic enrichment, a first-order dependence in [*rac*-LA]$_0$ has usually been observed.[37, 60, 61, 68, 85, 96-99]

A second-order regime became apparent at high conversion, when the concentration of *rac*-LA was low. The half-life, $t_{½}$, is inversely proportional to [*rac*-LA]$_0$, thus it takes a much longer time to reach full conversion at low concentration and the monomer persists in solution, as depicted in Figure 2.11 (left). According to the semi-logarithmic plot (Figure 2.11, right) and initial rates analysis, a first-order dependence in [*rac*-LA]$_0$ is plausible. The reaction may be first-order with respect to [*rac*-LA]$_0$

but the stereoselective enchainment may retard propagation further at high concentration, in addition to the usual slowing when the concentration of the monomer is low, thus a second-order model becomes appropriate.

In light of these proposals, a run with enantiopure *L*-LA was performed ([*L*-LA]$_0$:[BnNH$_2$]$_0$:[**1**]$_0$ = 200:3:1), but no conversion was recorded over a 20 minute period, consistent with the stereoselective nature of *rac*-LA polymerisations co-initiated by **1**. In another *L*-LA polymerisation experiment, [*L*-LA]$_0$:[BnNH$_2$]$_0$:[**1**]$_0$ = 100:5:1, 90% conversion of monomer to poly(*L*-LA) was achieved after 2 h, with an aliquot at 20 mins again showing no conversion. M_n(GPC) = 3,530 g mol^{-1} (PDI = 1.15) was in relatively poor agreement with M_n(calcd) = 2,700 g mol^{-1}. Kinetic analysis of *L*-LA polymerisation was not undertaken but the 200:6:1 run (Figure 2.12, *vide supra*) was repeated with [*rac*-LA]$_0$ = 1.0 M and a second-order dependence was observed once more. The second-order dependence in [*rac*-LA]$_0$ seems to be inherent to this catalytic system but its origin remains unresolved.

2.7.4 Preliminary NMR tube scale reactions and model of amine-initiated, immortal ROP

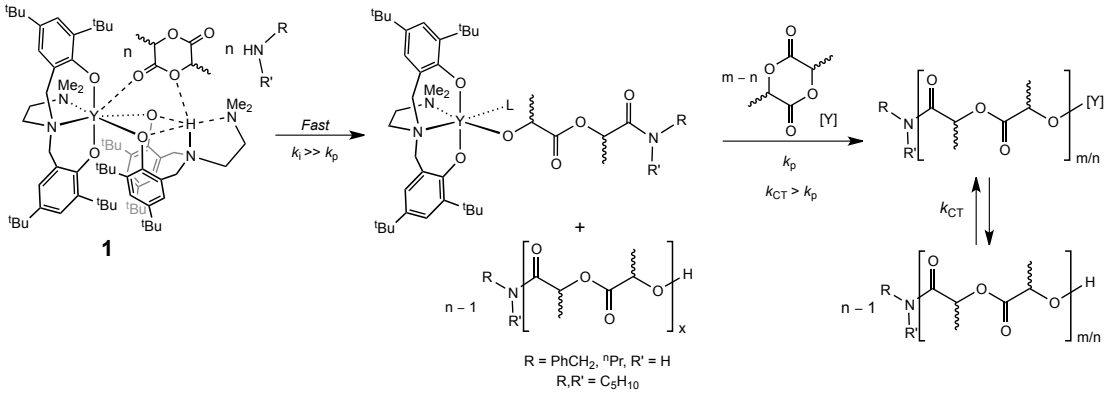

Figure 2.15. Proposed mechanism of amine-initiated, immortal ROP. L = THF, LA or PLA chelate.

NMR tube scale control experiments (C_6D_6) showed that BnNH$_2$ does not react with *rac*-LA in the absence of **1** and that BnNH$_2$ does not react with **1**. When an NMR tube scale polymerisation reaction, with the loading [*rac*-LA]$_0$:[BnNH$_2$]$_0$:[**1**] = 10:2:1 was performed in C_6D_6 or THF-d_8, one equivalent of $H_2O_2N^{NMe2}$ was shown to have been eliminated from **1** (Figure 2.16, top). Resonances corresponding to the active Y(O_2N^{NMe2})L (L = THF, LA or PLA chelate) fragment are broad in comparison to the C_s-symmetric [Y(O_2N^{NMe2})(OBn)L]$_n$ (**8**) (L = THF) species (Figure 2.17), but

resonances corresponding to benzyl amine-capped poly(*rac*-LA) are apparent, notably the methine and methyl CH(Me) internal protons (δ = 5.2 and 1.5 ppm) and benzylic environments (δ = 7.2 ppm and 4.3 ppm). Based on the experimental rate law and these NMR tube scale reactions it is proposed that initiation occurs *via* an activated-monomer type process, where $BnNH_2$ is consumed rapidly at the beginning of reaction in the ring opening of lactide units at the metal centre (Figure 2.15). Propagation then proceeds *via* coordination-insertion with facile exchange between dormant and active chains.

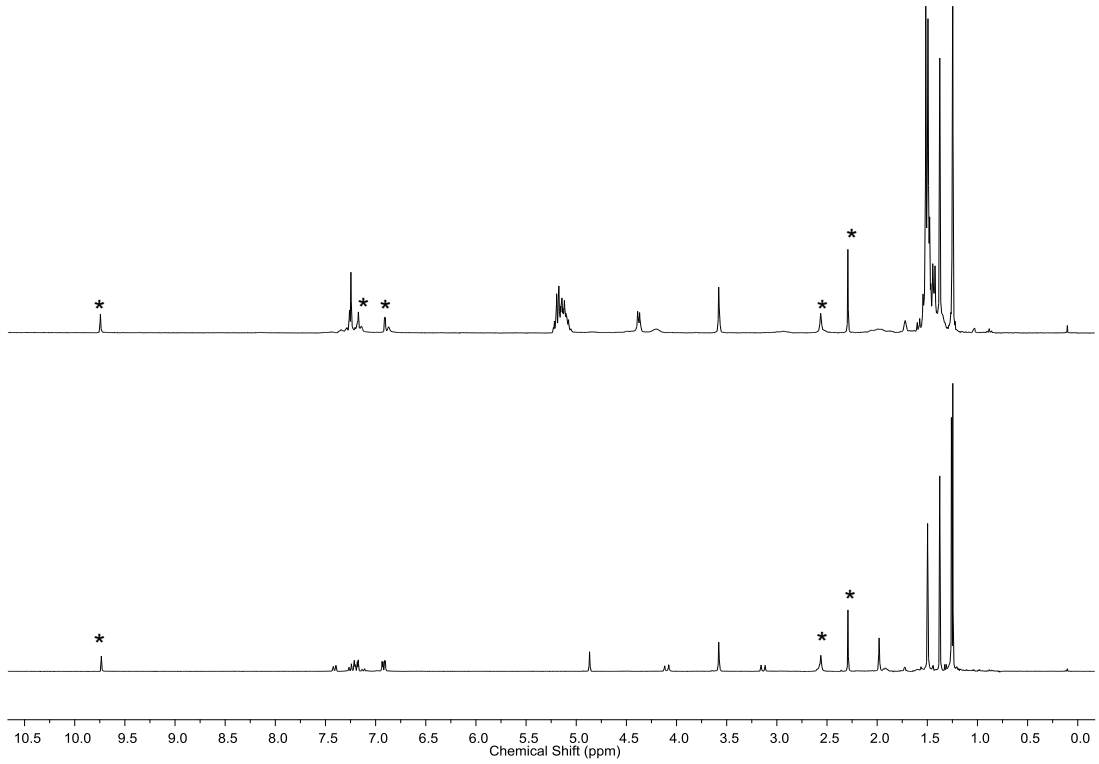

Figure 2.16. ^{1}H NMR (300.1 MHz, THF-d_8, 298 K) spectra of NMR tube scale reactions. Top, $[rac\text{-LA}]_0:[BnNH_2]_0:[\mathbf{1}]_0$ = 10:2:1. Bottom, spectrum of a 1:1 reaction between BnOH and **1**. * Denotes liberated $H_2O_2N^{NMe2}$. Residual protio-solvent, δ = 3.58 ppm.

Amine-capped macromonomers (Figure 2.15) with alcoholic end-groups are the likely protic sources responsible for removing the sacrificial HO_2N^{NMe2} ligand irrespective of the pK_as of phenols (10) and secondary alcohols (16), as well as the bidentate HO_2N^{NMe2} ligand of **1** being a chelating ligand. However, the retained proton of HO_2N^{NMe2} and competing PLA chain chelates, which have been proposed as catalyst resting states, may also force elimination.[30, 31, 61, 100-102] The poor performance of the

bimetallic complexes, $Sm(O_2N^{NMe2})(MO_2N^{NMe2})$ (M = Li (**2.8**) or Na (**2.9**)) (Table 2.2) may have resulted from inefficient elimination of MO_2N^{NMe2}, on account of the presence of the Group 1 metal. This was not investigated further but it is possible that the Group 1 metal hampers activation of *rac*-LA and attack by $BnNH_2$.

BnOH was also added to **1** and ^{1}H NMR analysis (Figure 2.16, bottom) confirmed that primary alcohols do eliminate $H_2O_2N^{NMe2}$ from the zwitterion, consistent with an observation made by Dyer using **1.24** and Feijen using **1.6** and ^{i}PrOH.[2, 103-105] The resultant complex, proposed as the C_s-symmetric $[Y(O_2N^{NMe2})(OBn)L]_n$ (**8**) species (Figures 2.16, bottom and 2.17) was not isolated but is a likely coordination-insertion type initiator. Alongside two *tert*-butyl resonances corresponding to eliminated $H_2O_2N^{NMe2}$, there were two signals corresponding to the bound bis(phenolate)-amino ligand. Aromatic protons and the singlet at δ = 4.8 ppm were assigned to the bound benzyl alkoxide, whilst characteristic diastereotopic methylene and methyl amino environments were consistent with the proposed C_s-symmetric structure. This species was stable in the presence of an excess of BnOH and since HO_2N^{NMe2} is removed during an initiation phase, propagation and chain transfer processes are likely to be mediated through a $Y(O_2N^{NMe2})L$ fragment, with a free site for propagation *via* a coordination-insertion mechanism. Polymerisation reactions using BnOH (and piperidine) were monitored by ^{1}H NMR and confirmed similar kinetic behaviour to $BnNH_2$ co-initiated ROP.

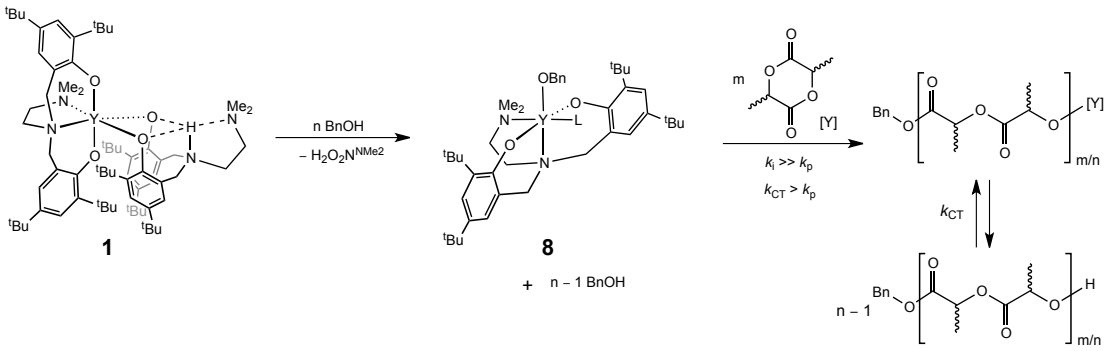

Figure 2.17. Immortal ROP using benzyl alcohol as the co-initiator. L = THF, LA or PLA chelate. **8** may also form a dimer in non-donor solvents.[30, 106]

2.7.5 Kinetic studies with BnOH and piperidine co-initiators

Investigations using BnOH and piperidine confirmed that other co-initiators behaved in a similar manner with regard to polymerisation propagation. The conditions for

these experiments were the same as those for experiments employing $BnNH_2$ as the co-initiator. Overall rate equations were determined as $R_p = k_p[rac\text{-LA}]^2[\mathbf{1}]$, with k_p determined as 290(18) M^{-2} min^{-1} for BnOH and 257(2) M^{-2} min^{-1} for piperidine. The slight variation from $k_{p,\ BnNH2}$ = 239(8) M^{-2} min^{-1} determined for $BnNH_2$ co-initiated ROP of *rac*-LA could reflect variation in initiation pathways, i.e. the direct removal of HO_2N^{NMe2} by BnOH. However, the overall rate constants are in agreement within two standard deviations. A minor induction period was observed for BnOH co-initiated polymerisations, and as in the case of analogous $BnNH_2$ co-initiated reactions, the induction period was included in the propagation model. Representative second-order rate plots for reactions using BnOH and piperidine are shown in Figure 2.18.

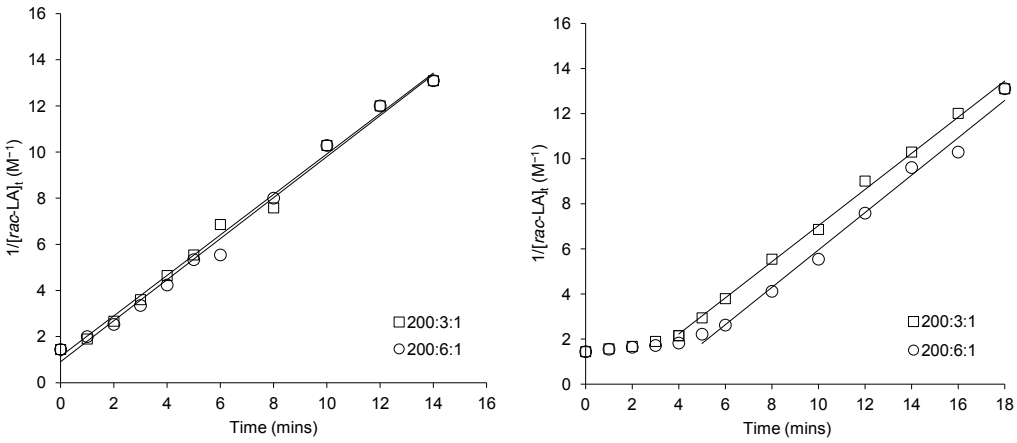

Figure 2.18. Second-order rate plots for polymerisations ([*rac*-LA]$_0$:[co-initiator]$_0$:[**1**]$_0$ = 200:3:1 and 200:6:1) co-initiated by BnOH (left), $k_{app,\ BnOH}$ = 0.877(24) (R^2 = 0.993) and 0.889(28) (R^2 = 0.992) M^{-1} min^{-1}; and piperidine (right), $k_{app,\ piperidine}$ = 0.802(16) (R^2 = 0.997) and 0.829(35) (R^2 = 0.989) M^{-1} min^{-1}. The vertical-axis intercepts of the BnOH second-order plots are 1.145(175) and 0.912(202) M^{-1}, with the expected intercept, 1/[*rac*-LA]$_0$ = 1.44 M^{-1}.

Reaction profiles for polymerisations co-initiated by BnOH were similar to $BnNH_2$, with 80% conversion achieved after 7 mins and the apparent rate constants for the reactions [*rac*-LA]$_0$:[BnOH]$_0$:[**1**]$_0$ = 200:2, 3, 4 and 6:1 were, $k_{app,\ BnOH}$ = 0.792(31) (R^2 = 0.986), 0.877(24) (R^2 = 0.993), 0.786(34) (R^2 = 0.983) and 0.889(28) (R^2 = 0.992) M^{-1} min^{-1}. With piperidine, a noticeable induction period was present that could reflect the lower nucleophilicity of the secondary amine *cf.* primary amines and alcohols. The length of this induction period was comparable to that observed in control experiments where no co-initiator was employed. However, the experimental

molecular weight data suggested that amine-initiation was the dominant initiation pathway. Apparent rate constants for the reactions [*rac*-LA]$_0$:[piperidine]$_0$:[**1**]$_0$ = 200:3 and 6:1 were, $k_{app,\ piperidine}$ = 0.802(16) (R^2 = 0.997) and 0.829(35) (R^2 = 0.989) M^{-1} min^{-1}.

Poly(*rac*-LA) molecular weights were shown to grow linearly with respect to conversion for both BnOH and piperidine co-initiated ROP reactions. Agreement between calculated and experimental M_n was excellent and PDI were narrow, ranging from 1.07–1.13 for BnOH and 1.16–1.20 for piperidine (Figure 2.19). It could be suggested that piperidine performed less well, based on the slightly broader PDI arising from slower initiation with respect to propagation.

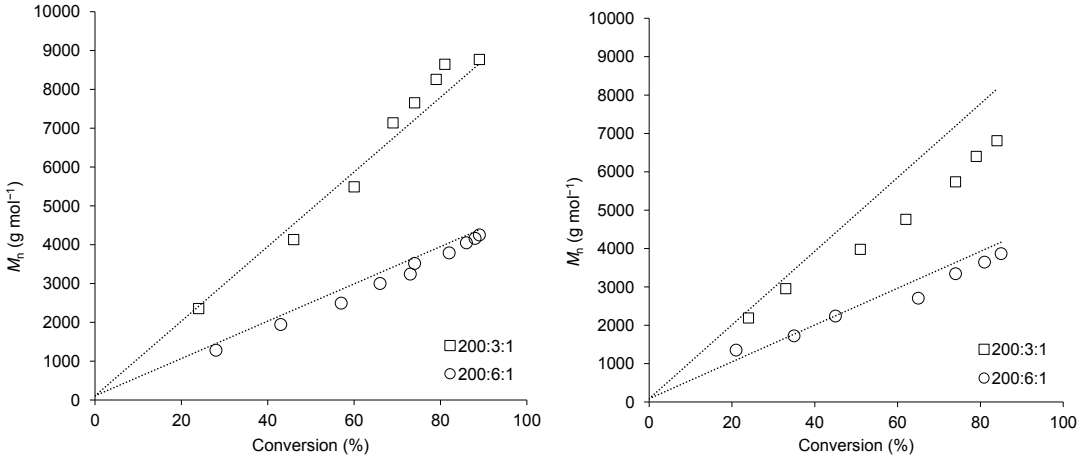

Figure 2.19. M_n(GPC) *vs*. Conversion plots for *rac*-LA polymerisations co-initiated by BnOH (left, PDIs = 1.07–1.13) and piperidine (right, PDIs = 1.16–1.20). The dashed lines represent M_n(calcd).

Polymerisation reactions co-initiated by BnOH or piperidine each displayed a linear dependency on [**1**]$_0$. As in the case of $BnNH_2$, [*rac*-LA]$_0$:[co-initiator]$_0$ was kept constant at 200:6, whilst [**1**]$_0$ was increased through 1–4 molar equivs.. Apparent rate constants, based on lines of least-squares fit were calculated as $k_{app,\ BnOH}$ = 0.889(28) (R^2 = 0.992), 1.670(23) (R^2 = 0.998), 3.346(212) (R^2 = 0.965) and 3.950(170) (R^2 = 0.984) M^{-1} min^{-1}. Plotting these rate constants against [**1**]$_0$, $k_{app} = k_p$[**1**]$_0$ (Figure 2.20), yielded the overall propagation rate constant, $k_{p,\ BnOH}$ = 290(18) M^{-2} min^{-1}. Similarly for piperidine, $k_{app,\ piperidine}$ = 0.829(35) (R^2 = 0.989), 1.757(87) (R^2 = 0.983), 2.580(85) (R^2 = 0.992) and 3.607(149) (R^2 = 0.993) M^{-1} min^{-1}. An overall propagation rate constant, $k_{p,\ piperidine}$ = 257(2) M^{-2} min^{-1} was determined in this

instance. Logarithmic plots, Figures A2.8–A2.10 (Chapter Two Appendix), also confirmed first-order dependencies in $[\mathbf{1}]_0$.

Molecular weight data were consistent with $[rac\text{-LA}]_0$:$[\text{co-initiator}]_0$ = 200:6 and can be found in Chapter Two Appendix (Figures A2.11 and A2.12). The kinetic and molecular weight data showed that the propagation processes of *rac*-LA polymerisations, initiated by **1** and a suitable co-initiator occurred *via* the same general mechanism. There were subtleties regarding initiation, but this largely reflected the nature of the co-initiator (as highlighted by the induction period with piperidine, Figure 2.18, right).

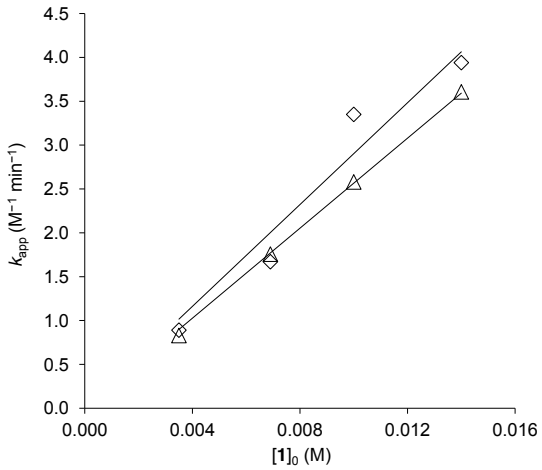

Figure 2.20. Linear plots of k_{app} *vs*. $[\mathbf{1}]_0$ for polymeriations co-initiated by BnOH (diamonds) and piperidine (triangles). Overall propagation rate constants were determined as $k_{p,\,BnOH}$ = 290(18) (R^2 = 0.944) M^{-2} min^{-1} and $k_{p,\,piperidine}$ = 257(2) (R^2 = 0.999) M^{-2} min^{-1}.

2.7.6 Initiation processes and competition experiments between co-initiators

Although chain propagation by coordination-insertion appears consistent for all suitable co-initiators, overall understanding is still limited by the initiation process. In Figure 2.15 (Section 2.7.4), it is proposed that lactide coordinates to the yttrium centre and is activated for attack by $BnNH_2$ in an activated-monomer type process. An interaction with the retained proton is depicted but investigations using model monomers to probe this possible interaction were not undertaken. As a first approximation, an empirical rate law, describing generation of an active species, **1***, could be described as $d[\mathbf{1}^*]/dt = k_i[rac\text{-LA}]^a[BnNH_2]^b[\mathbf{1}]^c$. Where initiation processes have been modelled in α-olefin polymerisations, a dependency in monomer was

determined, despite the monomer being in excess.[81-83] Using IR methods, it may be possible to quantify initiation based on consumption of the amine and when the bidentate HO_2N^{NMe2} ligand is eliminated from **1**.

However, in the case of piperidine-initiated polymerisations where there was a noticeable induction period, increasing the concentration of piperidine did not reduce the induction time. Experiments to investigate initiation directly were not attempted, but experiments where more than one co-initiator was present to try and establish relative k_i based on end-group integration and observed molecular weights were performed. Firstly, a run based on $[rac\text{-LA}]_0:[BnOH]_0:[BnNH_2]_0:[\mathbf{1}]_0 = 100:2.5:2.5:1$, under the conditions described in Table 2.3 was performed and 91% conversion of monomer to poly(*rac*-LA) was achieved after 20 mins. M_n(GPC) = 3,300 g mol^{-1} was slightly higher than that expected for five chains (M_n(calcd) = 2,730 g mol^{-1}) but the polydispersity remained narrow, PDI = 1.18.

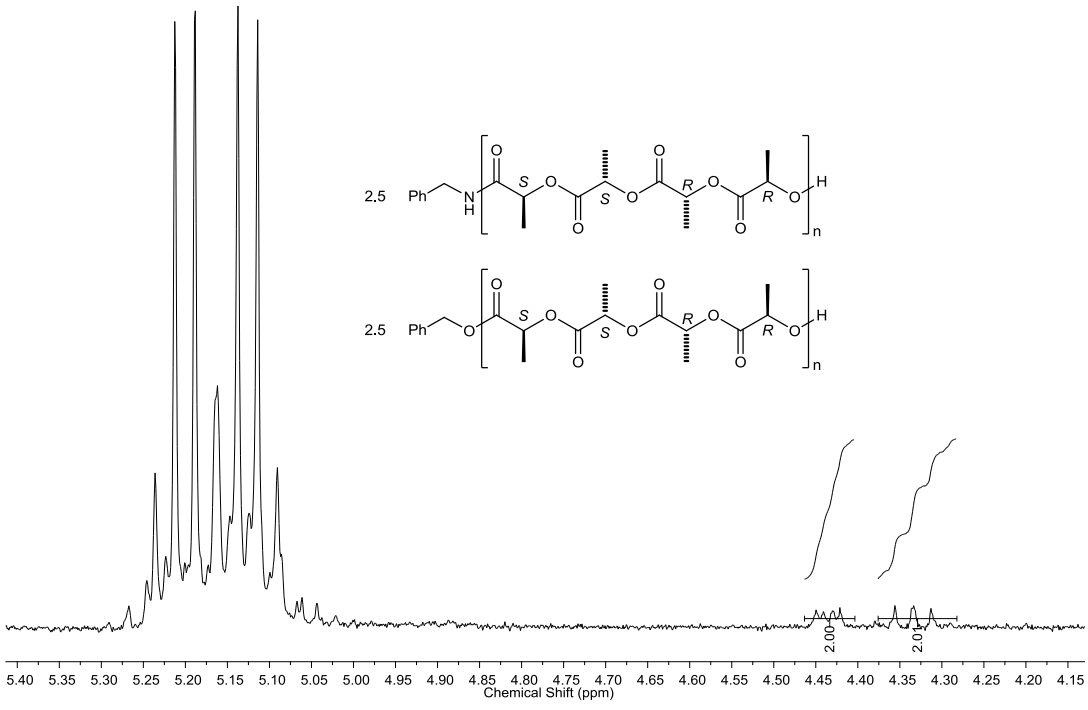

Figure 2.21. Expanded ^{1}H NMR (300.1 MHz, $CDCl_3$, 298 K) spectrum of benzyl alcohol and benzyl amine-capped poly(*rac*-LA).

From integration of the internal methine resonances (*ca*. 5.2 ppm) against the terminating HOC<u>H</u>(Me)– proton (*ca*. 4.32 ppm), an M_n(NMR) = 2,970 g mol^{-1} was calculated. The methylene resonance of the Ph$C\underline{H_2}$O– end-group was obscured by the internal methine resonances of the PLA chain, but the methylene signal of the benzyl

amine end-group was visible at δ = 4.43 ppm (Figure 2.21). It is likely that all co-initiator was consumed rapidly given M_n(NMR) = 2,970 g mol^{-1} was approximate to five chains per metal. The 1:1 integral between PhC<u>H</u>$_2$NH– and HOC<u>H</u>(Me)– (two of these end-groups) and the MADLI-ToF mass spectrum were also consistent with five chains per metal of M_n(calcd) = 2,970 g mol^{-1}. However, given that the molecular weights of $BnNH_2$ and BnOH differ only by 1 g mol^{-1}, it was not possible to resolve both benzyl alcohol and benzyl amine capped PLA chains in the MALDI-ToF mass spectrum, but the molecular weight distribution was centred on Δ(*m/z*) = 2,500 g mol^{-1}. Based on these observations, the initiation steps appear equally efficient with respect to propagation.

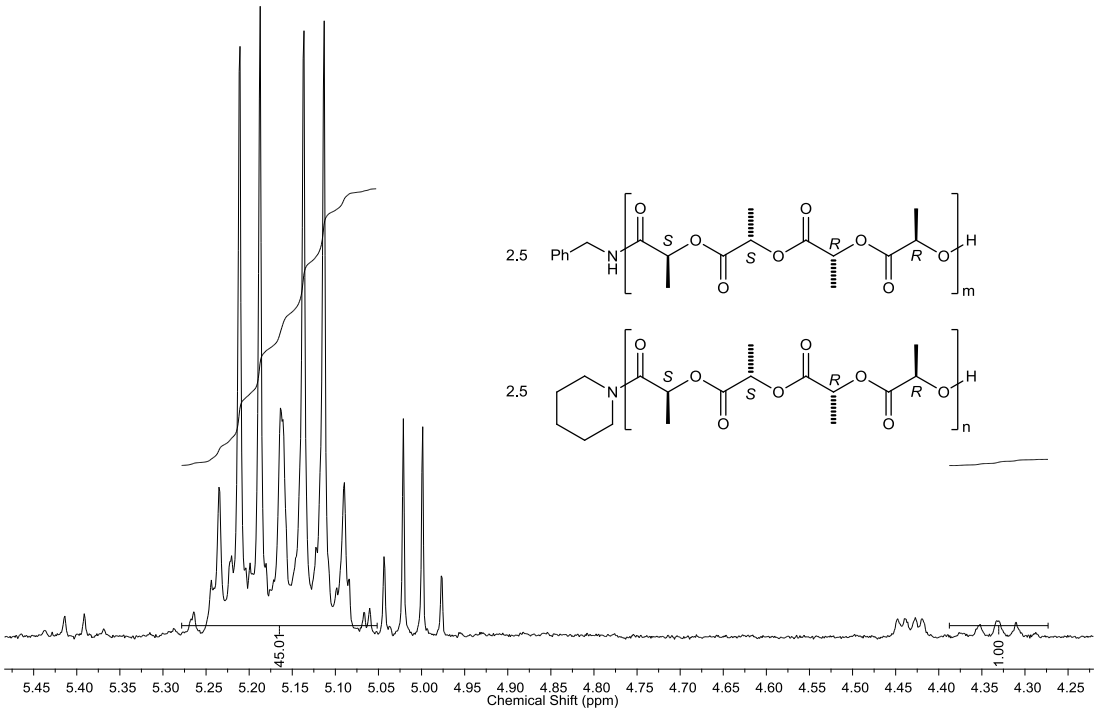

Figure 2.22. Expanded ^{1}H NMR (300.1 MHz, $CDCl_3$, 298 K) spectrum of crude benzyl amine and piperidine-capped poly(*rac*-LA).

When benzyl alcohol was replaced by piperidine in a run [*rac*-LA]$_0$:[piperidine]$_0$:[$BnNH_2$]$_0$:[**1**]$_0$ = 100:2.5:2.5:1, the observed M_n(GPC) = 3,400 g mol^{-1} (PDI = 1.17) was in close agreement to that calculated by NMR, M_n(NMR) = 3,280 g mol^{-1}. Comparison of end-group resonances suggested that all of the benzyl amine and piperidine was consumed eventually, despite the induction period with piperidine. Figure 2.22 shows the ^{1}H NMR spectrum of a crude mixture of piperidine and benzyl amine-capped poly(*rac*-LA). Additional features in this spectrum include unreacted

rac-LA at δ = 5.0 ppm and a unique C<u>H</u>(Me) quartet at δ = 5.4 ppm representing the alpha lactide unit adjacent to the piperidine end-group.

The slightly higher M_n(NMR) = 3,280 g mol^{-1} in this instance suggested a weighting in favour of benzyl amine-initiated chains. Integration of the internal methine resonances (*ca*. 5.2 ppm) against the terminating C<u>H</u>(Me) proton (*ca*. 4.32 ppm) suggested an average of 23 lactide units per chain, compared to the expected 18, based on the 92% monomer to poly(*rac*-LA) conversion rate. A relative initiation rate constant, $k_{i,\ BnNH2}/k_{i,\ piperidine}$ = 1.2–1.3 is tentatively suggested, but is likely to be higher based on the actual M_n of benzyl amine and piperidine-capped chains, rather than a combined average (Figure 2.22). The benzyl amine-capped chains should have a greater M_n than piperidine-capped polymers, based on the kinetic profiles. However, piperidine chains eventually initiate, thus there are five chains present according to end-group analysis, albeit not of equal M_n. It is also possible that initiation by piperidine was promoted because of the activation of the metal centre by benzyl amine-capped poly(*rac*-LA), in which case the suggested relative k_i may be appropriate. In an experiment with benzyl amine and *tert*-butyl amine as competing initiators, M_n(GPC) = 4,650 g mol^{-1} and PDI = 1.13 were recorded. A greater relative k_i in favour of $BnNH_2$ was apparent in this case and based on the initial experiments with $^tBuNH_2$ (Table 2.4, Section 2.6.2), it is unlikely that all $^tBuNH_2$ was consumed. M_n(GPC) data from *tert*-butyl amine co-initiated experiments (Table 2.4, Section 2.6.2) resembled one growing chain, despite 5 added equivs. of $^tBuNH_2$. However, the remaining data in Table 2.4 for the $^tBuNH_2$ loading experiments were suggestive of non-stoichiometric incorporation of $^tBuNH_2$. The propagation profiles of *tert*-butyl amine co-initiated polymerisations were also not determined, thus it is not possible to estimate the relative populations of benzyl amine and *tert*-butyl amine-capped poly(*rac*-LA).

End-group integration is limited by the length of polymer chains, as end-group resolution diminishes as the polymer chain increases in length. An elegant method for determining relative population would be analysis of GPC chromatograms, assuming that bimodal distributions could be produced deliberately. This was not attempted, but low temperature NMR tube scale reactions were performed to follow consumption of benzyl amine and benzyl alcohol and subsequent propagation.

2.7.7 Low temperature NMR tube scale reactions

In an attempt to observe *rac*-LA, co-initiators and **1** in solution before initiation, a pre-cooled solution of *rac*-LA was added to a THF-d_8 solution of $BnNH_2$ or BnOH and **1** at −35 °C ([*rac*-LA]$_0$:[co-initiator]$_0$:[**1**]$_0$ = 10:2:1). ^{1}H NMR analysis at this temperature showed incomplete consumption of $BnNH_2$ and BnOH and initial formation of poly(*rac*-LA). Liberated $H_2O_2N^{NMe2}$ was observed at this point and suggested that the protonolysis step occurs during the initiation phase, i.e. the initially formed BnNH-[LA]$_x$-H macromonomers may remove HO_2N^{NMe2} from **1** before the remaining $BnNH_2$ has been consumed. Upon warming in five-degree increments, complete consumption of the co-initiator was observed, confirming the facile initiation processes for both systems, despite the aforementioned difference in mechanism (Figures 2.15 and 2.17, *vide supra*). Poly(*rac*-LA) signals began to grow-in at approximately the same rate for both amine and alcohol-capped chains but propagation did not reach completion until each solution was warmed to 0 °C. This observation compliments the similar reaction profiles seen for both $BnNH_2$ and BnOH co-initiated immortal ROP of *rac*-LA experiments (Figures 2.12 and 2.18).

2.8 ROP with $Y(O_2N^{NMe2})\{N(SiHMe_2)_2\}(THF)$ (1.15)

To provide further insight into the initiation and propagation processes, control experiments were performed with a well-established initiator for immortal ROP of lactide. Carpentier's bis(phenolate)-amino yttrium amide complex, $Y(O_2N^{NMe2})\{N(SiHMe_2)_2\}(THF)$ (**1.15**) was chosen as a representative complex based on the identity of the ancillary ligand and readily removed $Y–N(SiHMe_2)_2$ amide ligand when exposed to alcohol substrates. Carpentier has most often exploited the ethereal donor arm complex, $Y(O_2N^{OMe})\{N(SiHMe_2)_2\}(THF)$ (**1.14**) for immortal ROP in the presence of alcohol co-initiators as described in Chapter One. Initial studies with $Y(O_2N^{NMe2})\{N(SiHMe_2)_2\}(THF)$ (**1.15**) were concerned with utilising $BnNH_2$ and BnOH in representative loading studies ([*rac*-LA]$_0$:[Co-initiator]$_0$:[**1**]$_0$ = 100:5:1, 20 mins) and results matching those of **1** were obtained (M_n(calcd) ≈ 2,700 g mol^{-1}, M_n(GPC) ≈ 2,400 g mol^{-1} and PDI = 1.2, Table 2.6). A high degree of heterotactic enrichment was measured (P_r = 0.9), owing to the presence of the bis(phenolate)-amino ligand and high conversion rates of monomer to poly(*rac*-LA) were recorded. Molecular weight data were consistent with one chain per co-initiator and the likely active propagating species is the $Y(O_2N^{NMe2})L$ (L = THF, LA or PLA

chelate) fragment. No –N(SiHMe$_2$)$_2$ or hydrolysed –NH(SiHMe$_2$) end-groups were detected in MALDI-ToF mass spectra, confirming that metal amides of this type are inefficient for coordination-insertion type polymerisation reactions and that this sacrificial amide ligand is readily eliminated by the alcoholic poly(*rac*-LA) end-groups (or BnOH).

Table 2.6. ROP of *rac*-LA using Y(O$_2$N^{NMe2}){N(SiHMe$_2$)$_2$}(THF) (**1.15**)

Co-initiator	Conv. (%)[b]	M_n(calcd) (g mol^{-1})[c]	M_n(GPC) (g mol^{-1})[d]	M_w/M_n[d]	P_r[b]
-	92	13,260	24,200	1.72	0.91
BnNH$_2$	87	2,620	2,350	1.19	0.91
BnOH	90	2,700	2,530	1.20	0.92

[a] [*rac*-LA]$_0$:[Co-initiator]$_0$:[**1.15**]$_0$ = 100:0:1 or 100:5:1, 2 mL THF, [*rac*-LA]$_0$ = 0.69 M, rt, 20 mins. [b] Conversion and P_r (by integration of appropriate tetrads) measured by ^{1}H and ^{1}H-{^{1}H} NMR in $CDCl_3$. [c] M_n(calcd) = (Conv. (%) × [*rac*-LA]$_0$:[Co-initiator]$_0$ × 144.1 + M_R Co-initiator). [d] Measured by GPC against polystyrene standards using the appropriate Mark-Houwink corrections for poly(*rac*-LA) in THF at 30 °C.

2.8.1 Kinetic studies on Y(O$_2$N^{NMe2}){N(SiHMe$_2$)$_2$}(THF) (1.15)

Studies using BnNH$_2$ and **1.15** were performed under the same conditions as **1** (Figure 2.12). A solution of monomer was added to a mixture of **1.15** and BnNH$_2$ to ensure an initial excess of BnNH$_2$ over the yttrium bound, Y–N(SiHMe$_2$) amide. As in the case of **1**, consumption of *rac*-LA was modelled with a second-order dependence and there was no systematic dependence in [BnNH$_2$]$_0$ (Figure 2.23). Apparent rate constants (k_{app}) were marginally lower than those found in the corresponding runs using **1**, which may reflect a variation in the initiation process or route to the active catalyst, given initiation was included in the propagation model. For example, for the run [*rac*-LA]$_0$:[BnNH$_2$]$_0$:[**1**]$_0$ = 200:3:1, k_{app} = 0.712(18) M^{-1} min^{-1} (Table 2.5), but in the analogous run with **1.15** (Figure 2.23, left), k_{app} = 0.673(25) M^{-1} min^{-1}. A first-order dependence in **1.15** was also determined (Figure 2.23, right), based on $k_{app} = k_p$[**1.15**], leading to an overall rate law for propagation, $R_p = k_p$[*rac*-LA]^2[**1.15**], with k_p = 209(6) (R^2 = 0.997) M^{-2} min^{-1} (k_p = 239(8) M^{-2} min^{-1} for ROP of *rac*-LA co-initiated by BnNH$_2$ and **1**).

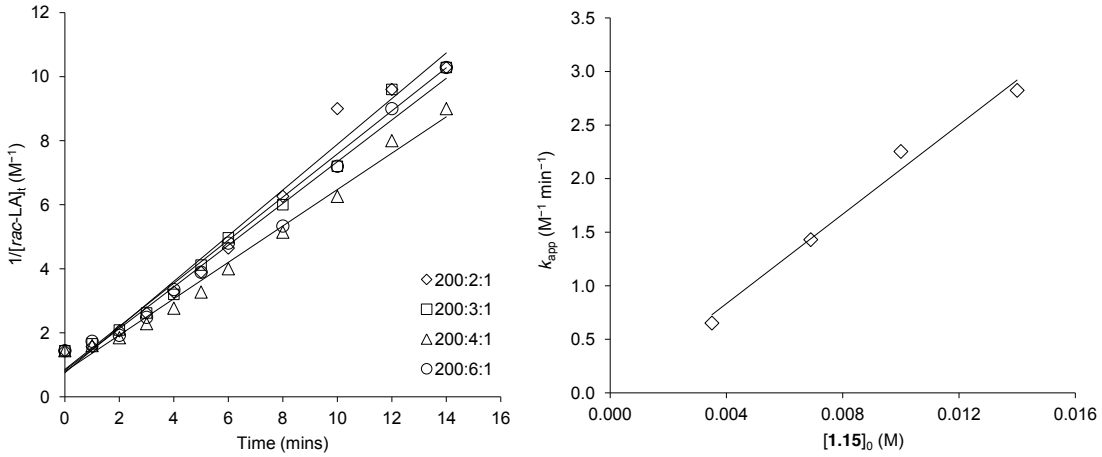

Figure 2.23. Apparent second-order rate constants showing no systematic dependence in $[BnNH_2]_0$ (left), $[rac\text{-LA}]_0$:$[BnNH_2]_0$:[**1.15**]$_0$ = 200:2, 3, 4 and 6:1. k_{app} = 0.713(37) (R^2 = 0.977), 0.673(25) (R^2 = 0.987), 0.568(24) (R^2 = 0.984) and 0.652(27) (R^2 = 0.985) M^{-1} min^{-1}. The vertical-axis intercepts of the plots are 0.754(271), 0.858(187), 0.791(176) and 0.827(198) M^{-1}, with the expected intercept, $1/[rac\text{-LA}]_0$ = 1.44 M^{-1}. Right, overall k_p determined as 209(6) (R^2 = 0.997) M^{-2} min^{-1} from plots of k_{app} *vs.* [**1.15**]$_0$, with k_{app} determined from $[rac\text{-LA}]_0$:$[BnNH_2]_0$:[**1.15**]$_0$ = 200:6:1, 2, 3 and 4. k_{app} = 0.652(27) (R^2 = 0.985), 1.430(51) (R^2 = 0.989), 2.254(142) (R^2 = 0.973) and 2.824(128) (R^2 = 0.982) M^{-1} min^{-1}.

2.8.2 NMR tube scale experiments with Y(O_2N^{NMe2}){$N(SiHMe_2)_2$}(THF) (1.15)

Analogous NMR tube scale experiments (Figure 2.24) were also performed with **1.15** to support the proposal that **1** and **1.15** form the same active species in solution. As expected, **1.15** was inert to $BnNH_2$ in both C_6D_6 and THF-d_8 at room temperature. Upon addition of *rac*-LA, $BnNH_2$ was consumed and poly(*rac*-LA) signals (δ = 5.2 and 1.5 ppm) were detected along with eliminated $HN(SiHMe_2)_2$ (δ = 0.1 ppm). No $H_2O_2N^{NMe2}$ was observed and resonances corresponding to the active species were consistent with the active species formed from **1**. Broad aromatic signals were assigned to the Y(O_2N^{NMe2})L (L = THF, LA or PLA chelate) fragment and the benzylic poly(*rac*-LA) end-group, with the remaining environments consistent with benzyl amine-capped poly(*rac*-LA) (δ = 4.4 ppm).

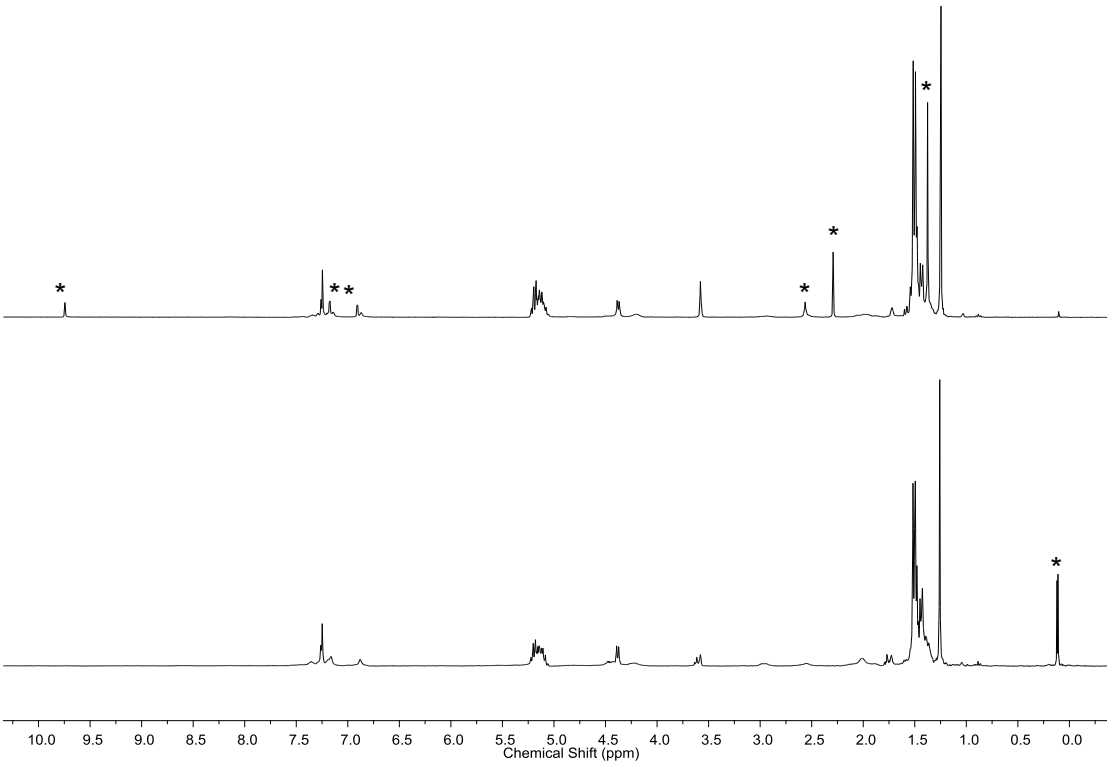

Figure 2.24. ^{1}H NMR (300.1 MHz, THF-d_8, 298 K) spectra of NMR tube scale reactions between [*rac*-LA]$_0$:[BnNH$_2$]$_0$:[**1**]$_0$ = 10:2:1 (top) and [*rac*-LA]$_0$:[BnNH$_2$]$_0$:[**1.15**]$_0$ = 10:2:1 (bottom). * Denotes liberated $H_2O_2N^{NMe2}$ (top) and HN(SiHMe$_2$)$_2$ (bottom). Residual protio-solvent, δ = 3.58 ppm.

2.9 Further mechanistic experiments

Although attempts to gain a quantitative insight into initiation processes with co-initiators have achieved limited success, aforementioned experiments support a propagation mechanism where poly(*rac*-LA) chains grow at a yttrium metal centre, Y(O_2N^{NMe2})L (L = THF, LA or PLA), through a coordination-insertion process. Based on post-polymerisation analysis, facile chain transfer reactions account for the multiple, well-defined polymers per metal centre. In order to cement this model, two resumption experiments were undertaken. One where classical living behaviour was demonstrated through adding extra monomer equivalents to a system that had reached completion and a second experiment utilising an isolated benzyl amine-capped poly(*rac*-LA) sample, **9**, as the co-initiator.

2.9.1 Resumption experiment

The [*rac*-LA]$_0$:[BnNH$_2$]$_0$:[**1**]$_0$ = 200:6:1 run was repeated in a living type experiment, where the reaction was followed to high conversion in the usual manner before the

addition of a further 200 equivs. of *rac*-LA ([*rac*-LA]$_0$ = 0.69 M). The system was shown to remain active and M_n effectively doubled between the two end-points. At the first end-point, t = 15 min, 89% conversion was recorded with M_n(calcd) = 4,380 g mol^{-1}, M_n(GPC) = 4,440 g mol^{-1} and PDI = 1.09. This favourable agreement between calculated and experimental M_n (8,520 and 9,310 g mol^{-1}) was repeated at the second end-point (86% conversion), with a PDI = 1.05. The Conversion *vs*. Time plot is shown in Figure 2.25.

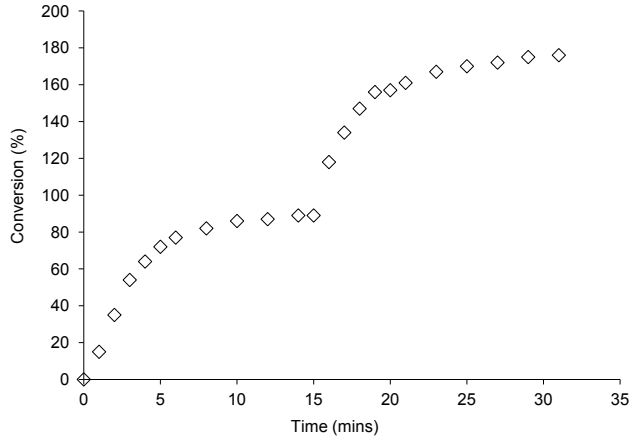

Figure 2.25. Conversion *vs*. Time plot, demonstration of living-type behaviour, with the resumption of polymerisation. [*rac*-LA]$_0$:[BnNH$_2$]$_0$:[**1**]$_0$ = 200:6:1, [*rac*-LA]$_{t\,=\,16}$:[**1**]$_{t\,=\,16}$ = 200:1.

2.9.2 Macromonomers as co-initiators

Following on from the successful resumption experiment, and to provide support for the generation of macromonomers at the beginning of the reaction, that in turn protonate off a sacrificial ligand (HO_2N^{NMe2} (**1**) or N(SiHMe$_2$)$_2$ (**1.15**)), a short chain polymer was isolated and utilised as a co-initiator. From a loading experiment, [*rac*-LA]$_0$:[BnNH$_2$]$_0$:[**1**]$_0$ = 100:10:1, a poly(*rac*-LA) sample, M_n = 1,600 g mol^{-1} and PDI = 1.14 was purified and used directly. This macromonomer (**9**) was added to **1** or **1.15** in stoichiometric reactions in C_6D_6 with ^{1}H NMR analysis once again showing elimination of $H_2O_2N^{NMe2}$ or HN(SiHMe$_2$)$_2$ (Figure 2.26 and 2.67). With **1**, addition of one equivalent of the macromonomer was shown to cause elimination of $H_2O_2N^{NMe2}$. Likewise, with **1.15**, HN(SiHMe$_2$)$_2$ was liberated from the complex and the bis(phenolate)-amino ligand remained coordinated. Comparable environments in the aromatic region were likely to correspond to [Y(O_2N^{NMe2})L]$_n$ (L = THF, LA or PLA chelate) and were consistent with the aromatic environments observed in the ^{1}H

NMR spectrum for the NMR tube scale reaction, [*rac*-LA]$_0$:[BnNH$_2$]$_0$:[**1**]$_0$ = 10:2:1 (Figure 2.16, top).

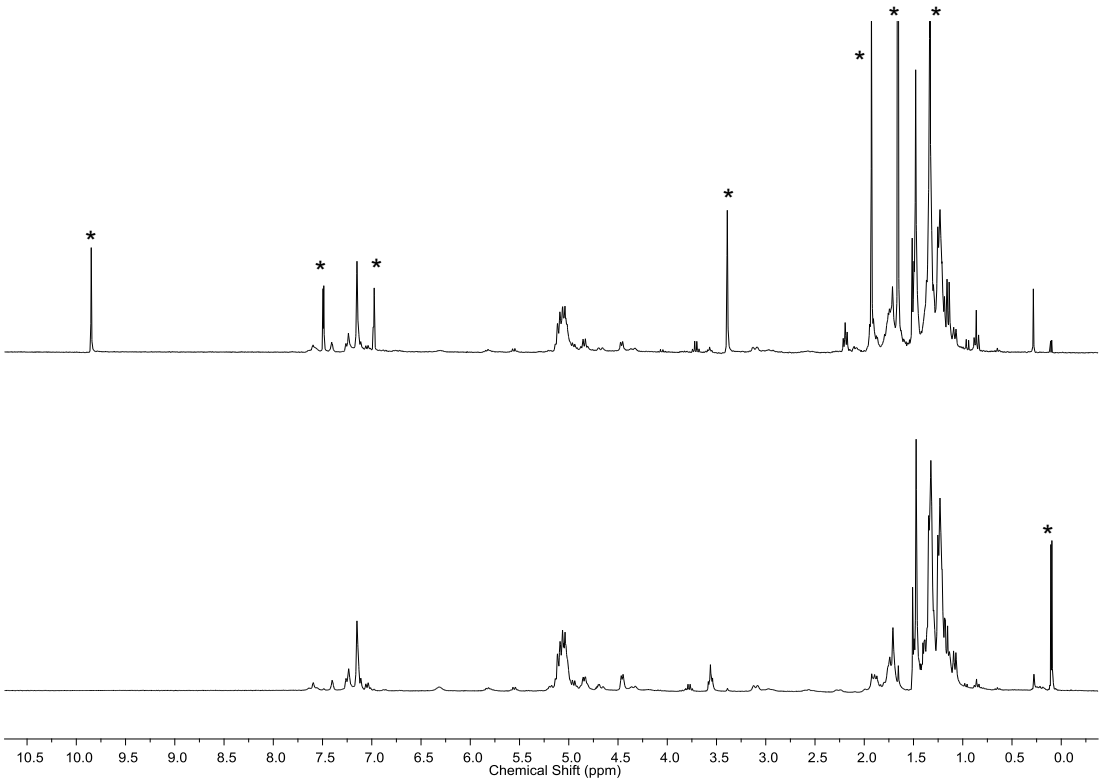

Figure 2.26. ^{1}H NMR (300.1 MHz, C_6D_6, 298 K) spectra of stoichiometric NMR tube scale reactions between **9** and **1** (top) and **9** and **1.15** (bottom). ***** Denotes liberated $H_2O_2N^{NMe2}$ (top) and $HN(SiHMe_2)_2$ (bottom). Residual protio-solvent, δ = 7.15 ppm.

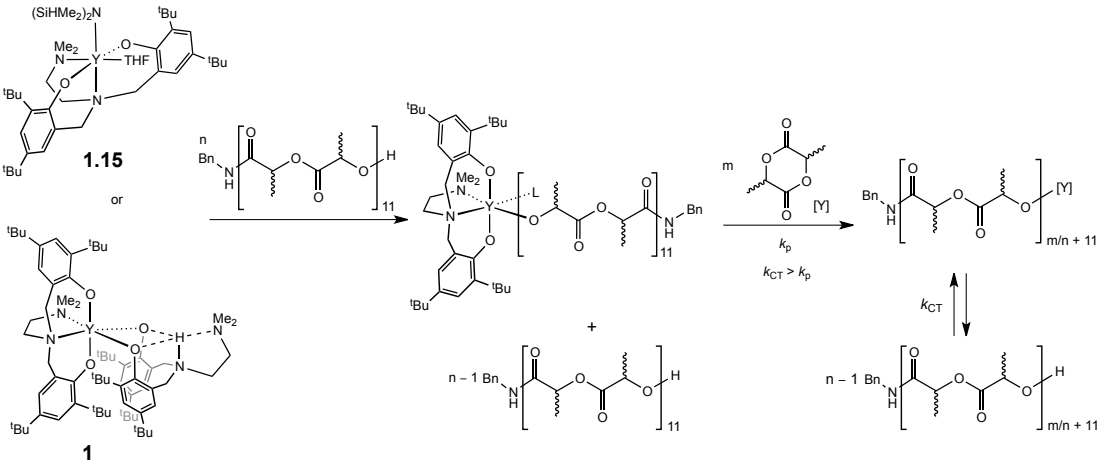

Figure 2.27. Macromonomer reactivity and polymerisation resumption. L = THF, LA or PLA chelate.

Three kinetic runs were also performed using the isolated macromonomer, **9**, and comparable rate constants were determined. Using [*rac*-LA]$_0$:[**9**]$_0$:[**1**]$_0$ = 200:2:1,

200:3:1 and 200:6:1, under the same experimental conditions as reactions using amines or benzyl alcohol, apparent second-order rate constants, k_{app} = 0.883(33), 0.838(20) and 0.836(16) M^{-1} min^{-1} were measured (Figure 2.28).

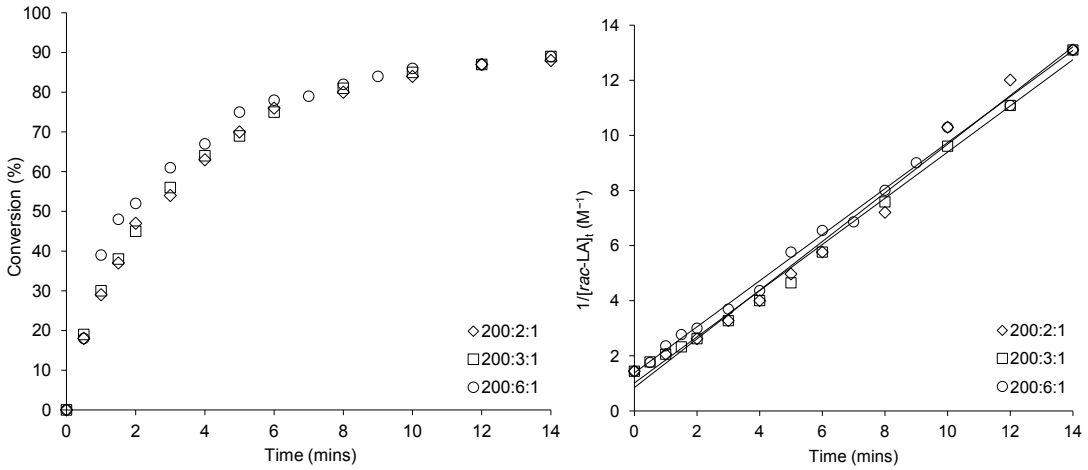

Figure 2.28. Left, Conversion *vs*. Time plots. Right, second-order rate plots for the polymerisation reactions, [*rac*-LA]$_0$:[**1**]$_0$ = 200:1, [**9**]$_0$:[**1**]$_0$ = 2, 3 or 6:1. k_{app} = 0.883(33) (R^2 = 0.987), 0.838(20) (R^2 = 0.994) and 0.836(16) (R^2 = 0.996) M^{-1} min^{-1}. The vertical-axis intercepts of these plots are 0.848(244), 1.010(136) and 1.379(108) M^{-1}, with the expected intercept, 1/[*rac*-LA]$_0$ = 1.44 M^{-1}.

Selected M_n data showed that 2 or 3 poly(*rac*-LA) chains had regrown during the polymerisation (Figure 2.29) for [*rac*-LA]$_0$:[**9**]$_0$:[**1**]$_0$ = 200:2:1 or 200:3:1 respectively. These kinetic and the molecular weight data further support a polymerisation mechanism where multiple polymer chains can be present in a system with facile exchange between growing and dormant chains to maintain control over M_n and PDI (Figure 2.27).

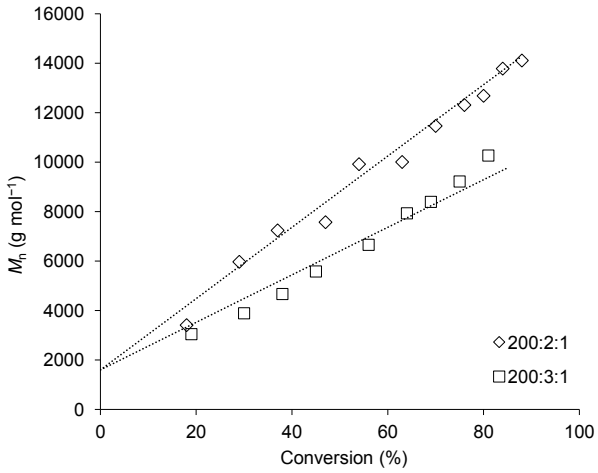

Figure 2.29. M_n(GPC) *vs*. Conversion plot for the runs, [*rac*-LA]$_0$:[**1**]$_0$ = 200:1, [**9**]$_0$:[**1**]$_0$ = 2 or 3:1. PDI = 1.07–1.13, with M_n(calcd) represented by the dashed lines.

2.10 Summary and Conclusions for Chapter Two

ROP of *rac*-LA in the presence of amines and rare earth zwitterionic complexes leads to the generation of multiple, well-defined poly(*rac*-LA) chains which are systematically capped with amine end-groups. Owing to the nature of the supporting ligand, poly(*rac*-LA) chains displayed a high degree of heterotactic enrichment and MALDI-ToF mass spectra showed little evidence of detrimental transesterification. A mechanism for the amine-initiated, immortal ring opening polymerisation using bis(phenolate)-amino supported yttrium catalysts has been established through kinetic studies and NMR tube scale reactivity. This methodology has been transferred to other neutral and cationic catalysts, where primary amines, such as $BnNH_2$ were shown to be the most efficient co-initiators.[1, 85, 107-109]

Regarding $Y(O_2N^{NMe2})(HO_2N^{NMe2})$ (**1**), one equivalent of $H_2O_2N^{NMe2}$ is eliminated from **1** to generate the active species, likely to be based on the $Y(O_2N^{NMe2})L$ (L = THF, LA or PLA chelate) fragment. NMR tube scale polymerisation reactions with BnOH, $BnNH_2$ or a macromonomer and *rac*-LA have shown that this ligand is removed by alcoholic poly(*rac*-LA) end-groups, and comparable reactions with $Y(O_2N^{NMe2})\{N(SiHMe_2)_2\}(THF)$ (**1.15**) confirmed that the tetradentate (O_2N^L) ligand remained coordinated. The propagation behaviour of **1** and **1.15** were also consistent with the same active species forming in solution.

There were subtleties regarding initiation, but these were likely to have been reflective of the nature of the co-initiator or pre-catalyst. Both **1** and **1.15** have a

sacrificial ligand that has to be removed to generate the active species. Alcohol co-initiators are capable of removing both the bidentate HO_2N^L ligand as well as the silyl-amide, $N(SiHMe_2)_2$ to generate a well-established coordination-insertion type catalyst. The sacrificial ligands are removed during or post initiation when amines are employed as the co-initiator. Following initial ring opening by an activated-monomer process, alcoholic poly(*rac*-LA) end-groups generate the active propagating species.

2.11 References for Chapter Two

1. L. Clark, M. G. Cushion, H. E. Dyer, A. D. Schwarz, R. Duchateau and P. Mountford, *Chem. Commun.*, 2010, **46**, 273.
2. H. E. Dyer, D.Phil Thesis, University of Oxford, 2009.
3. H. E. Dyer, S. Huijser, A. D. Schwarz, C. Wang, R. Duchateau and P. Mountford, *Dalton Trans.*, 2008, 32.
4. H. E. Dyer, S. Huijser, N. Susperregui, F. Bonnet, A. D. Schwarz, R. Duchateau, L. Maron and P. Mountford, *Organometallics*, 2010, **29**, 3602.
5. R. H. Platel, L. M. Hodgson and C. K. Williams, *Polym. Rev.*, 2008, **48**, 11
6. H. Yasuda, *J. Organomet. Chem.*, 2002, **647**, 128.
7. F. Bonnet, A. R. Cowley and P. Mountford, *Inorg. Chem.*, 2005, **44**, 9046.
8. F. Bonnet, A. C. Hillier, A. Collins, S. R. Dubberley and P. Mountford, *Dalton Trans.*, 2005, 421.
9. J. G. Stark and H. G. Wallace, *Chemistry Data Book*, John Murray, SI Ed., 1975.
10. C.-X. Cai, L. Toupet, C. W. Lehmann and J.-F. Carpentier, *J. Organomet. Chem.*, 2003, **683**, 131.
11. C.-X. Cai, A. Amgoune, C. W. Lehmann and J.-F. Carpentier, *Chem. Commun.*, 2004, 330.
12. A. Amgoune, C. M. Thomas, E. Balnois, Y. Grohens, P. J. Lutz and J.-F. Carpentier, *Macromol. Rapid Commun.*, 2005, **26**, 1145.
13. A. Amgoune, C. M. Thomas, T. Roisnel and J.-F. Carpentier, *Chem. Eur. J.*, 2006, **12**, 169.
14. A. Amgoune, C. M. Thomas and J.-F. Carpentier, *Macromol. Rapid Commun.*, 2007, **28**, 693.
15. A. Amgoune, C. M. Thomas and J.-F. Carpentier, *Pure Appl. Chem.*, 2007, **79**, 2013.

16. N. Ajellal, J.-F. Carpentier, C. Guillaume, S. M. Guillaume, M. Helou, V. Poirier, Y. Sarazin and A. Trifonov, *Dalton Trans.*, 2010, **39**, 8363.
17. E. Y. Tshuva, I. Goldberg, M. Kol, H. Weitman and Z. Goldschmidt, *Chem. Commun.*, 2000, 379.
18. E. Y. Tshuva, I. Goldberg and M. Kol, *J. Am. Chem. Soc.*, 2000, **122**, 10706.
19. E. Y. Tshuva, I. Goldberg, M. Kol and Z. Goldschmidt, *Inorg. Chem. Commun.*, 2000, **3**, 611.
20. E. Y. Tshuva, I. Goldberg, M. Kol and Z. Goldschmidt, *Organometallics*, 2001, **20**, 3017.
21. E. Y. Tshuva, I. Goldberg, M. Kol and Z. Goldschmidt, *Inorg. Chem.*, 2001, **40**, 4263.
22. E. Y. Tshuva, S. Groysman, I. Goldberg, M. Kol and Z. Goldschmidt, *Organometallics*, 2002, **21**, 662.
23. S. Groysman, I. Goldberg, M. Kol, E. Genizi and Z. Goldschmidt, *Organometallics*, 2003, **22**, 3013.
24. S. Gendler, S. Segal, I. Goldberg, Z. Goldschmidt and M. Kol, *Inorg. Chem.*, 2006, **45**, 4783.
25. S. Segal, I. Goldberg and M. Kol, *Organometallics*, 2005, **24**, 200.
26. M. E. G. Skinner, B. R. Tyrrell, B. D. Ward and P. Mountford, *J. Organomet. Chem.*, 2002, **647**, 145.
27. T. Toupance, S. R. Dubberley, N. H. Rees, B. R. Tyrrell and P. Mountford, *Organometallics*, 2002, **21**, 1367.
28. C. L. Boyd, T. Toupance, B. R. Tyrrell, B. D. Ward, C. R. Wilson, A. R. Cowley and P. Mountford, *Organometallics*, 2005, **24**, 309.
29. H. Ma, T. P. Spaniol and J. Okuda, *Dalton Trans.*, 2003, 4770.
30. H. Ma and J. Okuda, *Macromolecules*, 2005, **38**, 2665.
31. H. Ma, T. P. Spaniol and J. Okuda, *Angew. Chem. Int. Ed.*, 2006, **45**, 7818.
32. H. Ma, T. P. Spaniol and J. Okuda, *Inorg. Chem.*, 2008, **47**, 3328.
33. J.-C. Buffet, A. Kapelski and J. Okuda, *Macromolecules*, 2010, **43**, 10201.
34. A. J. Chmura, M. G. Davidson, M. D. Jones, M. D. Lunn and M. F. Mahon, *Dalton Trans.*, 2006, 887.
35. A. J. Chmura, M. G. Davidson, M. D. Jones, M. D. Lunn, M. F. Mahon, A. F. Johnson, P. Khunkamchoo, S. L. Roberts and S. S. F. Wong, *Macromolecules*, 2006, **39**, 7250.

36. M. G. Davidson, C. T. O'Hara, M. D. Jones, C. G. Keir, M. F. Mahon and G. Kociok-Koehn, *Inorg. Chem.*, 2007, **46**, 7686.
37. A. J. Chmura, M. G. Davidson, C. J. Frankis, M. D. Jones and M. D. Lunn, *Chem. Commun.*, 2008, 1293.
38. F. M. Kerton, A. C. Whitwood and C. E. Willans, *Dalton Trans.*, 2004, 2237.
39. C. E. Willans, M. A. Sinenkov, G. K. Fukin, K. Sheridan, J. M. Lynam, A. A. Trifonov and F. M. Kerton, *Dalton Trans.*, 2008, 3592.
40. H. Guo, H. Zhou, Y. Yao, Y. Zhang and Q. Shen, *Dalton Trans.*, 2007, 3555.
41. K. Nie, X. Gu, Y. Yao, Y. Zhang and Q. Shen, *Dalton Trans.*, 2010, **39**, 6832.
42. P. R. Woodman, N. W. Alcock, I. J. Munslow, C. J. Sanders and P. Scott, *J. Chem. Soc., Dalton Trans.*, 2000, 3340.
43. H. Kawaguchi and T. Matsuo, *J. Organomet. Chem.*, 2004, **689**, 4228.
44. X. Liu, X. Shang, T. Tang, N. Hu, F. Pei, D. Cui, X. Chen and X. Jing, *Organometallics*, 2007, **26**, 2747.
45. S. Barroso, J. Cui, J. M. Carretas, A. Cruz, I. C. Santos, M. T. Duarte, J. P. Telo, N. Marques and A. M. Martins, *Organometallics*, 2009, **28**, 3449.
46. O. Wichmann, R. Sillanpää and A. Lehtonen, *Coord. Chem. Rev.*, 2012, **256**, 371.
47. A. Kowalski, A. Duda and S. Penczek, *Macromolecules*, 2000, **33**, 7359.
48. A. Kowalski, J. Libiszowski, T. Biela, M. Cypryk, A. Duda and S. Penczek, *Macromolecules*, 2005, **38**, 8170.
49. M. Adeli and R. Haag, *J. Polym. Sci., Part A: Polym. Chem.*, 2006, **44**, 5740.
50. X. Cao, Z. Li, X. Song, X. Cui, P. Cao, H. Liu, F. Cheng and Y. Chen, *Eur. Polym. J.*, 2008, **44**, 1060.
51. P. Dubois, P. Degee, R. Jerome and P. Teyssie, *Macromolecules*, 1992, **25**, 2614.
52. M. Marzorati, K. Hult, S. Riva and B. Danieli, *Adv. Synth. Catal.*, 2007, **349**, 1963.
53. Q. Cai, Y. Zhao, J. Bei, F. Xi and S. Wang, *Biomacromolecules*, 2003, **4**, 828.
54. O. Coulembier, M. K. Kiesewetter, A. Mason, P. Dubois, J. L. Hedrick and R. M. Waymouth, *Angew. Chem., Int. Ed.*, 2007, **46**, 4719.
55. H. R. Kricheldorf, M. Garaleh and G. Schwarz, *J. Macromol. Sci., Part A*, 2005, **42**, 139.

56. H. R. Kricheldorf, N. Lomadze and G. Schwarz, *Macromolecules*, 2008, **41**, 7812.
57. H. Liu, Z. Shen, S.-E. Stiriba, Y. Chen, W. Zhang and L. Wei, *J. Polym. Sci., Part A: Polym. Chem.*, 2006, **44**, 4165.
58. N. E. Kamber, W. Jeong, R. M. Waymouth, R. C. Pratt, B. G. G. Lohmeijer and J. L. Hedrick, *Chem. Rev.*, 2007, **107**, 5813.
59. T. M. Ovitt and G. W. Coates, *J. Am. Chem. Soc.*, 1999, **121**, 4072.
60. B. M. Chamberlain, M. Cheng, D. R. Moore, T. M. Ovitt, E. B. Lobkovsky and G. W. Coates, *J. Am. Chem. Soc.*, 2001, **123**, 3229.
61. T. M. Ovitt and G. W. Coates, *J. Am. Chem. Soc.*, 2002, **124**, 1316.
62. M. H. Chisholm, J. C. Gallucci and K. Phomphrai, *Inorg. Chem.*, 2005, **44**, 8004.
63. M. H. Chisholm, J. Gallucci and K. Phomphrai, *Chem. Commun.*, 2003, 48.
64. M. H. Chisholm, J. C. Gallucci and K. Phomphrai, *Inorg. Chem.*, 2004, **43**, 6717.
65. M. H. Chisholm, S. S. Iyer, M. E. Matison, D. G. McCollum and M. Pagel, *Chem. Commun.*, 1997, 1999.
66. M. H. Chisholm, S. S. Iyer, D. G. McCollum, M. Pagel and U. Werner-Zwanziger, *Macromolecules*, 1999, **32**, 963.
67. M. T. Zell, B. E. Padden, A. J. Paterick, K. A. M. Thakur, R. T. Kean, M. A. Hillmyer and E. J. Munson, *Macromolecules*, 2002, **35**, 7700.
68. P. Hormnirun, E. L. Marshall, V. C. Gibson, A. J. P. White and D. J. Williams, *J. Am. Chem. Soc.*, 2004, **126**, 2688.
69. K. A. M. Thakur, R. T. Kean, M. T. Zell, B. E. Padden and E. J. Munson, *Chem. Commun.*, 1998, 1913.
70. K. A. M. Thakur, R. T. Kean, E. S. Hall, J. J. Kolstad, T. A. Lindgren, M. A. Doscotch, J. I. Siepmann and E. J. Munson, *Macromolecules*, 1997, **30**, 2422.
71. H. R. Kricheldorf, C. Boettcher and K.-U. Tonnes, *Polymer*, 1992, **33**, 2817.
72. J. E. Kasperczyk, *Macromolecules*, 1995, **28**, 3937.
73. M. Bouyahyi, N. Ajellal, E. Kirillov, C. M. Thomas and J.-F. Carpentier, *Chem. Eur. J.*, 2011, **17**, 1872.
74. N. Spassky, V. Simic, M. S. Montaudo and L. Hubert-Pfalzgraf, *Macromol. Chem. Phys.*, 2000, **201**, 2432.

75. P. B. Hitchcock, M. F. Lappert and A. Singh, *J. Chem. Soc., Chem. Commun.*, 1983, 1499.
76. C. K. Williams, *Chem. Soc. Rev.*, 2007, **36**, 1573.
77. M. Skotak, A. P. Leonov, G. Larsen, S. Noriega and A. Subramanian, *Biomacromolecules*, 2008, **9**, 1902.
78. M. A. Gauthier, M. I. Gibson and H.-A. Klok, *Angew. Chem., Int. Ed.*, 2009, **48**, 48.
79. J. L. Espartero, I. Rashkov, S. M. Li, N. Manolova and M. Vert, *Macromolecules*, 1996, **29**, 3535.
80. K. Thorshaug, J. A. Støvneng, E. Rytter and M. Ystenes, *Macromolecules*, 1998, **31**, 7149.
81. Z. Liu, E. Somsook and C. R. Landis, *J. Am. Chem. Soc.*, 2001, **123**, 2915.
82. Z. Liu, E. Somsook, C. B. White, K. A. Rosaaen and C. R. Landis, *J. Am. Chem. Soc.*, 2001, **123**, 11193.
83. F. Song, R. D. Cannon and M. Bochmann, *J. Am. Chem. Soc.*, 2003, **125**, 7641.
84. P. I. Binda and E. E. Delbridge, *Dalton Trans.*, 2007, 4685.
85. M. P. Blake, A. D. Schwarz and P. Mountford, *Organometallics*, 2011, **30**, 1202.
86. T.-P.-A. Cao, A. Buchard, X. F. Le Goff, A. Auffrant and C. K. Williams, *Inorg. Chem.*, 2012, **51**, 2157.
87. G. W. Coates, *J. Chem. Soc., Dalton Trans.*, 2002, 467.
88. J. A. Ewen, *J. Am. Chem. Soc.*, 1984, **106**, 6355.
89. W. Spaleck, F. Kueber, A. Winter, J. Rohrmann, B. Bachmann, M. Antberg, V. Dolle and E. F. Paulus, *Organometallics*, 1994, **13**, 954.
90. P. Longo, A. Proto, A. Grassi and P. Ammendola, *Macromolecules*, 1991, **24**, 4624.
91. L. Cavallo, G. Guerra, M. Vacatello and P. Corradini, *Macromolecules*, 1991, **24**, 1784.
92. T. A. Herzog, D. L. Zubris and J. E. Bercaw, *J. Am. Chem. Soc.*, 1996, **118**, 11988.
93. S. Miyake and J. E. Bercaw, *J. Mol. Cat. A: Chem.*, 1998, **128**, 29.
94. D. Veghini, L. M. Henling, T. J. Burkhardt and J. E. Bercaw, *J. Am. Chem. Soc.*, 1998, **121**, 564.

95. M. Ystenes, *J. Catal.*, 1991, **129**, 383.
96. H.-Y. Chen, H.-Y. Tang and C.-C. Lin, *Macromolecules*, 2006, **39**, 3745.
97. S. K. Russell, C. L. Gamble, K. J. Gibbins, K. C. S. Juhl, W. S. Mitchell, A. J. Tumas and G. E. Hofmeister, *Macromolecules*, 2005, **38**, 10336.
98. A. Pietrangelo, M. A. Hillmyer and W. B. Tolman, *Chem. Commun.*, 2009, 2736.
99. A. Pietrangelo, S. C. Knight, A. K. Gupta, L. J. Yao, M. A. Hillmyer and W. B. Tolman, *J. Am. Chem. Soc.*, 2010, **132**, 11649.
100. M. H. Chisholm, J. Gallucci and K. Phomphrai, *Inorg. Chem.*, 2002, **41**, 2785.
101. M. H. Chisholm, E. E. Delbridge and J. C. Gallucci, *New J. Chem.*, 2004, **28**, 145.
102. Z. Zhong, P. J. Dijkstra and J. Feijen, *J. Am. Chem. Soc.*, 2003, **125**, 11291.
103. W. M. Stevels, M. J. K. Ankone, P. J. Dijkstra and J. Feijen, *Macromolecules*, 1996, **29**, 3332.
104. W. M. Stevels, M. J. K. Ankone, P. J. Dijkstra and J. Feijen, *Macromolecules*, 1996, **29**, 6132.
105. W. M. Stevels, M. J. K. Ankone, P. J. Dijkstra and J. Feijen, *Macromolecules*, 1996, **29**, 8296.
106. Z. Zhang, X. Xu, W. Li, Y. Yao, Y. Zhang, Q. Shen and Y. Luo, *Inorg. Chem.*, 2009, **48**, 5715.
107. M. G. Cushion, D.Phil Thesis, University of Oxford, 2011.
108. M. G. Cushion and P. Mountford, *Chem. Commun.*, 2011, **47**, 2276.
109. Y. Sarazin, V. Poirier, T. Roisnel and J.-F. Carpentier, *Eur. J. Inorg. Chem.*, 2010, 3423.

Chapter Three

Multiarm PLA and amine-initiated, immortal ROP of *rac*-β-butyrolactone

3.1 Overview

This Chapter details further ROP experiments using $Y(O_2N^{NMe2})(HO_2N^{NMe2})$ (**1**) and amine co-initiators. These include the use of polyamines to prepare multiarm PLA and the extension of amine-initiated, immortal ROP to the cyclic esters, ε-caprolactone (ε-CL) and β-butyrolactone (BBL). As in Chapter Two, there is an emphasis on kinetic studies and polymer characterisation.

3.2 Introduction: multiarm polymers

A wide range of non-linear polylactone architectures have been developed utilising polyalcohol cores, with the intention of broadening the scope of these polymeric materials for medical applications and nanotechnology.[1-3] Typically, the highly functionalised core is hydrophilic owing to a large number of alcohol or amine end-groups, whilst the hydrophobic PLA shell structure results in novel amphiphilic core-shell architectures that lend themselves to guest encapsulation and release experiments, as well as self-assembly studies.

Multiarm or star-shaped polylactones have been prepared by post-polymerisation, "polymer-first" methods,[4, 5] where linear polylactones are attached to a hyperbranched or dendritic core; or by "core-first" processes, where the polymer is grown from the core using metal or organocatalysts. Whilst there are numerous reports of polyalcohol cores,[6-14] polyamine cores have also been employed and represent some of the earliest examples of the use of amine co-initiators in polymerisation mixtures. Duda and Penczek reported the use of $^{n}BuNH_2$ as a co-initiator alongside $Sn(Oct)_2$ for *L*-LA polymerisations, but also investigated hyperbranched polyamines with 8 (**3.1**) or 32 (**3.2**) terminal amine groups (Figure 3.1).[15] Kinetic analysis along with molecular weight and NMR data led to the proposal that all the amine groups were active in polymerisation reactions. In a run with **3.2**, 2,075 equivs. of *L*-LA were polymerised and M_n(GPC) = 376,900 g mol^{-1} (PDI = 1.02) was in reasonable agreement with M_n(calcd) = 302,600 g mol^{-1}. ε-CL (2,067 equivs.) was also polymerised and once again, M_n(GPC) = 373,000 g mol^{-1} (PDI = 1.05) was in favourable agreement with M_n(calcd) = 301,100 g mol^{-1}.

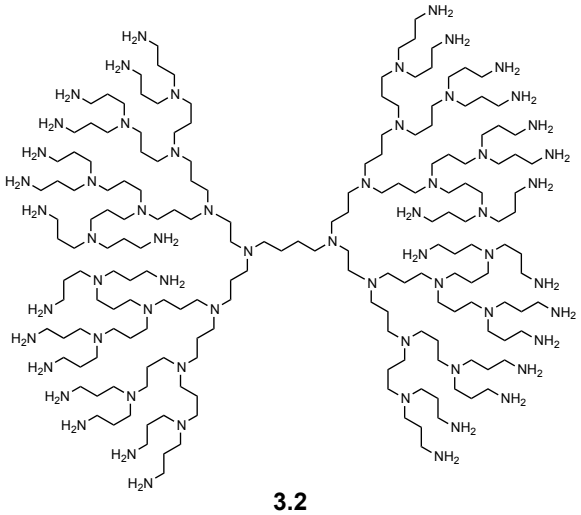

3.2

Figure 3.1. An example of a hyperbranched polyamine core.[15]

Hydrophilic poly(ethylene imine) cores, **3.3** (Figure 3.2), have been used in several reports for ε-CL and LA "core-first" polymerisations, also in the presence of $Sn(Oct)_2$. Adeli prepared multiarm polylactides under melt conditions and subsequent dye encapsulation experiments showed that longer polylactide arms improved the transport capacity of the so-called nanocarriers.[16] Chen was able to prepare multiarm PCL from the same amine core using $Sn(Oct)_2$ as the catalyst and also demonstrated dye encapsulation and release processes between organic and aqueous phases.[17, 18] Polylactides have also been propagated from poly(amidoamine) dendrimers, **3.4**, in the presence of $Sn(Oct)_2$ to prepare microsphere host molecules.[19] The drug release capability of the host was investigated, with polymer degradation a key factor in the rate of release.

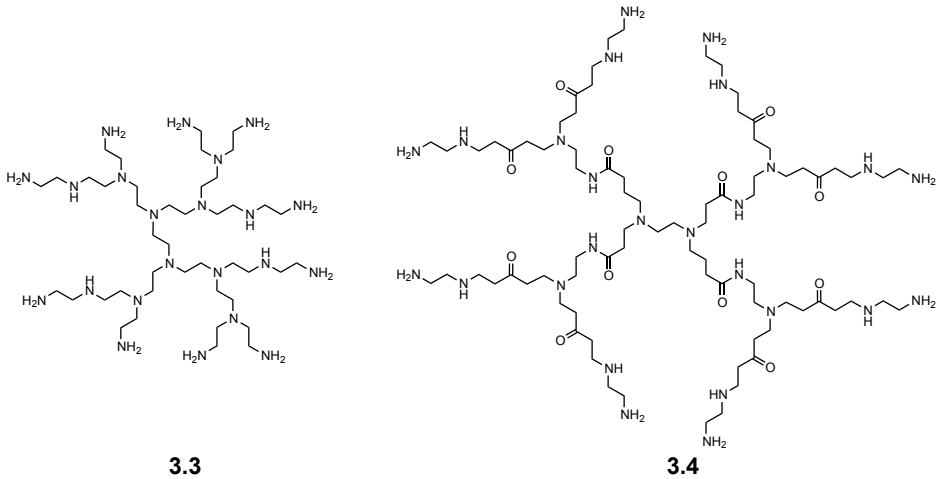

3.3 **3.4**

Figure 3.2. Poly(ethylene imine) (PEI), **3.3**, and poly(amidoamine), **3.4**, dendrimers.[16-19]

Waymouth has exploited a triazole carbene organocatalyst, **3.6**, to generate H-shaped and "super-H" shaped macromolecules (Figure 3.3).[20] In contrast to organometallic promoters (e.g. **1**), two PLA chains were shown to propagate from the active primary amine. Kinetic studies revealed first-order dependencies in $[rac\text{-LA}]_0$ and $[\mathbf{3.6}]_0$ and a doubling of observed rate when **3.5**, rather than a primary alcohol core was employed. These observations are consistent with a doubling of the number of active O–H propagating end-groups in an activated-monomer process.

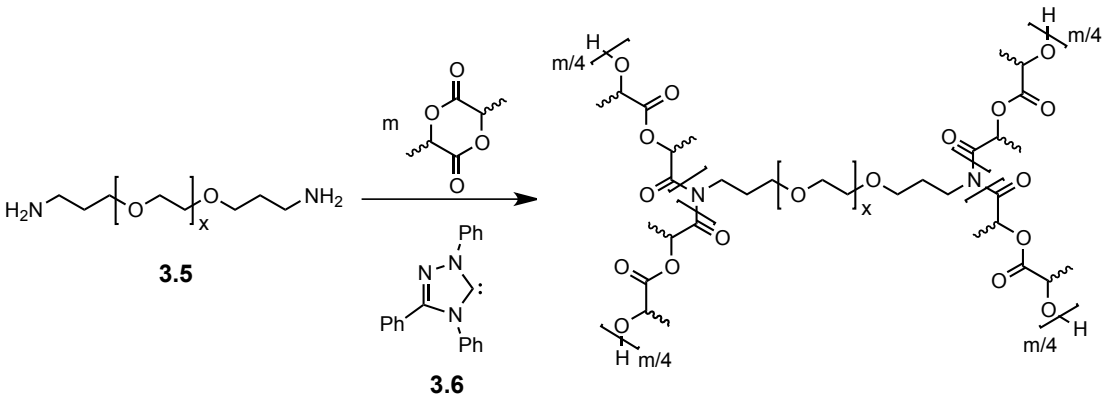

Figure 3.3. H-shaped macromolecules generated by organocatalysis.[20]

Regarding well-defined, single-site organometallic catalysts, Cui used triethanolamine alongside $Y(O_2N^{NMe2})(CH_2SiMe_3)(THF)$ (**1.22**) to prepare three-arm PLA.[21] Up to 8,100 equivs. of *rac*-LA were polymerised in the presence of 81 triethanolamine (TEA) equivs. (243 alcohols per **1.22**) in THF at 10 °C. Complete conversion was achieved in 1,440 mins and M_n(GPC) = 14,200 g mol^{-1} was in excellent agreement with M_n(calcd) = 14,600 g mol^{-1}. The molecular weight distribution was also narrow (PDI = 1.09) and heterotactic enrichment was expectedly high at P_r = 0.98. A first-order dependence in $[rac\text{-LA}]_0$ was determined, in contrast to **1** and **1.15** for the polymerisation of *rac*-LA in the presence of both primary amines and alcohols. Interestingly a negative order of –0.352 in $[TEA]_0$ was calculated ($[TEA]_0$:$[\mathbf{1.22}]_0$ = 0.33–9.0:1, $[rac\text{-LA}]_0$:$[\mathbf{1.22}]_0$ = 900:1) and represents a slowing in the rate of polymerisation at higher concentrations of co-initiator. Propagation in this system was expected to occur *via* a coordination-insertion mechanism, with prior liberation of $SiMe_4$ from **1.22** by TEA generating a new metal-alkoxide initiating species. During propagation, chain transfer processes were also expected to be fast and reversible, but the increased competition for the metal centre with more chains present may have

inhibited monomer coordination and enchainment, accounting for the negative order in $[TEA]_0$.

3.3 Introduction: β-butyrolactone and poly(3-hydroxybutanoate)

The polyester, poly(3-hydroxybutanoate) (PHB) is produced naturally by microorganisms and algaes.[22, 23] These biodegradable and biocompatible materials, commonly referred to as poly(hydroxyalkonates) (PHA), combine the film-barrier properties of polyesters and the mechanical performance of polyethylene and polypropylene.[24] The natural polymer occurs in an isotactic form with all stereocentres in the *R* configuration, leading to high crystallinity (T_m = 180 °C). The associated low thermostability means that processing is difficult and the commercial viability of the product is reduced.[25] However, a co-polymer of poly(3-hydroxybutanoate-*co*-3-hydroxyvalerate) has shown to have properties similar to those of polypropylene, but the high production costs of naturally synthesised PHA is a limiting factor in its applicability.[22, 23]

Another route to PHB is ring opening polymerisation of BBL.[25-28] The polymerisation reaction is driven by the release of ring-strain but BBL is generally less reactive than higher lactones and lactide.[28] ROP of BBL is attracting more attention but historical reports have described lower activities and the inability to produce PHB of high molecular weight (M_n > 100,000) in a controlled manner.[25] With regard to established single-site *rac*-LA polymerisation catalysts, Coates was able to show that bulky β-diiminate zinc alkoxides, Zn(BDI)(O^{i}Pr) (**3.7**), were excellent catalysts for the ROP of BBL.[25] In a typical run, 200 equivs. of *rac*-BBL were polymerised in 70 mins (91% conversion) in C_6D_6 at room temperature. M_n(GPC) = 26,100 g mol^{-1} for this polymer and a linear dependence between M_n and $[rac\text{-BBL}]_0$:$[\mathbf{3.7}]_0$ was established with PDIs remaining narrow (1.06–1.13). In general, polymerisations were faster in aromatic solvents (C_6D_6) than dichloromethane or THF, but atactic PHB was produced as judged by $^{13}C\text{-}\{^1H\}$ NMR (PLA produced by this family of catalysts displayed heterotactic enrichment). End-group analysis and retention of configuration when *R*-BBL was polymerised confirmed a coordination-insertion polymerisation mechanism and first-order dependencies in $[rac\text{-BBL}]_0$ and $[\mathbf{3.7}]_0$ were determined. Coates also identified PHB degradation products that can arise through prolonged reaction times. In addition to transesterification products, Lewis acidic metal residues can catalyse dehydration reactions with subsequent formation of unsaturated end-groups.

Gold(I) N-heterocyclic carbene complexes have also been shown to effect the ROP of *rac*-BBL under solvent-free conditions at 50 °C.[29] Interestingly, amide initiators, Au(NHC){N(SiR_3)$_2$}, were found to be more active than alkoxide analogues. In a representative [*rac*-BBL]$_0$:[Au]$_0$ = 100:1 run with Au(NHC){N($SiHMe_2$)$_2$} (**3.8**), 83% conversion of monomer to PHB was recorded after 2 h, whereas the *iso*-propoxide initiator only converted 46% of available monomer over a 24 h period. M_n(GPC) = 14,890 g mol^{-1} (PDI = 1.27) for the PHB produced by **3.8**, although at higher loadings and over longer reaction times, conversion was incomplete and polydispersities were broader. Nevertheless, propagation *via* a coordination-insertion mechanism was established.

3.3.1 Stereoselective polymerisation of *rac*-BBL

Racemic BBL has been polymerised to produce atactic PHB,[30-35] as well as PHB enriched in isotactic[36-38] and syndiotactic diads.[26, 33, 39-45] Early reports of stereoselective *rac*-BBL polymerisations were performed by aluminum and zinc-based initiators but the polymer products were inhomogeneous and contained mixtures of atactic, isotactic and syndiotactic polymer products.[27, 36, 38] Spassky reported the isospecific ROP of *rac*-BBL by kinetic resolution when diethyl zinc was used as a catalyst in the presence of *R*-3,3-dimethylenebutane-1,2-diol.[37] Cr(III) salen complexes (**3.9**, Figure 3.4) employed by Rieger generated PHB with modest isotactic enrichment (P_m = 0.63–0.66) ([*rac*-BBL]$_0$:[Cr]$_0$ = 1000, 100 °C, 5 h)[46] and Gross was able to prepare PHB with modest syndiotactic enrichment (P_r = 0.70) using alkyl tin derivatives (Bu_3SnOMe).[41] These reactions and polymerisations with related organo tin compounds were typically very slow, even at elevated temperature (18 d at 75 °C) and showed no inherent control over molecular weight.[33, 39, 40, 47] However, Kricheldorf showed that increasing the steric bulk of these relatively simple systems improved stereoselectivity.[42, 43]

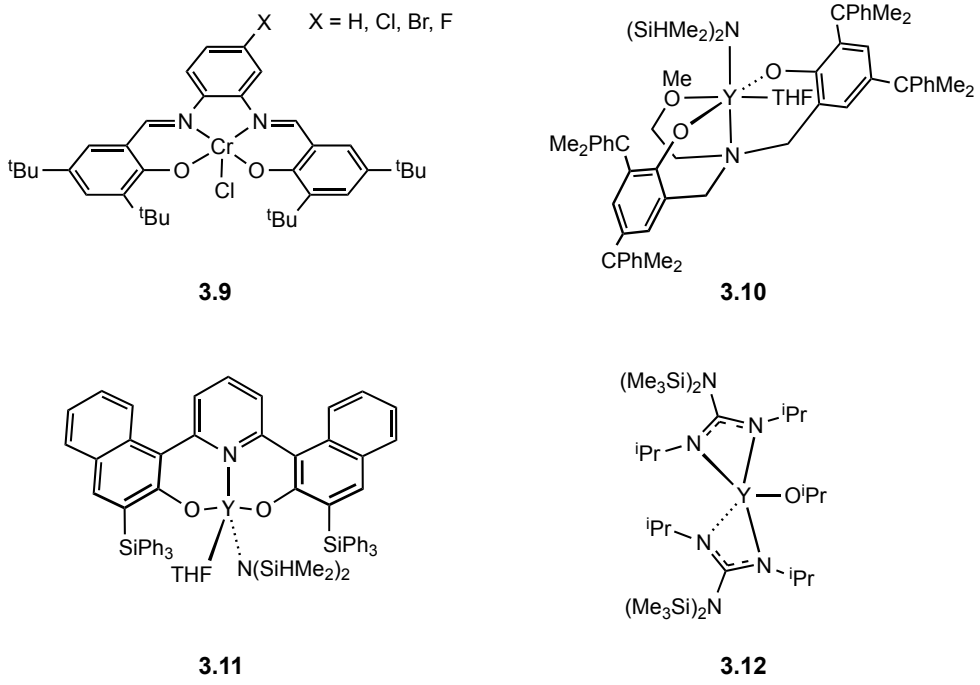

Figure 3.4. Single-site initiators for the stereoselective polymerisation of *rac*-BBL.[26, 44, 46, 48, 49]

Carpentier utilised bis(phenolate)-amino complexes with *ortho* and *para*-cumyl phenolate substituents, $Y(O_2^{(CPhMe2)2}N^{OMe})(O^iPr)(THF)$ (**3.10**), for the highly controlled, syndioselective polymerisations of *rac*-BBL.[26, 44] For example, 200 equivs. of *rac*-BBL were polymerised in 1 min in toluene at room temperature to produce a PHB with M_n(GPC) = 22,600 g mol^{-1} and PDI = 1.15. The probability of forming racemic diads, P_r, was judged to be 0.88 based on the intensities of the respective *racemic* and *meso* diads in $^{13}C\text{-}\{^1H\}$ NMR spectra. The bulkier catalyst, **3.10**, was citied as an optimal system for generating PHB with a high degree of syndiotactic enrichment and P_r = 0.94 (T_m = 183 °C) was measured in a run performed at –20 °C ([*rac*-BBL]$_0$:[**3.10**]$_0$ = 400:1). Accompanied by Bernoullian statistical analysis, stereosequence assignments (Figure 3.5) at the triad level have been proposed in the CO, CH_2 and CH_3 regions of PHB $^{13}C\text{-}\{^1H\}$ NMR spectra.[44] The enrichment is believed to arise again through a chain-end control mechanism for achiral catalysts, owing to the dependence on the steric bulk of the catalyst and solvent choice. P_r was found to be higher for polymerisations performed in toluene, rather in THF, in contrast to stereoselective *rac*-LA polymerisations.

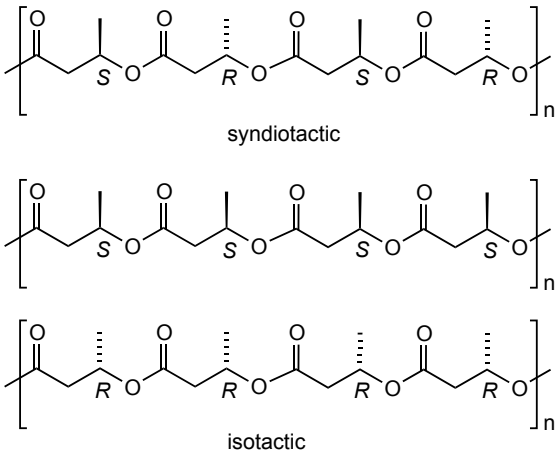

Figure 3.5. Regular stereosequences along PHB chains.[28]

Other rare earth complexes capable of preparing PHB with a high degree of syndiotactic enrichment include Carpentier's 2,6-bis(naphtholate)pyridine yttrium amide complex, Y(ONO^{SiPh3}){N(SiHMe$_2$)$_2$}(THF) (**3.11**), that adopts a C_s-symmetric structure.[48] P_r up to 0.87 were measured when **3.11** was employed as the catalyst to polymerise up to 300 equivs. of *rac*-BBL in toluene solution at room temperature. The bis(guanidinate) yttrium alkoxide complex, **3.12**, also produced PHB with P_r = 0.80–0.84, in contrast to ROP of *rac*-LA experiments using this initiator where the PLA products were atactic.[49] This observation, along with Coates' experiments with **3.7** has made it difficult to predict which catalysts will generate PHB with isotactic or syndiotactic enrichment, based on their performance in the ROP of *rac*-LA.

3.3.2 Immortal ROP of BBL

The suitability of BBL for immortal polymerisation has also been examined. In a comparative study, Carpentier utilised Coates' zinc β-diiminate complex, Zn(BDI){N(SiHMe$_2$)$_2$} (**3.13**) for solution and solvent-free ROP of *rac*-BBL in the presence of ^{i}PrOH or BnOH.[50, 51] In a solvent free experiment with [*rac*-BBL]$_0$:[BnOH]$_0$:[**3.13**]$_0$ = 500:10:1 at 60 °C, 73% conversion was recorded after 60 mins and M_n(GPC) = 4,800 g mol^{-1} was in reasonable agreement with M_n(calcd) = 3,300 g mol^{-1}. The PDI = 1.05 was consistent with a well-controlled polymerisation process, with facile chain transfer between dormant and active chains. Coates' zinc β-diiminate, **3.13**, was more active than Carpentier's bis(morpholinomethyl)phenoxy zinc complexes, **3.14** (Figure 3.6). In a comparable run, 95% conversion was achieved only after 180 mins but M_n(calcd) = 4,140 g mol^{-1} was in good agreement with M_n(GPC) = 4,300 g mol^{-1} and the molecular weight distribution was narrow (PDI =

1.07).[52] In a non-optimised reaction with a zinc catalyst supported by multidentate amino-ether phenolate ligands, **3.15**, 63% conversion was achieved after 3 hours and good agreement between M_n(calcd) = 2,700 g mol^{-1} and M_n(GPC) = 2,900 g mol^{-1} was recorded.[53] However, the polydispersity index was broader (PDI = 1.26) in this comparable run, [*rac*-BBL]$_0$:[^{i}PrOH]$_0$:[**3.15**]$_0$ = 500:10:1.

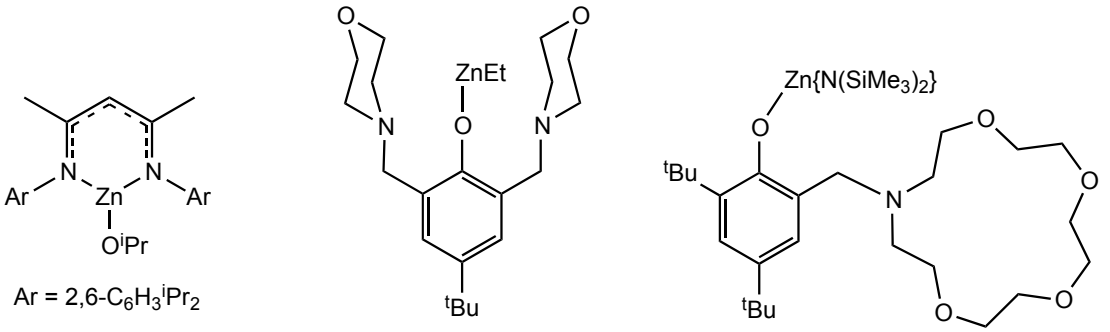

3.7 **3.14** **3.15**

Figure 3.6. Zinc based systems for immortal ROP of BBL.[50-53]

3.3.3 Carbonylation of epoxides and β-lactones and CO_2 co-polymerisations

ROP of BBL does have its drawbacks. BBL is toxic (and a suspected carcinogen) and requires rigorous purification and drying to ensure reliable polymerisation performance. PHB can be produced through co-polymerisation of propylene oxide and carbon monoxide, using simple cobalt carbonyl promoters. However, low molecular weight oligomers or mixtures of products are typically produced, despite some optimisation of conditions.[54]

Alongside the development of single-site homogeneous catalysts for the ROP of cyclic esters, Coates has reported the catalytic carbonylation of epoxides to β-lactones, as well as the carbonylation of β-lactones to succinic anhydrides.[55-58] The double carbonylation of epoxides to succinic anhydrides has also been demonstrated using the same salen or porhyrin bimetallic catalysts.[59] Production of β-lactones from epoxides was optimised using the cationic aluminium salen complex, [Al(salen)(THF)$_2$][Co(CO)$_4$] (**3.16**), whereas the porhyrin complex [Al(CITPP)(THF)$_2$][Co(CO)$_4$] (**3.17**), showed selectivity for double carbonylation of epoxides in reactions performed at 60 °C in 1,4-dioxane. Moncarbonylation could be achieved with **3.17** if THF was employed as the solvent.

These investigations have culminated in the development of a "one-pot" tandem catalytic approach to generate BBL from propylene oxide and CO using **3.17**, with subsequent ROP by Zn(BDI)(O^{i}Pr) **3.7** (and its analogues).[60] Zn(BDI)(OAc) (**3.18**, Ar = 2,6-$C_6H_3Et_2$) was shown to be the optimal polymerisation catalyst during initial screening and in a run with 0.1 mol% Al and 1.0 mol% Zn in THF at 60 °C, complete consumption of propylene oxide and subsequent polymerisation was achieved in 6 h. PHB with M_n(GPC) = 38,000 g mol^{-1} and PDI = 1.3 was produced. This route to high molecular weight PHB, with BBL as an intermediate eliminated the need for isolation and purification of the toxic monomer.

Related zinc β-diiminate ROP catalysts and Cr(III) and Co(III) salen and salan based complexes have also featured in CO_2 and epoxide (cyclohexene oxide and propylene oxide) co-polymerisation studies.[54, 61, 62] CO_2 co-polymerisations, as well as the homopolymerisation of six-membered carbonates e.g. trimethylenecarbonate (TMC), are attractive strategies for CO_2 functionalisation, but CO_2 and epoxide co-polymerisations can be prone to homopolymerisation of the epoxide or co-polymer decarboxylation, with the formation of ether linkages, as well as inert five-membered cyclic carbonates. Coates' zinc β-diiminates, although not the earliest reported CO_2/epoxide co-polymerisation catalysts were shown to produce co-polymers with 99% carbonate linkages and narrow PDIs (1.15).[62-64] Following structure-activity investigations, and noting that the more active co-polymerisation pre-catalysts form loosely bound dimers in solution, Coates proposed that these co-polymerisations operate through a bimetallic transition state. In this bimetallic pathway, one metal centre activates a pre-coordinated epoxide for attack by the growing co-polymer chain, which is presented by the second metal centre.[65, 66]

In light of Coates' proposal, a range of bimetallic zinc, transition metal and main group complexes have been developed, which are detailed in several other leading reviews and individual contributions from Darensbourg and Williams (who also reported selective coupling of CO_2 and epoxides), amongst others.[67-74] The use of mononuclear Cr(III) and Co(III) salen or salan and macrocyclic complexes is also detailed in these reviews, and whilst bimetallic transition metal complexes have been prepared, the catalytic activity of mononuclear complexes was promoted through the inclusion of ionic co-catalysts or functionalisation of the ligand periphery. There have been few reports of homogeneous rare earth complexes able to effect the co-

polymerisation of CO_2 and cyclohexene oxide, although Cui utilised half-sandwich metallocene lanthanide alkyl complexes to effect these transformations but polymer products with broad PDIs were produced.[75]

Homopolymerisation of isolated TMC monomers or co-polymerisation of CO_2 and a four-membered oxetane has also been effected with main group and transition metal salen and salan complexes.[69, 76-78] Furthermore, Carpentier has been able to demonstrate immortal type ROP of TMC in the presence of zinc catalysts (**3.7**, **3.14** and **3.15**) or simple metal triflates and alcohol chain transfer agents, although molecular weight distributions were moderately broad (PDI = 1.2–1.9).[79-82]

3.4 Preparation of multiarm PLA using 1 and tris(2-aminoethyl)amine as a co-initiator

Tris(2-aminoethyl)amine (tren) or a comparable model amine co-initiator, *N*,*N*-dimethylethylenediamine ($Me_2NCH_2CH_2NH_2$) were included in polymerisation mixtures based on [*rac*-LA]$_0$:[**1**]$_0$ = 200:1, [co-initiator]$_0$:[**1**]$_0$ = 10:1, as per $BnNH_2$ and related experiments (Equation 3.1). High conversion of monomer to poly(*rac*-LA) was achieved within 20 mins and experimental M_n were reflective of ten polymers per metal forming. For example, with tren as the co-initiator, 92% conversion was measured after 20 mins and M_n(GPC) and M_n(NMR) of 2,830 and 2,810 g mol^{-1}, with a PDI = 1.20 were in close agreement with M_n(calcd) = 2,800 g mol^{-1}. Likewise, using $Me_2NCH_2CH_2NH_2$, 91% conversion was achieved in the same time and M_n(calcd), M_n(NMR) and M_n(GPC) were 2,710, 2,320 and 2,740 g mol^{-1} respectively for the run, [*rac*-LA]$_0$:[$Me_2NCH_2CH_2NH_2$]$_0$:[**1**]$_0$ = 200:10:1 (PDI = 1.20).

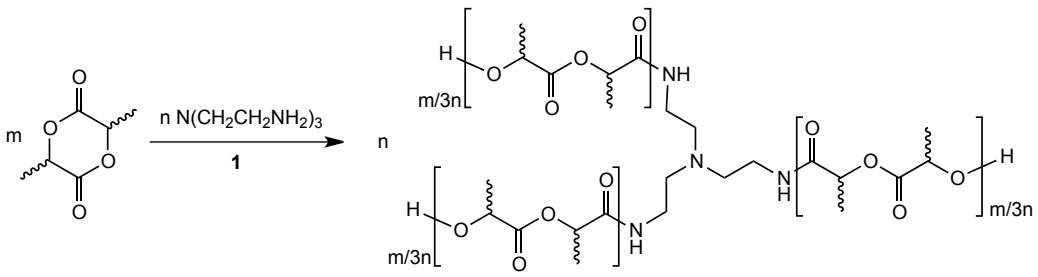

Equation 3.1

Since non-linear polymers are formed when tren is employed as a co-initiator, the applied Mark-Houwink corrections, used to calculate M_n(GPC) for linear PLA may not be appropriate. Absolute molecular weight determination can be achieved using viscometry and multiangle laser light scattering (MALLS) techniques in addition to

refractive-index methods. To compensate for the shortcoming with GPC calibration, M_n(NMR) of tren-core poly(*rac*-LA) were also calculated by integration of end-group resonances against internal enchained lactide units in ^{1}H NMR spectra. The PDIs of the tren-core PLA remained narrow, suggesting that chain transfer reactions were facile, with appropriate averaging of polymer chains occurring (Table 3.1). In a second tren-core *rac*-LA polymerisation reaction, [*rac*-LA]$_0$:[tren]$_0$:[**1**]$_0$ = 200:5:1, 89% conversion was achieved within 20 mins with M_n(GPC) = 4,660 g mol^{-1}, M_n(NMR) = 5,550 g mol^{-1}, M_n(calcd) = 5,280 g mol^{-1} and PDI = 1.20. Figure 3.7 shows the full ^{1}H NMR spectrum of the purified polymer with the internal methine (δ = 5.2 ppm) and methyl (δ = 1.5 ppm) environments being the dominant features. The terminal methine proton multiplets, HOC<u>H</u>(Me)–, were again detected at δ = 4.3 ppm along with broad tren-NH and OH signals at δ = 6.8 and 2.7 ppm. The broad features at δ = 2.5 ppm were assigned to a tren methylene (CH_2CH_2) environment. The sharp, overlapping C<u>H</u>(Me) quartets (δ = 5.2 ppm) were again consistent with high heterotactic enrichment and P_r = 0.9 were typically measured for tren-core poly(*rac*-LA) from homonuclear decoupled ^{1}H-{^{1}H} NMR experiments.

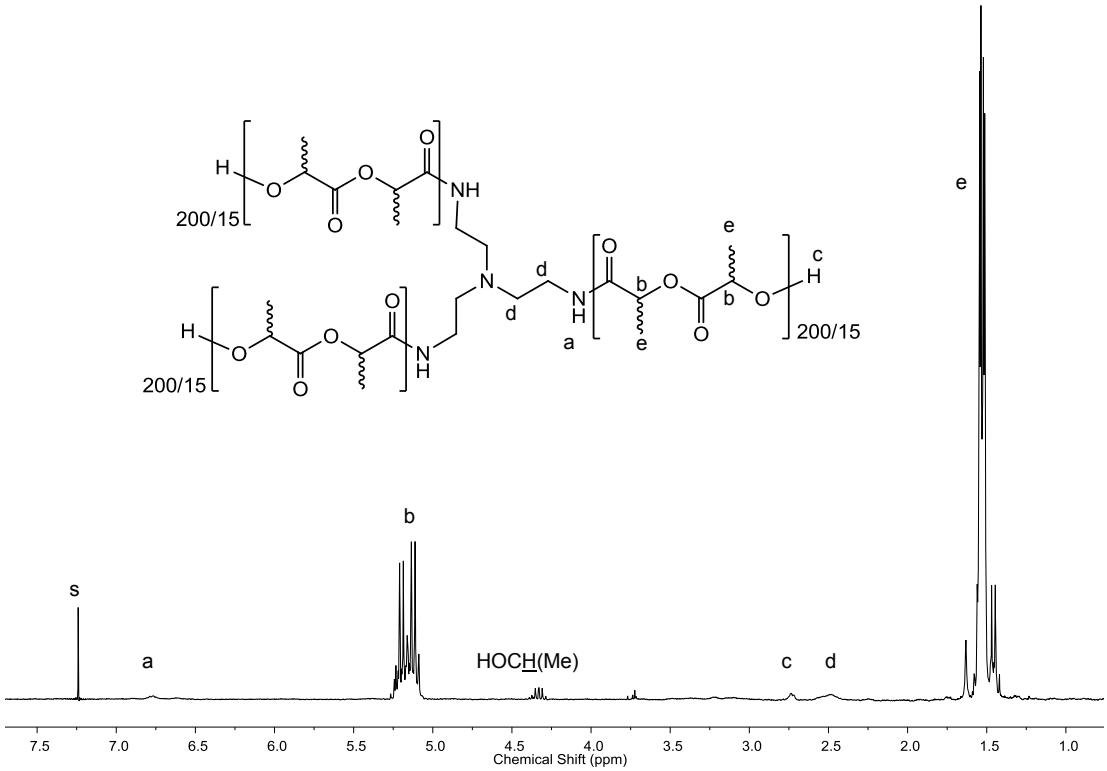

Figure 3.7. ^{1}H NMR spectrum (300.1 MHz, $CDCl_3$, 298 K) of purified tren-core poly(*rac*-LA). $[rac\text{-LA}]_0$:$[\text{tren}]_0$:$[\mathbf{1}]_0$ = 200:5:1. Residual protio-solvent, δ = 7.24 ppm.

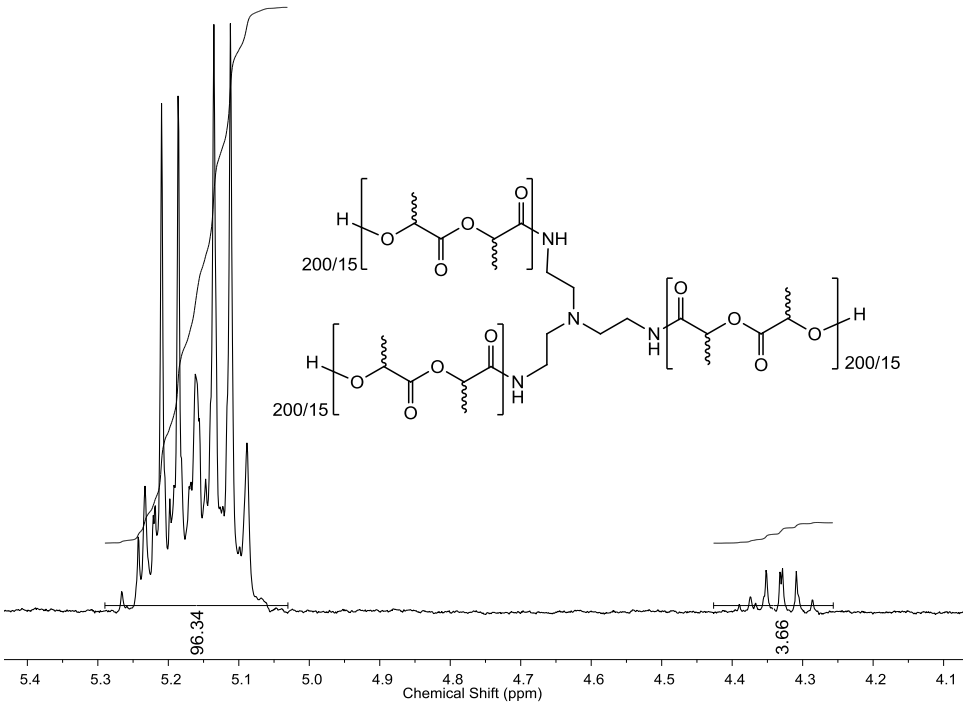

Figure 3.8. Expanded ^{1}H NMR spectrum (300.1 MHz, $CDCl_3$, 298 K), showing the CH(Me) region of tren-core poly(*rac*-LA). $[rac\text{-LA}]_0$:$[\text{tren}]_0$ = 200:5.

An expansion of Figure 3.7 with integrals is shown in Figure 3.8. Based on the [*rac*-LA]$_0$:[tren]$_0$ loading 200:5 and a conversion of 89%, 36 lactide units would be expected to form a linear chain for one active –NH_2 group per co-initiator (Figure 3.9, right). The ratio of the internal C<u>H</u>(Me) protons (δ = 5.2 ppm) to the terminal C<u>H</u>(Me) proton (δ = 4.4 ppm) would then approximate to 71:1 (two C<u>H</u>(Me) per lactide). However, in the tren-core polymer, there are three HOC<u>H</u>(Me)– groups per molecule, and the available lactide units are shared between each arm, hence an approximate ratio of C<u>H</u>(Me)–: HOC<u>H</u>(Me)– of 23:1 (96:4, Figure 3.8), or 12–13 lactide units per arm is observed. Based on this end-group integration of a relatively low molecular weight polymer, it would appear that each arm is active and that the average chain length is representative of the number of –NH_2 equivalents (Figure 3.9). If only one –NH_2 group was active, as described in Figure 3.9 (right), then multiple NH and tren methylene (CH_2CH_2) signals would appear in the ^{1}H NMR spectrum, but the ^{1}H NMR spectrum shown in Figure 3.7 was consistent with single NH and CH_2CH_2 environments and multiarm PLA forming.

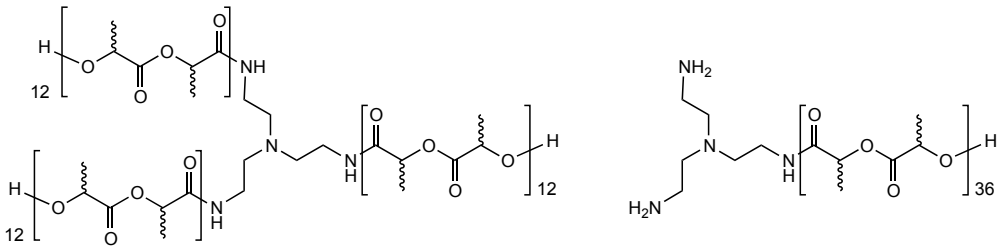

Figure 3.9. Multiarm tren-core and linear tren-capped poly(*rac*-LA).

It is difficult to calculate M_n(NMR) for linear poly(*rac*-LA) above loadings of [*rac*-LA]$_0$:[co-initiator]$_0$ = 200:5, as the relative intensities of the end-groups diminish as the polymer chain length increases. However, with the multiarm polymers, due to the sharing of lactide monomers around each arm, the chains are shorter and end-groups appear more intense. This was evident in a series of loading studies with [*rac*-LA]$_0$:[tren]$_0$ = 200:1, 2, 5, 8 or 10, where M_n(NMR) could be estimated down to a tren loading of [*rac*-LA]$_0$:[tren]$_0$ = 200:2 (Table 3.1). However, in the comparable runs with $Me_2NCH_2CH_2NH_2$, M_n(NMR) was only effectively measured for shorter polymers ([*rac*-LA]$_0$:[$Me_2NCH_2CH_2NH_2$]$_0$ = 200:8 or 200:10). M_n(GPC) for tren-core poly(*rac*-LA) were in reasonable agreement with the M_n(GPC) of $Me_2NCH_2CH_2NH_2$-capped PLA, which may indicate that $Me_2NCH_2CH_2NH_2$ is a "non-optimal" primary amine or that satisfactory GPC analysis of tren-core PLA could be undertaken in this

instance. At lower loadings of co-initiator, [*rac*-LA]$_0$:[co-initiator]$_0$ = 200:1 or 200:2, M_n(GPC) were lower than expected for both tren and $Me_2NCH_2CH_2NH_2$ runs, which was also seen in $BnNH_2$ runs (Chapter Two, Figure 2.12). Higher loadings of co-initiator ([*rac*-LA]$_0$:[co-initiator]$_0$ = 200:5, 8 or 10) generally achieved better control between M_n(calcd) and M_n(GPC) under these conditions.

Table 3.1. Polymerisation data for tren and $Me_2NCH_2CH_2NH_2$ co-initiated ROP of *rac*-LA.[a]

Equivs. [tren]$_0$	Conv. (%)[b]	M_n(calcd) (g mol^{-1})[c]	M_n(GPC) (g mol^{-1})[d]	M_n(NMR) (g mol^{-1})[e]	M_w/M_n[d]	P_r[b]
1	90	26,090	18,270	[f]	1.14	0.93
2	90	13,120	11,060	9,660	1.18	0.93
5	89	5,280	4,660	5,550	1.20	0.91
8	89	3,350	3,080	3,470	1.21	0.89
10	92	2,800	2,830	2,810	1.20	0.86
Equivs. [$Me_2NCH_2CH_2NH_2$]$_0$	Conv. (%)[b]	M_n(calcd) (g mol^{-1})[c]	M_n(GPC) (g mol^{-1})[d]	M_n(NMR) (g mol^{-1})[e]	M_w/M_n[d]	P_r[b]
1	90	26,030	19,980	[f]	1.13	0.90
2	92	13,350	10,820	[f]	1.18	0.93
5	90	5,280	5,040	[f]	1.20	0.92
8	90	3,330	3,110	3,170	1.21	0.89
10	91	2,710	2,740	2,320	1.20	0.88

[a] [*rac*-LA]$_0$:[**1**]$_0$ = 200:1, 4 mL THF, [*rac*-LA]$_0$ = 0.69 M, rt, 20 mins. [b] Conversion and P_r (by integration of appropriate tetrads) measured by ^{1}H and ^{1}H-{^{1}H} NMR in $CDCl_3$. [c] M_n(calcd) = (Conv. (%) × [*rac*-LA]$_0$:[Co-initiator]$_0$ × 144.1 + M_R Co-initiator). [d] Measured by GPC against polystyrene standards using the appropriate Mark-Houwink corrections for poly(*rac*-LA) in THF at 30 °C. [e] Calculated from the relative integrals of the internal C<u>H</u>(Me) resonances of the PLA chain against the unique HOC<u>H</u>(Me)– end-group. [f] Polymer chain too long for reliable M_n estimation by ^{1}H NMR.

Additional loading studies were performed where [co-initiator]$_0$:[**1**]$_0$ was held constant at 5:1, but [*rac*-LA]$_0$:[**1**]$_0$ was increased through 100, 200, 500, 800 and 1000 molar equivs. The M_n data are plotted as a function of ([*rac*-LA]$_0$ – [*rac*-LA]$_t$):[co-initiator]$_0$ in Figure 3.10. At lower loadings of *rac*-LA ([*rac*-LA]$_0$:[**1**]$_0$ = 100, 200 or 500), the agreement between expected and observed M_n are comparable for both tren

and $Me_2CH_2CH_2NH_2$, but at higher loadings, the M_n(GPC) values for tren-core PLA began to diverge more from M_n(calcd), perhaps a reflection of the unsuitable Mark-Houwink corrections for this polymer architecture.

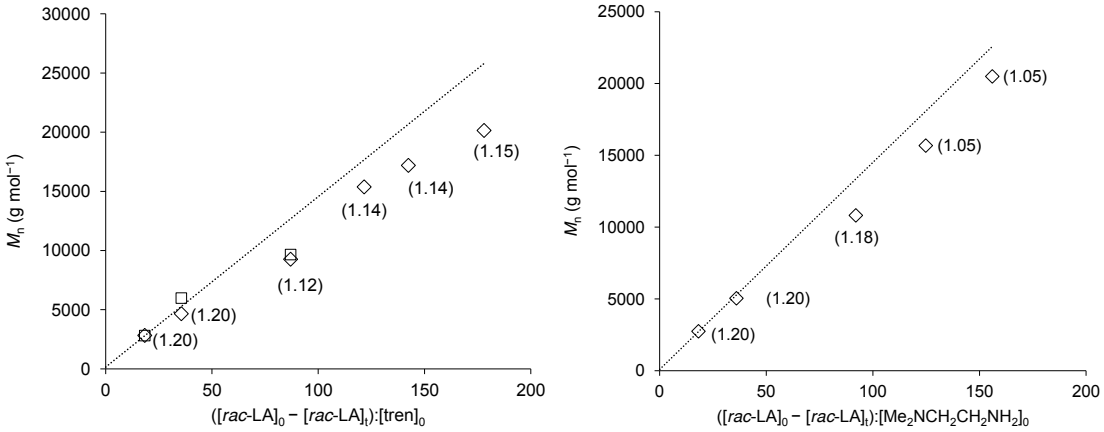

Figure 3.10. M_n as a function of ([*rac*-LA]$_0$ – [*rac*-LA]$_t$):[tren]$_0$ or ([*rac*-LA]$_0$ – [*rac*-LA]$_t$):[$Me_2NCH_2CH_2NH_2$]$_0$ with [*rac*-LA]$_0$:[**1**]$_0$ = 100, 200, 500, 800 (duplicated for tren) or 1000 and [co-initiator]$_0$:[**1**]$_0$ = 5:1. The dashed lines represent M_n(calcd), diamonds represent M_n(GPC) and squares represent M_n(NMR). The PDIs are given in parentheses.

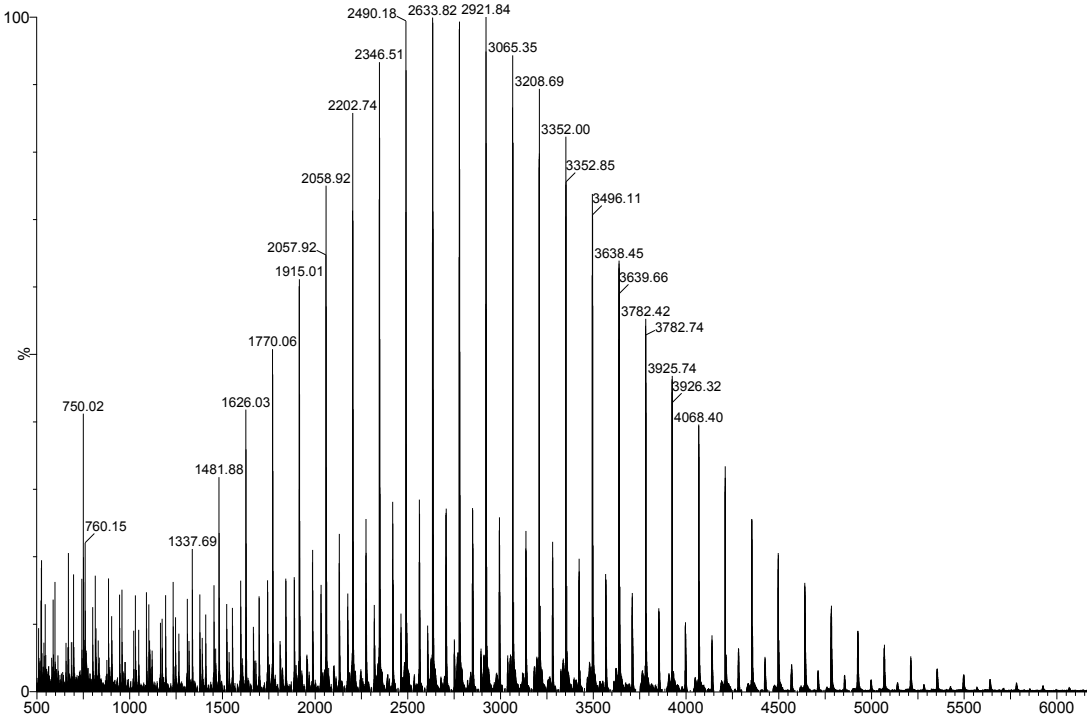

Figure 3.11. Full MALDI-ToF mass spectrum of crude poly(*rac*-LA) formed from a tren-core, [*rac*-LA]$_0$:[tren]$_0$:[**1**]$_0$ = 100:5:1. K^+ dopant, Δ(*m/z*) = 144 g mol^{-1}.

MALDI-ToF mass spectra of tren-core poly(*rac*-LA) (Figure 3.11) consistently showed more evidence for tranesterification than linear amine-capped poly(*rac*-LA) prepared using **1**, but it should be noted that MALDI-ToF MS is not a quantitative technique and care should be taken when trying to estimate the relative populations of polymer products. Furthermore, it is not clear if tren-core poly(*rac*-LA) will be doped with K^+ ions as effectively as linear poly(*rac*-LA), and thus the low *m/z* cyclic products may appear more dominant. There was a greater divergence between M_n(GPC) and M_n(calcd) in the M_n *vs*. ([*rac*-LA]$_0$ – [*rac*-LA]$_t$) plots (Figure 3.10, left) at higher [*rac*-LA]$_0$ loadings than in the comparable plots for $Me_2NCH_2CH_2NH_2$ (Figure 3.10, right), which may have arisen from chain shortening transesterification processes. During polymerisation, dormant chains attached to tren-cores may be in closer proximity to the metal centre, thus tranesterification processes may be promoted. However, the major distribution, $\Delta(m/z) = 144$ g mol^{-1} was consistent with systematic formation of tren-core poly(*rac*-LA).

The described experimental evidence suggested that tren co-initiators consumed the requisite number of *rac*-LA units, based on the initial [*rac*-LA]$_0$:[tren]$_0$ loading and that each terminal $–NH_2$ amine initiated ring-opening. The average arm length was consistent with the number of $–NH_2$ equivalents, although a distribution of arm lengths was likely to form. Appropriate kinetic analysis was undertaken with the tren and $Me_2NCH_2CH_2NH_2$ co-initiators under the same conditions as the $BnNH_2$ runs (Chapter Two, Section 2.7.1) to investigate whether the change in polymer architecture had an effect on initiation and propagation behaviour, particular in light of Cui's report of a negative rate dependence in triethanolamine when $Y(O_2N^{NMe2})(CH_2SiMe_3)(THF)$ (**1.22**) and TEA were used as co-initiators in the immortal ROP of *rac*-LA.[21]

3.4.1 Kinetics of tren and $Me_2NCH_2CH_2NH_2$ co-initiated ROP reactions

Kinetic studies using the tren co-initiator were pursued to investigate whether the architecture of the co-initiator and of the resultant polymer would affect the polymerisation kinetics. Reactions were performed with [*rac*-LA]$_0$:[**1**]$_0$ = 200:1 ([*rac*-LA]$_0$ = 0.69 M) and [tren]$_0$:[**1**]$_0$ = 1, 2 or 3:1, equivalent to 3, 6 or 9 active $–NH_2$ amine initiating groups. 3, 6 or 9 equivs. of $Me_2NCH_2CH_2NH_2$ were used as a comparable model amine in separate polymerisation runs. As in the case of $BnNH_2$ co-initiated ROP of *rac*-LA, 80% conversion monomer to poly(*rac*-LA) was achieved

within 7 mins and *rac*-LA consumption was modelled with a second-order dependence. These Conversion *vs*. Time and second-order rate plots (Figures 3.12 and 3.13) indicated no systematic dependence in $[tren]_0$ or $[Me_2NCH_2CH_2NH_2]_0$ and suggested that propagation occurred *via* a metal mediated coordination-insertion mechanism, as proposed in Chapter Two, Figure 2.15. k_{app} = 0.813(29) M^{-1} min^{-1} for the run $[rac\text{-LA}]_0:[tren]_0:[\mathbf{1}]_0$ = 200:1:1 was comparable to that observed for both $[rac\text{-LA}]_0:[Me_2NCH_2CH_2NH_2]_0:[\mathbf{1}]_0$ = 200:3:1 (k_{app} = 0.854(27) M^{-1} min^{-1}) and $[rac\text{-LA}]_0:[BnNH_2]_0:[\mathbf{1}]_0$ = 200:*n*:1 ($k_{app} \approx 0.8$ M^{-1} min^{-1}). The vertical-axis intercepts of each second-order rate plot (0.8–1.2 M^{-1}) were consistently lower than expected ($1/[rac\text{-LA}]_0$ = 1.44 M^{-1}) and were indicative of a small induction period, as noted for the kinetic runs with $BnNH_2$ (Chapter Two, Figure 2.12). However, owing to the appreciable conversion (*ca*. 10%) in the first minute, this induction period was included in the propagation model. The dependence in $[\mathbf{1}]_0$ was not measured for tren or $Me_2NCH_2CH_2NH_2$ co-initiated polymerisations but is presumed to follow the first-order dependence found for the $BnNH_2$ (Chapter Two, Figure 2.13) co-initiated reactions. A reduced overall propagation rate law, $R_p = k_{\mathbf{1}}[rac\text{-LA}]^2$ with $k_{\mathbf{1}} = k_p[\mathbf{1}]_0$ is proposed in this case.

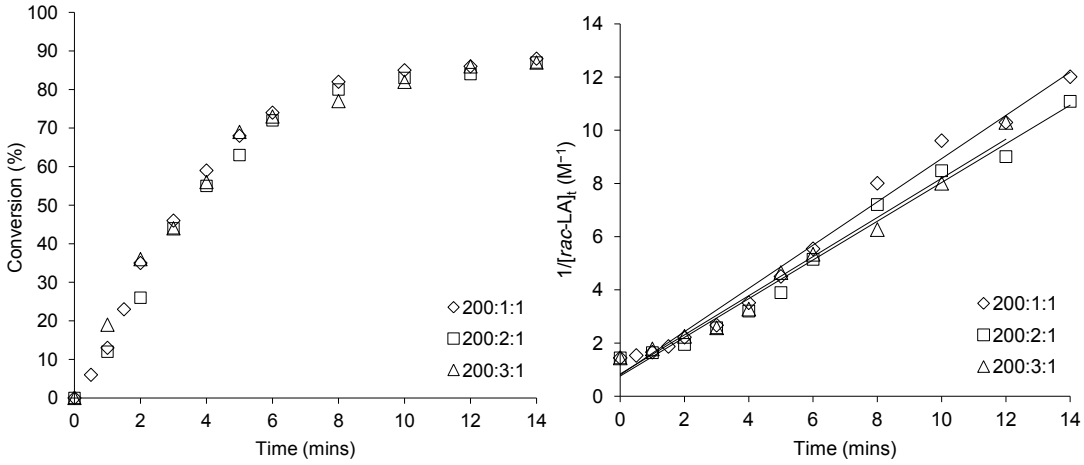

Figure 3.12. Conversion *vs*. Time profiles (left) and second-order rate plots (right) for polymerisation runs using tren as a co-initiator. $[rac\text{-LA}]_0:[tren]_0:[\mathbf{1}]_0$ = 200:1:1, 200:2:1 or 200:3:1; k_{app} = 0.813(29) (R^2 = 0.986), 0.728(33) (R^2 = 0.982) and 0.735(37) (R^2 = 0.980) M^{-1} min^{-1}. The vertical-axis intercepts of the plots are 0.800(199), 0.757(239) and 0.837(236) M^{-1}, with the expected intercept, $1/[rac\text{-LA}]_0$ = 1.44 M^{-1}.

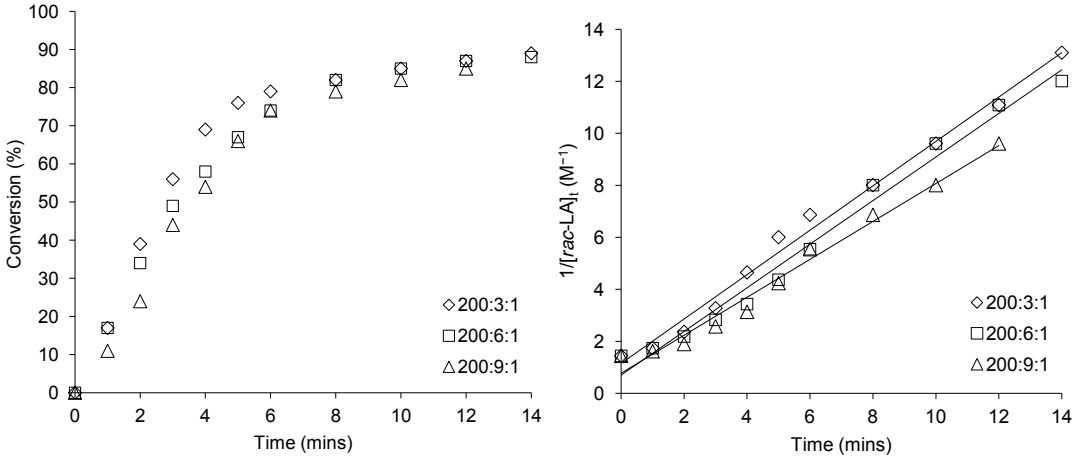

Figure 3.13. Conversion *vs*. Time profiles (left) and second-order rate plots (right) for polymerisation runs using $Me_2NCH_2CH_2NH_2$ as a co-initiator [*rac*-LA]$_0$:[$Me_2NCH_2CH_2NH_2$]$_0$:[**1**]$_0$ = 200:3:1, 200:6:1, 200:9:1; k_{app} = 0.854(27) (R^2 = 0.991), 0.839(36) (R^2 = 0.984) and 0.729(34) (R^2 = 0.983) M^{-1} min^{-1}. The vertical-axis intercepts of the plots are 1.149(199), 0.701(261) and 0.774(216) M^{-1}, with the expected intercept, 1/[*rac*-LA]$_0$ = 1.44 M^{-1}.

Molecular weight data for selected aliquots were measured and showed that M_n increased linearly with conversion, although data for the run, [*rac*-LA]$_0$:[tren]$_0$ = 200:1 showed relatively poor agreement between M_n(GPC) and M_n(calcd) (Figure 3.14, left). This poor agreement at a loading of 200:1 was consistent with the data point described in Table 3.1 for this comparable run and again may have arisen because of the inappropriate correction factor for M_n(GPC). The corresponding run with [*rac*-LA]$_0$:[$Me_2NCH_2CH_2NH_2$]$_0$ = 200:3 also showed relatively poor agreement between M_n(GPC) and M_n(calcd) and may indicate that $Me_2NCH_2CH_2NH_2$ is a "non-optimal" amine for amine-initiated, ROP in this instance. The apparent rate constants and selected M_n data for these kinetic runs are also summarised in Table 3.2.

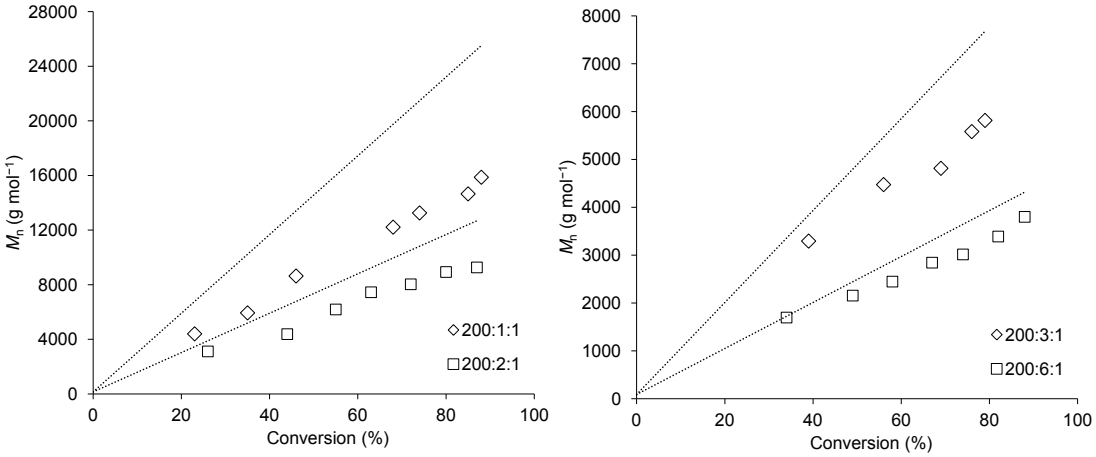

Figure 3.14. M_n(GPC) *vs*. Conversion plots for polymerisation of *rac*-LA runs (left), [*rac*-LA]$_0$:[tren]$_0$ = 200:1 or 200:2, [*rac*-LA]$_0$:[**1**]$_0$ = 200:1 and right, the equivalent polymeriation runs with $Me_2NCH_2CH_2NH_2$ as the co-initiator. PDIs = 1.10–1.20.

3.5 Summary of tren co-initiated, ROP of *rac*-LA

The polyamine, tris(2-aminoethyl)amine, has been shown to effect the amine-initiated, immortal ROP of *rac*-LA and the first examples of poly(*rac*-LA) grown from a polyamine core with heterotactic enrichment were described. Kinetics experiments have shown tren co-initiated polymerisations to behave like the equivalent benzyl amine and $Me_2NCH_2CH_2NH_2$ runs, with no systematic dependence in [tren]$_0$. This was in contrast in Cui's observation with $Y(O_2N^{NMe2})(CH_2SiMe_3)(THF)$ (**1.22**) and TEA in which a negative rate dependence was determined in [TEA]$_0$ over a range of [TEA]$_0$ loadings from 0.33 up to 9.0 molar equivs. ([*rac*-LA]$_0$:[**1.22**]$_0$ = 900:1).[21] Representative tren-core PLA have shown that each "arm" of the tren-core participates in ROP but a distribution of chain lengths is likely to form, despite M_n generally reflecting [*rac*-LA]$_0$:[tren]$_0$. Narrow PDIs also confirmed facile initiation and chain transfer processes and the immortal nature of these polymerisations.

Table 3.2. Summary of rate constants and molecular weight data from *rac*-LA polymerisations co-initiated by **1** and tren or $Me_2NCH_2CH_2NH_2$.

Entry	Co-initiator	[*rac*-LA]$_0$:[Co-initiator]$_0$:[**1**]$_0$ [a]	k_{app} (M^{-1} min^{-1}) [b]	R^2 [b]	Conv. (%) [c]	M_n(calcd) (g mol^{-1}) [c]	M_n(GPC) (g mol^{-1}) [d]	M_w/M_n [d]
1	tren	200:1:1	0.813(29)	0.986	88	25,510	15,870	1.10
2	tren	200:2:1	0.728(33)	0.982	87	12,690	9,260	1.12
3	tren	200:3:1	0.735(37)	0.980	82	8,030	6,370	1.19
4	$Me_2NCH_2CH_2NH_2$	200:3:1	0.854(27)	0.991	79	7,680	5,820	1.18
5	$Me_2NCH_2CH_2NH_2$	200:6:1	0.839(36)	0.984	88	4,320	3,800	1.20
6	$Me_2NCH_2CH_2NH_2$	200:9:1	0.729(34)	0.983	79	3,880	3,390	1.21

[a] [*rac*-LA]$_0$ = 0.69 M, 4 mL THF, rt. [b] Apparent second-order rate constants for consumption of *rac*-LA with standard error and R^2 determined by linear regression analysis. [c] Reactions monitored by ^{1}H NMR ($CDCl_3$). All quoted conversions refer to the last point where M_n(GPC) was determined. M_n(calcd) = (Conv. (%) × [*rac*-LA]$_0$:[Co-initiator]$_0$ × 144.1 + M_R Co-initiator). [d] Measured by GPC against polystyrene standards using Mark-Houwink corrections for linear poly(*rac*-LA) in THF at 30 °C.

3.6 ε-Caprolactone and β-butyrolactone polymerisation studies

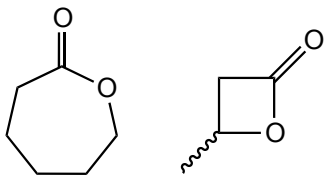

Figure 3.15. ε-caprolactone (ε-CL) (left) and β-butyrolactone (BBL) (right).

The *rac*-LA ROP studies have demonstrated that inclusion of suitable amines in polymerisation mixtures can lead to well-controlled, immortal type polymeriations. Whilst this methodology has been shown to be successful for primary, secondary and polyamines, the range of suitable monomers has not yet been considered. The seven-membered lactone, ε-CL (Figure 3.15), was selected initially owing to its prevalence in the ROP literature as a desirable biodegradable polymer and its use as a co-monomer in co-polymerisations with lactide,[83, 84] and there are numerous examples of ε-CL polymeriation in the presence of co-initiators, including amines.[15, 17, 18, 85, 86] In light of the successful ROP reactions with *rac*-BBL reported by Coates and Carpentier, *rac*-BBL polymerisations co-initiated by **1** and a range of amines and benzyl alcohol will also be described.[25, 26, 44]

3.6.1 ε-caprolactone (ε-CL) polymerisation studies

In a benchmarking run with no co-initiator, 100 equivs. of ε-CL were added to **1** in THF solution at room temperature and complete conversion was achieved within 20 mins. M_n(GPC) = 18,680 g mol^{-1} was in reasonable agreement for one chain per metal (M_n(calcd) = 14,410 g mol^{-1}). However, a very broad PDI of 2.65 was also suggestive of an uncontrolled polymerisation that was likely to have been initiated by trace water or caproic acid. When 5 equivs. of $BnNH_2$ were included in the polymerisation mixture, M_n(GPC) was reduced to 5,790 g mol^{-1} (and the PDI narrowed to 1.82) but was more than twice that expected for five chains (M_n(calcd) = 2,170 g mol^{-1}). In an attempt to prepare short chain PCL ([ε-CL]$_0$:[$BnNH_2$]$_0$:[**1**]$_0$ = 20:5:1) for characterisation by MALDI-ToF MS, the M_n(GPC) = 6,640 g mol^{-1} of the resultant polymer was much greater than expected (M_n(calcd) = 560 g mol^{-1}) and was suggestive of a non-systematic relationship between M_n and [ε-CL]$_0$:[$BnNH_2$]$_0$. From these initial experiments it would seem that ε-CL is not suited to amine co-initiated,

ROP with **1**. The amine-initiation phase does not appear to be as competitive as chain propagation based on the consistently higher than expected M_n(GPC) and broad PDI.

In a low temperature NMR tube scale reaction, ε-CL (10 equivs.) in THF-d_8 was added to a mixture of $BnNH_2$ (2 equivs.) and **1** (to ensure an initial excess of amine over any impurity capable of co-initiating polymerisation) at –35 °C. Initial analysis at this temperature showed ring-opened products along with unreacted $BnNH_2$. The solution was warmed in five-degree increments and unreacted $BnNH_2$ persisted in solution as conversion of ε-CL to PCL approached completion at 0 °C. Approximately two thirds of the $BnNH_2$ remained unreacted, based on the relative integrals between $BnNH_2$ and a presumed BnNH– end-group. In light of these observations and the aforementioned molecular weight data, it would seem that chain propagation processes are competitive with co-initiation by $BnNH_2$. Once a ε-CL unit has been ring-opened by $BnNH_2$, the newly formed macromonomer, with a hydroxyl/alkoxide end-group is likely to react faster with ε-CL monomers than remaining $BnNH_2$. Trace water or other impurities may have also outcompeted $BnNH_2$ in this case.

3.6.2 β-butyrolactone (BBL) polymerisation studies

The four-membered lactone, β-butyrolactone (BBL), proved to be more successful and Carpentier has shown it to be a suitable monomer for immortal ROP in the presence of alcohol co-initiators.[26] Thus, in a benchmarking run, 100 equivs. of *rac*-BBL were added to a stoichiometric mixture of **1.15** and ^{i}PrOH in toluene at room temperature. Complete conversion of monomer to PHB was achieved within minutes and a M_n(GPC) = 10,340 g mol^{-1}, with a PDI = 1.19 was in reasonable agreement with M_n(calcd) = 8,600 g mol^{-1}.

When 5 equivs. of $BnNH_2$ were included in a polymerisation mixture, [*rac*-BBL]$_0$:[$BnNH_2$]$_0$:[**1**]$_0$ = 100:5:1 ([*rac*-BBL]$_0$ = 1.16 M, toluene, room temperature), complete conversion of monomer to PHB was achieved within 5 mins. M_n(GPC) = 2,620 g mol^{-1} (treating PHB as a polystyrene for GPC analysis) was in reasonable agreement with one PHB chain forming per amine (M_n(calcd) = 1,830 g mol^{-1}), and the PDI = 1.12 was suggestive of a well-controlled polymerisation reaction displaying immortal behaviour. M_n(NMR) was also calculated by integration of the internal C<u>H</u>(Me) resonance against the terminal HOC<u>H</u>(Me)– signal, and the value of

M_n(NMR) = 1,760 g mol^{-1} for this polymer was in favourable agreement with M_n(calcd). When no co-initiator was included in the polymerisation mixture, a high molecular weight gel, not suitable for GPC analysis was formed within 5 mins.

Table 3.3. Immortal ROP of BBL with incorporation of amine end-groups.[a]

Co-initiator	M_n(calcd) (g mol^{-1})[b]	M_n(GPC) (g mol^{-1})[c]	M_n(NMR) (g mol^{-1})[d]	M_w/M_n[c]
BnOH	1,830	2,700	1,900	1.13
$BnNH_2$	1,830	2,620	1,760	1.12
$C_5H_{10}NH$	1,810	2,690	1,840	1.12
tren	1,870	2,020	1,770	1.07

[a] [*rac*-BBL]$_0$:[Co-initiator]$_0$:[**1**]$_0$ = 100:5:1, [*rac*-BBL]$_0$ = 1.16 M, 2 mL toluene, 5 mins, rt. [b] Measured conversions > 99% by ^{1}H NMR ($CDCl_3$). M_n(calcd) = ([*rac*-BBL]$_0$:[$BnNH_2$]$_0$ × 86.0 + M_R Co-initiator). [c] Measured by GPC using Mark-Houwink corrections for polystyrene in THF at 30 °C. [d] Calculated from the relative integrals of the internal C<u>H</u>Me resonances of the PHB chain against the unique HOC<u>H</u>(Me)– end-group.

The scope of end-group incorporation was extended to BnOH, piperidine and tren with the results summarised in Table 3.3, along with the data for benzyl amine capped-PHB. M_n(NMR) were calculated and were in very good agreement with M_n(calcd). Each new PHB product was isolated and further characterised by ^{1}H and ^{13}C-{^{1}H} (for stereosequence assignment) NMR and MALDI-ToF MS, with a full ^{1}H NMR spectrum of purified benzyl amine-capped PHB shown in Figure 3.16. Significant PHB features include the internal C<u>H</u>(Me) multiplet at δ = 5.2 ppm, diastereotopic CH_2 multiplets at δ = 2.5 ppm and overlapping CH(<u>Me</u>) doublets at δ = 1.3 ppm. The terminal HOC<u>H</u>(Me)– proton was observed at δ = 4.2 ppm and the OH doublet was present at δ = 3.1 ppm. $PhCH_2NH$– features include aromatic environments, a broad NH environment at δ = 6.3 ppm and $PhC\underline{H}_2NH$– methylene multiplets at δ = 4.4 ppm that integrated in a 2:1 ratio against the terminal HOC<u>H</u>(Me)– proton at δ = 4.2 ppm.

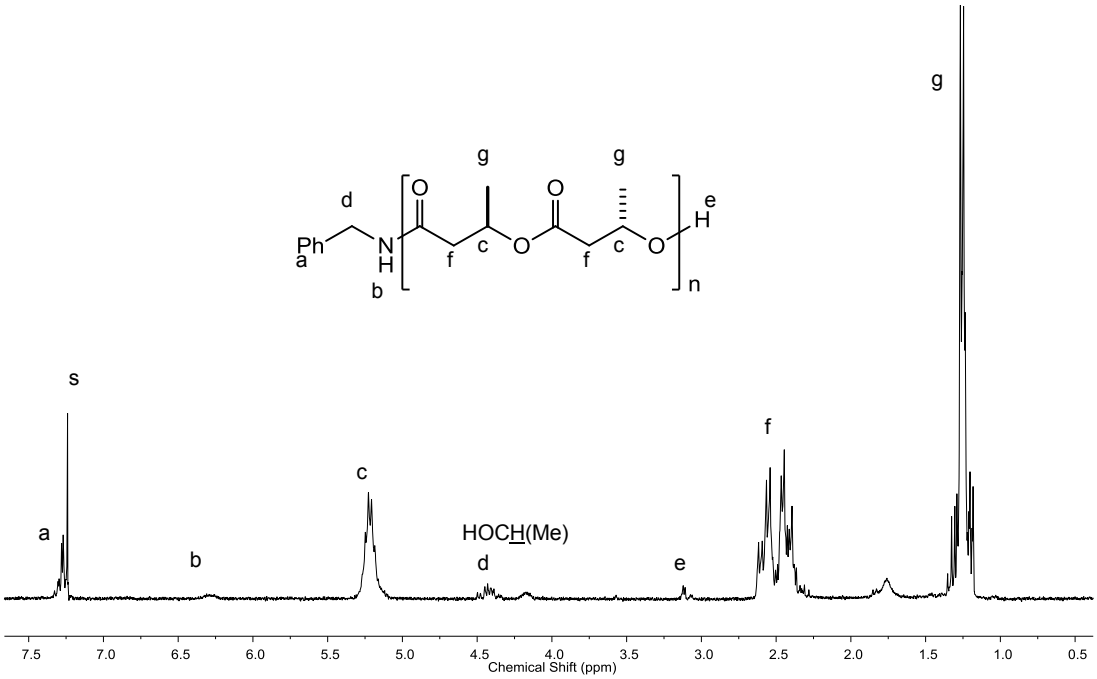

Figure 3.16. Full ^{1}H NMR spectrum (300.1 MHz, $CDCl_3$, 298 K) of benzyl amine-capped PHB isolated from the run, $[rac\text{-BBL}]_0$:$[BnNH_2]_0$:$[\mathbf{1}]_0$ = 100:5:1. Residual protio-solvent, δ = 7.24 ppm.

Expanded regions of the ^{1}H NMR spectra of tren, piperidine and benzyl alcohol-capped PHB, along with the benzyl amine example are shown in Figure 3.17. Terminal HOCH(Me)– environments are common to each spectrum (δ = 3.1 and 4.2 ppm), but significantly for tren-core PHB (Figure 3.17, top), the broad NH singlet was present at δ = 6.9 ppm, with NCH_2CH_2NH– signals at δ = 3.2 ppm. Distinct end-group triplets (δ = 3.6 and 3.4 ppm) were observed in the spectrum of piperidine-capped PHB (Figure 3.17, second from top) and aromatic environments and a methylene doublet, $PhCH_2O$– (δ = 5.1 ppm) were present in the benzyl alcohol-capped PHB spectrum (Figure 3.17, third from top).

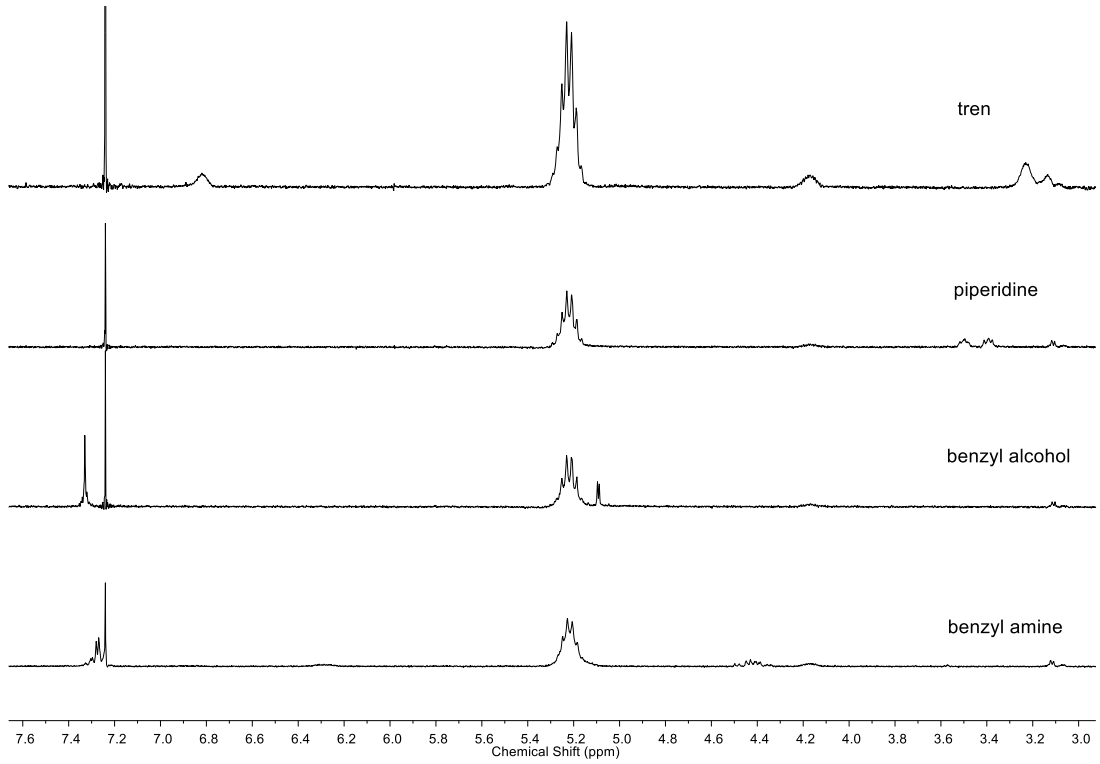

Figure 3.17. Expanded regions of the ^{1}H NMR spectra (300.1 MHz, $CDCl_3$, 298 K) of functionalised PHB. From top to bottom: tren, piperidine, benzyl alcohol and benzyl amine. Residual protio-solvent, δ = 7.24 ppm.

3.6.3 PHB stereosequence assignment

Carpentier has reported PHB with a high degree of syndiotactic enrichment, i.e. alternating enchainment of *R*- (or *S*-) followed by *S*- (or *R*-) BBL enantiomers and has used ^{13}C-{^{1}H} NMR along with Bernoullian statistical analysis to resolve stereosequences in PHB produced by $Y(O_2N^{OMe})\{N(SiHMe_2)_2\}(THF)$ (**1.14**) and its bulkier analogues.[26, 44] The probabilities of forming racemic linkages, P_r, have been determined by integration of *racemic* (*r*) and *meso* (*m*) diad (and at the triad level) resonances. Selected regions of the ^{13}C-{^{1}H} NMR spectrum of benzyl amine-capped PHB produced by **1** are shown in Figure 3.18. A $P_r \approx 0.8$ was suggested from integration of the *racemic* (*r*) and *meso* (*m*) diads in the methyl region (δ = 19.8 ppm) of PHB, which was consistent with that measured by Carpentier for syndiotactic PHB prepared using **1.14**.

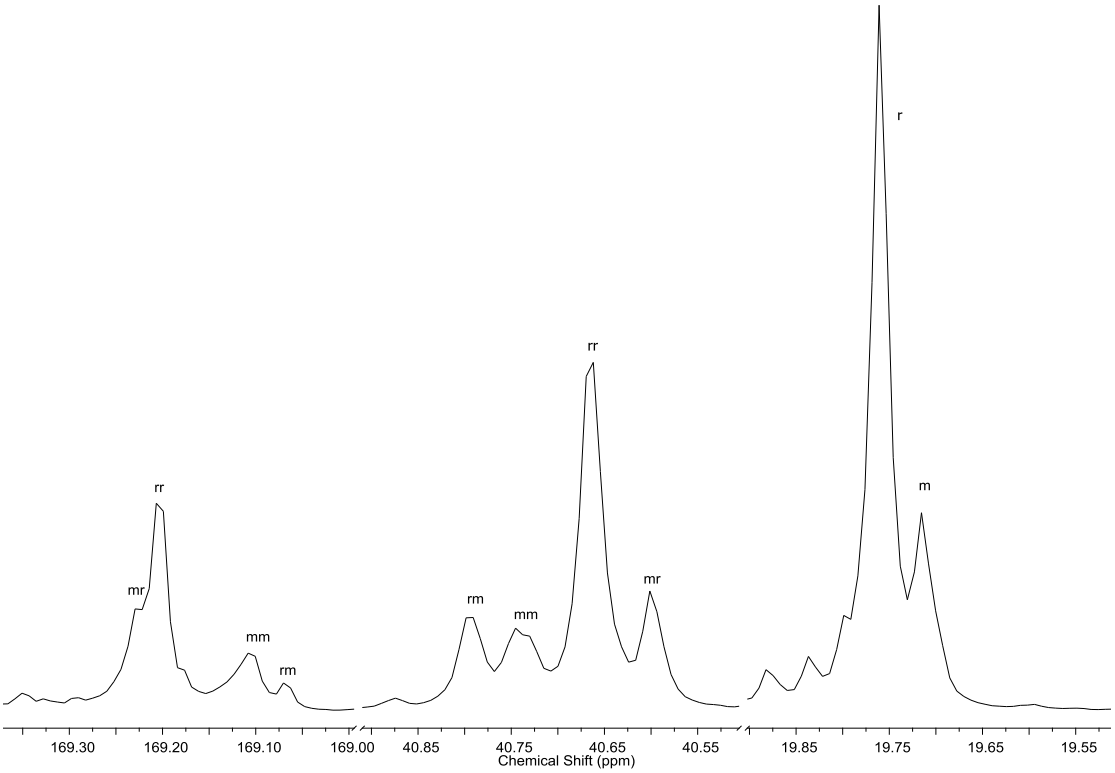

Figure 3.18. Selected regions of the ^{13}C-{^{1}H} NMR spectrum (125.8 MHz, $CDCl_3$, 298 K) of benzyl amine-capped PHB ([*rac*-BBL]$_0$:[$BnNH_2$]$_0$:[**1**]$_0$ = 100:5:1) with stereosequence assignment. δ = 169 ppm, CO; δ = 40.7 ppm, CH_2; δ = 19.8 ppm CH_3.[26, 44]

Carpentier has shown that the probability of forming racemic linkages is improved as the steric bulk of the phenolate *ortho* substituents is increased. For example, with Y($O_2^{2\text{-CPh3-4-Me}}N^{OMe}$){N($SiHMe_2$)$_2$}(THF) (**3.18**), a P_r = 0.94 was measured for a PHB produced from a loading of *rac*-BBL to initiator of 400:1.[44] In the ^{13}C-{^{1}H} NMR spectrum of this polymer, the *mr* and *rm* triads in the CO and CH_2 regions were much less intense and the relative population of *mm* triads, corresponding to *RRR* or *SSS* enchained BBL units was negligible. Significant populations of *mm* triads were present in the ^{13}C-{^{1}H} NMR spectra of PHB produced by **1** (Figure 3.18); hence **1** is a "non-optimal" catalyst for production of PHB with syndiotactic enrichment. Carpentier has also suggested that the phenyl flanking groups of **3.18** may influence stereoselectivity in the ROP of *rac*-BBL through C–H•••π interactions between the ligand and monomer.[87]

3.6.4 MALDI-ToF MS analysis and loading studies

The major distributions present in the MALDI-ToF mass spectra of isolated PHB were consistent with systematic end-group incorporation (Figure 3.19). A minor distribution corresponding to cyclic PHB products with no apparent end-group was also present, indicating that some transesterification processes were operating during polymerisation. However, Coates has noted the propensity of PHB to undergo post-polymerisation tranesterification in the presence of Lewis acid metal residues and has isolated PHB degradation products.[25] Although the polymerisation reaction times for the preparation of amine capped-PHB were short (5 mins) and the kinetic experiments (*vide infra*) showed that a 5 minute reaction time was the optimal timeframe for these preparative reactions, it remains unclear whether the majority of cyclic forming processes occurred during or post-polymerisation.

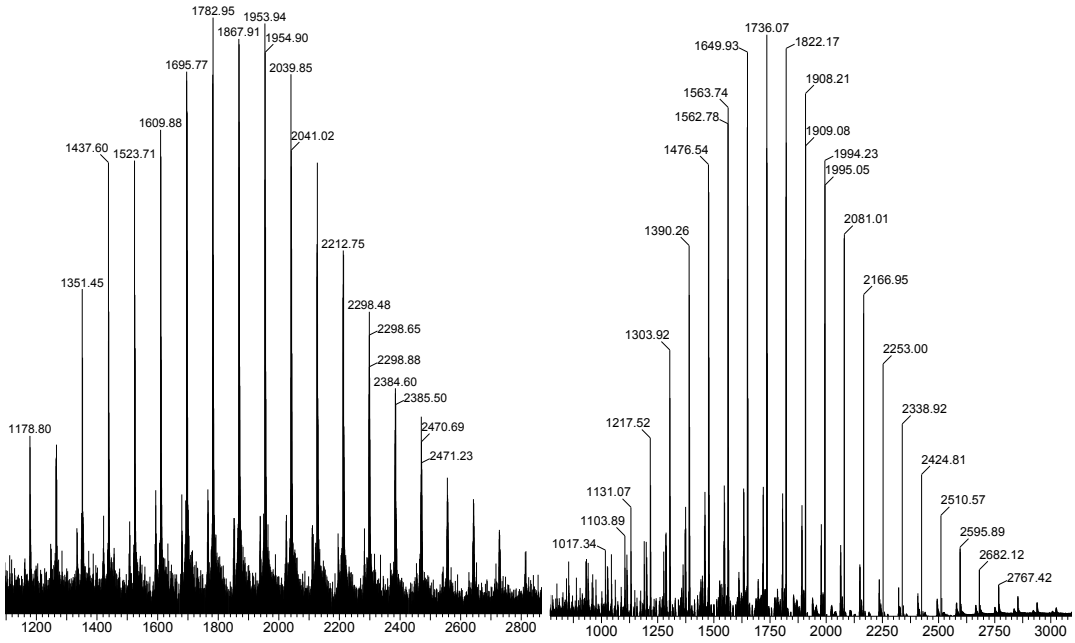

Figure 3.19. MALDI-ToF mass spectra of $BnNH_2$-capped (left) and tren-core (right) PHB. K^+ dopant, $\Delta(m/z)$ = 86.0 g mol^{-1}.

Further loading experiments were performed to establish the suitability of PHB for amine-initiated, immortal ROP of [*rac*-BBL]$_0$. The number of [*rac*-BBL]$_0$ equivalents were increased through 100, 200, 500, 800 and 1000 with [$BnNH_2$]$_0$:[**1**]$_0$ = 5:1 (Figure 3.20.). In light of the success using tren and *rac*-LA, 5 equivs. of tren were also included in *rac*-BBL polymerisation mixtures to compare with $BnNH_2$ co-initiated runs. Despite treating each PHB as a polystyrene for GPC analysis, M_n(GPC) were in

good agreement with M_n(calcd) and PDI were narrow. Figure 3.20 also shows that there was little variation in M_n(GPC) for both benzyl-amine capped and tren-core PHB and further established the suitability of *rac*-BBL for amine-initiated, immortal ROP.

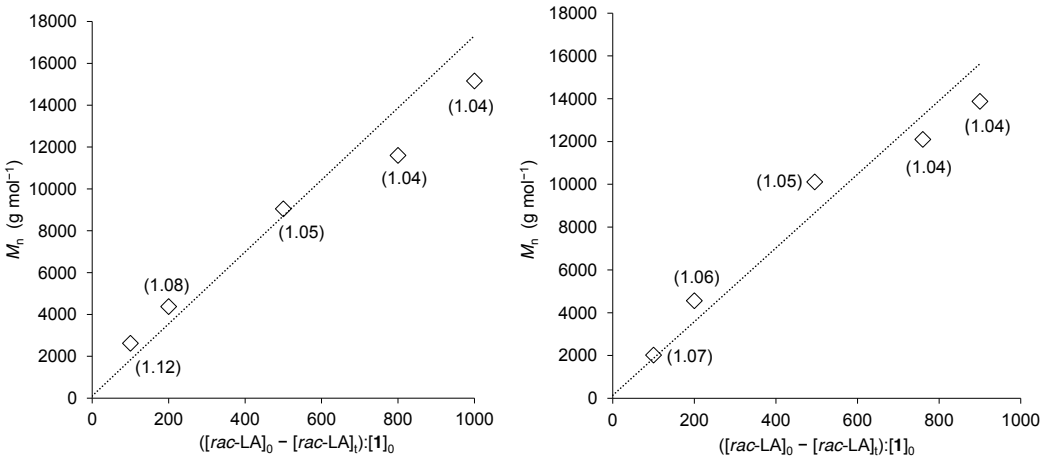

Figure 3.20. M_n(GPC) as a function of ([*rac*-LA]$_0$ − [*rac*-LA]$_t$):[**1**]$_0$ for *rac*-BBL polymerisations co-initiated by $BnNH_2$ (left), and tren (right). The dashed lines represent M_n(calcd) based on [*rac*-BBL]$_0$:[co-initiator]$_0$ = *n*:5 and the PDIs are given in parentheses.

3.7 Kinetic analysis of BBL polymerisations co-initiated by $BnNH_2$ and 1

The *rac*-BBL loading experiments (Figure 3.20) have demonstrated that the M_n of PHB can be tuned by systematic variation of [*rac*-BBL]$_0$:[co-initiator]$_0$. Along with narrow PDIs and successful amine end-group incorporation, *rac*-BBL polymerisations proceed in an immortal fashion. Following initial ring opening of activated BBL units by the amine co-initiator, propagation *via* coordination-insertion with facile chain transfer ensured that multiple PHB chains were generated with narrow PDIs. As was the case for *rac*-LA polymeriations, kinetic investigation was crucial to establish that propagation occurred *via* a coordination-insertion, not an activated-monomer type process. Although Carpentier has demonstrated the suitability of *rac*-BBL for immortal ROP, kinetic analysis was lacking in these initial reports.[50-53] Coates undertook kinetic analysis for *rac*-BBL polymerisations initiated by Zn(BDI)(O^{i}Pr) (**3.7**) complexes and determined first-order dependencies in *rac*-BBL and metal.[25]

3.7.1 $BnNH_2$ dependence

In order to obtain meaningful and consistent room temperature kinetic data for *rac*-BBL polymerisations co-initiated by **1** and $BnNH_2$, a relatively high benzyl amine loading had to be employed. $[rac\text{-BBL}]_0:[\mathbf{1}]_0 = 200:1$ ($[rac\text{-BBL}]_0 = 0.58$ M, 0.40 g, 8 mL toluene; $[\mathbf{1}]_0 = 0.003$ M) was held constant and $[BnNH_2]_0:[\mathbf{1}]_0$ was increased through 10.0 (0.029 M), 12.5 (0.036 M), and 15.0 (0.044 M) molar equivalents.

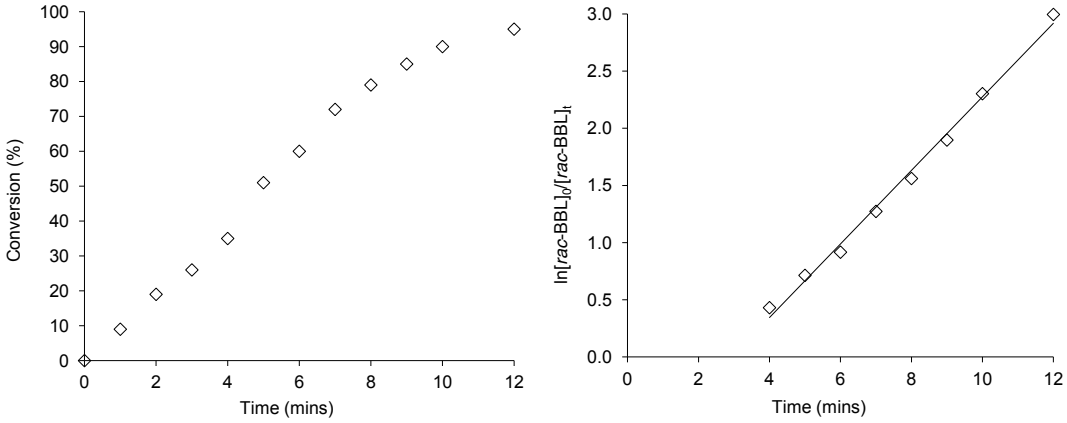

Figure 3.21. Conversion *vs*. Time plot (left) and semi-logarithmic plot (right) for the run $[rac\text{-BBL}]_0:[BnNH_2]_0:[\mathbf{1}]_0 = 200:10.0:1$. $k_{app} = 0.322(10)$ ($R^2 = 0.994$).

Figure 3.21 shows a Conversion *vs*. Time and a *pseudo* first-order plot for the run, $[rac\text{-BBL}]_0:[BnNH_2]_0:[\mathbf{1}]_0 = 200:10.0:1$. Whilst the consumption of *rac*-BBL could be modelled with first-order dependence, a 4 minute induction period was evident from the semi-logarithmic plot (Figure 3.21, right). Significant conversion of monomer to PHB occurred in this 4 minute period (35%) but a possible change in the propagation model was apparent from the Conversion *vs*. Time profile (Figure 3.21, left). This "induction period" was neglected when the apparent rate constant (k_{app}) was calculated, despite the appreciable conversion in this period. Further runs (Figure 3.22) were also modelled with a first-order dependence in $[rac\text{-BBL}]_0$ and showed evidence of an induction period (4 mins). k_{app} for the runs $[rac\text{-BBL}]_0:[\mathbf{1}]_0 = 200:1$, $[BnNH_2]_0:[\mathbf{1}]_0 = 10.0$, 12.5 or 15.0:1 were determined as 0.322(10) ($R^2 = 0.994$), 0.351(26) ($R^2 = 0.978$) and 0.398(22) ($R^2 = 0.991$) min^{-1}. As in the case of *rac*-LA polymerisations co-initiated by benzyl amine, these rate constants indicated no systematic dependence in $[BnNH_2]_0$, and were suggestive of fast initiation with respect to propagation to generate the amine-capped macromonomers. However, at a lower loading of amine, $[rac\text{-BBL}]_0:[BnNH_2]_0 = 200:7.5$, non-reproducible kinetic

data were obtained and complete conversion of monomer to PHB was shown to occur much more rapidly for the loadings [*rac*-BBL]$_0$:[BnNH$_2$]$_0$ = 200:3.0 or 200:5.0 (complete conversion within 5 mins *cf*. 10 mins when [*rac*-BBL]$_0$:[BnNH$_2$]$_0$ = 200:10.0). It should be noted that M_n(GPC) were in good agreement with M_n(calcd) for these runs (Table 3.4, *vide infra*), and were supportive of immortal ROP type behaviour. It would have been preferable to determine k_{app} from these loadings since PHB of significant M_n were generated, rather than oligomers when the loading of [BnNH$_2$]$_0$:[**1**]$_0$ is high (Entries 4, 5 and 6, Table 3.4). Attempts were made to vary conditions but no further meaningful data could be obtained.

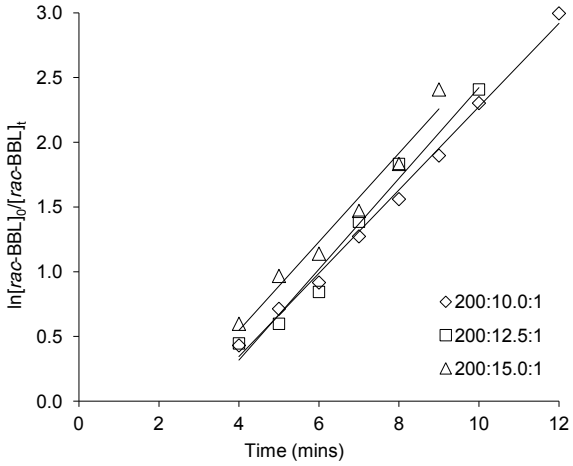

Figure 3.22. Combined semi-logarithmic plots for the runs [*rac*-BBL]$_0$:[**1**]$_0$ = 200:1, [BnNH$_2$]$_0$:[**1**]$_0$ = 10.0, 12.5 or 15.0:1. k_{app} = 0.322(10) (R^2 = 0.994), 0.351(26) (R^2 = 0.978) and 0.398(22) (R^2 = 0.991) min^{-1}.

3.7.2 Dependence in [1]$_0$ and mechanistic discussion

The dependence in [**1**]$_0$ was also determined from runs based on the loading, [*rac*-BBL]$_0$:[BnNH$_2$]$_0$ = 200:10. The initial concentration of [**1**]$_0$ was increased through 1 (0.003 M), 2 (0.006 M) and 3 (0.009 M) molar equivs. and the apparent rate constants are plotted in Figure 3.23 (left). Based on the linear plot, $k_{app} = k_p[\mathbf{1}]_0$, an overall propagation rate constant, k_p = 134(5) (R^2 = 0.986) M^{-1} min^{-1} was determined, and a plot of $-\ln k_{app}$ against $-\ln[\mathbf{1}]_0$ was suggestive of an order in [**1**]$_0$ of 1.19(10) (R^2 = 0.994) (Figure 3.23, right). When a run, [*rac*-BBL]$_0$:[BnNH$_2$]$_0$:[**1**]$_0$ = 200:10:4 was attempted, the rate of monomer consumption increased with a non-linear dependence and k_{app} could not be determined. As the equivs. of **1** were increased, [BnNH$_2$]$_0$:[**1**]$_0$ reduced and as was observed in the amine dependence determination experiments (Figures 3.21 and 3.22), fewer equivalents of amine per metal led to faster

propagation, which may account for the effective order in **1** of 1.19(10) (although first-order within error).

Molecular weight data for the runs, [*rac*-BBL]$_0$:[$BnNH_2$]$_0$:[**1**]$_0$ = 200:10:2 and 200:10:3 were also obtained (Entries 7 and 8, Table 3.4) and M_n(calcd) = 1,740 g mol^{-1}, M_n(GPC) = 1,880 g mol^{-1} and M_n(NMR) = 1,500 g mol^{-1} (for the run [*rac*-BBL]$_0$:[$BnNH_2$]$_0$:[**1**]$_0$ = 200:10:2) were in very good agreement for one PHB chain per $BnNH_2$ forming. In general, M_n (NMR) and M_n(GPC) were reflective of [*rac*-BBL]$_0$:[$BnNH_2$]$_0$ = 200:*n* and independent of [**1**]$_0$, as in the case of *rac*-LA polymerisations co-initiated by $BnNH_2$ and **1** (Chapter Two, Section 2.7). However, these polymer chains are short, and isolated PHB from lower conversion points were below the lower calibration limit, thus the linear increase in M_n could not be established from M_n(GPC) *vs*. Conversion plots. Nevertheless, isolated PHB from aliquots representing high conversions of BBL to PHB had narrow PDIs (1.07–1.10), indicative of well-controlled, immortal ROP reactions.

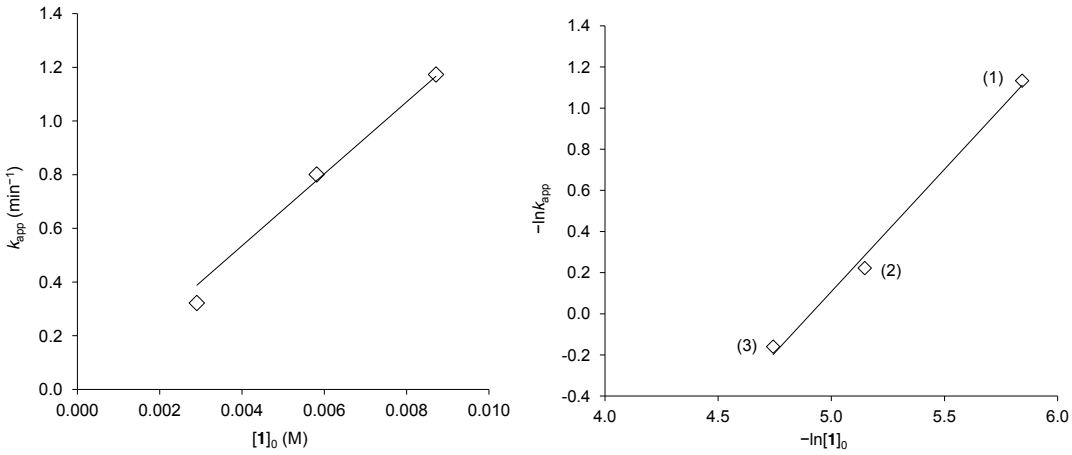

Figure 3.23. Plots of k_{app} *vs*. [**1**]$_0$ (left) and –lnk_{app} *vs*. –ln[**1**]$_0$ (right). k_{app} = 0.322(10) (R^2 = 0.994), 0.801(52) (R^2 = 0.983) and 1.173(103) (R^2 = 0.970) min^{-1}, with k_p = 134(5) (R^2 = 0.986) M^{-1} min^{-1} and order in [**1**]$_0$ = 1.19(10) (R^2 = 0.994). Numbers in parentheses indicate molar equivs. of **1**.

An overall propagation rate law, $R_p = k_p$[*rac*-BBL][**1**], is suggested from kinetic runs with *rac*-BBL, $BnNH_2$ and **1**. Despite the loading experiments effectively showing that M_n could be tuned at relatively low concentrations of amine ([*rac*-BBL]$_0$:[$BnNH_2$]$_0$ = 200:5, Figure 3.20), yielding kinetic data at lower amine loadings proved problematic. At higher amine loadings, where kinetic analysis was successful, more polymer chains were generated that could only propagate (and exchange) at the

metal centre (under a coordination-insertion regime). The rate of chain transfer is expected to be greater than the rate of propagation (irrespective of $[BnNH_2]_0$) but an increased number of chains may serve to temper the rate of propagation by competing with monomer molecules for the active metal centre (i.e. propagation is competitive with chain transfer when $[BnNH_2]_0$ is low). Cui noted a dependence of –0.352 in triethanolamine (TEA) co-initiated ROP of *rac*-LA (using $Y(O_2N^{NMe2})(CH_2SiMe_3)(THF)$ (**1.22**) as the catalyst) and suggested that the increase in competition for the metal centre at higher loadings of TEA accounted for the reduction in reaction rate.[21] It is unclear whether there is a dependence in $[BnNH_2]_0$ in the region represented by the polymerisation runs, $[rac\text{-BBL}]_0:[BnNH_2]_0$ = 200:3.0, 200:5.0 and 200:7.5, $[rac\text{-LA}]_0:[\mathbf{1}]_0$ = 200:1, but a negative dependence in $[BnNH_2]_0$ is a possibility based on Cui's observation. The kinetic runs where $[BnNH_2]_0:[\mathbf{1}]_0$ = 10.0:1, 12.5:1 or 15.0:1, may represent a region where the minimum k_{app} has been reached, and the generation of more chains does not affect competition for the metal centre significantly. When kinetic analysis of *rac*-LA ROP was performed (Chapter Two, Section 2.7), the maximum loading was $[rac\text{-LA}]_0:[BnNH_2]_0$ = 200:6 and there was no apparent rate dependency in $[BnNH_2]_0$. Additional competing chains ($[BnNH_2]_0$ > 6 equivs.) may have had an effect on the rate of propagation but this had to be measured against the desire to generate poly(*rac*-LA) of appreciable M_n.

Table 3.4. Summary of kinetic and molecular weight data from ROP of *rac*-BBL co-initiated by **1** and $BnNH_2$.

Entry	[*rac*-BBL]$_0$:[$BnNH_2$]$_0$:[**1**]$_0$ [a]	k_{app} (min^{-1}) [b]	R^2 [b]	Conv. (%) [c]	M_n(calcd) ($g\ mol^{-1}$) [c]	M_n(GPC) ($g\ mol^{-1}$) [d]	M_n(NMR) ($g\ mol^{-1}$) [d]	M_w/M_n [d]
1	200:3.0:1	[e]	[e]	> 99	5,840	5,380	[f]	1.10
2	200:5.0:1	[e]	[e]	> 99	3,550	4,380	[f]	1.08
3	200:7.5:1	[e]	[e]	98	2,360	3,260	1,740	1.08
4	200:10.0:1	0.322(10)	0.994	90	1,660	2,290	1,720	1.08
5	200:12.5:1	0.351(26)	0.978	91	1,360	1,940	1,160	1.08
6	200:15.0:1	0.398(22)	0.991	94	1,180	1,920	1,030	1.07
7	200:10.0:2	0.801(52)	0.983	95	1,740	1,880	1,500	1.09
8	200:10.0:3	1.173(103)	0.970	90	1,660	1,940	1,450	1.10

[a] [*rac*-BBL]$_0$ = 0.58 M, 8 mL toluene, rt. [b] Apparent first-order rate constants for consumption of *rac*-BBL with standard error and R^2 determined by linear regression analysis. [c] Reactions monitored by ^{1}H NMR ($CDCl_3$). All quoted conversions refer to the last point where M_n(GPC) was determined. M_n(calcd) = (Conv. (%) × [*rac*-BBL]$_0$:[$BnNH_2$]$_0$ × 86.0 + 107.2). [d] Measured by GPC using Mark-Houwink corrections for polystyrene in THF at 30 °C. [e] No meaningful kinetic data obtained but complete conversion was achieved within 5 mins. [f] Polymer too long for reliable M_n estimation by ^{1}H NMR.

3.7.3 Resumption experiment

To establish the living character of *rac*-BBL polymerisations co-initiated by **1** and $BnNH_2$, the run [*rac*-BBL]$_0$:[$BnNH_2$]$_0$:[**1**]$_0$ = 200:10:1 was repeated and followed to high conversion (Figure 3.24). A further 200 equivs. of *rac*-BBL was added to the polymerisation mixture at t = 13 mins and the polymerisation resumed.

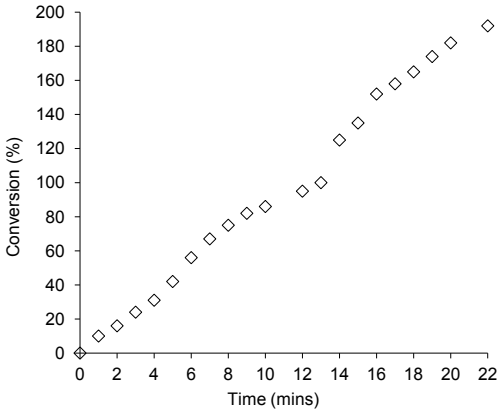

Figure 3.24. Resumption of polymerisation, demonstrating living behaviour.

At the first end-point" (95% conversion), M_n(GPC) = 1,880 g mol^{-1} (PDI = 1.08) was in good agreement with M_n(NMR) = 1,870 g mol^{-1} and M_n(calcd) = 1,740 g mol^{-1} and at the second end-point and M_n(GPC) = 2,950 g mol^{-1} (M_n(calcd) = 3,270 g mol^{-1}, 92% conversion). Narrow PDIs of 1.07 were measured for these points.

3.7.4 Low temperature NMR tube scale reaction

Despite the limited kinetic investigations with *rac*-BBL, it is proposed that amine-initiated, immortal ROP of BBL occurred *via* the same general mechanism as per *rac*-LA polymerisation. To support this proposal, a low temperature NMR tube scale reaction was performed with [*rac*-BBL]$_0$:[$BnNH_2$]$_0$:[**1**]$_0$ = 10:2:1. A cold toluene-d_8 solution of *rac*-BBL was added to a mixture of $BnNH_2$ and **1** at –35 °C, with ^{1}H NMR analysis at this temperature showing liberation of the sacrificial HO_2N^{NMe2} ligand from **1**. Complete consumption of $BnNH_2$ was also observed but PHB resonances were broad at this temperature. This observation contrasts the analogous experiment with *rac*-LA in which some unreacted $BnNH_2$ was present in solution alongside "free" $H_2O_2N^{NMe2}$ at –35 °C. In this instance, it was suggested that the initially formed macromonomers (lactide) could remove HO_2N^{NMe2} before complete consumption of $BnNH_2$. Since unreacted $BnNH_2$ and liberated $H_2O_2N^{NMe2}$ were not observed in the reaction with *rac*-BBL, it is difficult to conclude whether or not protonolysis occurred

before $BnNH_2$ was completely consumed. However, it can be concluded that the amine-initiation phase is fast and the initial ring opening is likely to occur *via* an activated-monomer process.

As the mixture was warmed in five degree increments, the remaining *rac*-BBL was consumed, but complete conversion was not achieved until the mixture was warmed to room temperature. Figure 3.25 shows the ^{1}H NMR spectrum of the NMR tube scale reaction, $[rac\text{-BBL}]_0:[BnNH_2]_0:[\mathbf{1}]_0$ = 10:2:1, at 10 °C. Features of this spectrum include the internal PHB C<u>H</u>(Me) and CH(<u>Me</u>) environments at δ = 5.2 and 1.2 ppm but the internal PHB methylene regions (δ ≈ 2.0 ppm) were overlapping with protio-ligand and residual protio-solvent peaks. The PhC<u>H$_2$</u>NH– methylene end-group doublet was present at δ = 4.2 ppm and overlapped with the PHB HOC<u>H</u>(Me)– methine end-group multiplet (δ = 4.3 ppm). Unreacted *rac*-BBL signals were also present at δ = 3.6, 2.5 and 0.7 ppm. Since HO_2N^{NMe2} was eliminated from **1** again, with likely formation of an active $Y(O_2N^{NMe2})L$ (L = PHB chelate of BBL monomer) fragment for propagation *via* coordination-insertion mechanism, it would seem that amine-initiated, immortal ROP of *rac*-BBL occurs *via* the general mechanism shown in Figure 3.26.

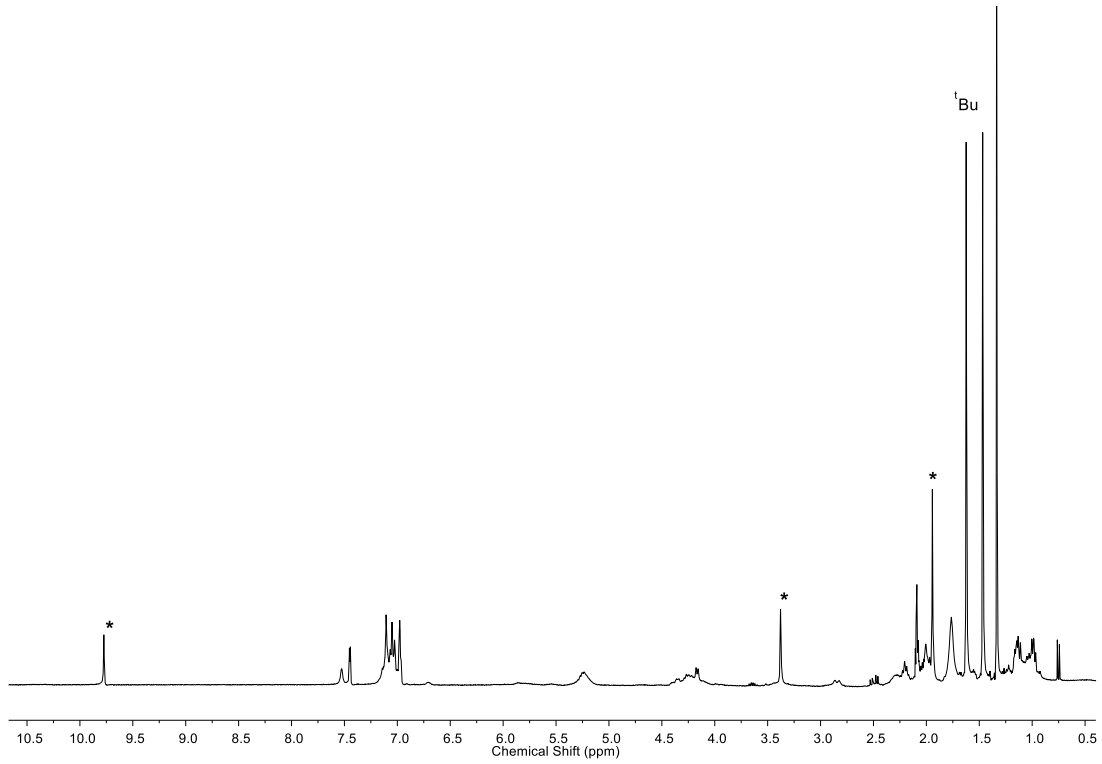

Figure 3.25. ^{1}H NMR (299.9 MHz, toluene-d_8, 283 K) spectrum of the NMR tube scale reaction [*rac*-BBL]$_0$:[BnNH$_2$]$_0$:[**1**]$_0$ = 10:2:1. ***** Denotes liberated $H_2O_2N^{NMe2}$. Residual protio-solvent, δ = 7.09, 7.00, 6.98 and 2.09 ppm.

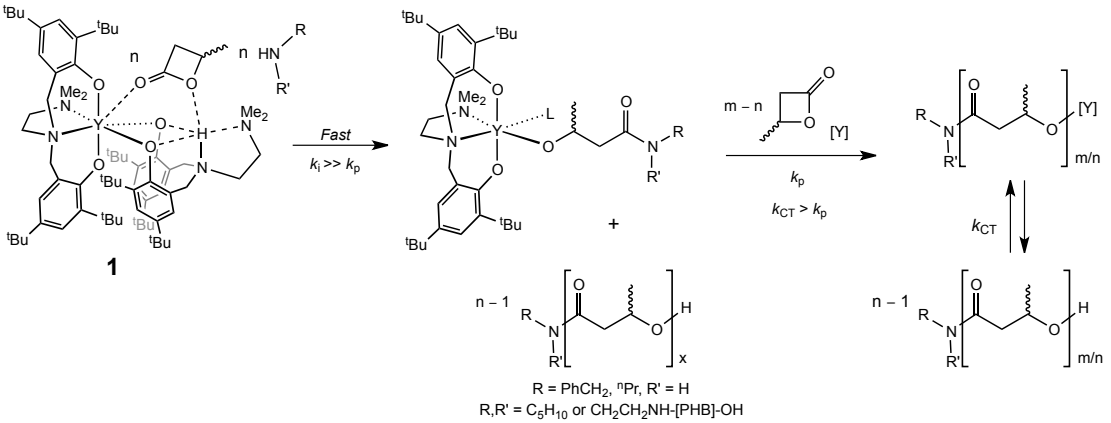

Figure 3.26. Amine-initiated, immortal ROP of *rac*-BBL in the presence of **1**. L = PHB chelate or BBL monomer.

3.8 Summary and Conclusions for Chapter Three

The amine-initiated, immortal ROP methodology has been successfully extended to *rac*-BBL for the first time. Model runs with a range of amine co-initiators, including tren have led to the formation of well-defined PHB with systematic amine end-group incorporation and loading experiments demonstrated a linear relationship between the

M_n of PHB samples and [*rac*-BBL]$_0$:[co-initiator]$_0$. First-order dependencies in [*rac*-BBL]$_0$ and [**1**]$_0$ were determined over a limited range of amine and metal loadings, but supporting low temperature NMR tube scale reactions suggested that amine-initiated, immortal ROP of *rac*-BBL occurs *via* an activated-monomer initiation step followed by propagation *via* a coordination-insertion mechanism with facile chain transfer between dormant and growing PHB chains. No systematic dependence in [$BnNH_2$]$_0$ was determined when the loading of $BnNH_2$ was relatively high, confirming that propagation was limited by the metal. However, the rate of propagation may be competitive with chain transfer when [$BnNH_2$]$_0$:[**1**]$_0$ is low. Isolated PHB also displayed moderate syndiotactic enrichment.

Tren was also included in *rac*-LA (and *rac*-BBL) polymerisation mixtures and each terminal primary amine was shown to participate in ROP. Kinetic analysis revealed a second-order dependence in [*rac*-LA]$_0$ and there was no systematic dependence in [tren]$_0$. The general amine-initiated, immortal ROP methodology is applicable to polyamines as well as $BnNH_2$.

3.9 References for Chapter Three

1. D. J. A. Cameron and M. P. Shaver, *Chem. Soc. Rev.*, 2011, **40**, 1761.
2. M. Trollsås and J. L. Hedrick, *J. Am. Chem. Soc.*, 1998, **120**, 4644.
3. D. Konkolewicz, M. J. Monteiro and S. Perrier, *Macromolecules*, 2011, **44**, 7067.
4. M. J. Stanford and A. P. Dove, *Macromolecules*, 2008, **42**, 141.
5. C. Hua, C.-M. Dong and Y. Wei, *Biomacromolecules*, 2009, **10**, 1140.
6. L. M. Pitet, B. M. Chamberlain, A. W. Hauser and M. A. Hillmyer, *Macromolecules*, 2010, **43**, 8018.
7. R. Wu, T. F. Al-Azemi and K. S. Bisht, *Chem. Commun.*, 2009, 1822.
8. J. Cheng, J.-X. Ding, Y.-C. Wang and J. Wang, *Polymer*, 2008, **49**, 4784.
9. A. S. Karikari, W. F. Edwards, J. B. Mecham and T. E. Long, *Biomacromolecules*, 2005, **6**, 2866.
10. A. S. Karikari, B. D. Mather and T. E. Long, *Biomacromolecules*, 2007, **8**, 302.
11. H. R. Kricheldorf and S.-R. Lee, *Macromolecules*, 1996, **29**, 8689.
12. H. R. Kricheldorf and B. Fechner, *J. Polym. Sci., Part A: Polym. Chem.*, 2002, **40**, 1047.

13. K. A. George, F. Schué, T. V. Chirila and E. Wentrup-Byrne, *J. Polym. Sci., Part A: Polym. Chem.*, 2009, **47**, 4736.
14. M. P. Shaver and D. J. A. Cameron, *Biomacromolecules*, 2010, **11**, 3673.
15. A. Kowalski, J. Libiszowski, T. Biela, M. Cypryk, A. Duda and S. Penczek, *Macromolecules*, 2005, **38**, 8170.
16. M. Adeli and R. Haag, *J. Polym. Sci., Part A: Polym. Chem.*, 2006, **44**, 5740.
17. H. Liu, Z. Shen, S.-E. Stiriba, Y. Chen, W. Zhang and L. Wei, *J. Polym. Sci., Part A: Polym. Chem.*, 2006, **44**, 4165.
18. X. Cao, Z. Li, X. Song, X. Cui, P. Cao, H. Liu, F. Cheng and Y. Chen, *Eur. Polym. J.*, 2008, **44**, 1060.
19. Q. Cai, Y. Zhao, J. Bei, F. Xi and S. Wang, *Biomacromolecules*, 2003, **4**, 828.
20. O. Coulembier, M. K. Kiesewetter, A. Mason, P. Dubois, J. L. Hedrick and R. M. Waymouth, *Angew. Chem., Int. Ed.*, 2007, **46**, 4719.
21. W. Zhao, D. Cui, X. Liu and X. Chen, *Macromolecules*, 2010, **43**, 6678.
22. H.-M. Müller and D. Seebach, *Angew. Chem. Int. Ed. Engl.*, 1993, **32**, 477.
23. K. Sudesh, H. Abe and Y. Doi, *Prog. Polym. Sci.*, 2000, **25**, 1503.
24. M. Okada, *Prog. Polym. Sci.*, 2002, **27**, 87.
25. L. R. Rieth, D. R. Moore, E. B. Lobkovsky and G. W. Coates, *J. Am. Chem. Soc.*, 2002, **124**, 15239.
26. A. Amgoune, C. M. Thomas, S. Ilinca, T. Roisnel and J.-F. Carpentier, *Angew. Chem. Int. Ed.*, 2006, **45**, 2782.
27. C. M. Thomas, *Chem. Soc. Rev.*, 2010, **39**, 165.
28. J.-F. Carpentier, *Macromol. Rapid Commun.*, 2010, **31**, 1696.
29. E. Brulé, S. Gaillard, M.-N. Rager, T. Roisnel, V. Guérineau, S. P. Nolan and C. M. Thomas, *Organometallics*, 2011, **30**, 2650.
30. N. C. Billingham, M. G. Proctor and J. D. Smith, *J. Organomet. Chem.*, 1988, **341**, 83.
31. A. Le Borgne, C. Pluta and N. Spassky, *Macromol. Rapid Commun.*, 1994, **15**, 955.
32. M. Möller, R. Kånge and J. L. Hedrick, *J. Polym. Sci., Part A: Polym. Chem.*, 2000, **38**, 2067.
33. Z. Jedliński, M. Kowalczuk, P. Kurcok, G. Adamus, A. Matuszowicz, W. Sikorska, R. A. Gross, J. Xu and R. W. Lenz, *Macromolecules*, 1996, **29**, 3773.

34. E. F. Connor, G. W. Nyce, M. Myers, A. Möck and J. L. Hedrick, *J. Am. Chem. Soc.*, 2002, **124**, 914.
35. P. Kurcok, M. Śmiga and Z. Jedliński, *J. Polym. Sci., Part A: Polym. Chem.*, 2002, **40**, 2184.
36. S. Bloembergen, D. A. Holden, T. L. Bluhm, G. K. Hamer and R. H. Marchessault, *Macromolecules*, 1989, **22**, 1656.
37. A. Le Borgne and N. Spassky, *Polymer*, 1989, **30**, 2312.
38. B. Wu and R. W. Lenz, *Macromolecules*, 1998, **31**, 3473.
39. Y. Hori and T. Hagiwara, *Int. J. Biol. Macromol.*, 1999, **25**, 237.
40. J. E. Kemnitzer, S. P. McCarthy and R. A. Gross, *Macromolecules*, 1993, **26**, 6143.
41. J. E. Kemnitzer, S. P. McCarthy and R. A. Gross, *Macromolecules*, 1993, **26**, 1221.
42. H. R. Kricheldorf, S.-R. Lee and N. Scharnagl, *Macromolecules*, 1994, **27**, 3139.
43. H. R. Kricheldorf and S. Eggerstedt, *Macromolecules*, 1997, **30**, 5693.
44. N. Ajellal, M. Bouyahyi, A. Amgoune, C. M. Thomas, A. Bondon, I. Pillin, Y. Grohens and J.-F. Carpentier, *Macromolecules*, 2009, **42**, 987.
45. J. W. Kramer, D. S. Treitler, E. W. Dunn, P. M. Castro, T. Roisnel, C. M. Thomas and G. W. Coates, *J. Am. Chem. Soc.*, 2009, **131**, 16042.
46. M. Zintl, F. Molnar, T. Urban, V. Bernhart, P. Preishuber-Pflügl and B. Rieger, *Angew. Chem. Int. Ed.*, 2008, **47**, 3458.
47. Y. Hori, M. Suzuki, A. Yamaguchi and T. Nishishita, *Macromolecules*, 1993, **26**, 5533.
48. E. Grunova, E. Kirillov, T. Roisnel and J.-F. Carpentier, *Dalton Trans.*, 2010, **39**, 6739.
49. N. Ajellal, D. M. Lyubov, M. A. Sinenkov, G. K. Fukin, A. V. Cherkasov, C. M. Thomas, J.-F. Carpentier and A. A. Trifonov, *Chem. Eur. J.*, 2008, **14**, 5440.
50. C. Guillaume, J.-F. Carpentier and S. M. Guillaume, *Polymer*, 2009, **50**, 5909.
51. N. Ajellal, J.-F. Carpentier, C. Guillaume, S. M. Guillaume, M. Helou, V. Poirier, Y. Sarazin and A. Trifonov, *Dalton Trans.*, 2010, **39**, 8363.
52. V. Poirier, T. Roisnel, J.-F. Carpentier and Y. Sarazin, *Dalton Trans.*, 2009, 9820.

53. V. Poirier, T. Roisnel, J.-F. Carpentier and Y. Sarazin, *Dalton Trans.*, 2011, **40**, 523.
54. E. Brulé, J. Guo, G. W. Coates and C. M. Thomas, *Macromol. Rapid Commun.*, 2011, **32**, 169.
55. Y. D. Y. L. Getzler, V. Kundnani, E. B. Lobkovsky and G. W. Coates, *J. Am. Chem. Soc.*, 2004, **126**, 6842.
56. Y. D. Y. L. Getzler, V. Mahadevan, E. B. Lobkovsky and G. W. Coates, *J. Am. Chem. Soc.*, 2002, **124**, 1174.
57. V. Mahadevan, Y. D. Y. L. Getzler and G. W. Coates, *Angew. Chem. Int. Ed.*, 2002, **41**, 2781.
58. J. W. Kramer and G. W. Coates, *Tetrahedron*, 2008, **64**, 6973.
59. J. M. Rowley, E. B. Lobkovsky and G. W. Coates, *J. Am. Chem. Soc.*, 2007, **129**, 4948.
60. E. W. Dunn and G. W. Coates, *J. Am. Chem. Soc.*, 2010, **132**, 11412.
61. M. Cheng, E. B. Lobkovsky and G. W. Coates, *J. Am. Chem. Soc.*, 1998, **120**, 11018.
62. G. W. Coates and D. R. Moore, *Angew. Chem. Int. Ed.*, 2004, **43**, 6618.
63. M. Cheng, D. R. Moore, J. J. Reczek, B. M. Chamberlain, E. B. Lobkovsky and G. W. Coates, *J. Am. Chem. Soc.*, 2001, **123**, 8738.
64. D. R. Moore, M. Cheng, E. B. Lobkovsky and G. W. Coates, *Angew. Chem. Int. Ed.*, 2002, **41**, 2599.
65. S. D. Allen, D. R. Moore, E. B. Lobkovsky and G. W. Coates, *J. Am. Chem. Soc.*, 2002, **124**, 14284.
66. C. M. Byrne, S. D. Allen, E. B. Lobkovsky and G. W. Coates, *J. Am. Chem. Soc.*, 2004, **126**, 11404.
67. D. J. Darensbourg and M. W. Holtcamp, *Coord. Chem. Rev.*, 1996, **153**, 155.
68. D. J. Darensbourg, *Chem. Rev.*, 2007, **107**, 2388.
69. D. J. Darensbourg, *Inorg. Chem.*, 2010, **49**, 10765.
70. D. J. Darensbourg and E. B. Frantz, *Inorg. Chem.*, 2008, **47**, 4977.
71. X.-B. Lu and D. J. Darensbourg, *Chem. Soc. Rev.*, 2012, **41**, 1462.
72. M. R. Kember, A. Buchard and C. K. Williams, *Chem. Commun.*, 2011, **47**, 141.
73. A. Buchard, M. R. Kember, K. G. Sandeman and C. K. Williams, *Chem. Commun.*, 2011, **47**, 212.

74. A. Cyriac, S. H. Lee, J. K. Varghese, E. S. Park, J. H. Park and B. Y. Lee, *Macromolecules*, 2010, **43**, 7398.
75. D. Cui, M. Nishiura and Z. Hou, *Macromolecules*, 2005, **38**, 4089.
76. D. J. Darensbourg, W. Choi, P. Ganguly and C. P. Richers, *Macromolecules*, 2006, **39**, 4374.
77. D. J. Darensbourg, W. Choi, O. Karroonnirun and N. Bhuvanesh, *Macromolecules*, 2008, **41**, 3493.
78. D. J. Darensbourg, O. Karroonnirun and S. J. Wilson, *Inorg. Chem.*, 2011, **50**, 6775.
79. M. Helou, O. Miserque, J.-M. Brusson, J.-F. Carpentier and Sophie M. Guillaume, *Chem. Eur. J.*, 2008, **14**, 8772.
80. M. Helou, O. Miserque, J.-M. Brusson, J.-F. Carpentier and S. M. Guillaume, *Adv. Synth. Cat.*, 2009, **351**, 1312.
81. M. Helou, O. Miserque, J.-M. Brusson, J.-F. Carpentier and S. M. Guillaume, *Macromol. Rapid Commun.*, 2009, **30**, 2128.
82. M. Helou, O. Miserque, J.-M. Brusson, J.-F. Carpentier and Sophie M. Guillaume, *ChemCatChem*, 2010, **2**, 306.
83. M. Labet and W. Thielemans, *Chem. Soc. Rev.*, 2009, **38**, 3484.
84. M. Florczak and A. Duda, *Angew. Chem. Int. Ed.*, 2008, **47**, 9088.
85. P. Dubois, P. Degee, R. Jerome and P. Teyssie, *Macromolecules*, 1992, **25**, 2614.
86. M. Marzorati, K. Hult, S. Riva and B. Danieli, *Adv. Synth. Catal.*, 2007, **349**, 1963.
87. M. Bouyahyi, N. Ajellal, E. Kirillov, C. M. Thomas and J.-F. Carpentier, *Chem. Eur. J.*, 2011, **17**, 1872.

Chapter Four

Alkaline earth and rare earth phenolate complexes for the ROP of *rac*-LA

4.1 Overview

This Chapter details experimental work undertaken as part of a collaborative project with the groups of Professors Glen B. Deacon and Peter C. Junk at Monash University, Melbourne, Australia. A family of Group 2 and lanthanide phenolate complexes, originally prepared by Dr. Joshua P. Townley are introduced and initial ROP screening is summarised. The results of more in-depth ROP studies undertaken by the author are then presented. Some synthetic and structural discussion has already been published and the reader is directed to this reference for further information.[1]

4.2 Introduction

Whilst there are numerous examples of ROP catalysts bearing chelating phenolate ligands, as well as alkoxide initiating groups for ROP *via* the coordination-insertion mechanism, an opportunity arose to study new poly- and mono-nuclear Group 2 and lanthanide phenolate complexes that do not contain a recognised initiating group. These lanthanide (and Group 2) complexes are related to the tris(phenolate) complex, $Y(O\text{-}2,6\text{-}C_6H_3{}^tBu_2)_3$ (**1.6**) that was used in conjunction with ^{i}PrOH to initiate ROP of *L*-LA.[2, 3] It is known that simple Lewis acidic metal salts or complexes with non-chelating ligands catalyse ROP.[4-8] However, polymerisation reactions using these catalysts generally show poor control over M_n and PDI. Addition of co-initiators such as alcohols has led to improved polymerisation systems although there are few examples of conclusive mechanistic elucidation.[9-15] Studying these phenolate complexes has proved useful in developing a further understanding of alternative initiation, propagation and chain transfer processes in immortal ROP i.e. activated-monomer propagation pathways.

4.2.1 Group 2 and lanthanide complexes bearing phenolate ligands

Group 2, Group 3 and lanthanide phenolate complexes are commonly prepared by protonolysis routes between an appropriate metal precursor, such as $M\{N(SiR_3)_2\}_3(L)_n$ (L = THF or Et_2O), with a phenol, or metathesis reactions between metal salts and anionic ligand precursors. Group 2, Group 3 and lanthanide metal-amides are themselves products of metathesis reactions between metal halides and alkali metal-amides,[16-18] but despite the publication of several reliable syntheses of $Ln\{N(SiR_3)_2\}_3(THF)_n$-type lanthanide precursors,[19, 20] these preparative reactions

alone can be prone to complications arising from the often poor solubility of lanthanide halides or retention of alkali metals i.e. "ate" complex formation.

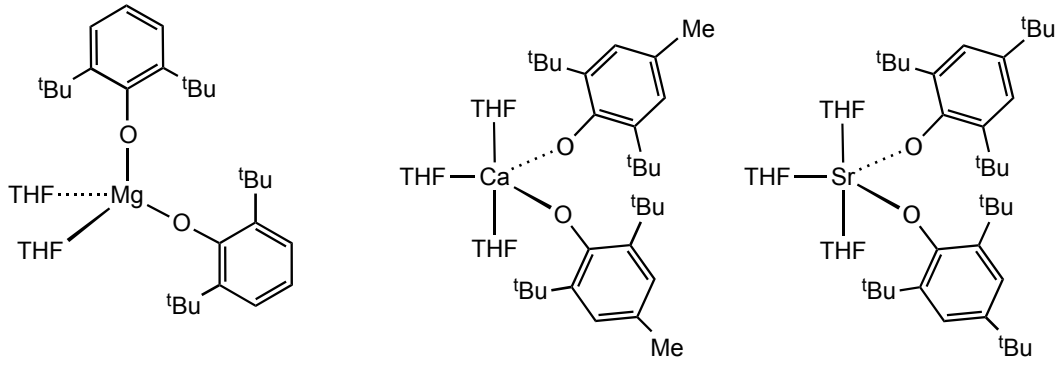

4.2 **4.5** **4.13**

Figure 4.1. Examples of structurally characterised, monomeric Group 2 phenolate complexes.[21-23]

As in the case of Group 3 and lanthanides, there are numerous early examples of homo- and hetero-leptic Group 2 phenolate complexes. Similar examples have been reported by a number of research groups and various synthetic routes have been employed, including direct reactions between metals and phenols as well as salt metathesis. Monomeric magnesium aryloxides, $Mg(O\text{-}2,4,6\text{-}C_6H_2{}^tBu_2Me)_2(THF)_2$ (**4.1**), with di-*ortho*-^{t}Bu substituents[24] and $Mg(O\text{-}2,6\text{-}C_6H_3{}^tBu_2)_2(THF)_2$ (**4.2**)[21] (Figure 4.1), displaying tetrahedral coordination geometry were obtained by treatment of di-*n*-butylmagnesium with HO-2,4,6-$C_6H_2{}^tBu_2Me$ (BHT) or HO-2,6-$C_6H_3{}^tBu_2$ in THF. An unsolvated species, $[Mg(O\text{-}2,4,6\text{-}C_6H_2{}^tBu_2Me)_2]_2$ (**4.3**), could be obtained when the reaction was performed in a hydrocarbon solvent.[25]

In 1990, Hanusa described the preparation of $Ca(O\text{-}2,4,6\text{-}C_6H_2{}^tBu_2Me)_2(THF)_2$ (**4.4**) by a reaction between reactive calcium powder (prepared by reduction of CaI_2 with potassium metal) and BHT in THF.[26] **4.4** was isolated in moderate yield and was the first example of a hydrocarbon soluble calcium phenolate complex. In the same year, Lappert reported and structurally characterised the tris(THF) solvate, $Ca(O\text{-}2,4,6\text{-}C_6H_2{}^tBu_2Me)_2(THF)_3$ (**4.5**, Figure 4.1), also prepared by direct reaction of calcium powder and BHT.[22] The calcium (and barium) powders in this case were activated by metal vapour synthesis techniques. The preparative reaction with barium powder required heating at reflux and a tetra(THF) solvate formed, whilst **4.5** was successfully prepared at room temperature. Crystallographic analysis of **4.5**

established a trigonal bipyramidal structure with THF molecules occupying the axial positions. A dinuclear species, with a bridging phenolate ligand [Ca(O-2,4,6-$C_6H_2{}^tBu_2Me$)(μ-O-2,4,6-$C_6H_2{}^tBu_2Me$)]$_2$ (**4.6**), could be accessed through treatment of **4.5** with calcium metal at elevated temperature (80 °C) and low pressure (10^{-2} Torr). Sr(O-2,4,6-$C_6H_2{}^tBu_2Me)_2(THF)_4$ (**4.7**) and Sr(O-2,4,6-$C_6H_2{}^tBu_2Me)_2$ (**4.8**) were reported later and were synthesised by the same synthetic methodology as their calcium congeners.[27]

Hanusa was later able to access monomeric BHT-derived complexes of the type M(O-2,4,6-$C_6H_2{}^tBu_2Me)_2(THF)_3$ (M = Ca (**4.5**) and Ba (**4.9**)) by metathesis reactions between CaI_2 or BaI_2 and the potassium salt of BHT in THF at room temperature.[28] These complexes were characterised in the solid state as M(O-2,4,6-$C_6H_2{}^tBu_2Me)_2(THF)_3$ solvates, each possessing a trigonal bipyramidal coordination geometry with axial THF ligands. In the same year, Drake and Hursthouse reported a family of Ca, Sr and Ba compounds bearing tri-*tert*-butyl phenolate (O-2,4,6-$C_6H_2{}^tBu_3$) ligands.[23] Unsolvated oligomeric compounds were characterised in addition to mononuclear THF, toluene, DME and HMPA solvates and/or adducts. Interestingly, elemental Ca, Sr and Ba were used in the preparation of the complexes. HO-2,4,6-$C_6H_2{}^tBu_3$ was added in the appropriate solvent to the metal before ammonia gas was bubbled through each solution at low temperature until complete dissolution of the metal was observed. Ammonia is a relatively poor solvent for the Group 2 metals but solvation of the metal could be achieved when an organic co-solvent was employed. [M(O-2,4,6-$C_6H_2{}^tBu_3)_2]_n$ (M = Ca (**4.10**), Sr (**4.11**) and Ba (**4.12**)) homoleptic complexes were isolated when toluene was employed as the co-solvent with ammonia adducts of the type, M(O-2,4,6-$C_6H_2{}^tBu_3)_2(NH_3)_n$, being the likely first-formed products. Dissolution of the homoleptics **4.10**–**4.12** in Lewis base solvents (THF, DME and HMPA) produced monomeric, base-stabilised species, e.g. **4.13** (Figure 4.1), which could also be prepared in one-step from the elemental metal when ammonia and the appropriate Lewis base solvent combination was utilised. Finally, the homoleptics **4.10**–**4.12**, could be regained when the monomeric solvates were dissolved in toluene and heated to reflux. Later examples of calcium phenolates were prepared from highly reactive phenyl calcium hydride precursors prepared by metal vapour synthesis techniques.[29]

As alluded to in Chapter One, lanthanide aryloxide complexes have attracted considerable interest owing to the range of accessible structural motifs through systematic metal and ligand variation. Although Lappert's complexes, Sc(O-2,4,6-$C_6H_2{}^tBu_2Me)_3$ (**2.13**) and Y(O-2,6-$C_6H_3{}^tBu_2)_3$ (**1.6**) are cited as prime examples of this compound class,[30, 31] Mehrotra and co-workers were able to prepare $Ln(OPh)_3$ (Ln = Y (**4.14**) and Sm (**4.15**)) type complexes *via* alkoxide/phenol exchange over a decade earlier.[32-34] No structural characterisation was provided but it is likely that these complexes were multinuclear with bridging phenolate ligands. The cerium congener of **1.6** was reported in 1988 and was prepared by treatment of $Ce\{N(SiMe_3)_2\}_3$ with three equivalents of HO-2,6-$C_6H_3{}^tBu_2$ in pentane.[35] Boyle has also generated a family of monomeric, dimeric and oligomeric Ce(III) phenolate complexes through systematic variation of steric bulk on the phenyl ring.[36] Progress in this field of lanthanide phenolate complexes has also been documented in historical and more recent reviews.[37, 38]

The groups of Deacon and Junk have utilised redox transmetallation/protonolyis reactions (Scheme 4.1, Section 4.3) as versatile alternatives to metathesis or amide protonolysis reactions for the synthesis of low coordinate alkaline earth and rare earth complexes.[37, 39-43] These techniques offer a number of advantages over metathesis, such as simple "one-pot" synthesis and avoidance of possible halide or alkali metal retention. Using these methods, well-defined monomeric divalent and trivalent analogues and derivatives of **1.6** have been prepared. Bulky substituents such as *tert*-butyl, phenyl or substituted phenyl groups in the 2,6- positions are essential to ensure formation of monomeric species, whereas less bulky or 3,5-substituted phenolates lead to the formation of multinuclear complexes that are often stabilised by donor solvents. Deacon and Junk have recently shown that asymmetric substitution patterns can lead to interesting structural variation that is often dependent on the choice of donor solvent.[1]

4.2.2 Polymerisation studies

There are few reports of Group 2 phenolate complexes of the type $M(OAr)_2(L)_n$ (L = Lewis base) being used in the ROP of cyclic esters. In contrast, Group 3 and lanthanide complexes have received considerably more attention. As described in Chapter One, Feijen utilised Lappert's tris(phenolate), Y(O-2,6-$C_6H_3{}^tBu_2)_3$ (**1.6**) in

combination with ^{i}PrOH to generate well-defined PLA with narrow PDI. In a representative procedure, 150 equivs. of *L*-LA were polymerised in 2 mins in the presence of three equivs. of ^{i}PrOH, in dichloromethane at room temperature. The experimental M_n(GPC) = 12,300 g mol^{-1} (PDI = 1.24) was greater than that expected for three chains forming, M_n(calcd) = 7,200 g mol^{-1}, and represented the general trend for the ROP of lactones using **1.6** and alcohols.[2, 3] First-order dependencies in *L*-LA and **1.6** were determined by Feijen, but the orders in ^{i}PrOH could not be determined reliably. Shen and Zhang have prepared lanthanide tris(phenolates) for the ROP of lactones.[44-49] In the absence of a co-initiator, La(O-4-$C_6H_4{}^{t}Bu)_3$ (**4.16**) could polymerise 1000 equivs. of *L*-LA in 110 mins at 70 °C in toluene.[50, 51] The resultant polymer product had an experimental M_n that was indicative of three chains per metal, M_n(GPC) = 45,700 g mol^{-1} (PDI = 1.49), whilst kinetic investigations revealed first-order dependencies in both *L*-LA and catalyst. A derivative of Lappert's complex, Y(O-2,4,6-$C_6H_2{}^{t}Bu_2Me)_3$ (**4.17**) with a *para*-methyl phenolate substituent, also demonstrated immortal type behaviour when ε-CL was polymerised in the presence of functionalised alcohols, but no kinetic analysis was undertaken.[52, 53] The scandium analogue, Sc(O-2,4,6-$C_6H_2{}^{t}Bu_2Me)_3$ (**2.13**), has also been exploited by Shen to homo- and co-polymerise ε-CL and trimethylene carbonate (TMC), with mild heating being required to effect complete conversion of ε-CL to PCL. Incorporation of ^{i}PrOH end-groups was shown to be successful when the alcohol was included in the polymerisation mixture but no kinetic investigations were reported.[54]

4.3 Synthesis and characterisation

Owing to the lack of study on asymmetric aryl-ring substituted phenolates, Deacon and Junk have investigated 2,4-di-*tert*-butyl substituted phenolate complexes and the potential for variations in the bonding and bridging ability of the ligand. Steric bulk at the *ortho* position provides some saturation of the coordination sphere, while the *para*-*tert*-butyl group assists with solubility in non-polar solvents. Incidentally, the 2,4-di-*tert*-butyl substitution pattern on the phenolate ring is identical to that of $H_2O_2N^{NMe2}$, with the exception of the linking amino bridge of the bis(phenol)-amine.

The compounds Nd(O-2,4-$C_6H_3{}^{t}Bu_2)_3(THF)_3$ (**10**), Gd(O-2,4-$C_6H_3{}^{t}Bu_2)_3(THF)_3$ (**11**), Ca_2(O-2,4-$C_6H_3{}^{t}Bu_2)_4(DME)_5$ (**12**), Sr_2(O-2,4-$C_6H_3{}^{t}Bu_2)_4(DME)_3$ (**13**) and Sr_3(O-2,4-$C_6H_3{}^{t}Bu_2)_6(THF)_6$ (**14**) were successfully prepared according to Scheme 4.1. Reactions were carried out as a "one-pot" synthesis in which $Hg(C_6F_5)_2$ and HO-2,4-

$C_6H_3{}^tBu_2$ were added to an excess of Ca, Sr, Nd or Gd metal (with 1-2 drops of mercury for activation) in the donor solvents, THF or DME, to produce **10**–**14** in good yields. Following initial formation of $M(C_6F_5)_2$ or $Ln(C_6F_5)_3$, C_6F_5H was eliminated from each organometallic intermediate owing to the greater Brønsted acidity of the phenol. The structure of **10** with meridional phenolate ligands is shown in Figure 4.2 alongside related Group 2 complexes.[1, 55]

Since the ionic radii of Ca(II) (1.14 Å) and Sr(II) (1.32 Å) are comparable to Yb(II) (1.16 Å) and Eu(II) (1.31 Å) respectively,[56] these divalent examples provide suitable structural and catalytic mimics for Ln(II) analogues whilst avoiding potential complicating redox reactions. The ionic radii of Nd(III) (1.12 Å) and Gd(III) (1.08 Å) permitted formation of monomeric species with non-bridging phenolate ligands in this instance. In **12**, whilst each phenolate ligand is terminally bound, each calcium centre is seven-coordinate. The coordination sphere of each calcium centre is satisfied by two chelating DME ligands and one non-chelating DME ligand that forms a linkage between the calcium centres, a coordination mode that has been reported in Ca_2(O-2,4,6-$C_6H_2Me_3)_2(\kappa^2$-DME)$_2(\kappa^1$-DME)$_2$ (**4.18**).[57] The calcium THF solvate, Ca(O-2,4-$C_6H_3{}^tBu_2)_2(THF)_4$ (**4.19**) is monomeric, akin to **10** and **11** but with *trans* phenolate ligands.[55] Monomeric DME solvates, Ca(O-2,6-$C_6H_3R_2)_2(DME)_2$ (R = Me (**4.20**) or ^{i}Pr (**4.21**)) were obtained when 2,6-substituted phenolates were employed.[58, 59]

In contrast, the strontium DME solvate, **13**, has a curious dinuclear but unsymmetrical structure with three bridging and one terminal phenolate ligand bound to Sr(1) (Figure 4.2). Chelating DME ligands complete the coordination sphere of each strontium centre with Sr(1) being six coordinate, whilst Sr(2) is seven coordinate. Analogous connectivity was observed in Eu_2(O-2,6-$C_6H_3Me_2)_4(DME)_3$ (**4.22**)[58] and similar coordination modes were observed in the *N*-methylimidazole solvated complex, Eu_2(O-2,6-$C_6H_3Me_2)_4$(*N*-methylimidazole)$_5$ (**4.23**).[60] Further examples include the unsolvated M_2(O-2,6-$C_6H_3Ph_2)_4$ (M = Sr (**4.24**), Ba (**4.25**) or Eu (**4.26**))[61, 62] dimers and the heterobimetallics, MEu(O-2,6-$C_6H_3Ph_2)_4$ (M = Sr (**4.27**) or Ba (**4.28**)) and SrBa(O-2,6-$C_6H_3Ph_2)_4$ (**4.29**), where intramolecular aromatic π-donation from flanking phenyl rings stabilised each metal centre.[63] The DME ligands of **13** were shown to be liberated when the complex was dissolved in THF-d_8 and the ^{1}H NMR spectrum (THF-d_8) of the resultant complex was similar to that of **14** (THF-d_8), suggesting that **13** and **14** form the same species in THF solution.

The THF solvate, **14**, is trinuclear with bridging phenolate ligands only. Capping THF molecules ensure that each Sr centre is six-coordinate with precedents for this unusual structural motif including $Eu_3(O\text{-}2,6\text{-}C_6H_3Me_2)_6(THF)_6$ (**4.30**)[64] and $M_3(O\text{-}2,4,6\text{-}C_6H_2Me_2)_6(THF)_6$ (M = Sr (**4.31**), Ba (**4.32**) or Eu (**4.33**)).[43, 57] Further structural discussion and data can be found in the appropriate reference.[1]

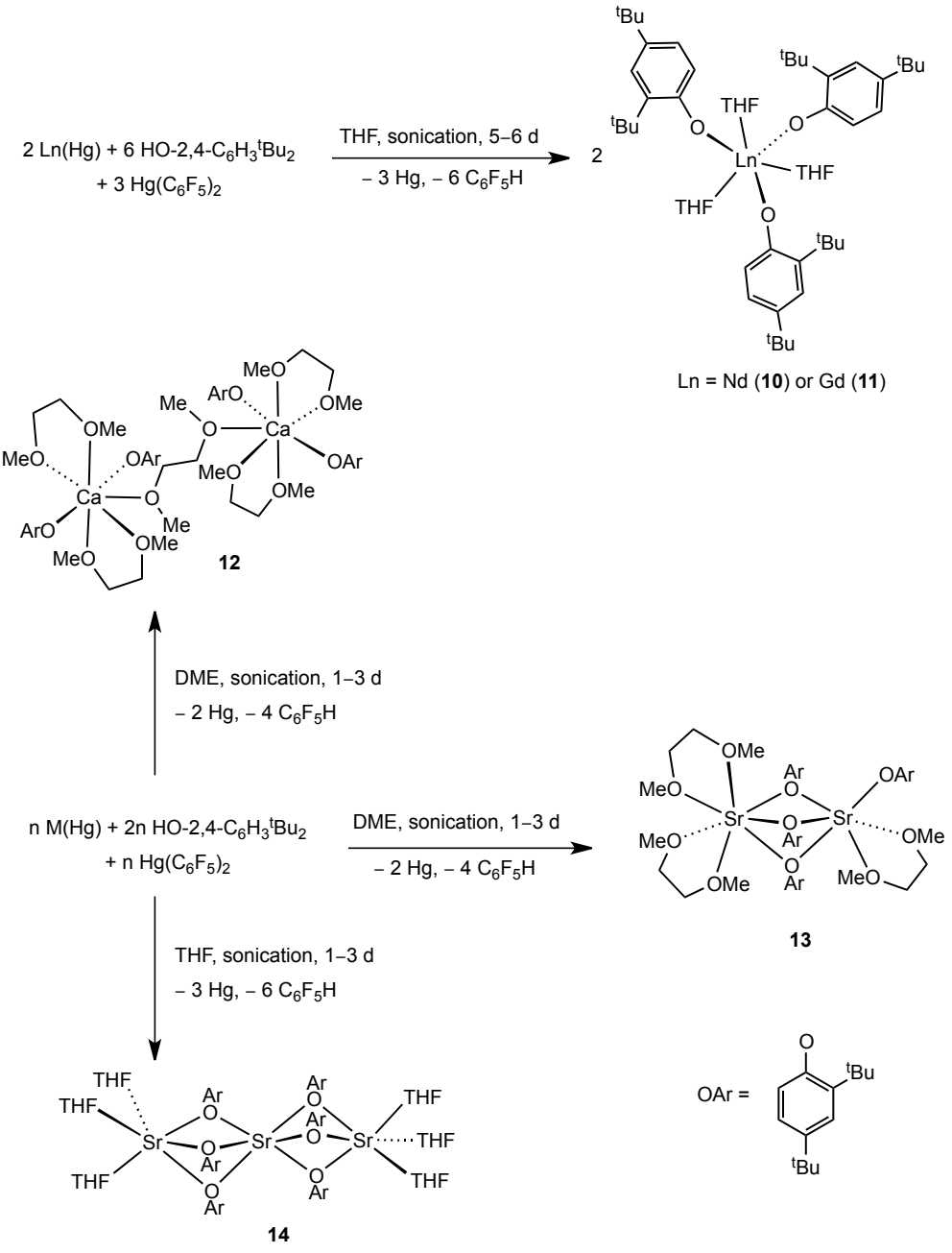

Scheme 4.1. Room temperature syntheses of Group 2 and lanthanide phenolate complexes *via* redox transmetallation/protonolysis methods.[1, 55]

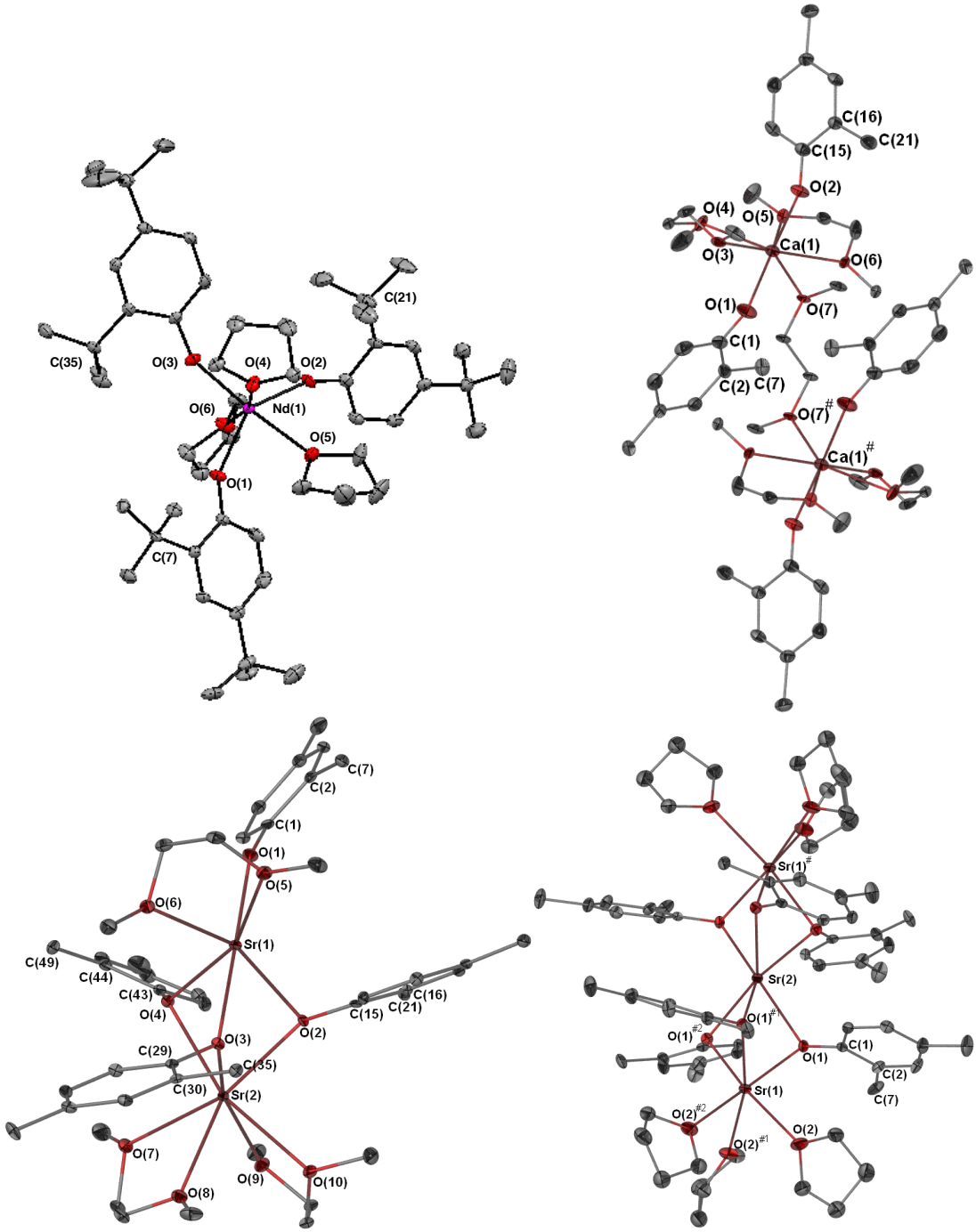

Figure 4.2. Molecular structures of **10** (analogous to **11**, top and left) and molecular structures of **12** (top, right), **13** (bottom, left) and **14** (bottom, right) All C-bound H atoms and $(CH_3)_3$ groups of **11**–**14** omitted for clarity.[1, 55]

4.4 Preliminary polymerisation studies

Nd(O-2,4-$C_6H_3{}^tBu_2)_3(THF)_3$ (**10**), Gd(O-2,4-$C_6H_3{}^tBu_2)_3(THF)_3$ (**11**), Ca_2(O-2,4-$C_6H_3{}^tBu_2)_4(DME)_5$ (**12**), Sr_2(O-2,4-$C_6H_3{}^tBu_2)_4(DME)_3$ (**13**) and Sr_3(O-2,4-$C_6H_3{}^tBu_2)_6(THF)_6$ (**14**) were selected as representative examples and their ability to effect the ROP of *rac*-LA in THF was assessed in collaboration with Dr. Joshua P. Townley. Both compounds **10** and **11** were reacted with 100 equivs. of *rac*-LA ([*rac*-LA]$_0$:[Ln]$_0$ = 100:1) in THF and > 90% conversion of monomer to poly(*rac*-LA) was achieved within 30 mins. For both **10** and **11** the experimental molecular weights, M_n(GPC) = 7,570 and 10,100 g mol^{-1} (Table 4.1), were significantly higher than those predicted for one polymer chain growing per Ln-O-2,4-$C_6H_3{}^tBu_2$ bond (M_n(calcd) ≈ 4,400 g mol^{-1}). If insertion of LA monomers into a Ln-O-2,4-$C_6H_3{}^tBu_2$ bond is possible, a likely interpretation of these molecular weight data is that once one or more LA monomers have inserted, the propagation rate for the so-formed Ln-[LA]$_x$-O-2,4-$C_6H_3{}^tBu_2$ moiety is significantly larger than that for initiation due to reduced steric hindrance. Phenol-capped PLA chains have been detected in previous reports but the PLA samples produced by **10** and **11** were unsuitable for MALDI-ToF MS analysis because of their high molecular weight.[65, 66] The very broad PDIs of 2.7 and 2.2 were also consistent with a poorly-controlled polymerisation process, with poly(*rac*-LA) chains of considerably different molecular weights being formed.

The results of preliminary screening experiments undertaken in collaboration with Dr. Joshua P. Townley using **12**–**14** are also summarised in Table 4.1. Treating **12** and **13** as dinuclear molecules, these runs were performed with [*rac*-LA]$_0$:[Complex]$_0$ = 100. In the case of **12**, 89% conversion of monomer to poly(*rac*-LA) was achieved in 150 mins, with intermediate aliquots at 30 and 60 mins showing 73% and 80% conversion of monomer to poly(*rac*-LA), respectively. The equivalent reaction with **13** proceeded over a similar timescale and 86% conversion of monomer to poly(*rac*-LA) was achieved in 150 mins. Intermediate aliquots were taken at 30, 60 and 120 mins and showed 51%, 70% and 83% conversion, respectively. A higher loading of [*rac*-LA]:[**14**] = 150:1 was employed in the analogous reaction with **14** (representing the trinuclear molecule) to ensure a [*rac*-LA]$_0$:[Sr metal centre]$_0$ loading of 50:1. 94% conversion of monomer to poly(*rac*-LA) was measured after 150 mins for this run.

Table 4.1. Polymerisation of *rac*-LA co-initiated by Nd(O-2,4-$C_6H_3{}^tBu_2)_3(THF)_3$ (**10**), Gd(O-2,4-$C_6H_3{}^tBu_2)_3(THF)_3$ (**11**), Ca_2(O-2,4-$C_6H_3{}^tBu_2)_4(DME)_5$ (**12**), Sr_2(O-2,4-$C_6H_3{}^tBu_2)_4(DME)_3$ (**13**) and Sr_3(O-2,4-$C_6H_3{}^tBu_2)_6(THF)_6$ (**14**).[a]

Complex	[*rac*-LA]$_0$: [BnOH]$_0$	Time (mins)	Conv. (%)[b]	M_n(calcd) (g mol^{-1})	M_n(GPC) (g mol^{-1})[c]	M_w/M_n[c]
10	[d]	30	92	4,420[e]	7,570	2.7
11	[d]	30	90	[i]	[i]	[i]
11	[d]	60	91	4,370[e]	10,100	2.2
12	[d]	30	73	[i]	[i]	[i]
12	[d]	150	89	3,200[f]	4,050	2.6
13	[d]	30	51	[i]	[i]	[i]
13	[d]	150	86	12,400[g]	13,200[j]	1.5[j]
14	[d]	30	84	[i]	[i]	[i]
14	[d]	150	94	20,300[g]	14,500[k]	1.4[k]
10	20:1	30	96	2,880[h]	3,530	1.5
11	20:1	30	95	2,850[h]	3,190	1.6
12	20:1	30	95	2,850[h]	3,000	1.8
13	20:1	30	96	2,880[h]	3,010	1.8
14	20:1	30	99	2,920[h]	1,880	2.2

[a] [*rac*-LA]$_0$:[Complex]$_0$ = 100:1, [*rac*-LA]$_0$:[**14**]$_0$ = 150:1, 2 mL THF, [*rac*-LA]$_0$ = 0.69 M, rt. [b] Measured by ^{1}H NMR in $CDCl_3$. [c] Measured by GPC against polystyrene standards using the appropriate Mark-Houwink corrections for poly(*rac*-LA) in THF at 30 °C. [d] No BnOH added. [e] M_n (calcd) = (Conv. (%) × 144.1)/3. [f] M_n(calcd) = (Conv. (%) × 144.1)/4. [g] M_n(calcd) = (Conv. (%) × [*rac*-LA]$_0$:[Complex]$_0$ × 144.1). [h] M_n(calcd) = (Conv. (%) × [*rac*-LA]$_0$:[BnOH]$_0$ × 144.1 + 108.1). [i] Not measured. [j] Bimodal distribution, major peak area measured (87%). [k] Bimodal distribution, major peak area measured (90%).

For **12**, the experimental molecular weight, M_n(GPC) = 4,050 g mol^{-1} was consistent with two chains per calcium centre (M_n(calcd) = 3,200 g mol^{-1}), and in the case of **13** an experimental molecular weight, M_n(GPC) = 13,200 g mol^{-1} (M_n(calcd) = 12,400 g mol^{-1}) was suggestive of one chain per strontium dimer. These experimental molecular weights correlate with the solid state structures of **12** and **13** if the terminal

O-2,4-$C_6H_3{}^tBu_2$ ligand can act as a suitable initiator. For instance, in **13** there is one terminal but three bridging O-2,4-$C_6H_3{}^tBu_2$ ligands in the dinuclear structure (Figure 4.2), whilst in **12**, all four O-2,4-$C_6H_3{}^tBu_2$ ligands are terminal. However, the ^{1}H NMR spectrum of **13** in THF-d_8 was consistent with one time averaged O-2,4-$C_6H_3{}^tBu_2$ environment and was identical to that of **14** in THF-d_8 (with the exception of free DME signals with **13**). When **14** was tested for ROP, with a loading representative of [*rac*-LA]$_0$:[Sr]$_0$ = 50:1, M_n(GPC) = 14,500 g mol^{-1} was close to that observed for **13** (13,200 g mol^{-1}). These M_n(GPC) values and the comparable PDIs of 1.5 (**13**) and 1.4 (**14**) (Table 4.1) were calculated from the major peak area (*ca*. 90%) of a bimodal distribution of molecular weights.

–O-2,4-$C_6H_3{}^tBu_2$ end-groups could not be detected in the MALDI-ToF mass spectra of crude PLA produced by **12**–**14**. In fact only cyclic poly(*rac*-LA) products arising from transesterification side reactions and an unassignable minor secondary distribution were present. The very broad PDIs of 2.7 (**10**), 2.2 (**11**) and 2.6 (**12**) and bimodal distribution of polymers (**13** and **14**) were consistent with poorly-controlled polymerisation processes, with poly(*rac*-LA) chains of different molecular weights forming. Taking the PDIs and susceptibility of the growing polymer chains to undergo transesterification into consideration, some caution should be taken in drawing conclusions between the solid state structures of **12** and **13** and the experimental molecular weights observed. With the absence of a conventional initiating group in complexes **10**–**14**, initiation by trace water or lactic acid cannot be ruled out, despite the rigorous purification of solvent and *rac*-LA monomer.

Mindful of Feijen's aforementioned reports that addition of certain alcohols to Y(O-2,6-$C_6H_3{}^tBu_2)_3$ (**1.6**) could lead to better controlled catalyst systems, and the growing interest in using chain transfer agents and co-initiators in polymerisation reactions, further ROP experiments with complexes **10**–**14** in the presence of 5 equivs. of BnOH ([*rac*-LA]$_0$:[BnOH]$_0$ = 20:1, Table 4.1) were undertaken. The reduced molecular weights of 3,530 and 3,190 g mol^{-1} with **10** and **11** and 3,000 and 3,010 g mol^{-1} with **12** and **13** were in reasonable agreement with the expected formation of benzyl alcohol-capped poly(*rac*-LA) chains containing *ca*. 20 monomer units ($M_n \approx$ 2,900 g mol^{-1}). Furthermore, the reduced PDIs of 1.5 and 1.6 (**10** and **11**) were consistent with better-controlled systems. With **12** and **13** the time taken to achieve complete

conversion of monomer to poly(*rac*-LA) was reduced significantly (30 mins) compared to when no alcohol was present (150 mins in the case of **13**) and each molecular weight distribution was monomodal, although broad (PDI = 1.8). 150 equivs. of *rac*-LA were added to a mixture of BnOH and **14** ($[BnOH]_0$:$[\mathbf{14}]_0$ = 7.5:1) and 99% conversion was achieved in 30 mins. The molecular weight agreement was not as good with **14** *cf.* **13** and M_n(GPC) = 1,880 g mol^{-1} was lower than expected (M_n(calcd) = 2,920 g mol^{-1}). As with **13**, the PDI = 2.2 was broad. This variation in experimental molecular weight data contrasts NMR tube scale reactions (Figure 4.10, *vide infra*), which suggested that **13** and **14** formed the same species under polymerisation conditions. The variation in polymerisation performance may lie within the range of acceptable experimental error, but polymer products of similar molecular weight would have been expected to form.

^{1}H NMR and MALDI-ToF mass spectra of the resultant poly(*rac*-LA) featured only HOCH(Me)– and $PhCH_2O$– end groups. Unfortunately, the poly(*rac*-LA) formed in these and other ROP experiments described herein exhibited no isotactic or heterotactic bias. The $\Delta(m/z)$ of 72.0 g mol^{-1} between the adjacent peak envelopes in the MALDI-ToF mass spectra was indicative of extensive transesterification and cyclic transesterification products with no apparent end-group were also detected.

4.5 Reactions with $BnNH_2$ as a co-initiator

ROP reactions with BnOH were important to establish the potential of **10**–**13** as immortal ROP catalysts and further reactions with $BnNH_2$ were undertaken. Nd(O-2,4-$C_6H_3{}^tBu_2)_3(THF)_3$ (**10**) was selected as a suitable lanthanide candidate, whereas the strong paramagnetic properties of its gadolinium congener (**11**) prevented accurate ^{1}H NMR analysis of poly(*rac*-LA) products and no further studies were performed with **11**. The potential of Ca_2(O-2,4-$C_6H_3{}^tBu_2)_4(DME)_5$ (**12**), Sr_2(O-2,4-$C_6H_3{}^tBu_2)_4(DME)_3$ (**13**) and Sr_3(O-2,4-$C_6H_3{}^tBu_2)_6(THF)_6$ (**14**) to produce benzyl amine-capped poly(*rac*-LA) was also assessed. The results are presented in Table 4.2 and Figures 4.3 and 4.4.

Table 4.2. Polymerisation of *rac*-LA co-initiated by Nd(O-2,4-$C_6H_3{}^tBu_2)_3(THF)_3$ (**10**), Gd(O-2,4-$C_6H_3{}^tBu_2)_3(THF)_3$ (**11**), Ca_2(O-2,4-$C_6H_3{}^tBu_2)_4(DME)_5$ (**12**), Sr_2(O-2,4-$C_6H_3{}^tBu_2)_4(DME)_3$ (**13**) and Sr_3(O-2,4-$C_6H_3{}^tBu_2)_6(THF)_6$ (**14**).[a]

Complex	[*rac*-LA]$_0$:[$BnNH_2$]$_0$	Time (mins)	Conv. (%)[b]	M_n(calcd) (g mol^{-1})	M_n(GPC) (g mol^{-1})[c]	M_w/M_n[c]
10	[d]	30	92	4,420[e]	7,570	2.7
12	[d]	30	73	[i]	[i]	[i]
12	[d]	150	89	3,200[f]	4,050	2.6
13	[d]	30	51	[i]	[i]	[i]
13	[d]	150	86	12,400[g]	13,200[j]	1.5[j]
14	[d]	30	84	[i]	[i]	[i]
14	[d]	150	94	20,300[g]	14,500[k]	1.4[k]
10	20:1	10	94	2,820[h]	3,110	1.3
12	20:1	10	95	2,850[h]	3,070	1.8
13	20:1	10	96	2,870[h]	3,320	2.0
14	20:1	10	96	2,870[h]	2,360	2.3

[a] [*rac*-LA]$_0$:[Complex]$_0$ = 100:1, [*rac*-LA]$_0$:[**14**]$_0$ = 150:1, 2 mL THF, [*rac*-LA]$_0$ = 0.69 M, rt. [b] Measured by ^{1}H NMR in $CDCl_3$. [c] Measured by GPC against polystyrene standards using the appropriate Mark-Houwink corrections for poly(*rac*-LA) in THF at 30 °C. [d] No $BnNH_2$ added. [e] M_n (calcd) = (Conv. (%) × 144.1)/3). [f] M_n(calcd) = (Conv. (%) × 144.1)/4. [g] M_n(calcd) = (Conv. (%) × [*rac*-LA]$_0$:[Complex]$_0$ × 144.1). [h] M_n(calcd) = (Conv. (%) × [*rac*-LA]$_0$:[$BnNH_2$]$_0$ × 144.1 + 107.2). [i] Not measured. [j] Bimodal distribution, major peak area measured (87%). [k] Bimodal distribution, major peak area measured (90%).

ROP of 100 equivs. of *rac*-LA in the presence of 5 equivs. of $BnNH_2$ and **10**, **12** or **13** in THF at room temperature gave *ca*. 95% conversion to benzyl amine-capped poly(*rac*-LA) within 10 mins. To compare **13** with **14**, the loading for **14** was scaled appropriately to [*rac*-LA]$_0$:[$BnNH_2$]$_0$:[**14**]$_0$ = 150:7.5:1. Measured (and expected) molecular weights were 3,110 (2,820), 3,070 (2,850) and 3,320 (2,870) and 2,360 (2,870) g mol^{-1} for **10**, **12**, **13** and **14** respectively. With **10**, **12** and **13**, each measured molecular weight, M_n(GPC), was higher than that expected for five benzyl amine-capped poly(*rac*-LA) chains forming, and the PDIs ranged from 1.3 (**10**) to 1.8 for **12** and 2.0 for **13**, indicating a wide variation in the degree of control in each ROP

reaction. For compound **10**, the PDI = 1.3 represented an improvement in control compared to when 5 equivs. of BnOH were used (PDI = 1.5, Table 4.1), whereas little variation was observed for complex **12** (PDI = 1.8). However, in the case of **13** and **14**, slightly broader PDIs of 2.0 and 2.3 were noted when $BnNH_2$ was used, rather than BnOH (PDI = 1.8 and 2.2). The M_n(GPC) = 2,360 g mol^{-1} for **14** was lower than M_n(GPC) = 3,320 g mol^{-1} for **13**. However, NMR tube scale polymerisations performed in THF-d_8 (Section 4.6, *vide infra*), strongly suggested that **13** and **14** formed the same active species in solution. The inconsistencies with molecular weight data are likely to lie within the range of acceptable experimental error and are not as conclusive as analysis of NMR tube scale reactions in this instance.

On the basis of **10** and **12** displaying better controlled ROP reactions when $BnNH_2$ was utilised as a co-initiator, further runs were performed where [*rac*-LA]$_0$:[Complex]$_0$ was increased through 100–500 equivs., holding [$BnNH_2$]$_0$:[Complex]$_0$ constant at 5:1. These data are plotted in Figure 4.3 along with lines of least-squares fit. The expected gradient of the least-squares fit is 28.8 g mol^{-1} (not shown) for 5 polymer chains growing per complex in each case. With **10**, the gradient of 35(2) g mol^{-1} (R^2 = 0.986) is higher than expected, although very close within error, and suggests that the rate of initiation is not quite as competitive with propagation given the higher than expected experimental molecular weights. Conversely, the gradient of least-squares fit of 27(1) g mol^{-1} (R^2 = 0.991) for experiments performed with **12** is in better agreement, despite the poorer PDIs (1.3–2.0).

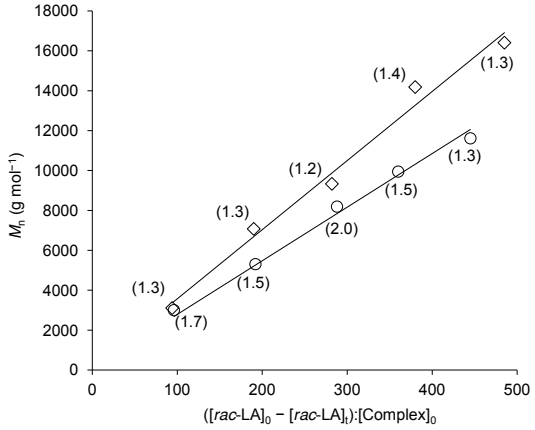

Figure 4.3. M_n(GPC) *vs.* [*rac*-LA]$_0$ – [*rac*-LA]$_t$):[Complex]$_0$, [*rac*-LA]$_0$:[Complex]$_0$ = 100, 200, 300, 400 or 500, using **10** (diamonds) or **12** (circles) and 5 equivs. of $BnNH_2$ as a co-initiator. PDIs are given in parentheses and intercepts were set to 107.2 g mol^{-1} (M_R $BnNH_2$).

Figure 4.4 shows plots of M_n(GPC) *vs.* ([*rac*-LA]$_0$ – [*rac*-LA]$_t$):[$BnNH_2$]$_0$ for the ROP of *rac*-LA, [*rac*-LA]$_0$:[Complex]$_0$ = 200:1, using **10**, **12** and **13** and 3, 5, 7 or 10 equivs. of $BnNH_2$ co-initiator. In these plots the expected line of least-squares fit has a gradient of 144 g mol^{-1} (*rac*-LA unit) for one chain per added amine. The gradient of the least-squares fitted line for **10** was higher than expected at 176(5) g mol^{-1} (R^2 = 0.985), with **12** and **13** having fitted lines with lower gradients of 133(6) g mol^{-1} (R^2 = 0.950) and 122(6) (R^2 = 0.954) g mol^{-1}.

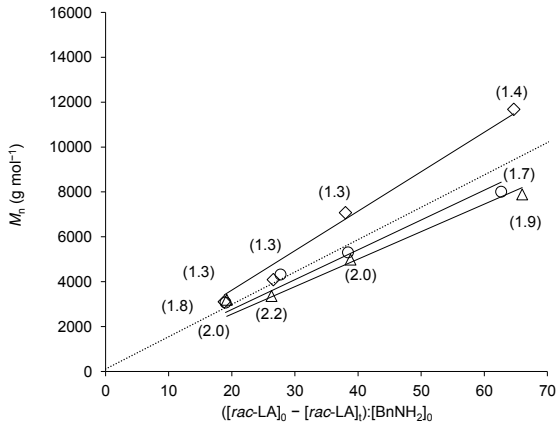

Figure 4.4. M_n(GPC) *vs.* ([*rac*-LA]$_0$ – [*rac*-LA]$_t$):[$BnNH_2$]$_0$ for the ROP of *rac*-LA ([*rac*-LA]$_0$:[Complex]$_0$ = 200:1) using **10** (diamonds), **12** (circles) or **13** (triangles) and 3, 5, 7 or 10 equivs. of $BnNH_2$ as a co-initiator. The numbers in parentheses are the PDIs and the intercepts were set to 107.2 g mol^{-1} (M_R $BnNH_2$). The dashed line represents M_n(calcd) based on [*rac*-LA]$_0$:[$BnNH_2$]$_0$ = 200:*n*.

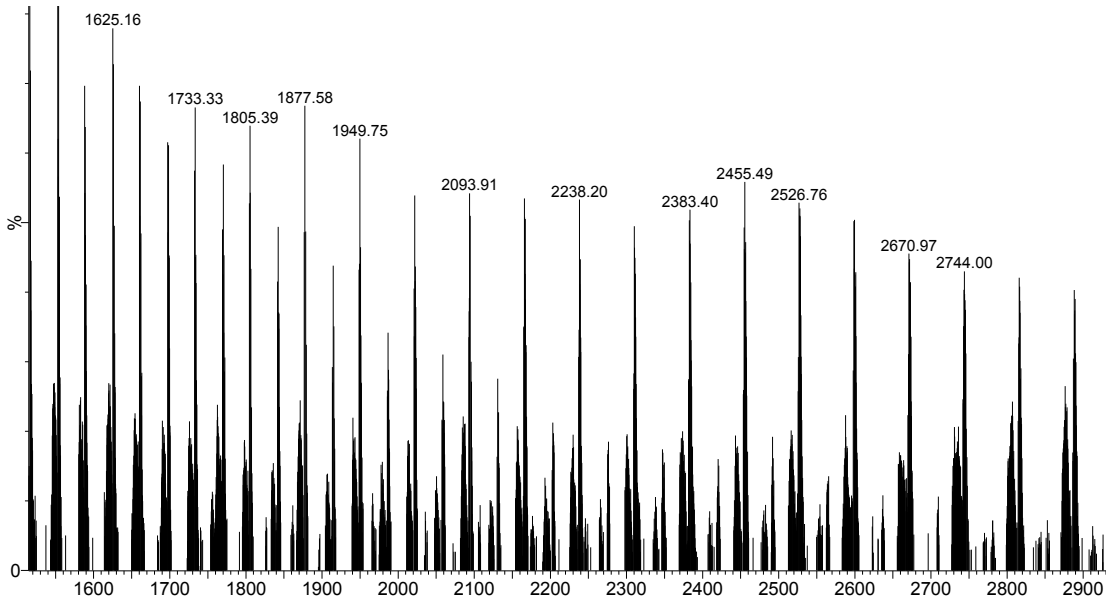

Figure 4.5. Representative MALDI-ToF mass spectrum of benzyl amine-capped (annotated peaks) poly(*rac*-LA) produced by **10**, **12**, **13** and **14**. Example shown is from the run with $[rac\text{-LA}]_0$:$[BnNH_2]_0$:$[\mathbf{13}]_0$ = 100:5:1. K^+ dopant, $\Delta(m/z)$ = 72.0 g mol^{-1}.

The ^{1}H NMR and MALDI-ToF mass spectra (Figure 4.5) of the poly(*rac*-LA) products formed were consistent with the formation of benzyl amine-capped poly(*rac*-LA) for **10**, **12**, **13** and **14**, although once again the polymers were atactic and had $\Delta(m/z)$ separations of 72.0 g mol^{-1} between adjacent peak envelopes. Cyclic polymer products with no apparent end-group were also present as well as an unassigned secondary distribution with $\Delta(m/z)$ = 72.0 g mol^{-1} (present in samples produced by **12**, **13** and **14**).

At lower $[rac\text{-LA}]_0$:$[Complex]_0$ loadings, the observed M_n(GPC) values for benzyl amine-capped poly(*rac*-LA) produced by **10**, **12** and **13** were in good agreement with that expected based on the measured conversion by ^{1}H NMR and presumption of one growing chain per added amine. However, at higher *rac*-LA loadings (Figure 4.3) or lower $BnNH_2$ loadings (Figure 4.4), the agreement between observed and predicted M_n began to diverge. With **10**, M_n(GPC) values were higher than expected, possibly as a result of the rate of initiation not competing with propagation or incomplete consumption of $BnNH_2$. The lower than expected M_n(GPC) values with **12** and **13** are reminiscent of polymerisation reactions where transesterification side reactions compete with linear chain growth.[67, 68] The larger Sr centres of **13** *cf.* Ca (**12**) may

have facilitated intramolecular back-biting and/or intermolecular pathways more readily, accounting for the poorer agreement.

Attempts to extend the amine co-initiated ROP of *rac*-LA to $^{t}BuNH_2$ or piperidine as representative bulky primary or secondary amines were unsuccessful based on initial screening experiments. Agreement between observed and expected polymer molecular weights was much worse, with observed molecular weights being approximately twice that expected for a typical $[rac\text{-LA}]_0$:$[\text{co-initiator}]_0$:$[\text{Complex}]_0$ = 100:5:1 run. These preliminary findings suggest a much slower initiation step with these amine co-initiators, as was found when **1** was employed as the catalyst.

4.6 NMR tube scale reactions

In order to gain some initial mechanistic insight, a series of NMR tube scale reactions were performed. As the paramagnetic properties of Nd(III) are not conducive to reliable study by ^{1}H NMR, no further reactions were performed with **10**. It was shown that neither BnOH (4 equivs.) nor $BnNH_2$ (4 equivs.) reacted with **12** or **13**, to generate new benzyl alkoxide (in contrast to $Y(O_2N^{NMe2})(HO_2N^{NMe2})$ (**1**)) or benzyl amide species as expected based on the relative pK_as of phenols and primary alcohols and amines.[69] However, both BnOH and $BnNH_2$ may compete with DME as a donor ligand based on a general shift of the DME resonances to lower field compared to the pure DME solvates. When *rac*-LA (20 equivs.) was added to mixtures of BnOH and **12** or **13**, or $BnNH_2$ and **12** or **13** (Figure 4.6, bottom), ^{1}H NMR analysis indicated complete consumption of BnOH and $BnNH_2$ and formation of PLA (broad signals at *ca*. δ = 5.1 and 1.3 ppm) with liberation of DME from each metal complex (singlets at δ = 3.3 and 3.1 ppm). This supports the proposed model that in ROP reactions that successfully incorporate co-initiators or chain transfer reagents, the co-initiator is consumed rapidly at the beginning of the reaction in order to generate the multiple PLA chains.

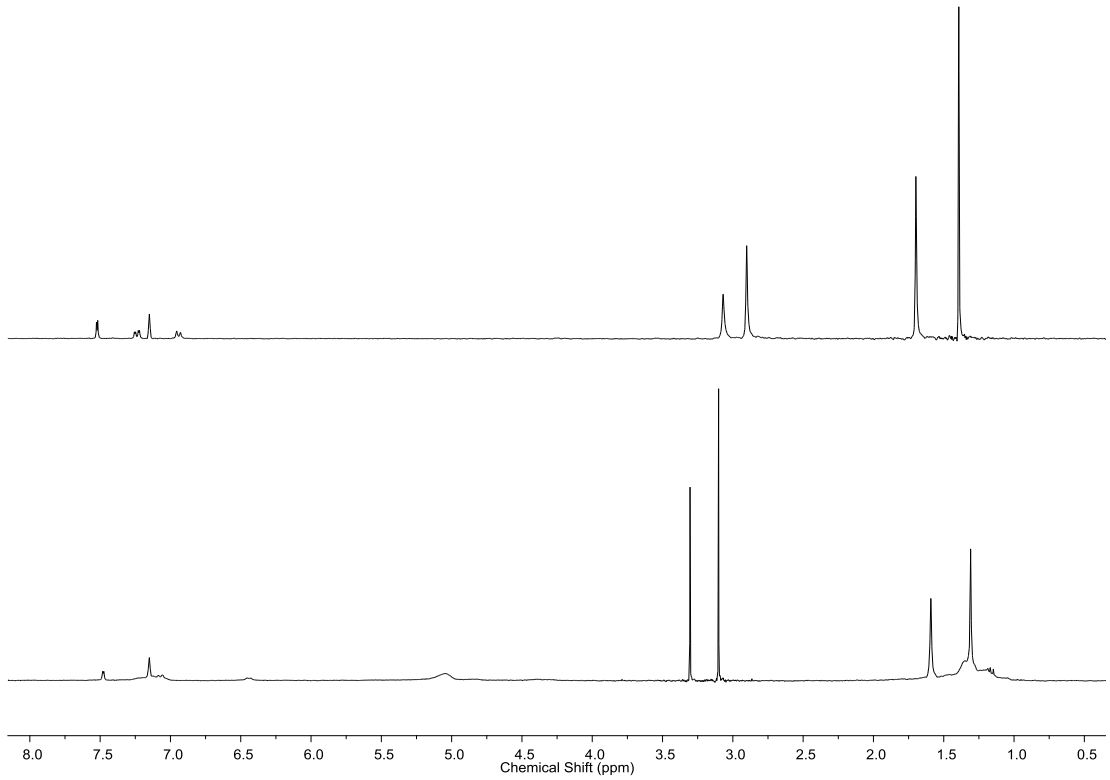

Figure 4.6. ^{1}H NMR (300.1 MHz, C_6D_6, 298 K) spectra of **12** (top), and the NMR tube scale reaction [*rac*-LA]$_0$:[$BnNH_2$]$_0$:[**12**] = 20:4:1 (bottom). Residual protio-solvent, δ = 7.15 ppm.

Interestingly, the presence of liberated HO-2,4-$C_6H_3{}^tBu_2$ from **12** and **13** was not apparent in these reactions. If propagation were to proceed *via* a coordination-insertion mechanism then displacement of HO-2,4-$C_6H_3{}^tBu_2$ would be expected to occur in order to permit a formal bond between the metal centre and a growing PLA chain, which is widely accepted as the reactive bond through which chain propagation occurs. This observation raises the possibility of chain propagation proceeding *via* an activated-monomer process, where rather than having a well-defined metal-alkoxide bond, there are associative interactions between the metal centre, a lactide monomer and an exogenous PLA chain as shown in Figure 1.11 (Chapter One) and Figure 4.7.

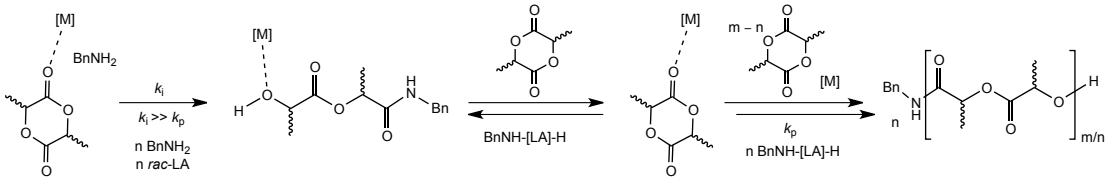

Figure 4.7. Activated-monomer initiation and propagation pathways.

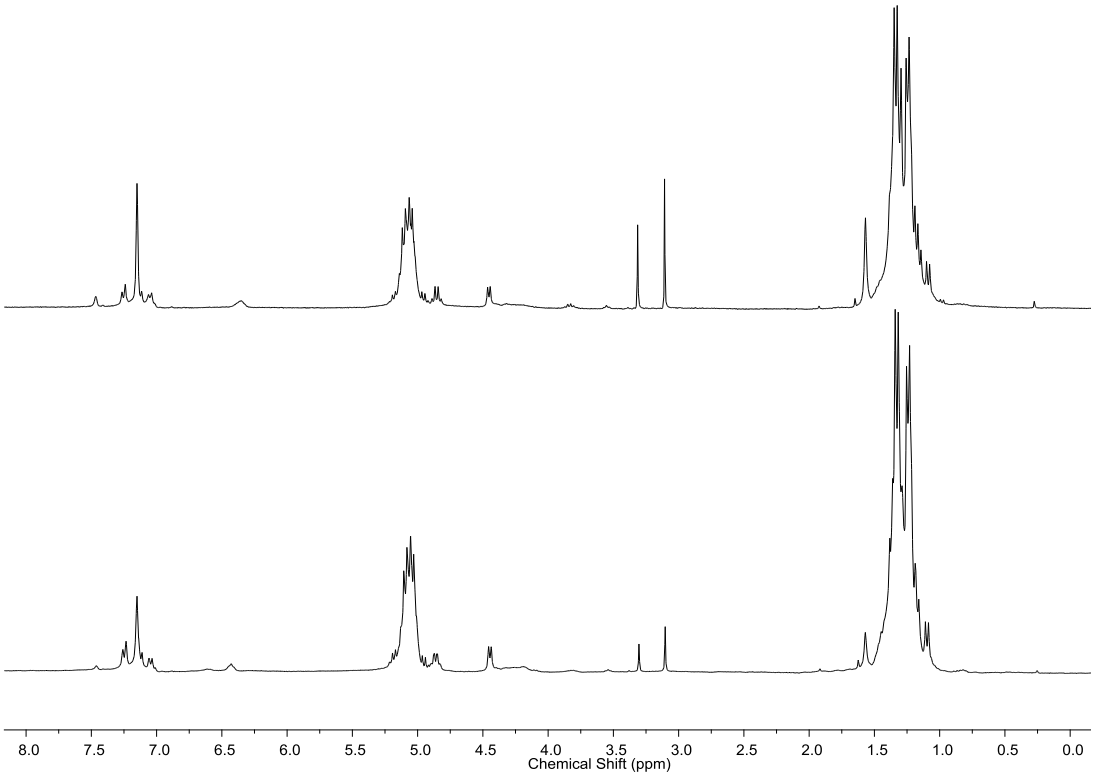

Figure 4.8. ^{1}H NMR (300.1 MHz, C_6D_6, 298 K) spectra from NMR tube scale reactions between macromonomer (**9**) and **13** (4:1, top) and *rac*-LA, macromonomer (**9**) and **13** (20:4:1, bottom). Residual protio-solvent, δ = 7.15 ppm.

This hypothesis was supported by further NMR tube scale experiments where an isolated benzyl amine-terminated PLA macromonomer (**9**) (M_n = 1,600 g mol^{-1}, PDI = 1.11), prepared using Y(O_2N^{NMe2})(HO_2N^{NMe2}) (**1**), was added to **12** or **13** in C_6D_6. Successive equivalents (up to 4 equivs.) of this macromonomer were added to **12** or **13** with subsequent ^{1}H NMR analysis showing no liberation of HO-2,4-$C_6H_3{}^{t}Bu_2$, but again DME was displaced indicating that PLA chains effectively interact with calcium and strontium centres (Figure 4.8, top). *rac*-LA (20 equivs.) was added to each mixture of **12** or **13** and macromonomer (**9**), with ^{1}H NMR analysis confirming that each system was active for ROP (Figure 4.8, bottom), based on the consumption of *rac*-LA and the increase in relative intensity of backbone PLA resonances (broad signals at *ca*. δ = 5.1 and 1.3 ppm) against liberated DME (singlets at δ = 3.3 and 3.1 ppm).

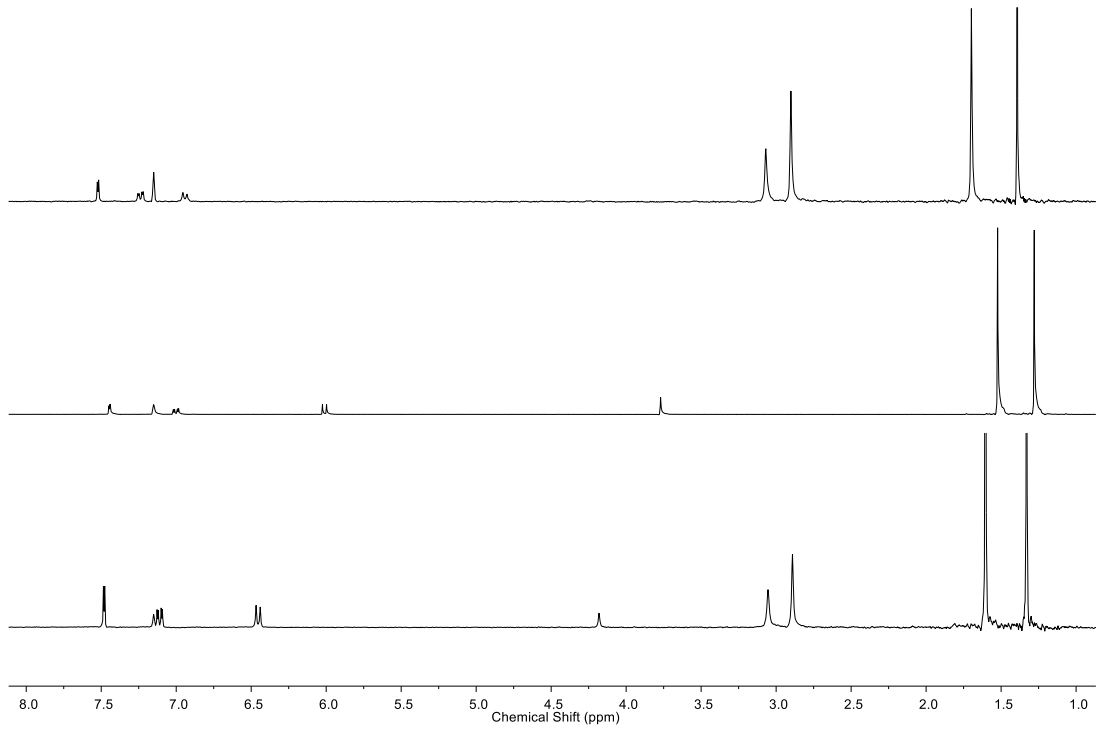

Figure 4.9. ^{1}H NMR (300.1 MHz, C_6D_6, 298 K) spectra from NMR tube scale reactions between HO-2,4-$C_6H_3{}^{t}Bu_2$ and **12**. Top, spectrum of **12**; middle, HO-2,4-$C_6H_3{}^{t}Bu_2$ and bottom, a mixture of HO-2,4-$C_6H_3{}^{t}Bu_2$ and **12** (4:1). Residual protio-solvent, δ = 7.15 ppm.

When protio HO-2,4-$C_6H_3{}^{t}Bu_2$ (4 equivs.) was added to **12** (or **13**) in C_6D_6, "free" HO-2,4-$C_6H_3{}^{t}Bu_2$ was also not apparent in the ^{1}H NMR spectra (Figure 4.9, bottom), suggesting that fast exchange between HO-2,4-$C_6H_3{}^{t}Bu_2$ and bound M-O-2,4-$C_6H_3{}^{t}Bu_2$ may occur. Figure 4.9 (middle) shows the spectrum of HO-2,4-$C_6H_3{}^{t}Bu_2$ with the *ortho*-H doublet and the hydroxyl singlet at δ = 6.0 and 3.7 ppm respectively. The ^{1}H NMR spectrum of the mixture of **12** and HO-2,4-$C_6H_3{}^{t}Bu_2$ (Figure 4.9, bottom), shows a low field shift of this hydroxyl singlet to δ = 4.2 ppm and an averaged *ortho*-H doublet environment at δ = 6.5 ppm. Exchange between liberated HO-2,4-$C_6H_3{}^{t}Bu_2$ and M–O-2,4-$C_6H_3{}^{t}Bu_2$ remains possible during polymerisation reactions and consequently, polymerisation by a coordination-insertion pathway cannot be ruled out if HO-2,4-$C_6H_3{}^{t}Bu_2$ is liberated from **12** or **13**.

To address the uncertainty regarding the fate of **13** and **14** under polymerisation conditions (Tables 4.1 and 4.2), independent NMR tube scale polymerisation reactions were performed in THF-d_8. The top ^{1}H NMR spectrum in Figure 4.10 is that

of **13** dissolved in THF-d_8. Liberated DME (δ = 3.4 and 3.2 ppm) is present, but otherwise, the spectrum is identical to that of **14** (Figure 4.10, second from top). The ^{1}H NMR spectrum of the reaction [*rac*-LA]$_0$:[BnNH$_2$]$_0$:[**13**]$_0$ = 20:4:1 (Figure 4.10, third from top), is also identical to the ^{1}H NMR spectrum of the analogous reaction with **14** ([*rac*-LA]$_0$:[BnNH$_2$]$_0$:[**14**]$_0$ = 30:6:1, Figure 4.10, bottom). Despite the presence of DME singlets (δ = 3.4 and 3.2 ppm) from the reaction with **13**, diagnostic aromatic doublets at δ = 7.0 and 6.6 ppm and ^{t}Bu singlets at δ = 1.4 and 1.2 ppm (Figure 4.10, third from top and bottom) do suggest that **13** and **14** form the same active species in solution.

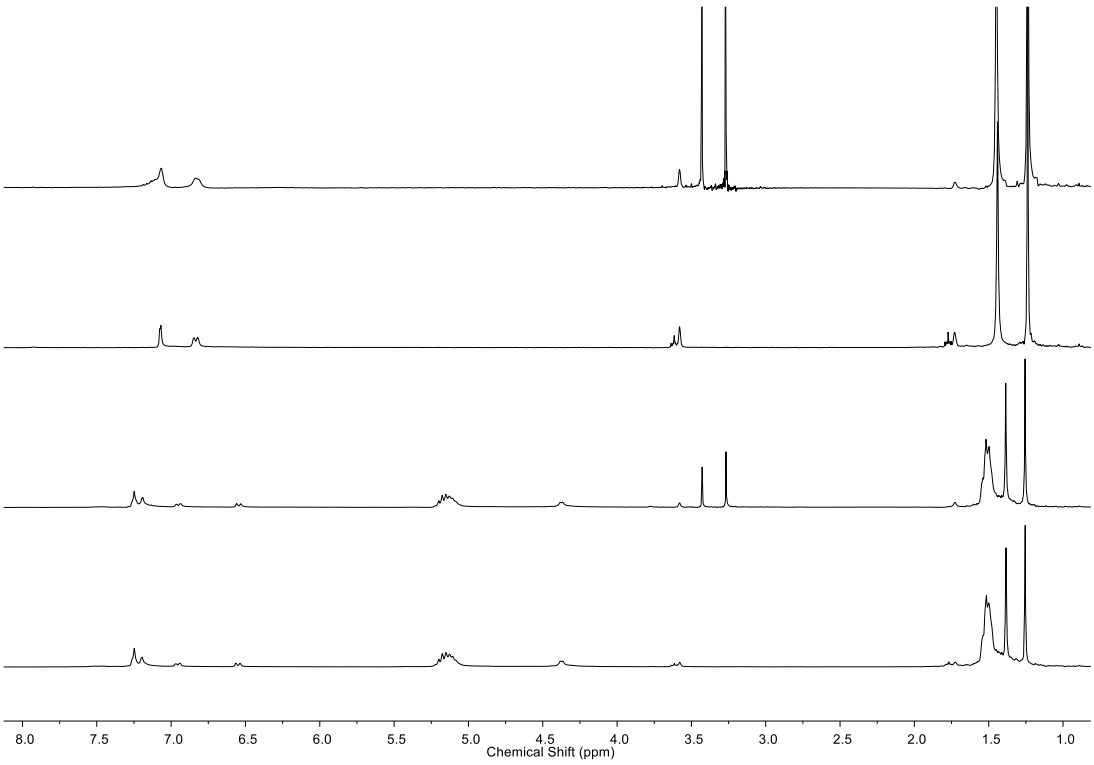

Figure 4.10. From top to bottom, ^{1}H NMR (300.1 MHz, THF-d_8, 298 K) spectra of **13**, **14**, [*rac*-LA]$_0$:[BnNH$_2$]$_0$:[**13**]$_0$ = 20:4:1 and [*rac*-LA]$_0$:[BnNH$_2$]$_0$:[**14**]$_0$ = 30:6:1. Residual protio-solvent, δ = 3.58 and 1.73 ppm.

4.7 Summary of preliminary polymerisation studies

The inclusion of co-initiators in polymerisation mixtures led to a marked improvement in the polymerisation performance of **10**–**14**. In general, experimental M_n(GPC) were reflective of [*rac*-LA]$_0$:[BnNH$_2$]$_0$ and loading experiments showed a systematic increase in M_n if [*rac*-LA]$_0$ was increased (or [BnNH$_2$]$_0$ reduced). The broad PDIs and propensity for transesterification products to form during

polymerisation reactions are "non-ideal" for immortal ROP, but systematic amine end-group incorporation highlighted the broader scope of the amine co-initiated methodology.

Given the paucity of ROP reports utilising simple Group 2 phenolates and the potential for activated-monomer propagation pathways, as indicated by NMR tube scale experiments (Figures 4.6–4.9), further investigation of **12** and **13** was warranted. Immortal ROP *via* coordination-insertion propagation was firmly established by polymerisation studies with **1** and by Carpentier using related complexes,[70, 71] but the development of immortal ROP behaviour with complexes not bearing chelating ligands or initiating group should lead to a redevelopment in the design of future ROP catalysts.

4.8 Kinetic studies

Detailed kinetic studies on both **12** and **13** were undertaken to investigate the nature of the dinuclear species under polymerisation conditions and the acceleration in rate of monomer consumption when $BnNH_2$ was included in the polymerisation mixture. Orders in *rac*-LA, $BnNH_2$ and complex were determined in each case and ^1H NMR ($CDCl_3$) analysis of aliquots taken from polymerisation reactions was used to monitor consumption of *rac*-LA.

4.8.1 Dependence in 12 and 13

Initial room temperature analysis focused on **13**, using a loading of [*rac*-LA]$_0$:[$BnNH_2$]$_0$:[**13**]$_0$ = 400:5:1, ([*rac*-LA]$_0$ = 0.69 M, **13** represents Sr_2(O-2,4-^{t}Bu$_2$-C_6H_3)$_4$(DME)$_3$ containing two Sr centres). Runs were performed where the initial *rac*-LA and $BnNH_2$ concentrations were held constant ([*rac*-LA]$_0$:[$BnNH_2$]$_0$ = 400:5, 0.69 M and 0.009 M respectively) and the concentration of **13** was increased through 0.5–2.5 molar equivs. A representative Conversion *vs*. Time plot for the run [*rac*-LA]$_0$:[$BnNH_2$]$_0$:[**13**]$_0$ = 400:5:1.5 is shown in Figure 4.11 alongside the corresponding second-order plot, modelling consumption of *rac*-LA for this run.

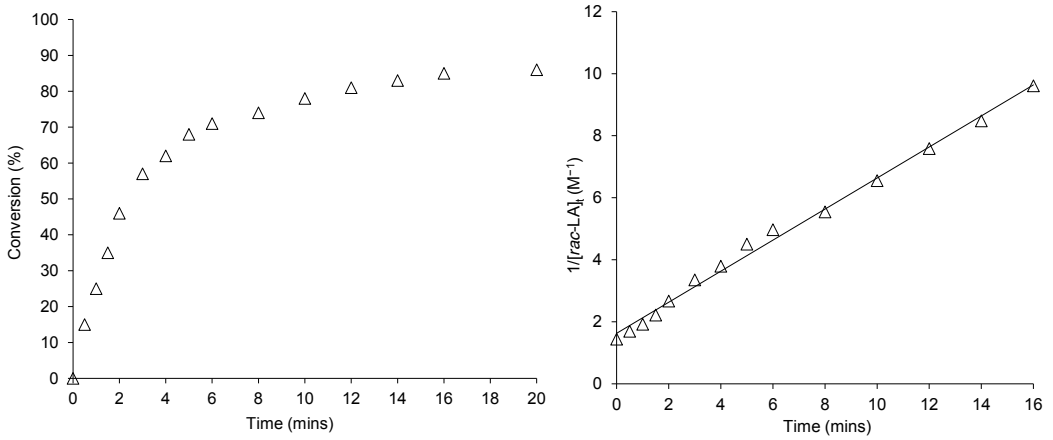

Figure 4.11. Conversion *vs*. Time profile (left) and a second-order rate plot (right) for the run [*rac*-LA]$_0$:[BnNH$_2$]$_0$:[**13**]$_0$ = 400:5:1.5. k_{app} = 0.501(11) (R^2 = 0.994) M^{-1} min^{-1}, vertical-axis intercept = 1.627(84) M^{-1} (1/[*rac*-LA]$_0$ = 1.44 M^{-1}).

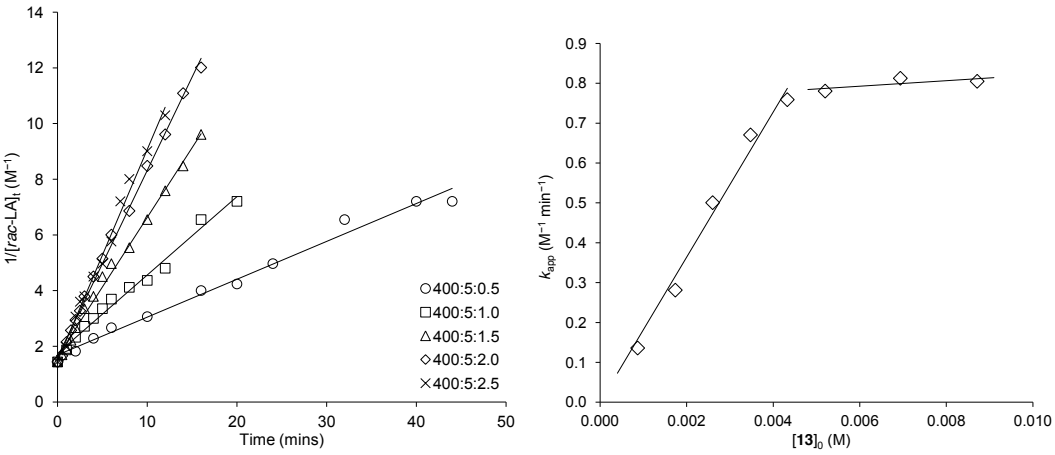

Figure 4.12. Left, second-order plots of 1/[*rac*-LA]$_t$ *vs*. Time with increasing concentrations of [**13**]$_0$. Rate constants, k_{app} = 0.136(5) (R^2 = 0.986), 0.281(11) (R^2 = 0.984), 0.501(11) (R^2 = 0.994), 0.671(11) (R^2 = 0.997) and 0.759(23) (R^2 = 0.991) M^{-1} min^{-1}. The vertical-axis intercepts of these plots are 1.685(127), 1.749(105), 1.627(84), 1.614(79) and 1.477(139) M^{-1}, with the expected intercept, 1/[*rac*-LA]$_0$ = 1.44 M^{-1}. Right, plots of k_{app} *vs*. [**13**]$_0$ for the polymerisation of *rac*-LA. [*rac*-LA]$_0$:[BnNH$_2$]$_0$ = 400:5. Molar equivs. [**13**]$_0$ = 0.5–2.5, 3.0, 4.0 or 5.0, k_{Sr2} = 182(5) M^{-2} min^{-1} (R^2 = 0.983).

Plots of 1/[*rac*-LA]$_t$ *vs.* Time (Figure 4.12, left) were linear over all concentrations of **13** assessed, indicating that the polymerisation reaction proceeded with a second-order dependence in [*rac*-LA]$_0$ concentration as was observed with Y(O$_2$N^{NMe2})(HO$_2$N^{NMe2}) (**1**) and Y(O$_2$N^{NMe2}){N(SiHMe$_2$)$_2$}(THF) (**1.15**). A linear plot of the apparent second-order rate constants, k_{app} *vs*. [**13**]$_0$ (k_{app} = k_{Sr2}[**13**] and k_{Sr2}

= $k_p[BnNH_2]^x$) provided k_{Sr2} = 182(5) M^{-2} min^{-1} (Figure 4.12, right) leading to an experimental rate law of $R_{p,\ Sr2} = k_{Sr2}[rac\text{-LA}]^2[\mathbf{13}]$. Further runs were performed where the molar equivs. of strontium metal centres, Sr_{Tot} (two per molar equivalent of **13**) were increased to exceed $[BnNH_2]_0$ ($[rac\text{-LA}]_0$:$[BnNH_2]_0$:$[\mathbf{13}]_0$ = 400:5:3.0, 400:5:4.0 and 400:5:5.0, $[BnNH_2]_0$:$[Sr_{Tot}]_0$ = 5:6.0, 5:8.0 and 5:10.0). Although **13** can polymerise *rac*-LA in the absence of $BnNH_2$, the reaction is very slow (150 mins to convert 100 equivs.) compared to when an amine or alcohol is present, so polymerisations reactions initiated by **13** alone could be neglected over the timescale of these experiments. As expected, k_{app} increased only marginally from the 400:5:2.5 run (k_{app} = 0.759(23) M^{-1} min^{-1}) in this region and demonstrated saturation within the system, where propagation has become limited by the number of propagating chains, i.e. $[BnNH_2]_0$. Increasing the number of metal equivs. provides more active sites for chain propagation as seen by the increase in k_{app} up to 2.5 equivs. of **13**. However, since propagation is limited by the number of chains, an excess of metal sites does not yield further increases in k_{app} once the concentration of metal centres (i.e. $[Sr_{Tot}]_0$) exceeds initial amine equivs. $[BnNH_2]_0$.

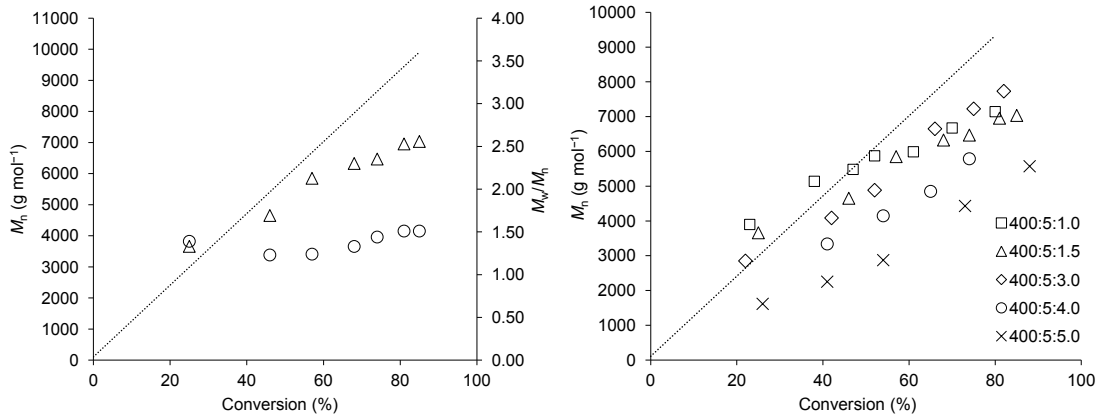

Figure 4.13. Left, M_n(GPC) *vs*. Conversion (triangles) and M_w/M_n *vs*. Conversion (circles) plots for the run $[rac\text{-LA}]_0$:$[BnNH_2]_0$:$[\mathbf{13}]_0$ = 400:5:1.5. Right, M_n(GPC) *vs*. Conversion plots for $[rac\text{-LA}]_0$:$[\mathbf{13}]_0$ = 400:1.0, 1.5, 3.0, 4.0 or 5.0, $[rac\text{-LA}]_0$:$[BnNH_2]_0$ = 400:5, PDIs = 1.4–1.7. The dashed lines represent M_n(calcd) based on $[rac\text{-LA}]_0$:$[BnNH_2]_0$ = 400:5.

Molecular weight data were acquired for select points. In general, the expected and observed molecular weights of early aliquots taken from the reaction mixture were in reasonable agreement, but as the reaction progressed experimental molecular weights began to diverge from those expected. Figure 4.13 (left) shows molecular weight data

and PDI for the run, [*rac*-LA]$_0$:[$BnNH_2$]$_0$:[**13**]$_0$ = 400:5:1.5 (M_n(calcd) = 9,910 g mol^{-1}, M_n(GPC) = 7,040 g mol^{-1} and PDI = 1.51, Entry 3, Table 4.3, *vide infra*). The lower than expected molecular weights at higher monomer to poly(*rac*-LA) conversion and the general increase in PDI during polymerisation were consistent with detrimental chain-shortening transesterification side reactions competing with linear chain growth and resembled the poorer agreement seen in the catalyst loading experiments (Figure 4.4) at lower loadings of amine ([*rac*-LA]$_0$:[$BnNH_2$]$_0$).

Up to the saturation limit, adding more **13** to the polymerisation mixture resulted in a linear increase in k_{app} (Figure 4.12), whereas M_n(GPC) showed no systemmatic dependence on [**13**]$_0$ (Figure 4.13, right). However, the data for [$BnNH_2$]$_0$:[**13**]$_0$ = 5:4.0 or 5:5.0, where the molar equivalents of [Sr_{Tot}]$_0$ considerably exceeded [$BnNH_2$]$_0$ (i.e. the number of growing chains), showed poor agreement between observed and expected M_n (M_n(calcd) = 10,250 g mol^{-1}, M_n(GPC) = 5,570 g mol^{-1} and PDI = 1.44 for [$BnNH_2$]$_0$:[**13**]$_0$ = 5:5.0, Entry 8, Table 4.3, *vide infra*). The excess of metal sites did not yield a net increase in rate, but could have increased the number of metal-catalysed chain-shortening transesterification processes, resulting in poor molecular weight agreement. PDIs ranged from 1.4–1.7 and showed no systematic variation as [**13**]$_0$ was increased.

Compound **12** was conveniently examined under the same polymerisation conditions as **13**. In general the rate of consumption of *rac*-LA was twice as fast in the presence of **12** compared to **13**, and plots of 1/[*rac*-LA]$_t$ *vs*. Time once again suggested a second-order dependence in [*rac*-LA]$_0$ (Figure 4.14, left). The stoichiometry [*rac*-LA]$_0$:[$BnNH_2$]$_0$ = 400:5 ([*rac*-LA]$_0$ = 0.69 M, $BnNH_2$ = 0.009 M) was used again and held constant as the concentration of [**12**]$_0$ (**12** contains two Ca metal centres) was increased through 0.5, 1.0, 1.5 and 2.5 molar equivs. (Figure 4.14, right). The apparent second-order rate constant (k_{app}) values were plotted against [**12**]$_0$ (k_{app} = k_{Ca2}[**12**]) and revealed a first-order dependence in [**12**]$_0$ with k_{Ca2} = 315(10) M^{-2} min^{-1}, nearly two times k_{Sr2} (k_{Sr2} = 182(5) M^{-2} min^{-1}), which contrasts with the generally accepted relative activities of Ca and Sr initiators used in ROP.[72, 73]

Additional experiments with [**12**]$_0$ = 4.0 and 5.0 molar equivs. (Figure 4.14, right) demonstrated a similar saturation region to that observed in the corresponding strontium system, **13**, with the run at [*rac*-LA]$_0$:[$BnNH_2$]$_0$:[**12**]$_0$ = 400:5:2.5 providing an intermediate point of inflexion before the onset of saturation. However, comparing

this case to **13**, there did appear to be some residual activity in the region where the number of calcium centre equivalents, $[Ca_{Tot}]_0$, exceeded $[BnNH_2]_0$. For example, k_{app} for the run $[rac\text{-LA}]_0:[BnNH_2]_0:[\mathbf{12}]_0$ = 400:5:2.5 was determined as k_{app} = 1.323(52) M^{-1} min^{-1}, approximately five times k_{app} for $[rac\text{-LA}]_0:[BnNH_2]_0:[\mathbf{12}]_0$ = 400:5:0.5 (0.279(8) M^{-1} min^{-1}, Figure 4.14). The values of k_{app} for the points $[rac\text{-LA}]_0:[BnNH_2]_0:[\mathbf{12}]_0$ = 400:5:4.0 and 400:5:5.0 ($[BnNH_2]_0:[Ca_{Tot}]_0$ = 5:8.0 and 5:10.0) were 1.606(71) M^{-1} min^{-1} and 1.556(53) M^{-1} min^{-1} respectively, representing some smaller enhancement of rate. The gradient of the line of least-squares fit at the saturation region (29.1 M^{-1} min^{-1}, Figure 4.14) also reflected some rate enhancement under these conditions. In this saturation region (Figure 4.14, right), additional ROP of lactide by excess **12** relative to $BnNH_2$ may be occurring by an alternative propagation pathway not involving benzyl amine-capped PLA chains, for example by impurities.

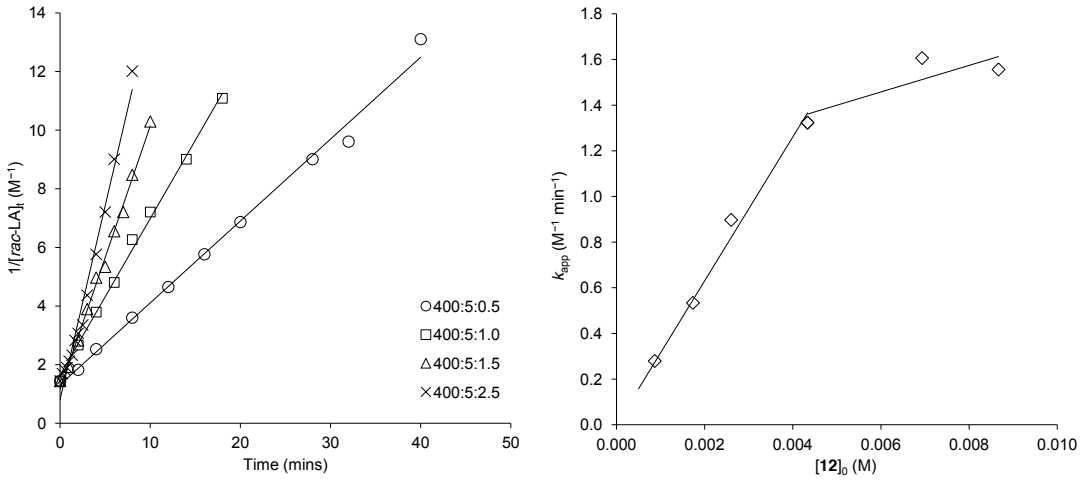

Figure 4.14. Left, second-order plots of $1/[rac\text{-LA}]_t$ *vs*. Time with increasing concentrations of $[\mathbf{12}]_0$. Rate constants, k_{app} = 0.279(8) (R^2 = 0.994), 0.534(13) (R^2 = 0.997), 0.897(22) (R^2 = 0.995) and 1.323(52) (R^2 = 0.982) M^{-1} min^{-1}. The vertical-axis intercepts of the plots are 1.315(165), 1.645(124), 1.165(122) and 0.806(181) M^{-1}, with the expected intercept, $1/[rac\text{-LA}]_0$ = 1.44 M^{-1}. Right, plots of k_{app} *vs*. $[\mathbf{12}]_0$. $[rac\text{-LA}]_0:[BnNH_2]_0$ = 400:5. Molar equivs. $[\mathbf{12}]_0$ = 0.5–1.5, 2.5, 4.0 or 5.0, k_{Ca2} = 315(10) M^{-2} min^{-1} (R^2 = 0.987).

The apparent second-order rate constants from the experiments described in Figures 4.12 and 4.14 are summarised in Tables 4.3 and 4.4 along with experimental M_n data for aliquots taken from polymerisation reactions. Figure 4.15 (left) is a M_n(GPC) *vs*. Conversion plot for $[rac\text{-LA}]_0:[BnNH_2]_0:[\mathbf{12}]_0$ = 400:5:1.5 (M_n(calcd) = 10,020 g

mol^{-1}, M_n(GPC) = 8,200 g mol^{-1} and PDI = 1.36, Entry 3, Table 4.4) and shows that M_n(GPC) values were consistently lower than M_n(calcd) based on the ratio [*rac*-LA]$_0$:[$BnNH_2$]$_0$ = 400:5. Over the course of the reaction the polydispersity indices remained consistent within error and a final PDI = 1.36 was recorded (Figure 4.15, left). In the comparable run with [*rac*-LA]$_0$:[$BnNH_2$]$_0$:[**13**]$_0$ = 400:5:1.5, the final PDI = 1.51 reflected the broader PDIs seen in ROP experiments with **13** *cf.* **12** (Tables 4.3 and 4.4 and Figure 4.4). Figure 4.15 (right) shows M_n(GPC) data for the loadings, [*rac*-LA]$_0$:[**12**]$_0$ = 400:1.0, 1.5, 2.5 and 4.0. In general (and taking note of the catalyst loading experiments, Figures 4.3 and 4.4), molecular weights were lower than expected based on [*rac*-LA]$_0$:[$BnNH_2$]$_0$ = 400:5. At higher metal loadings (saturation region), [*rac*-LA]$_0$:[$BnNH_2$]$_0$:[**12**]$_0$ = 400:5:4.0, the molecular weight agreement was poor, (M_n(calcd) = 10,020 g mol^{-1}, M_n(GPC) = 6,350 g mol^{-1} and PDI = 1.37, Entry 5, Table 4.4) and possibly reflected promotion of chain-shortening transesterification on account of the higher concentration of metal sites or extra chains growing per metal as highlighted by the residual activity of **12** (Figure 4.14, right). In the comparable run with **13**, [*rac*-LA]$_0$:[$BnNH_2$]$_0$:[**13**]$_0$ = 400:5:4.0, M_n(calcd) = 8,640 g mol^{-1}, M_n(GPC) = 5,790 g mol^{-1} and PDI = 1.36.

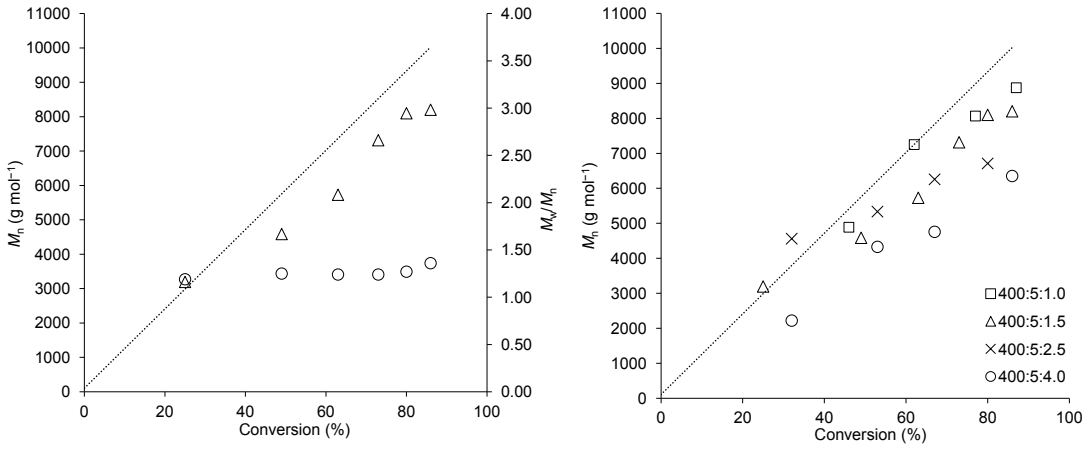

Figure 4.15. Left, M_n(GPC) *vs*. Conversion (triangles) and M_w/M_n *vs*. Conversion (circles) plots for the run [*rac*-LA]$_0$:[$BnNH_2$]$_0$:[**12**]$_0$ = 400:5:1.5. Right, M_n(GPC) *vs*. Conversion plots with [*rac*-LA]$_0$:[$BnNH_2$]$_0$ = 400:5 and [*rac*-LA]$_0$:[**12**]$_0$ = 400:1.0, 1.5, 2.5 or 4.0, PDIs = 1.4–1.5. The dashed lines represent M_n(calcd) based on [*rac*-LA]$_0$:[$BnNH_2$]$_0$ = 400:5.

Table 4.3. Apparent second-order rate constants (k_{app}) and molecular weight data from the metal dependence determination experiments for $Sr_2(O\text{-}2,4\text{-}C_6H_3{}^tBu_2)_4(DME)_3$ (**13**).

Entry	Complex	[*rac*-LA]$_0$:[BnNH$_2$]$_0$:[**13**]$_0$ [a]	k_{app} (M^{-1} min^{-1}) [b]	R^2 [b]	Conv. (%) [c]	M_n(calcd) (g mol^{-1}) [c]	M_n(GPC) (g mol^{-1}) [d]	M_w/M_n [d]
1	**13**	400:5:0.5	0.136(5)	0.986	[e]	[e]	[e]	[e]
2	**13**	400:5:1.0	0.281(11)	0.984	80	9,330	7,140	1.66
3	**13**	400:5:1.5	0.501(11)	0.994	85	9,910	7,040	1.51
4	**13**	400:5:2.0	0.671(11)	0.997	76	8,870	7,550	1.70
5	**13**	400:5:2.5	0.759(23)	0.991	[e]	[e]	[e]	[e]
6	**13**	400:5:3.0	0.780(29)	0.986	82	9,560	7,730	1.51
7	**13**	400:5:4.0	0.813(49)	0.975	74	8,640	5,790	1.36
8	**13**	400:5:5.0	0.805(45)	0.967	88	10,250	5,570	1.44

[a] [*rac*-LA]$_0$:[BnNH$_2$]$_0$ = 400:5, [*rac*-LA]$_0$ = 0.69 M, THF, rt. [b] Apparent second-order rate constants for consumption of *rac*-LA with standard error and R^2 determined by linear regression analysis. [c] Reactions monitored by ^{1}H NMR ($CDCl_3$). All quoted conversions refer to the last point where M_n(GPC) was determined. M_n(calcd) = (Conv. (%) × [*rac*-LA]$_0$:[BnNH$_2$]$_0$ × 144.1 + 107.2). [d] Measured by GPC against polystyrene standards with appropriate Mark-Houwink corrections for poly(*rac*-LA) in THF at 30 °C. [e] Molecular weight data not determined.

Table 4.4. Apparent second-order rate constants (k_{app}) and molecular weight data from the metal dependence determination experiments for $Ca_2(O\text{-}2,4\text{-}C_6H_3{}^tBu_2)_4(DME)_5$ (**12**).

Entry	Complex	[*rac*-LA]$_0$:[BnNH$_2$]$_0$:[**12**]$_0$ [a]	k_{app} (M^{-1} min^{-1}) [b]	R^2 [b]	Conv. (%) [c]	M_n(calcd) (g mol^{-1}) [c]	M_n(GPC) (g mol^{-1}) [d]	M_w/M_n [d]
1	**12**	400:5:0.5	0.279(8)	0.994	[e]	[e]	[e]	[e]
2	**12**	400:5:1.0	0.534(12)	0.997	87	10,140	8,880	1.35
3	**12**	400:5:1.5	0.897(22)	0.995	86	10,020	8,200	1.36
4	**12**	400:5:2.5	1.323(52)	0.982	80	9,330	6,710	1.46
5	**12**	400:5:4.0	1.606(71)	0.981	86	10,020	6,350	1.37
6	**12**	400:5:5.0	1.556(53)	0.986	[e]	[e]	[e]	[e]

[a] [*rac*-LA]$_0$:[BnNH$_2$]$_0$ = 400:5, [*rac*-LA]$_0$ = 0.69 M, THF, rt. [b] Apparent second-order rate constants for consumption of *rac*-LA with standard error and R^2 determined by linear regression analysis. [c] Reactions monitored by ^{1}H NMR ($CDCl_3$). All quoted conversions refer to the last point where M_n(GPC) was determined. M_n(calcd) = (Conv. (%) × [*rac*-LA]$_0$:[BnNH$_2$]$_0$ × 144.1 + 107.2). [d] Measured by GPC against polystyrene standards with appropriate Mark-Houwink corrections for poly(*rac*-LA) in THF at 30 °C. [e] Molecular weight data not determined.

4.8.2 $BnNH_2$ rate dependence in ROP experiments catalysed by 12 and 13

From the catalyst loading experiments (Table 4.2 and Figures 4.4 and 4.5) it was clear that $BnNH_2$ had a significant effect on the rate of *rac*-LA consumption when **12** and **13** were employed as catalysts. In the absence of a co-initiator, complete conversion was achieved in 150 mins, whereas comparable $BnNH_2$ co-initiated polymerisations were complete in 10 mins. When the first-order dependencies in $[\mathbf{12}]_0$ and $[\mathbf{13}]_0$ were determined (Figures 4.12 and 4.14), the rate increased until the concentration of catalyst metal centres was equal to $[BnNH_2]_0$ (i.e. the number of growing chains once all $BnNH_2$ had been consumed).

To determine the order in $[BnNH_2]_0$, $[rac\text{-LA}]_0:[\mathbf{13}]_0 = 400:1$ ($[rac\text{-LA}]_0 = 0.69$ M, $[\mathbf{13}]_0 = 0.002$ M) was selected as the constant *rac*-LA to complex loading and since k_{app} for the run $[rac\text{-LA}]_0:[BnNH_2]_0:[\mathbf{13}]_0 = 400:5.0:1$ had been determined (k_{app} = 0.281(11) M^{-1} min^{-1}, Entry 2, Table 4.3 and Entry 2, Table 4.5), a second run was performed where the initial $BnNH_2$ concentration was doubled ($[rac\text{-LA}]_0:[BnNH_2]_0:[\mathbf{13}]_0 = 400:10.0:1$). Again polymerisation was shown to proceed with a second-order dependence in $[rac\text{-LA}]_0$ but a much greater k_{app} = 2.033(92) M^{-1} min^{-1} (*cf.* 0.281(11) M^{-1} min^{-1} for the 400:5.0:1 run) clearly showed a non-linear rate dependence in $[BnNH_2]_0$. Due to this fast rate of reaction (> 90% conversion after 8 mins) being at the upper limit of the practical reaction-sampling window, intermediate runs at 2.5 and 7.5 $BnNH_2$ molar equivs. were performed (Entries 1 and 3, Table 4.5). The gradient of the line of least-squares fit ($R^2 = 0.984$) taken from the $-\ln k_{app}$ *vs.* $-\ln[BnNH_2]_0$ plot (Figure 4.16, left) provided an order in $[BnNH_2]_0$ of 2.6(2). Hence, $R_{p,\,BnNH2} = k_{BnNH2}[rac\text{-LA}]^2[BnNH_2]^{2.6}$ with $k_{BnNH2} \approx 60{,}000$ $M^{-3.6}$ min^{-1}, calculated from the vertical-axis intercept ($\ln k_{BnNH2} = 11.0(1.0)$). The overall rate law for propagation then becomes $R_p = k_p[rac\text{-LA}]^2[BnNH_2]^{2.6}[\mathbf{13}]$ and since $k_{BnNH2} = k_p[\mathbf{13}]_0$, with $[\mathbf{13}]_0 = 0.002$ M, $k_p \approx 3.5 \times 10^7$ $M^{-4.6}$ min^{-1}.

Since the majority of previous immortal ROP studies have utilised alcohols as a chain transfer agent, the $[rac\text{-LA}]_0:[BnNH_2]_0:[\mathbf{13}]_0 = 400:10:1$ and 400:5:1 runs were repeated using BnOH as the co-initiator in order to compare the performance of $BnNH_2$ with a more widely recognised immortal ROP chain transfer agent. Whilst consumption of *rac*-LA was modelled with a second-order dependence, the polymerisations co-initiated by BnOH were less well behaved, but similar

conversions were achieved over comparable timescales. For example with [*rac*-LA]$_0$:[BnNH$_2$]$_0$ or [*rac*-LA]$_0$:[BnOH]$_0$ = 400:10, 65% monomer to poly(*rac*-LA) conversion was achieved within 2 mins and conversions of 92% (BnNH$_2$) and 84% (BnOH) were achieved within 8 mins. Polymerisations were slower when [*rac*-LA]$_0$:[BnNH$_2$]$_0$ or [*rac*-LA]$_0$:[BnOH]$_0$ = 400:5, with 40% monomer to poly(*rac*-LA) conversion being achieved within 2 mins. 80% conversion was not achieved until 20 mins had elapsed in both runs and was indicative of a dependence in [BnOH]$_0$ in BnOH co-initiated experiments.

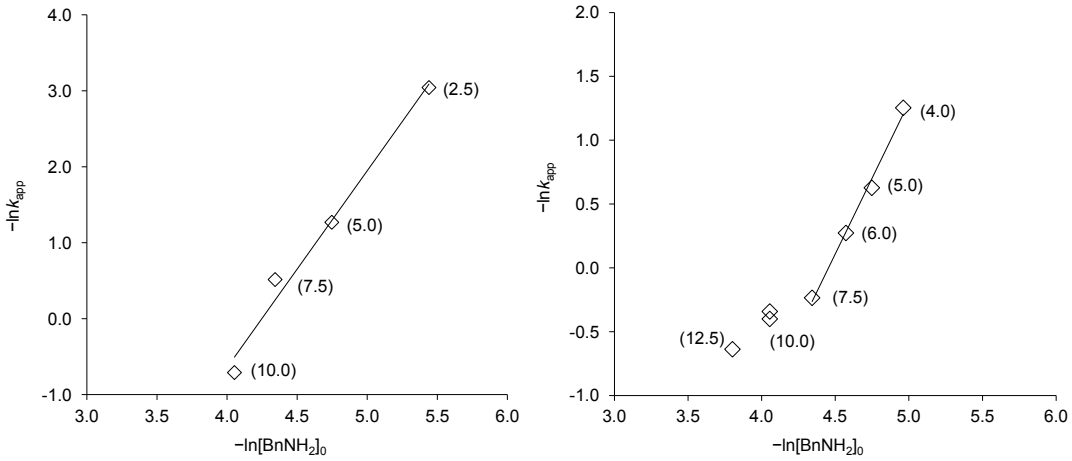

Figure 4.16. −lnk_{app} *vs*. −ln[BnNH$_2$]$_0$ plots for **13** (left) and **12** (right), with the vertical-axis intercept equal to −lnk_{BnNH2}. Numbers in parentheses indicate number of amine equivs. (*n*) for the runs [*rac*-LA]$_0$:[BnNH$_2$]$_0$:[Complex]$_0$ = 400:*n*:1.

A similar dependence in [BnNH$_2$]$_0$ was also found for **12**, but only for runs up to [BnNH$_2$]$_0$:[**12**]$_0$ = 7.5. As with **13**, [*rac*-LA]$_0$:[BnNH$_2$]$_0$:[**12**]$_0$ = 400:5.0:1 was taken as the initial point (k_{app} = 0.534(12) M^{-1} min^{-1}, Entry 2, Table 4.4 and Entry 2, Table 4.6). Holding [*rac*-LA]$_0$ and [**12**]$_0$ constant (0.69 M and 0.002 M respectively), the number of amine equivs. (*n*) were increased through 4.0, 5.0, 6.0, 7.5, 10.0 and 12.5 (Table 4.6). The addition of 10 equivs. of BnNH$_2$ did not result in as great an increase in rate as expected based on the fitted line for 4.0–7.5 BnNH$_2$ equivs. (Figure 4.16, right). The result was reproduced and a further point at 12.5 amine equivs. was suggestive of a tendency to saturation, representing the rate of propagation becoming limited by the calcium metal concentration.

An order of 2.4(1) in [BnNH$_2$]$_0$ was calculated from the plot of –lnk_{app} *vs*. −ln[BnNH$_2$], based on the line of least-squares fit (R^2 = 0.993) through the points representing 4.0, 5.0, 6.0 and 7.5 BnNH$_2$ molar equivs. (Figure 4.16, right). The

proposed overall rate law for propagation is $R_{p,\ BnNH2} = k_{BnNH2}[rac\text{-LA}]^2[BnNH_2]^{2.4}$, with $k_{BnNH2} \approx 39{,}000\ M^{-3.4}\ min^{-1}$ calculated from the vertical-axis intercept ($\ln k_{BnNH2} = 10.6(7)$) and since $k_{BnNH2} = k_p[\mathbf{12}]$ with $[\mathbf{12}]_0 = 0.002$ M, $k_p \approx 2.2 \times 10^7\ M^{-4.4}\ min^{-1}$, providing an overall propagation rate law, $R_p = k_p[rac\text{-LA}]^2[BnNH_2]^{2.4}[\mathbf{12}]$.

The overall propagation rate constants, k_p, determined for both **12** and **13** were approximately the same at $2.2 \times 10^7\ M^{-4.4}\ min^{-1}$ and $3.5 \times 10^7\ M^{-4.6}\ min^{-1}$ respectively. However, it is felt that the metal rate dependence experiments (Figures 4.12 and 4.14) provide a more accurate depiction of relative metal activity with **12** ($k_{Ca2} = 315(10)\ M^{-2}\ min^{-1}$) being approximately twice as active as **13** ($k_{Sr2} = 182(5)\ M^{-2}\ min^{-1}$). The greater overall k_p for **13** ($3.5 \times 10^7\ M^{-4.6}\ min^{-1}$) may have been biased by the greater order in $BnNH_2$ (2.6(2) for **13** and 2.4(1) for **12**) and the variation in the vertical-axis intercepts ($\ln k_{BnNH2} = 11.0(1.0)$ for **13** and 10.6(7) for **12**, Figure 4.16). The onset of the saturation limit evident in Figure 4.16 (right) may have also skewed the overall rate constant in this instance.

The order in $BnNH_2$ is approximately 2.5 within one standard deviation for ROP of *rac*-LA catalysed by both **12** and **13**. In the metal dependence determination experiments (Figures 4.12 and 4.14 and Tables 4.3 and 4.4), $[BnNH_2]_0$ was held constant at 0.009 M (5 molar equivs.). Given $k_{Complex} = k_p[BnNH_2]^{2.5}$ and $k_{Ca2} = 315(10)\ M^{-2}\ min^{-1}$, overall k_p for **12** is $4.1(1) \times 10^7\ M^{-4.5}\ min^{-1}$ and likewise, $k_p = 2.4(1) \times 10^7\ M^{-4.5}\ min^{-1}$ for **13**. These calculated overall rate constants are more reflective of the relative rates of ROP catalysed by **12** and **13** under the described experimental conditions (Tables 4.3–4.6). Regarding a mechanistic interpretation (*vide infra*), it may be more appropriate to describe the overall rate law for propagation with a second-order dependence in $[BnNH_2]_0$, in which case, $k_p = 3.9(1) \times 10^7\ M^{-4}\ min^{-1}$ for **12** and $k_p = 2.2(1) \times 10^7\ M^{-4}\ min^{-1}$ for **13**. These overall propagation rate constants, for a second-order dependence in $[BnNH_2]_0$ are consistent with the overall rate constants for an order in $[BnNH_2]_0$ of 2.5.

Table 4.5. Apparent second-order rate constants (k_{app}) and molecular weight data from the $[BnNH_2]_0$ dependence determination experiments for $Sr_2(O\text{-}2,4\text{-}C_6H_3{}^tBu_2)_4(DME)_3$ (**13**).

Entry	Complex	[*rac*-LA]$_0$:[$BnNH_2$]$_0$:[**13**]$_0$ [a]	k_{app} (M^{-1} min^{-1}) [b]	R^2 [b]	Conv. (%) [c]	M_n(calcd) (g mol^{-1}) [c]	M_n(GPC) (g mol^{-1}) [d]	M_w/M_n [d]
1	**13**	400:2.5:1	0.048(2) [e]	0.976	[f]	[f]	[f]	[f]
2	**13**	400:5.0:1	0.281(11)	0.984	80	9,330	7,140	1.66
3	**13**	400:7.5:1	0.598(20)	0.984	87	6,800	5,900	1.70
4	**13**	400:10.0:1	2.033(92)	0.982	88	5,180	5,840	1.50

[a] [*rac*-LA]$_0$:[**13**]$_0$ = 400:1, [*rac*-LA]$_0$ = 0.69 M, THF rt. [b] Apparent second-order rate constants for consumption of *rac*-LA with standard error and R^2 determined by linear regression analysis. [c] Reactions monitored by ^1H NMR ($CDCl_3$). All quoted conversions refer to the last point where M_n(GPC) was determined. M_n(calcd) = (Conv. (%) × [*rac*-LA]$_0$:[$BnNH_2$]$_0$ × 144.1 + 107.2). [d] Determined by GPC against polystyrene standards with appropriate Mark-Houwink corrections for poly(*rac*-LA) in THF at 30 °C. [e] Conversion of monomer to polymer did not proceed beyond 65%. [f] Molecular weight data not determined.

Table 4.6. Apparent second-order rate constants (k_{app}) and molecular weight data from the $[BnNH_2]_0$ dependence determination experiments for $Ca_2(O\text{-}2,4\text{-}C_6H_3{}^tBu_2)_4(DME)_5$ (**12**).

Entry	Complex	[*rac*-LA]$_0$:[BnNH$_2$]$_0$:[**12**]$_0$ [a]	k_{app} (M^{-1} min^{-1}) [b]	R^2 [b]	Conv. (%) [c]	M_n(calcd) (g mol^{-1}) [c]	M_n(GPC) (g mol^{-1}) [d]	M_w/M_n [d]
1	**12**	400:2.5:1	0.064(9) [e]	0.908	[f]	[f]	[f]	[f]
2	**12**	400:4.0:1	0.285(6)	0.994	[f]	[f]	[f]	[f]
3	**12**	400:5.0:1	0.534(13)	0.997	87	10,140	8,420	1.35
4	**12**	400:6.0:1	0.761(11)	0.998	[f]	[f]	[f]	[f]
5	**12**	400:7.5:1	1.264(33)	0.991	90	7,030	8,310	1.30
6	**12**	400:10.0:1	1.407(22)	0.997	85	5,010	5,950	1.42
7	**12**	400:10.0:1	1.492(49)	0.987	[f]	[f]	[f]	[f]
8	**12**	400:12.5:1	1.891(58)	0.989	88	4,170	4,260	1.25

[a] [*rac*-LA]$_0$:[**12**]$_0$ = 400:1, [*rac*-LA]$_0$ = 0.69 M, THF, rt. [b] Apparent second-order rate constants for consumption of *rac*-LA with standard error and R^2 determined by linear regression analysis. [c] Reactions monitored by ^{1}H NMR ($CDCl_3$). All quoted conversions refer to the last point where M_n(GPC) was determined. M_n(calcd) = (Conv. (%) × [*rac*-LA]$_0$:[BnNH$_2$]$_0$ × 144.1 + 107.2). [d] Determined by GPC against polystyrene standards with appropriate Mark-Houwink corrections for poly(*rac*-LA) in THF at 30 °C. [e] Conversion of monomer to polymer did not proceed beyond 65%. [f] Molecular weight data not determined.

4.9 Mechanistic interpretation

It is much harder to draw definitive mechanistic conclusions for ROP reactions performed with these phenolate supported calcium and strontium complexes (**12** and **13**) than the well-defined bis(phenolate)-amino supported yttrium (**1**) and related lanthanide catalysts. Regarding the second-order dependence in $[rac\text{-LA}]_0$ with **1** and related complexes, it was possible that the observed heteroselectivity played a role or that two *rac*-LA monomers were involved in a cooperative propagation mechanism. Given that no heterotactic enrichment was detected in PLA products produced by **12** and **13**, the second-order dependencies in both $[BnNH_2]_0$ and $[rac\text{-LA}]_0$ may arise from a possible cooperative mechanism where two monomers are involved in the transition state or may reflect the activated-monomer behaviour exhibited by **12** and **13**.

According to NMR tube scale experiments, the O-2,4-di-*tert*-butylphenolate ligands of **12** and **13** were not liberated during polymerisation by alcoholic PLA end-groups (as in the case of **1**), or are at least in fast exchange with bound PLA chains. In the former scenario, no formal metal-poly(*rac*-LA) bond is formed, thus propagation is likely to occur through an activated-monomer process (Figure 4.7, *vide supra*).

As shown in Figure 4.17, it may be possible that multiple chains propagate at the same time, accounting for the higher orders in both $[rac\text{-LA}]_0$ and $[BnNH_2]_0$ with the latter determining the number of PLA chains. If two lactide monomers can be enchained at the same time, then two PLA chains are likely to be involved thus the approximate 2.5 order in $[BnNH_2]_0$ may be closer to 2, providing an overall rate law for propagation, $R_p = k_p[rac\text{-LA}]^2[BnNH_2]^2[\text{Complex}]$. The fate of each pre-catalyst is unknown but if the dimeric structure is retained (and stabilised by THF solvent molecules or PLA chelates), then the dimeric molecule may cooperatively bind two lactide units with two exogenous PLA chains involved in enchainment. In the metal dependence determination experiments (Figures 4.12 and 4.14), the saturation region was reached when $[BnNH_2]_0$:$[\text{Complex}]_0$ = 5:2.5, which is equivalent to $[BnNH_2]_0$:$[M_{Tot}]_0$ = 5:5, given that each complex contains two metal centres. This suggests that each metal centre is involved in catalysing chain growth, irrespective of whether the dimeric structure is retained or not.

With **12**, the onset of a saturation limit at $[BnNH_2]_0$:[**12**]$_0$ = 10:1 (Figure 4.16, right) signified that the calcium coordination sphere was becoming saturated by PLA chains and monomer-activation was being inhibited. Under the same conditions, the larger strontium centres of **13** continued to facilitate efficient monomer coordination and the rate of reaction increased with a 2.5-order dependence in $[BnNH_2]_0$. A saturation limit may eventually be reached with **13** as the concentration of $BnNH_2$ is increased above $[BnNH_2]_0$:[**13**]$_0$ = 10:1, but these reactions were too fast to monitor reliably (> 90% conversion after 8 mins). In the proposed activated-monomer propagation phase, reversible chain transfer does not occur in the same vein as that described with **1** (Chapter Two, Figure 2.15). Since no poly(*rac*-LA) chain is formally bonded to the metal centre, each exogenous chain is competing for a coordinated lactide unit, which leads to overall averaging of M_n based on [*rac*-LA]$_0$:$[BnNH_2]_0$.

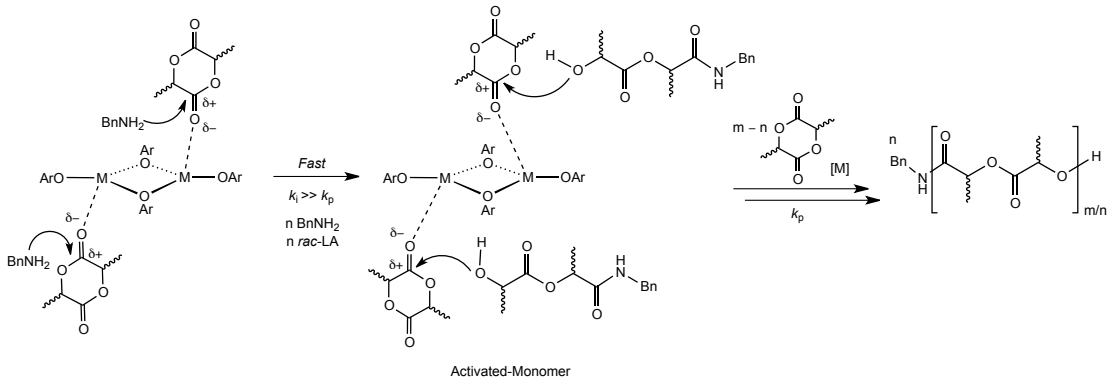

Figure 4.17. Schematic activated-monomer pathway for ROP with **12** and **13**. M = Ca or Sr, Ar = 2,4-$C_6H_3{}^tBu_2$.

There have been several recent reports of activated-monomer propagation pathways, including kinetic analysis. Whilst studying cationic Group 2 complexes, supported by well-defined (aza-crown ether)-fluorinated-alkoxide ligands (**3.15**), Carpentier noted a first-order dependency in $[BnOH]_0$ alongside first-order dependencies in lactide and catalyst.[72] A monomer-activated mechanism akin to that described in Figure 4.7 (*vide supra*) was proposed in the likelihood of the strontium based catalyst remaining monomeric under polymerisation conditions. First-order dependencies in *L*-LA and alcohol were also been determined by Lin, utilising neutral calcium bis(phenoxy-imine) catalysts and BnOH co-initiators.[74] It should be noted that the order in [monomer]$_0$ was equal to the order in [co-initiator]$_0$ in these studies, as was found with **12** and **13**, whilst Chakraborty has also quantified the enhancement of ε-CL

consumption when BnOH was employed in conjunction with titanium phenolate complexes.[75]

4.10 Y(O-2,4-$C_6H_3{}^tBu_2)_3(THF)_2$ (15)

In light of the complex experimental rate law for ROP with **12** and **13** and the inherent difficulties undertaking mechanistic studies with paramagnetic **10** and **11**, Y(O-2,4-$C_6H_3{}^tBu_2)_3(THF)_2$ (**15**) was prepared by a protonolysis reaction between $Y\{N(SiHMe_2)_2\}_3(THF)_2$ and three equivs. of HO-2,4-$C_6H_3{}^tBu_2$ in THF at room temperature (Scheme 4.2). Owing to the choice of supporting phenolate ligand, **15** should be a suitable mimic for **10** and **11**. Despite the lack of structural data for **15**, ^{1}H NMR (Figure 4.18, top) and C,H elemental analysis were consistent with the formation of a bis(THF) complex. Paramagnetism prevented ^{1}H NMR mechanistic studies with the neodymium and gadolinium congeners **10** and **11**, but solution phase NMR studies with **15** were possible.

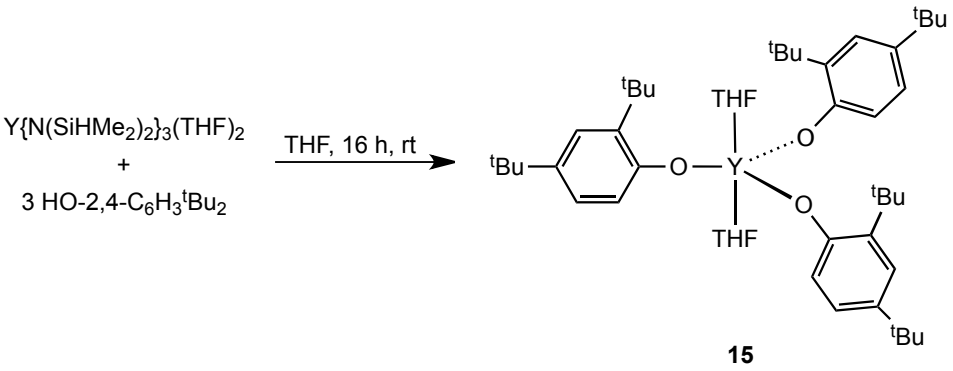

Scheme 4.2. Synthesis of Y(O-2,4-$C_6H_3{}^tBu_2)_3(THF)_2$ (**15**).

15 was treated with 100 equivs. of *rac*-LA ([*rac*-LA]$_0$ = 0.69 M) in THF at room temperature in the absence of any co-initiator and then with 5 equivs. of BnOH and $BnNH_2$ respectively. In the reaction without any co-initiator, conversion of monomer to poly(*rac*-LA) was sluggish with 34% conversion being recorded after 30 mins. At this point the catalyst was no longer active as no further progression was noted after 60 and 90 mins. M_n(GPC) = 7,460 g mol^{-1} was much higher than that calculated for one chain per metal, M_n(calcd) = 4,900 g mol^{-1}, and the PDI of 1.8 was comparable to values observed with **10** and **11**. Polymerisation performance improved when BnOH and $BnNH_2$ were included in the polymerisation mixture. 96% conversion was achieved within 20 mins for both runs and the agreement between M_n(GPC) (2,850 g mol^{-1}, BnOH) and M_n(calcd) (2,880 g mol^{-1}) was consistent with five chains forming

again. In the run with $BnNH_2$, M_n(GPC) = 3,230 g mol^{-1} was higher than expected but PDIs of 1.2 (BnOH) and 1.3 ($BnNH_2$) were also consistent with much better controlled ROP processes and respective ^{1}H NMR and MALDI-ToF mass spectra featured $PhCH_2O$– and $PhCH_2NH$–, as well as HOCH(Me)– poly(*rac*-LA) end-groups. However, no heterotactic bias was detected and transesterification processes were shown to operate, given the $\Delta(m/z)$ = 72.0 g mol^{-1} peak envelopes in the MALDI-ToF mass spectra.

Identical ^{1}H NMR studies to those for **12** and **13** (Figure 4.6) were also performed with **15**. Treatment of **15** with $BnNH_2$ or BnOH did not result in liberation of HO-2,4-$C_6H_3{}^tBu_2$ and both $BnNH_2$ and BnOH were consumed when *rac*-LA was added to each mixture. Despite the presence of unreacted *rac*-LA (δ = 3.7 and 1.2 ppm), broad PLA signals at δ = 5.0 and 1.2 ppm and $PhCH_2N\underline{H}$– at 6.5 ppm (Figure 4.18, middle) confirmed that the system was active. The diagnostic *ortho*-H doublet of HO-2,4-$C_6H_3{}^tBu_2$ at 6.0 ppm (Figure 4.18, bottom) was not present in the ^{1}H NMR of the polymerisation mixture (Figure 4.18, middle) and clearly showed that the Y–O-2,4-$C_6H_3{}^tBu_2$ ligands of **15** were retained under polymerisation conditions. It would seem that this class of lanthanide aryloxides behave in a similar manner to **12** and **13** regarding an activated-monomer type propagation pathway and based on these initial experiments it would seem reasonable to suggest that amine-initiated ROP with **10** and **11** may also operate *via* an activated-monomer type propagation mechanism.

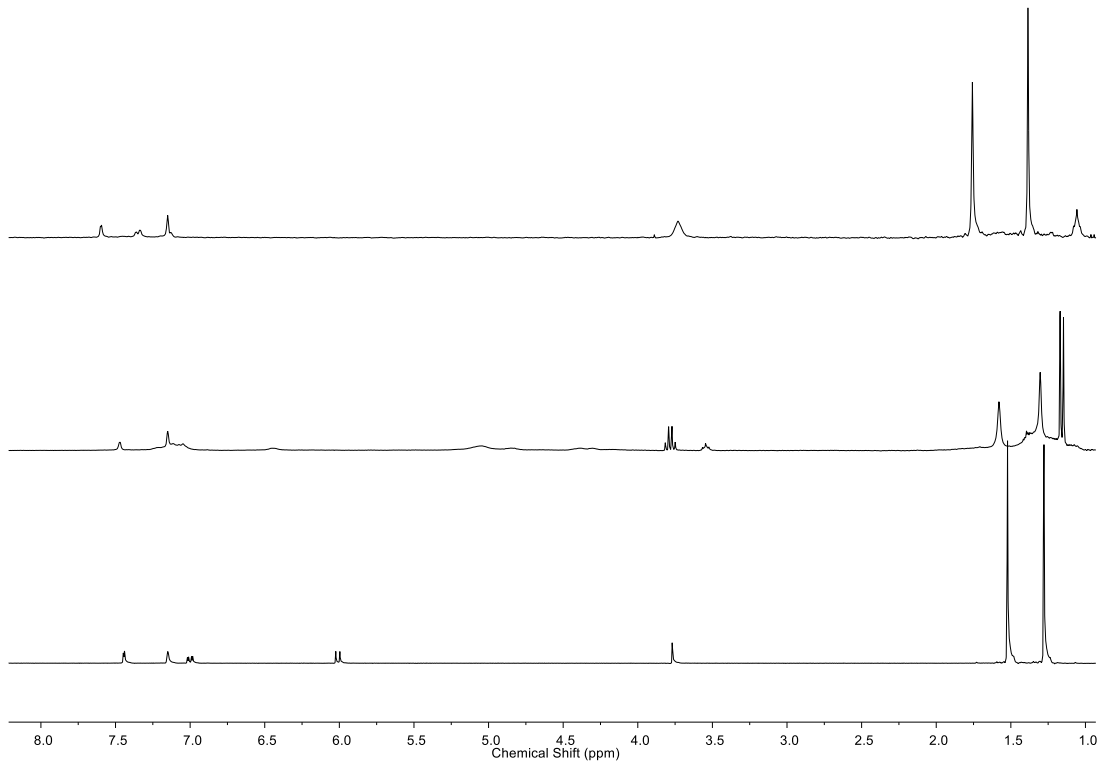

Figure 4.18. ^{1}H NMR (300.1 MHz, C_6D_6, 298 K) spectra of top, Y(O-2,4-$C_6H_3{}^{t}Bu_2)_3(THF)_2$ (**15**); middle, $[rac\text{-LA}]_0$:$[BnNH_2]_0$:[**15**]$_0$ = 10:2:1 (unreacted *rac*-LA at δ = 3.7 and 1.2 ppm) and bottom, HO-2,4-$C_6H_3{}^{t}Bu_2$. Residual protio-solvent, δ = 7.15 ppm.

4.11 Summary and Conclusions for Chapter Four

This Chapter has described polymerisation experiments undertaken using Group 2 and lanthanide bearing monodentate phenolate ligands. The briefly outlined synthetic route to these complexes *via* redox transmetallation/protonolysis represents an efficient pathway to low coordinate lanthanide and Group 2 complexes.

The polymerisation data obtained for complexes **10**–**14** demonstrated effectively the vast improvement in catalytic performance when suitable co-initiators were employed in ROP. Whilst it has long been understood that addition of certain alcohols to simple Lewis acidic salts or complexes bearing a relatively simple ligand framework can lead to the production of well-defined polylactides, in-depth mechanistic studies akin to those performed with highly developed single-site, coordination-insertion type systems have been limited.

Kinetic investigations revealed a likely activated-monomer propagation mechanism, based on the dependence in $[BnNH_2]_0$ in the overall propagation rate law and the

likely retention of the phenolate ligands by each metal centre. Whilst this may account for the less well-controlled polymeriation reactions and the complex rate law, these studies have revealed the generality of the amine-initiated ROP process. Over the past 15–20 years highly developed single-site coordination-insertion ROP initiators have developed but the interest in the use of alcohol and amine co-initiators has shown that relatively simple catalysts are effective in generating well-defined polylactides.

4.12 References for Chapter Four

1. L. Clark, G. B. Deacon, C. M. Forsyth, P. C. Junk, P. Mountford and J. P. Townley, *Dalton Trans.*, 2010, **39**, 6693.
2. W. M. Stevels, M. J. K. Ankone, P. J. Dijkstra and J. Feijen, *Macromolecules*, 1996, **29**, 3332.
3. W. M. Stevels, M. J. K. Ankone, P. J. Dijkstra and J. Feijen, *Macromolecules*, 1996, **29**, 6132.
4. M. Save, M. Schappacher and A. Soum, *Macromol. Chem. Phys.*, 2002, **203**, 889.
5. M. Save and A. Soum, *Macromol. Chem. Phys.*, 2002, **203**, 2591.
6. R. R. Gowda and D. Chakraborty, *J. Mol. Cat. A: Chem.*, 2009, **301**, 84.
7. Y. Shen, Z. Shen, J. Shen, Y. Zhang and K. Yao, *Macromolecules*, 1996, **29**, 3441.
8. C. Miola-Delaite, T. Hamaide and R. Spitz, *Macromol. Chem. Phys.*, 1999, **200**, 1771.
9. A. Pietrangelo, M. A. Hillmyer and W. B. Tolman, *Chem. Commun.*, 2009, 2736.
10. A. Pietrangelo, S. C. Knight, A. K. Gupta, L. J. Yao, M. A. Hillmyer and W. B. Tolman, *J. Am. Chem. Soc.*, 2010, **132**, 11649.
11. M.-L. Hsueh, B.-H. Huang, J. Wu and C.-C. Lin, *Macromolecules*, 2005, **38**, 9482.
12. M. H. Chisholm, C.-C. Lin, J. C. Gallucci and B.-T. Ko, *Dalton Trans.*, 2003, 406.
13. Z. Zhong, M. J. K. Ankon, P. J. Dijkstra, C. Birg, M. Westerhausen and J. Feijen, *Polym. Bull.*, 2001, **46**, 51.
14. Z. Zhong, P. J. Dijkstra, C. Birg, M. Westerhausen and J. Feijen, *Macromolecules*, 2001, **34**, 3863.

15. Z. Zhong, S. Schneiderbauer, P. J. Dijkstra, M. Westerhausen and J. Feijen, *J. Polym. Environ.*, 2001, **9**, 31.
16. D. C. Bradley, M. B. Hursthouse, A. A. Ibrahim, K. M. A. Malik, M. Motevalli, R. Möseler, H. Powell, J. D. Runnacles and A. C. Sullivan, *Polyhedron*, 1990, **9**, 2959.
17. M. Westerhausen, *Inorg. Chem.*, 1991, **30**, 96.
18. J. M. Boncella, C. J. Coston and J. K. Cammack, *Polyhedron*, 1991, **10**, 769.
19. D. C. Bradley, J. S. Ghotra and F. A. Hart, *J. Chem. Soc., Dalton Trans.*, 1973, 1021.
20. R. Anwander, O. Runte, J. Eppinger, G. Gerstberger, E. Herdtweck and M. Spiegler, *J. Chem. Soc., Dalton Trans.*, 1998, 847.
21. K. W. Henderson, G. W. Honeyman, A. R. Kennedy, R. E. Mulvey, J. A. Parkinson and D. C. Sherrington, *Dalton Trans.*, 2003, 1365.
22. P. B. Hitchcock, M. F. Lappert, G. A. Lawless and B. Royo, *J. Chem. Soc., Chem. Commun.*, 1990, 1141.
23. S. R. Drake, D. J. Otway, M. B. Hursthouse and M. K. M. Abdul, *Polyhedron*, 1992, **11**, 1995.
24. A. B. Goel and R. C. Mehrotra, *Indian J. Chem., Sect. A*, 1978, **16A**, 428.
25. A. W. Duff, P. B. Hitchcock, M. F. Lappert, R. G. Taylor and J. A. Segal, *J. Organomet. Chem.*, 1985, **293**, 271.
26. M. J. McCormick, K. B. Moon, S. R. Jones and T. P. Hanusa, *J. Chem. Soc., Chem. Commun.*, 1990, 778.
27. F. G. N. Cloke, P. B. Hitchcock, M. F. Lappert, G. A. Lawless and B. Royo, *J. Chem. Soc., Chem. Commun.*, 1991, 724.
28. K. F. Tesh, T. P. Hanusa, J. C. Huffman and C. J. Huffman, *Inorg. Chem.*, 1992, **31**, 5572.
29. J. P. Dunne, M. Tacke, C. Selinka and D. Stalke, *Eur. J. Inorg. Chem.*, 2003, 1416.
30. P. B. Hitchcock, M. F. Lappert and A. Singh, *J. Chem. Soc., Chem. Commun.*, 1983, 1499.
31. P. B. Hitchcock, M. F. Lappert and R. G. Smith, *Inorg. Chim. Acta*, 1987, **139**, 183.
32. S. N. Misra, T. N. Misra and R. C. Mehrotra, *Aust. J. Chem.*, 1968, **21**, 797.
33. K. C. Malhotra and R. L. Martin, *J. Organomet. Chem.*, 1982, **239**, 159.

34. R. C. Mehrotra and J. M. Batwara, *Inorg. Chem.*, 1970, **9**, 2505.
35. H. A. Stecher, A. Sen and A. L. Rheingold, *Inorg. Chem.*, 1988, **27**, 1130.
36. T. J. Boyle, L. J. Tribby and S. D. Bunge, *Eur. J. Inorg. Chem.*, 2006, 4553.
37. T. J. Boyle and L. A. M. Ottley, *Chem. Rev.*, 2008, **108**, 1896.
38. R. C. Mehrotra, A. Singh and U. M. Tripathi, *Chem. Rev.*, 1991, **91**, 1287.
39. G. B. Deacon, P. E. Fanwick, A. Gitlits, I. P. Rothwell, B. W. Skelton and A. H. White, *Eur. J. Inorg. Chem.*, 2001, 1505.
40. G. B. Deacon, C. M. Forsyth and S. Nickel, *J. Organomet. Chem.*, 2002, **647**, 50.
41. G. B. Deacon, C. M. Forsyth, R. Harika, P. C. Junk, J. W. Ziller and W. J. Evans, *J. Mater. Chem.*, 2004, **14**, 3144.
42. G. B. Deacon, G. D. Fallon, C. M. Forsyth, S. C. Harris, P. C. Junk, B. W. Skelton and A. H. White, *Dalton Trans.*, 2006, 802.
43. G. B. Deacon, P. C. Junk and G. J. Moxey, *Chem. Asian J.*, 2009, **4**, 1717.
44. Y. Wang, L.-f. Zhang, P. Wang and L.-j. Shen, *Chin. J. Polym. Sci.*, 2010, **28**, 509.
45. L. Zhang, Y. Niu, Y. Wang, P. Wang and L. Shen, *J. Mol. Cat. A: Chem.*, 2008, **287**, 1.
46. J. Ling, Z. Shen and Q. Huang, *Macromolecules*, 2001, **34**, 7613.
47. C. Yu, L. Zhang and Z. Shen, *Eur. Polym. J.*, 2003, **39**, 2035.
48. L. Zhang, C. Yu and Z. Shen, *Polym. Bull.*, 2003, **51**, 47.
49. F. Peng and Z. Shen, *J. Appl. Polym. Sci.*, 2007, **106**, 1828.
50. C. Yu, L. Zhang, X. Ni, Z. Shen and K. Tu, *J. Polym. Sci., Part A: Polym. Chem.*, 2004, **42**, 6209.
51. L. Zhang, Z. Shen, C. Yu and L. Fan, *J. Mol. Cat. A: Chem.*, 2004, **214**, 199.
52. N. Zhu, J. Ling, Y. Zhu, W. Sun and Z. Shen, *J. Polym. Sci., Part A: Polym. Chem.*, 2010, **48**, 4366.
53. J. Ling, J. Liu, Z. Shen and T. E. Hogen-Esch, *J. Polym. Sci., Part A: Polym. Chem.*, 2011, **49**, 2081.
54. J. Ling, W. Zhu and Z. Shen, *Macromolecules*, 2004, **37**, 758.
55. L. Clark, G. B. Deacon, C. M. Forsyth, P. C. Junk, P. Mountford, J. P. Townley and J. Wang, Unpublished Results.
56. R. D. Shannon, *Acta Crystallogr.*, 1976, **A32**, 2431.

57. G. B. Deacon, P. C. Junk, G. J. Moxey, M. Guino-o and K. Ruhlandt-Senge, *Dalton Trans.*, 2009, 4878.
58. W. J. Evans, W. G. McClelland, M. A. Greci and J. W. Ziller, *Eur. J. Solid State Inorg. Chem.*, 1996, **33**, 145.
59. G. B. Deacon, P. C. Junk and G. J. Moxey, *New J. Chem.*, 2010, **34**, 1731.
60. W. J. Evans, M. A. Greci and J. W. Ziller, *Chem. Commun.*, 1998, 2367.
61. G. B. Deacon, C. M. Forsyth and P. C. Junk, *J. Organomet. Chem.*, 2000, **607**, 112.
62. G. B. Deacon, C. M. Forsyth, P. C. Junk, B. W. Skelton and A. H. White, *Chem. Eur. J.*, 1999, **5**, 1452.
63. G. B. Deacon, P. C. Junk, G. J. Moxey, K. Ruhlandt-Senge, C. St. Prix and M. F. Zuniga, *Chem. Eur. J.*, 2009, **15**, 5503.
64. W. J. Evans, M. A. Greci and J. W. Ziller, *Inorg. Chem.*, 2000, **39**, 3213.
65. P. I. Binda and E. E. Delbridge, *Dalton Trans.*, 2007, 4685.
66. J. Ejfler, M. Kobylka, L. B. Jerzykiewicz and P. Sobota, *Dalton Trans.*, 2005, 2047.
67. H. E. Dyer, D.Phil Thesis, University of Oxford, 2009.
68. H. E. Dyer, S. Huijser, N. Susperregui, F. Bonnet, A. D. Schwarz, R. Duchateau, L. Maron and P. Mountford, *Organometallics*, 2010, **29**, 3602.
69. P. Sykes, *A Guidebook To Mechanism In Organic Chemistry*, Longman, Sixth Ed., 1986.
70. A. Amgoune, C. M. Thomas and J.-F. Carpentier, *Pure Appl. Chem.*, 2007, **79**, 2013.
71. A. Amgoune, C. M. Thomas and J.-F. Carpentier, *Macromol. Rapid Commun.*, 2007, **28**, 693.
72. Y. Sarazin, B. Liu, T. Roisnel, L. Maron and J.-F. Carpentier, *J. Am. Chem. Soc.*, 2011, **133**, 9069.
73. Y. Sarazin, V. Poirier, T. Roisnel and J.-F. Carpentier, *Eur. J. Inorg. Chem.*, 2010, 3423.
74. H.-Y. Chen, H.-Y. Tang and C.-C. Lin, *Polymer*, 2007, **48**, 2257.
75. R. R. Gowda, D. Chakraborty and V. Ramkumar, *Eur. J. Inorg. Chem.*, 2009, 2981.

Chapter Five

Group 3 amide complexes supported by phenolate-amino ligands and amine-initiated, ROP studies

5.1 Overview

This Chapter describes the synthesis and characterisation of rare earth amide complexes supported by bidentate or tridentate phenolate-amino ligands. The resultant bis and mono(amide) complexes were utilised as catalysts for amine-initiated, immortal ROP. Four new complexes are described and three X-ray structures are presented.

5.2 Introduction: immortal ROP *via* activated-monomer and coordination-insertion pathways

Chapters Two, Three and Four have described amine-initiated, immortal ROP processes with catalysts bearing both highly developed bis(phenolate)-amino chelating ligands (**1**–**7**) as well as relatively simple, non-chelating phenolate ligands (**10**–**15**). Whilst it was clear that the best performing catalyst for the amine-initiated, immortal ROP of *rac*-LA was the zwitterionic, bis(phenolate)-amino yttrium complex, **1**, the calcium and strontium phenolate complexes, **12** and **13**, showed that fast amine-initiation and reasonable molecular weight control could be achieved using catalysts with less well-developed ligand architectures. The rare earth catalyst, Y(O-2,4-$C_6H_3{}^tBu_2)_3(THF)_2$ (**15**), also demonstrated the applicability of complexes bearing relatively simple ligands for amine-initiated, immortal ROP and M_n(GPC) = 3,230 g mol^{-1} with a PDI = 1.3 were recorded in a representative polymerisation run ([*rac*-LA]$_0$:[$BnNH_2$]$_0$:[**15**]$_0$ = 100:5:1, M_n(calcd) = 2,880 g mol^{-1}). Owing to the robust nature of the non-chelating mono(phenolate) ligands under polymerisation conditions and from the results of kinetics experiments with **12** and **13**, initiation and propagation processes were shown to occur *via* activated-monomer pathways. Whilst molecular weights were generally reflective of [*rac*-LA]$_0$:[$BnNH_2$]$_0$ in polymerisation reactions co-initiated by **10**–**15**, the activated-monomer pathway for a given metal and ligand set is undesirable in terms of achieving optimal control over molecular weights, PDI and polymer tacticity.

In the amine-initiated, immortal ROP of *rac*-LA using **1** or **1.15** as catalysts, the HO_2N^{NMe2} or $–N(SiHMe_2)_2$ ligands were liberated at the beginning of the reaction, which permitted formation of a formal bond between the metal and the growing PLA chain. Propagation then ensued *via* a coordination-insertion mechanism and control over molecular weight and tacticity were excellent. Propagation *via* coordination-

insertion generally leads to better molecular weight control for a given metal and ligand set and, mechanistically, it is much easier to control polymerisations that are limited by $[monomer]_0$ and $[metal]_0$ only.

5.2.1 Rare earth amide complexes supported by phenolate-amino ligands

Whilst the bis(phenolate)-amino supported zwitterionic yttrium complex, **1**, represents an optimal class of catalyst, further investigation of $Y(O\text{-}2,4\text{-}C_6H_3{}^tBu_2)_3(THF)_2$ (**15**) is warranted in order to determine the level of development required in order to achieve better control over M_n(GPC) and PDI, as well as stereoselective polymerisations. In the amine-initiated, immortal ROP methodology, a suitable innocent leaving group that will be outcompeted during initiation will need to be incorporated into the pre-catalyst. This will enable a formal bond between the active metal centre and the alkoxide end-group of the growing PLA chains. From the experiments with $Y(O_2N^{NMe2})\{N(SiHMe_2)_2\}(THF)$ (**1.15**) (Chapter Two, Section 2.8), no $HN(SiHMe_2)_2$-capped PLA were detected in the MALDI-ToF mass spectra of isolated PLA products, thus metal amide complexes may be suitable candidates.

In order to measure incremental progression in catalyst development, it would be desirable to retain the monodentate phenolate ligands and develop a catalyst such as "$Y(O\text{-}2,4\text{-}C_6H_3{}^tBu_2)_2\{N(SiHMe_2)_2\}$." Mixed phenolate-amide or phenolate-alkyl rare earth species are known. Evans successfully prepared the mixed yttrium alkyl-alkoxide complex, $Y(O\text{-}2,6\text{-}C_6H_3{}^tBu_2)(CH_2SiMe_3)_2(THF)_2$ (**5.1**),[1] but the later described bis-substituted phenolate species, $[Y(O\text{-}2,6\text{-}C_6H_3{}^tBu_2)_2\text{-}(CH_2SiMe_3)_2][\{Li(THF)_3\}_2Cl]$ (**5.2**) was an 'ate' complex.[2] Clark *et al*. have also reported the synthesis and characterisation of mixed phenolate amide actinide complexes e.g. $U(O\text{-}2,6\text{-}C_6H_3{}^tBu_2)\{N(SiMe_3)_2\}_3$ (**5.3**), but such complexes are unsuitable for ROP, given the toxicity of the metal centre.[3] With regard to the successful formation of a $Y(O\text{-}2,4\text{-}C_6H_3{}^tBu_2)_2\{N(SiHMe_2)_2\}$-type complex, over-substitution of the metal centre is likely to occur, leading to the formation of **15** and during polymerisation, catalyst aggregation may also be promoted given the less encumbered metal centre.

Employment of a chelating phenolate ligand is more likely to prevent catalyst deactivation and maintain the single-site nature of the coordination-insertion catalyst. However, there are exceptions, such as the tridenate bis(phenolate)-amino ligands

without a pendant arm donor (HO_2N^{Me}) that were used to form the five-coordinate zwitterionic complexes, $Ln(O_2N^{Me})(HO_2N^{Me})$ (Ln = Y (**3**) or Sm (**2.2**)). These complexes showed poor activities, with typical ROP reactions, [*rac*-LA]$_0$:[$BnNH_2$]$_0$:[Ln]$_0$ = 100:5:1, taking over 3 h to reach *ca*. 50% conversion. The origin of this inactivity remains unresolved, although 1-hexene polymerisation catalysts, also possessing the "dummy arm" ligand (O_2N^{Me}) performed poorly. Kol noted that five-coordinate $Ti(O_2N^{Me})(Bn)_2$ (**2.10**) was more active than six-coordinate $Ti(O_2N^{NMe2})(Bn)_2$ (**2.11**). However, **2.10** produced only oligomers, whilst the six-coordinate **2.11** displayed living type behaviour. With the zirconium analogues, good activity was observed with $Zr(O_2N^{NMe2})(Bn)_2$ (**1.27**), whilst the five-coordinate species, $Zr(O_2N^{Me})(Bn)_2$ (**1.28**), was inactive.[4-6] $Sm(O_2N^{Me})(BH_4)(THF)$ (**1.26**) was also inactive for ROP.[7, 8] In light of these observations, the unsaturated metal centres of **1.26**, **1.28** and **2.2** may be more prone to deactivation through aggregation or potential PLA chelation.

Despite the ineffective application of the O_2N^{Me} ligand, there are numerous examples of di- and tri-valent main group and rare earth metal ROP catalysts bearing bi- and tri-dentate phenolate-amino ligands and a selection are presented in Figure 5.1. Sobota developed the bidentate phenolate-amino ligand, $ON^{Me,Cy}$,[9] and prepared the homoleptic complexes, $M(ON^{Me,Cy})_2$ (M = Mg (**5.4**) and Zn (**5.5**)) by addition of two equivs. of the protio-ligand, $HON^{Me,Cy}$, to either Mg^nBu_2 or $ZnEt_2$ in toluene at room temperature.[10, 11] **5.4** was used to polymerise 50 or 100 equivs. of *L*-LA in the presence of 1 equiv. of BnOH in toluene at room temperature.[10] Complete conversion was achieved within minutes and observed molecular weights were consistent with one PLA chain forming per equiv. of BnOH. In the 50 equivs. of *L*-LA run, M_n(calcd) = 6,880 g mol^{-1}, M_n(GPC) = 7,020 g mol^{-1} and PDI = 1.09. Excellent control was also observed in the 100 equivs. of *L*-LA run with M_n(calcd) = 15,580 g mol^{-1}, M_n(GPC) = 13,370 g mol^{-1} and PDI = 1.10. The narrow PDIs and control over M_n were consistent with living polymerisations and ^{1}H NMR confirmed that the PLA chains were benzyl alcohol-capped.

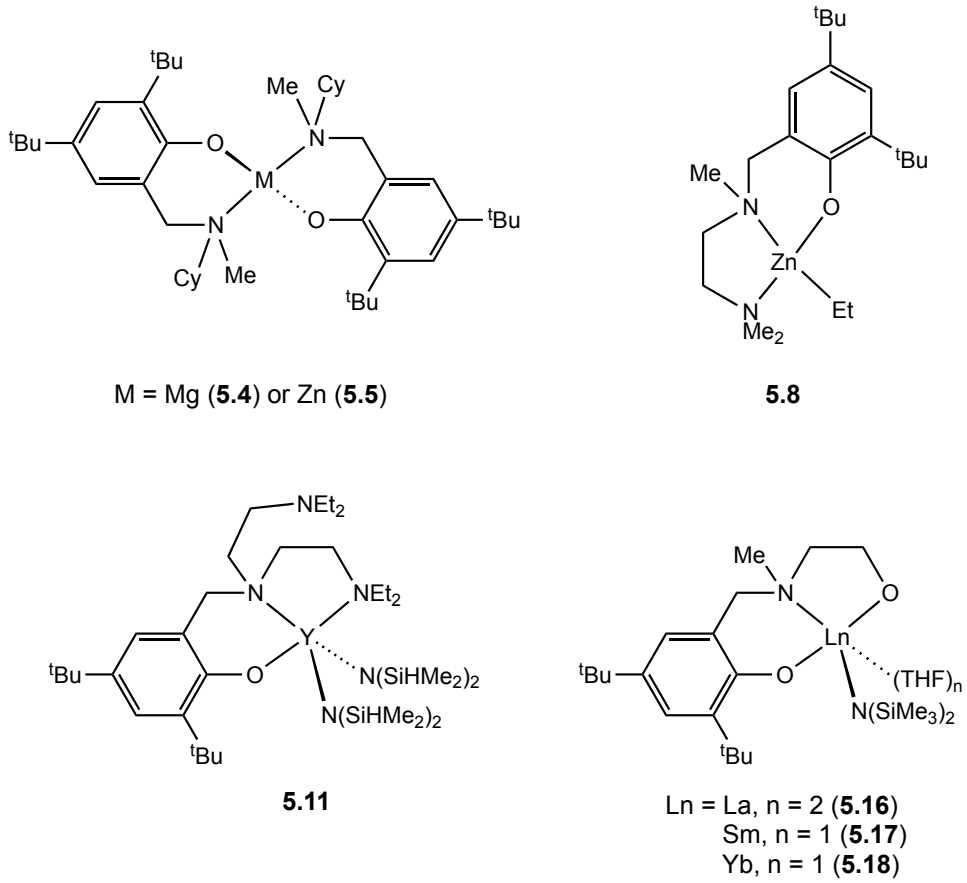

Figure 5.1. Main group and rare earth phenolate-amino complexes.[9-14]

5.5 (Figure 5.1) was also used to polymerise 100 equivs. of *L*-LA in the presence of 1 equiv. of BnOH in dichloromethane at room temperature.[11] 92% conversion of monomer to PLA was achieved after 60 mins and M_n(GPC) = 16,730 g mol^{-1} was suggestive of one chain forming per BnOH with M_n(calcd) = 14,380 g mol^{-1}. The narrow PDI = 1.16 was consistent with a living polymerisation and benzyl alcohol-capped PLA chains were again confirmed by ^{1}H NMR. To demonstrate the immortal character of the system, 2 equivs. of BnOH were included in the polymerisation mixture and the observed molecular weight reduced by a factor of 2 (M_n(GPC) = 8,420 g mol^{-1}). The PDI = 1.16 also remained narrow. The quoted reaction time for this run was 40 mins, in which time 99% conversion was achieved. Despite non-optimisation of reaction conditions and absence of kinetic analysis in this report, an activated-monomer propagation mechanism was reported, given that BnOH or alcoholic PLA end-groups did not liberate the phenolate-amino ligands (NMR tube scale experiments suggested that the phenolate remained bound to the zinc centre, but the neutral-amino donor may have decomplexed).[11] However, in an earlier report describing ROP reactions with a solvated species, Mg(ON^{Me,Cy})$_2$(THF)$_2$ (**5.6**),

$ON^{Me,Cy}$ was shown to be a non-innocent ligand in the ROP of *L*-LA as phenol-capped PLA chains were detected in the ^{1}H NMR spectra of purified PLA samples.[9] No co-initiator was included in this run and complete conversion took 30 mins to achieve. In the run with **5.4** and BnOH, complete conversion was achieved within 1 min, so it is likely that insertion of LA into the magnesium–phenolate bond was outcompeted by activated-monomer initiation under immortal-type conditions and the $ON^{Me,Cy}$ ligands remained bound to the metal centre.

A heteroleptic coordination-insertion initiator, $[Zn(ON^{Me,Cy})(OBn)]_2$ (**5.7**), was also prepared and its polymerisation performance was compared with **5.5** (which was shown to be an effective co-initiator alongside BnOH).[11] **5.7** was reacted with 100 equivs. of *L*-LA per Zn in dicholoromethane at room temperature but complete conversion (98%) took 120 mins to achieve compared to 60 mins when **5.5** was used in the presence of BnOH. However, M_n(GPC) = 15,380 g mol^{-1} was in better agreement with M_n(calcd) = 14,230 g mol^{-1} and the PDI = 1.09 was narrower (M_n(GPC) = 16,730 g mol^{-1}, M_n(calcd) = 14,380 g mol^{-1} and PDI = 1.16 for **5.5**). **5.5** and **5.7** form different active species under polymerisation conditions, and despite the limited experimental evidence, the polymerisation data do suggest that propagation *via* a coordination-insertion mechanism (**5.7**) is advantageous with regard to control over M_n and molecular weight distribution.

Tolman, Hillmyer and Williams incorporated a NMe_2 pendant arm into the phenolate-amino ligand framework and prepared $Zn(ON^{Me,NMe2})(Et)$ (**5.8**, Figure 5.1) by treatment of $ZnEt_2$ with $HON^{Me,NMe2}$ in aliphatic hydrocarbon solvents at –35 °C.[12] However, **5.8** was found to be inactive for ROP of LA. Treatment of **5.8** with EtOH in toluene at –35 °C yielded the dimeric alkoxide complex, $[Zn(ON^{Me,NMe2})(OEt)]_2$ (**5.9**), which was capable of polymerising up to 1500 equivs. of *rac*-LA per Zn in dichloromethane at room temperature. M_n(GPC) = 130,000 g mol^{-1} for this run and the PDI = 1.4 was indicative of the formation of a moderate distribution of molecular weights. A M_n(GPC) *vs*. Conversion plot for the run $[rac\text{-LA}]_0$:$[Zn]_0$ = 1000:1 confirmed the linear increase in M_n(GPC) with % conversion but M_n(GPC) values were consistently lower than expected. With regard to the run, $[rac\text{-LA}]_0$:$[Zn]_0$ = 1500:1, the expected M_n(calcd) = 214,000 g mol^{-1} but M_n(GPC) = 130,000 g mol^{-1}. In a series of loading experiments with varying monomer to metal ratios, observed molecular weights were lower than expected and the divergence was particularly

pronounced at higher loadings of $[rac\text{-LA}]_0:[Zn]_0$ (1000:1 and 1500:1). Catalyst deactivation and chain transfer processes were proposed as the main contributors to M_n reduction and the effective concentrations of chain transfer agents and deactivators were determined, leading to an effective $[Zn]_{eff}$ and appropriate recalculation of expected M_n(calcd). Chain transfer capability was established through the inclusion of BnOH in polymerisation mixtures and the reduction in M_n(GPC) was effectively modelled. Propagation *via* coordination-insertion was established but PLA chains showed no heterotactic enrichment.

ROP of *rac*-LA initiated by **5.9** at 0 and 25 °C was shown to proceed with a first-order dependence in $[rac\text{-LA}]_0$.[12] However, non-integer orders of 1.33 and 1.75 in $[Zn]_0$ were determined at these temperatures from logarithmic plots of $\ln k_{app}$ *vs*. $\ln[Zn]_0$. Lines of least-squares fit in non-logarithmic plots of k_{app} *vs*. $[Zn]_0$ intercepted the horizontal-axis at values of $[Zn]_0 > 0$, indicating that below certain catalyst concentrations, no polymerisation should occur. Further study concluded that the intrinsic impurity, the effective concentration of which, was dependent on the reaction conditions, was responsible for the non-integer orders in $[Zn]_0$. The tolerance of **5.9** to impurities was worse at lower temperature and higher monomer loadings and a minimum required catalyst concentration was determined for ROP at 0 °C. However, experiments conducted under rigorous anaerobic and moisture free conditions showed that ROP could be effected using a concentration of catalyst below the proposed minimum. First-order dependencies in catalyst concentration were proposed in light of the careful consideration of the influence of deactivation pathways but the impurities were not formally identified, although water and/or lactic acid are not unreasonable candidates.

Guillaume, Carpentier and Bourissou prepared a cationic complex, $[Zn(ON^{Me,NMe2})][B(C_6F_5)_4]$ (**5.10**) by treatment of **5.8** with $[PhMe_2NH][B(C_6F_5)_4]$ in THF at –78 °C and a dual catalytic approach to ROP was explored.[15] Treatment of **5.10** with 100 equivs. of *rac*-LA in the presence of 1 equiv. of *neo*-pentanol (Me_3CCH_2OH) in toluene resulted in no conversion of monomer to PLA. However, inclusion of an organic base activator such as 1,2,2,6,6-pentamethylpiperidine (PMP) led to complete conversion of *rac*-LA to poly(*rac*-LA) within 3 h. In a representative run, $[rac\text{-LA}]_0:[Me_3CCH_2OH]_0:[Zn^+]_0:[PMP]_0$ = 100:1:0.5:0.5 in toluene at 50 °C, 98% conversion was achieved within 3 h. M_n(GPC) = 11,700 g mol^{-1} was in good

agreement with M_n(calcd) = 14,200 g mol^{-1} and a PDI = 1.34 was indicative of a moderately broad distribution of molecular weights. A linear relationship between M_n and [*rac*-LA]$_0$:[Me_3CCH_2OH]$_0$ was also established in loading experiments. This approach to ROP demonstrated the effective combination of organic and organometallic methods and mirrored work by Tolman and Hillmyer using indium trihalides, triethylamine and BnOH for the stereoselective ROP of *rac*-LA.[16, 17]

Arnold incorporated a second pendant arm within the phenolate-amino ligand and prepared a mono-substituted yttrium bis(amide) complex, **5.11** (Figure 5.1, *vide supra*).[13] A complex with 2,4-methyl phenolate substituents was also prepared but the majority of polymerisation studies were performed with **5.11**. The molecular structure of **5.11** confirmed that the second pendant arm was non-coordinating and VT ^{1}H NMR studies consistently showed a non-coordinating arm alongside a coordinated NEt_2 donor. The majority of ROP polymerisation runs using **5.11** were performed in dichloromethane at room temperature over a range of monomer to catalyst loadings and high conversions were achieved within 30 mins. No co-initiators were included in polymerisation mixtures. In a run, [*rac*-LA]$_0$:[**5.11**]$_0$ = 1000:1, 97% was achieved and M_n(GPC) = 150,200 g mol^{-1} (PDI = 1.48) was in close agreement with M_n(calcd) ≈ 140,000 g mol^{-1} for one chain forming per metal. However, at a lower *rac*-LA loading, [*rac*-LA]$_0$:[**5.11**]$_0$ = 100:1, the M_n(GPC) = 28,000 g mol^{-1} was twice that expected for one chain forming. PDIs ranged from 1.2–1.5 and generally narrowed as the M_n increased. A –N($SiHMe_2$)$_2$ end-group was assigned in the ^{1}H NMR spectrum of isolated PLA but no MALDI-ToF mass spectra were described.

Delbridge also utilised the $HON^{Me,NMe2}$ protio-ligand used by Tolman, Hillmyer and Williams to prepare rare earth mono(amide) complexes.[18] Two equivs. of $HON^{Me,NMe2}$ were added to the tris(amide) precursors, Ln{N($SiMe_3$)$_2$}$_3$ (Ln = La, Nd, Sm or Yb) in THF at –40 °C and the mono(amide) complexes, La($ON^{Me,NMe2}$)$_2${N($SiMe_3$)$_2$} (Ln = La (**5.12**), Nd (**5.13**), Sm (**5.14**) and Yb (**5.15**)) were isolated. Crystallographic analysis of **5.14** and ^{1}H NMR studies on **5.12** showed that both NMe_2 pendant arms were non-coordinating. Each complex was treated with 100 equivs. of *L*-LA in toluene and **5.12** was able to effect complete conversion of *L*-LA to PLA within 1 min at room temperature. ROP reactions with **5.13**–**5.15** required heating at 80 °C to effect ROP, but the reactions were incomplete even after heating for 1 h. In a further run with [*L*-LA]$_0$:[**5.12**]$_0$ = 300:1, 96% conversion was achieved after 5 mins and

M_n(GPC) = 40,000 g mol^{-1} was in close agreement with M_n(calcd) = 41,000 g mol^{-1} although the broad PDI = 1.9 was typical of ROP reactions involving amide initiators. Kinetic analysis revealed a second-order dependence in [*L*-LA]$_0$ and a first-order dependence in [**5.12**]$_0$. The propagation rate constant, k_p = 8.1 M^{-2} h^{-1} or 486 M^{-2} min^{-1}, represented a ROP reaction that was twice as fast as ROP of *rac*-LA co-initiated by Y(O_2N^{NMe2})(HO_2N^{NMe2}) (**1**) and benzyl amine (k_p = 239(8) M^{-2} min^{-1}). Although **5.12** and **1** are non-comparable, these rate constants highlight the greater activity of the larger rare earth elements.

The phenolate-amino ligands present in **5.12** were shown to be non-innocent and phenol-capped PLA chains and cyclic PLA products were present in MALDI-ToF mass spectra.[18] In a later report, Delbridge described the synthesis and characterisation of rare earth mono(amide) complexes supported by a dianionic phenolate-amino ligand with an alkoxide pendant arm (Figure 5.1, *vide supra*).[14] Treatment of Ln{$N(SiMe_3)_2$}$_3$ (Ln = La, Sm or Yb) with $HON^{Me,OH}$ at –40 °C in THF led to the formation of the mononuclear amide complexes, Ln($ON^{Me,O}$){$N(SiHMe_2)_2$}$(THF)_n$ (Ln = La, n = 2 (**5.16**); Sm, n = 1 (**5.17**); Yb, n = 1 (**5.18**)).

The lanthanum centred complex, **5.16**, was the main focus of polymerisation studies owing to its high activity at room temperature.[14] 100 equivs. of *L*-LA were added to **5.16** in toluene at room temperature and 94% conversion was achieved within 1 min. M_n(GPC) = 23,500 g mol^{-1} was higher than expected (M_n(calcd) ≈ 14,000 g mol^{-1}), despite a narrow PDI = 1.23. When the reaction was allowed to run for 10 mins, M_n(GPC) reduced to 22,600 g mol^{-1} and the PDI broadened to 1.62. Detrimental post-polymerisation transesterification was the likely cause of the polymer degradation. There was limited evidence for $HN(SiMe_3)_2$-capped PLA in the MALDI-ToF mass spectra but kinetic analysis did reveal first-order dependencies in monomer and catalyst.

5.3 Synthesis and characterisation of rare earth amide initiators

The protio-ligand, $HON^{Me,Cy}$, developed by Sobota, and $HON^{Me,NMe2}$ employed by Tolman *et al*. and Delbridge were selected as suitable monoanionic, bidentate or tridentate phenolate-amino ligands. The cyclohexyl-group of $HON^{Me,Cy}$ should provide some steric protection of an active metal centre and there was scope to

investigate the influence of the pendant arm with $HON^{Me,NMe2}$. $HON^{Me,NMe2}$ is also related to the bis(phenol)-amine, $H_2O_2N^{NMe2}$, and is more illustrative of catalyst progression between $Y(O\text{-}2,4\text{-}C_6H_3{}^tBu_2)_3(THF)_2$ (**15**) and $Y(O_2N^{NMe2})(HO_2N^{NMe2})$ (**1**). The double-pendant arm ligand $HON^{(NEt2)2}$ was not utilised but studies by Arnold showed that bis(amide) complexes can be effectively employed as catalysts for ROP. The ROP experiments described in this Thesis have focused on the use of co-initiators to achieve efficient initiation and bis(amide) complexes offer a route to active systems where two PLA chains may possibly grow at the metal centre in coordination-insertion propagation processes.

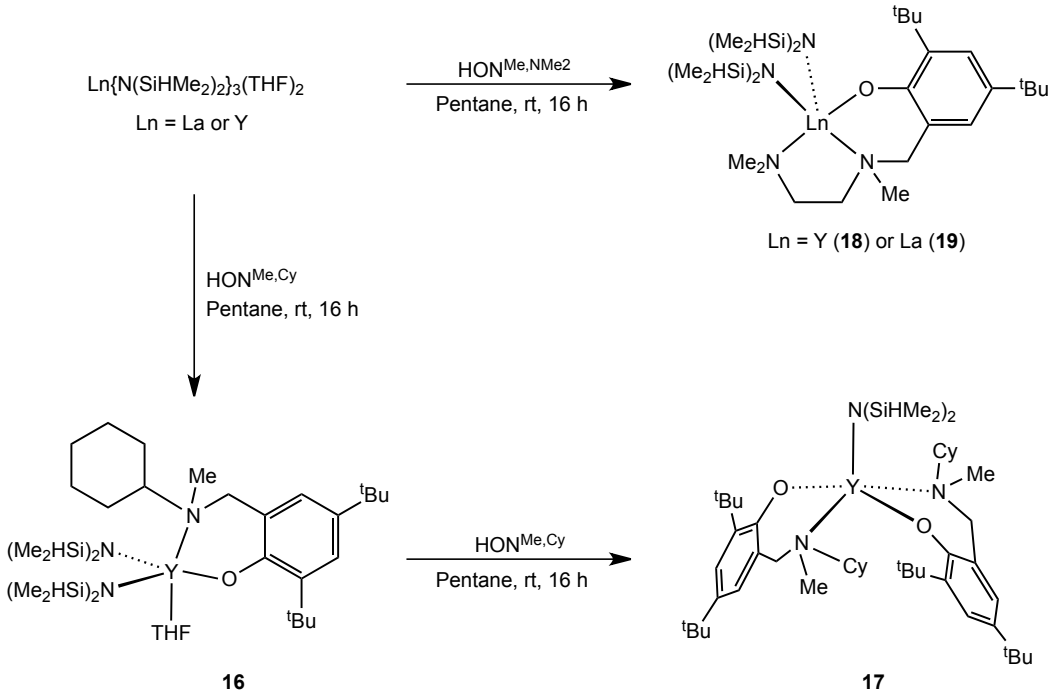

Scheme 5.1. Synthesis of phenolate-amino supported, rare earth amide complexes.

Treatment of $Ln\{N(SiHMe_2)_2\}_3(THF)_2$ (Ln = Y or La) with the appropriate protio-ligand in pentane led to the formation of the bis(amide) complexes, $Y(ON^{Me,Cy})\{N(SiHMe_2)_2\}_2(THF)$ (**16**) or $Ln(ON^{Me,NMe2})\{N(SiHMe_2)_2\}_2$ (Ln = Y (**18**) or La (**19**)) (Scheme 5.1). Addition of a further equiv. of $HON^{Me,Cy}$ to **16** resulted in the formation of the mono(amide) complex, $Y(ON^{Me,Cy})_2\{N(SiHMe_2)_2\}$ (**17**), but direct addition of two equivs. of $HON^{Me,Cy}$ to $Y\{N(SiHMe_2)_2\}_3(THF)_2$ was the optimal synthetic route to **17**. Each complex was soluble in hydrocarbon solvents and THF and were isolated in moderate to good yields of 45–65%.

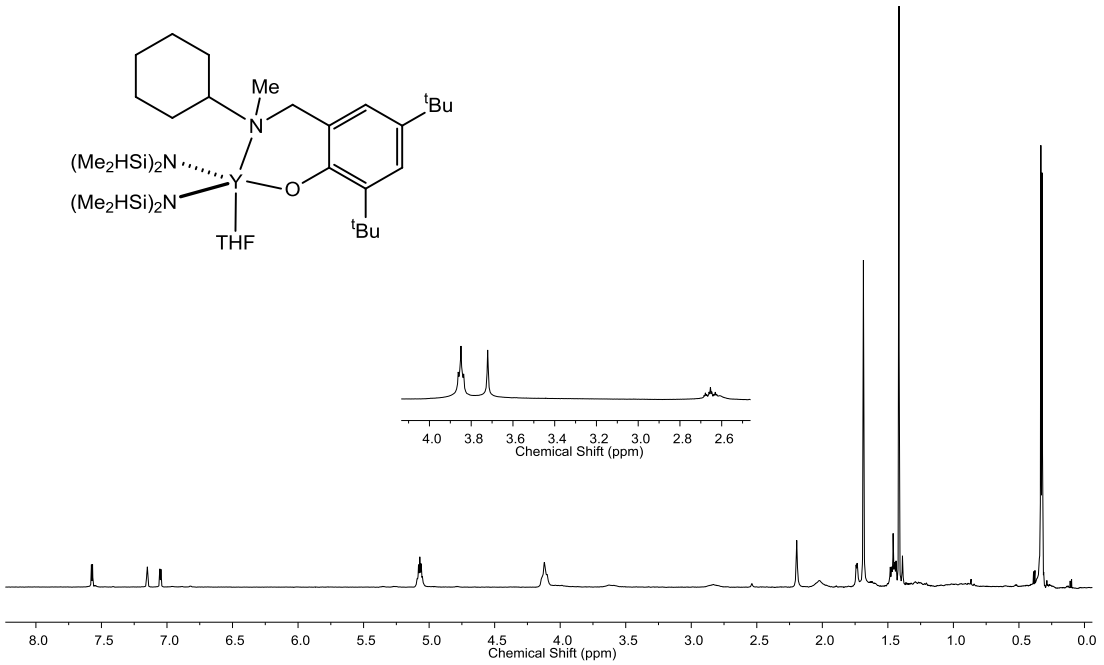

Figure 5.2. ^{1}H NMR (300.1 MHz, C_6D_6, 298 K) spectrum of $Y(ON^{Me,Cy})\{N(SiHMe_2)\}_2(THF)$ (**16**). Residual protio-solvent, δ = 7.15 ppm. Inset, expansion of the ^{1}H NMR (499.9 MHz, toluene-d_8, 363 K) spectrum of **16** showing bound THF (δ = 3.9 ppm), time-averaged methylene protons (δ = 3.7 ppm) and the 1-C_6H_{11} multiplet (δ = 2.6 ppm).

Solution phase NMR studies of **16**–**19** were undertaken and confirmed the formation of either mono(amide) (**17**) or bis(amide) (**16**, **18** and **19**) compounds. Figure 5.2 shows the room temperature ^{1}H NMR (C_6D_6) spectrum of **16**. The cyclohexyl environments and the diastereotopic methylene linking group protons (δ = 3.6 and 2.8 ppm) were broad at this temperature, whilst the remaining signals were sharp and relative peak integrations were consistent with formation of a bis(amide) complex. The Y–$N(SiHMe_2)_2$ groups were time-averaged to a single environment at room temperature (δ = 5.1 and 0.3 ppm) and a bound-THF molecule was also present (δ = 4.2 and 1.4 ppm) in the molecule. At elevated temperature (Figure 5.2, inset), the diasterotopic methylene protons coalesced to a time-averaged singlet (δ = 3.7 ppm) and the cyclohexyl proton, 1-C_6H_{11} (δ = 2.6 ppm, adjacent to the NMe), resolved as a multiplet. However, the remaining cyclohexyl environments remained broad over high and low temperature ranges. The ^{1}H NMR spectra of **17** were consistently broad over high and low temperature ranges but characteristic aromatic, $N(SiHMe_2)_2$,

methylene doublets, NMe and ^{t}Bu features were assigned. The solid state structure of **17** (*vide infra*) was consistent with a C_2-symmetric complex.

The room temperature ^{1}H NMR spectrum of **19** is shown in Figure 5.3 by way of example. Two aromatic protons at δ = 7.6 and 7.0 ppm were observed along with two characteristic ^{t}Bu environments at δ = 1.8 and 1.5 ppm. Peak integration was consistent with two bound La–N(SiHMe$_2$)$_2$ amide groups (δ = 5.0 and 0.4 ppm) that were time-averaged to a single environment in the ^{1}H NMR spectrum under the described conditions. In contrast to **16**, no THF was coordinated to the metal centre. The NMe singlet overlapped with one of the pendant arm NMe$_2$ singlets at 1.9 ppm, whilst the second NMe$_2$ singlet was present at δ = 2.1 ppm. The diastereotopic ArCH$_2$ methylene doublets (δ = 3.8 and 3.1 ppm) were sharp at this temperature. The ABCD spin system formed by the C<u>H$_2$</u>C<u>H$_2$</u>NMe$_2$ methylene groups (along with the presence of two NMe$_2$ singlets at δ = 2.1 and 1.9 ppm) was consistent with pendant arm coordination, which was confirmed by the solid state structure (*vide infra*). The ^{1}H NMR spectrum of **18** was broader at room temperature but identical features to those described for **19** were resolved at elevated temperature.

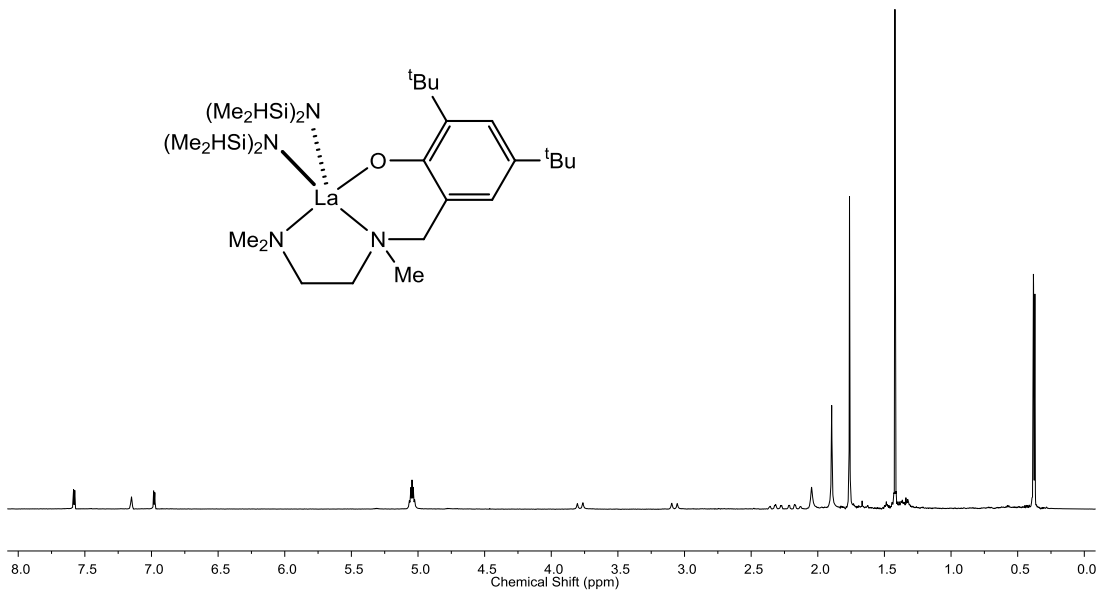

Figure 5.3. ^{1}H NMR (300.1 MHz, C_6D_6, 298 K) spectrum of La(ON^{Me,NMe2})-{N(SiHMe$_2$)$_2$}$_2$ (**19**). Residual protio-solvent, δ = 7.15 ppm.

The solid state structures of **16** and **17** were consistent with the formation of bis and mono(amide) complexes. The structure of **16** (Figure 5.4) clearly shows a five

coordinate yttrium centre with the Y–N(SiHMe$_2$)$_2$ groups in the trigonal plane along with the phenolate oxygen atom. The sum of the bond angles that formed the trigonal plane about the yttrium centre was 358.84(23)°. The Si(3)HMe$_2$ group was positionally disordered (40:60 relative orientations) and was refined subject to satisfactory restraints. The neutral amino donor and the coordinated THF molecule occupied the axial positions, completing the five-coordinate structure. There was some minor positional disorder in the THF ligand but a satisfactory split-site model could not be developed. The ligand was positionally and isotropically refined with soft restraints applied to the C–C distances and non-H atom displacement parameters.

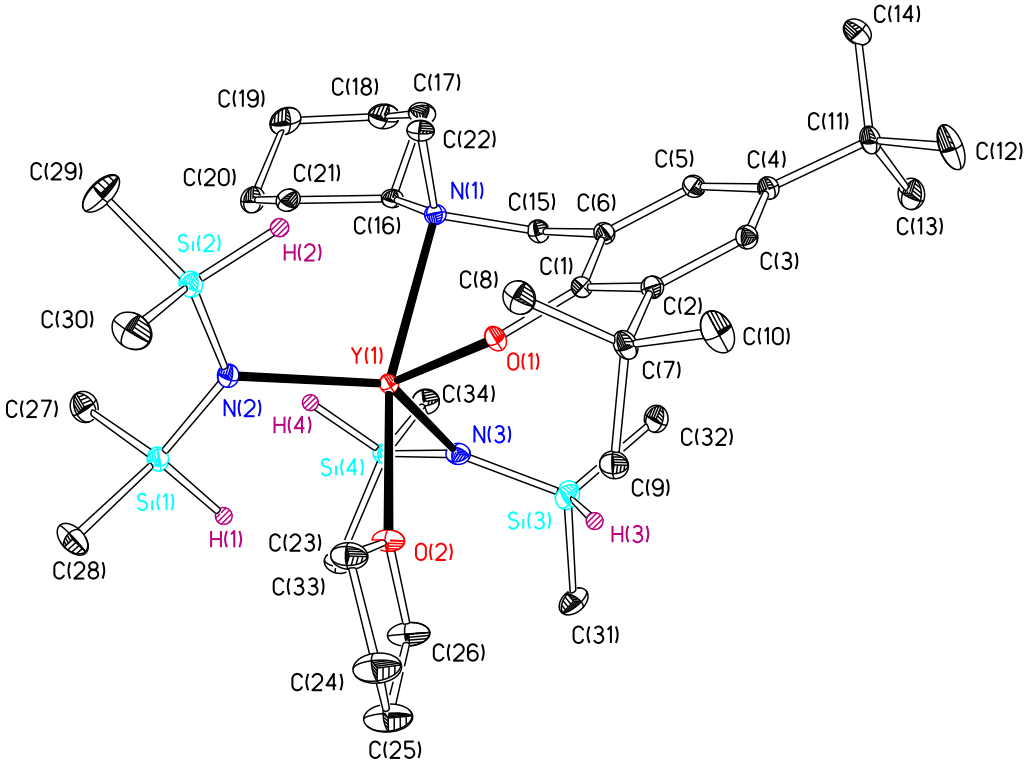

Figure 5.4. Molecular structure of Y(ON^{Me,Cy}){N(SiHMe$_2$)$_2$}$_2$(THF) (**16**), drawn at the 20% probability level. C-bound H atoms and minor disorder omitted. Si-bound H atoms are drawn as spheres of arbitrary radius. Selected bond lengths (Å) and angles (°): Y(1)–O(1) 2.0928(17), Y(1)–O(2) 2.3929(19), Y(1)–N(1) 2.586(2), Y(1)–N(2) 2.265(2), Y(1)–N(3) 2.267(2); N(2)–Y(1)–O(1) 117.67(7), N(2)–Y(1)–N(3) 130.54(8), N(3)–Y(1)–O(1) 110.63(8), N(1)–Y(1)–O(1) 75.30(6), N(1)–Y(1)–N(3) 95.43(7), N(1)–Y(1)–N(2) 105.66(7), O(1)–Y(1)–O(2) 86.25(7), Y(1)–O(1)–C(1) 139.54(15).

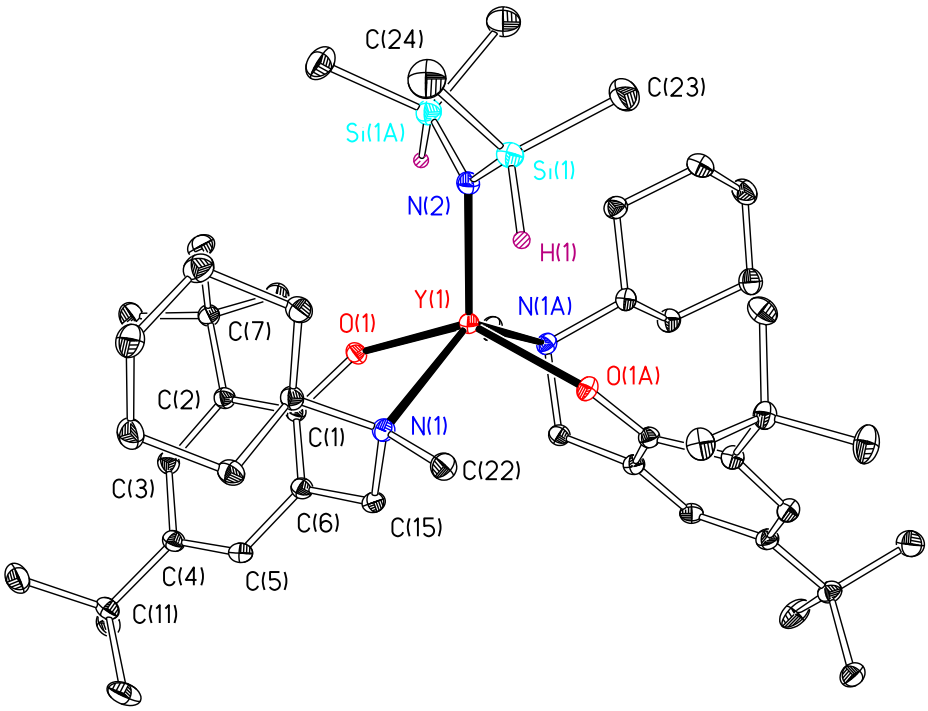

Figure 5.5. Molecular structure of $Y(ON^{Me,Cy})_2\{N(SiHMe_2)_2\}$ (**17**), drawn at the 20% probability level. C-bound H atoms omitted for clarity. Si-bound H atoms are drawn as spheres of arbitrary radius. Atoms labelled with the suffix 'A' are related to their counterparts by the symmetry operator $1 - x, y, -z + ½$). Selected bond lengths (Å) and angles (°): Y(1)–O(1) 2.1343(14), Y(1)–N(1) 2.5495(17), Y(1)–N(2) 2.233(2); N(1)–Y(1)–O(1) 75.54(5), N(1)–Y(1)–N(2) 113.27(4), N(2)–Y(1)–O(1) 111.25(4), C(1)–O(1)–Y(1) 141.20(12).

The molecular structure of **17**, with crystallographically-imposed C_2-symmetry and square-based pyramidal geometry about the yttrium centre is shown in Figure 5.5. The nitrogen and oxygen donors of the $ON^{Me,Cy}$ ligands form the basal plane and the Y–$N(SiHMe_2)_2$ group capped the pyramidal coordination site. The N(1)–Y(1)–O(1) bond angle in **17** of 75.54(5)° was consistent with the corresponding angle in **16** (75.30(6)°), but the N(1)–Y(1)–O(1) angle of 75.30(6)° in **16** was more acute that the O(1)–Y(1)–O(2) angle of 86.25(7)°, highlighting the associated strain in the chelating ligand.

The oxygen donors of the $ON^{Me,Cy}$ ligands are in a *trans* arrangement and the Y(1)–O(1) bond lengths in **17** (2.1343(14) Å) are longer than the Y(1)–O(1) bond length in **16** (2.0928(17) Å). However, the Y(1)–N(1) bond in **16** (2.586(2) Å) is longer than its counterpart in **17** (2.5495(17) Å). The longer Y(1)–O(1) bond lengths in **17** may

reflect the competition between the oxygen donors for the yttrium centre, given that in **16**, there is only one phenolate donor. In **16**, the shorter Y(1)–O(1) bond leads to a relative lengthening of the Y(1)–N(1) bond through associated geometric ligand strain.

There was a difference in the Y–N(SiHMe$_2$)$_2$ bond lengths in **16** and **17**. The bond lengths of 2.265(2) and 2.267(2) Å in **16** are longer than the corresponding bond in **17** (2.233(2) Å). In Arnold's complex, Y(O$_2$N$^{(NEt2)2}$){N(SiHMe$_2$)$_2$}$_2$ (**5.11**), there was a noticeable difference between the Y–N(SiHMe$_2$)$_2$ bond lengths (2.221(6) and 2.307(6) Å).[13] However, these literature examples and the Y–N(SiHMe$_2$)$_2$ bond distances in **16** and **17** lie within the range of other reported examples (2.209 – 2.504 Å, mean 2.271 Å, 40 examples)[19] and within the range for reported Y–N(SiMe$_3$)$_2$ bond distances (2.187 – 2.343 Å, mean 2.261 Å, 72 examples).[19]

The structure of La(ON^{Me,NMe2}){N(SiHMe$_2$)$_2$}$_2$ (**19**) is shown in Figure 5.6. Pendant NMe$_2$ arm coordination was confirmed from the structure and the [NNO] donors lie within a plane that bisects the N(3)–La(1)–N(4) angle. The La(1)–O(1) and La(1)–N(1) bond distances were 2.216(3) and 2.727(3) Å and reflect the associated increase in bond lengths with the larger metal centre (in **17**, Y(1)–O(1) = 2.1343(14) Å and Y(1)–N(1) = 2.5495(17) Å). The La(1)–N(3) and La(1)–N(4) bond distances of 2.411(3) and 2.406(3) Å were expectedly longer than the Y–N(SiHMe$_2$) distances in **16** (2.265(2) and 2.267(2) Å) and **17** (2.233(2) Å) and those reported by Arnold in **5.11** (2.221(6) and 2.307(6) Å),[13] but were consistent with non-bridging La–N(SiHMe$_2$)$_2$ moieties (2.344 – 2.449 Å, mean 2.397 Å, 11 examples)[19] and La–N(SiMe$_3$)$_2$ analogues (2.312 – 2.488 Å, mean 2.408 Å, 24 examples).[19]

Despite the presence of the NMe$_2$ pendant arm, the O(1)–La(1)–N(1) bond angle in **19** (70.03(1)°) was more acute than the N(1)–Y(1)–O(1) bond angle in **17** (75.54(5)°), again consistent with the larger metal covalent radius. The La(1)–N(1), La(1)–N(2) and N(1)–La(1)–N(2) bond lengths and angles of **19** were 2.727(3) and 2.750(4) Å and 66.65(10)° but in La(O$_2$N^{NMe2})(HO$_2$N^{NMe2}) (**2.4**), the corresponding bond distances were 2.711(3) and 2.861(3) Å and the angle was 64.42(10)°.[7]

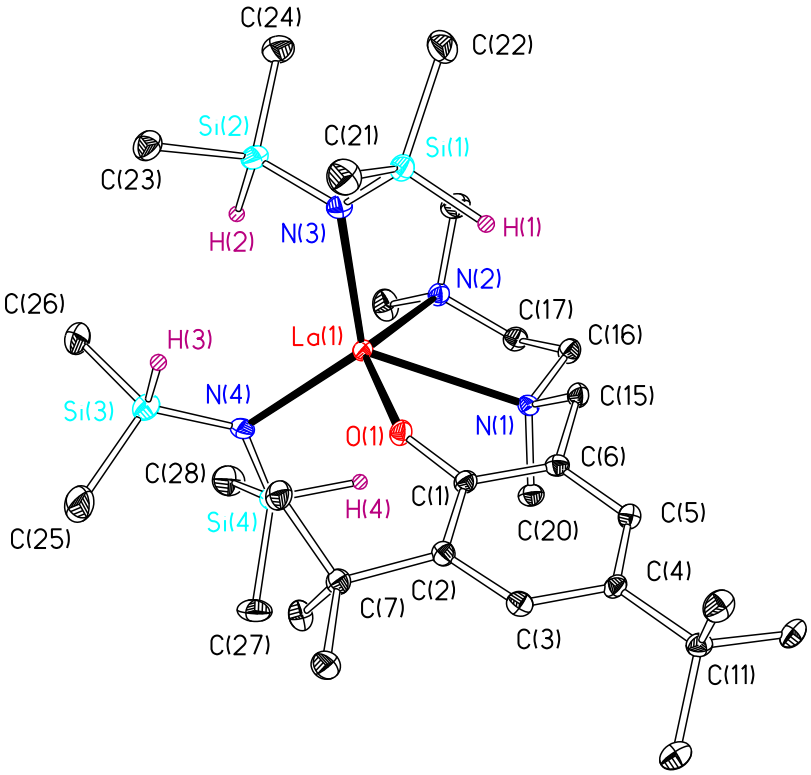

Figure 5.6. Molecular structure of La(ON^{Me,NMe2}){N(SiHMe$_2$)$_2$}$_2$ (**19**), drawn at the 20% probability level. C-bound H atoms omitted for clarity. Si-bound H atoms are drawn as spheres of arbitrary radius. Selected bond lengths (Å) and angles (°): La(1)–O(1) 2.216(3), La(1)–N(1) 2.727(3), La(1)–N(2) 2.750(4), La(1)–N(3) 2.411(3), La(1)–N(4) 2.406(3); O(1)–La(1)–N(1) 70.03(1), O(1)–La(1)–N(3) 100.85(12), O(1)–La(1)–N(4) 101.01(11), N(1)–La(1)–N(2) 66.65(10), N(1)–La(1)–N(3) 117.06(11), N(2)–La(1)–N(3) 96.97(12), C(1)–O(1)–La(1) 149.8(3).

5.4 Polymerisation studies

The suitability of complexes **16–19** as immortal ROP catalysts was investigated. In benchmarking runs in THF at room temperature, each complex was treated with 100 equivs. of *rac*-LA ([*rac*-LA]$_0$:[Ln]$_0$ = 100:1, [*rac*-LA]$_0$ = 0.69 M, Table 5.1) to determine whether one or two polymer chains formed per metal centre, given that **16**, **18** and **19** contain two potential Ln–N(SiHMe$_2$)$_2$ initiating groups. With **16**, **18** and **19**, monomer to poly(*rac*-LA) conversions above 90% were achieved within 20 mins and M_n(GPC) = 16,460, 14,570 and 11,580 g mol^{-1} were reflective of one chain forming and mirrored data reported by Arnold using **5.11** (*vide supra*).[13] The analogous polymerisation reaction with **17** was slower, with 80% conversion achieved

after 20 mins. The reaction was quenched after 40 mins and a conversion of 91% measured, as judged by the relative integrals of poly(*rac*-LA) products and unreacted monomer in the ^{1}H NMR spectrum of the crude poly(*rac*-LA) sample. M_n(GPC) = 13,170 g mol^{-1} for this polymer was also reflective of one chain per metal forming (M_n(calcd) = 13,120 g mol^{-1}). However, the broad PDIs of 2.0–2.4 for this sample and the poly(*rac*-LA) produced using **16**, **18** and **19** were indicative of poorly-controlled polymerisation reactions with propagation competing with initiation by insertion of lactide into the Ln–N(SiHMe$_2$)$_2$ bond. These polymerisation reactions remained un-optimised and it is likely that complete conversion was achieved in much shorter times that those quoted in Table 5.1. When Delbridge employed the lanthanum centred complex, La(ON^{Me,O}){N(SiHMe$_2$)$_2$}$_2$ (**5.16**), 100 equivs. of *L*-LA were converted to PLA within 1 min in toluene at room temperature.[14] It is also possible that the apparent agreement between M_n(calcd) and M_n(GPC) for each catalytic run may have arisen from post-polymerisation averaging of polymer chains by transesterification processes or chain shortening by the formation of cyclics during ROP. In an attempt to identify –N(SiHMe$_2$)$_2$ (or hydrolysed amide) polymer end-groups, a run with [*rac*-LA]$_0$:[**16**]$_0$ = 20:1 was performed. A bimodal distribution of poly(*rac*-LA) was detected by GPC analysis but the MALDI-ToF mass spectrum of the lower molecular weight distribution (M_n(GPC) = 3,190 g mol^{-1}, PDI = 1.11, 37% of total peak area) showed only cyclic polymer products with no apparent end-group. No –N(SiHMe$_2$)$_2$ or –NH(SiHMe$_2$) end-groups could be assigned.

M_n(GPC) for polymerisation reactions using **16**–**19** as initiators were in reasonable agreement with one poly(*rac*-LA) chain forming per metal but it is unlikely that initiation occurred exclusively by insertion of LA into a Ln–N(SiHMe$_2$)$_2$ bond. Given the notoriously poor performance of amide initiators with regard to incomplete initiation (or slow initiation with respect to propagation), competing initiation pathways involving trace lactic acid or water impurities were also likely to have occurred. Extensive transesterification and prolonged reaction times may have also led to the broad PDIs observed. All polymer products were atactic, although a slight heterotactic bias (P_r = 0.65) was measured for PLA produced by **17**.

Table 5.1. Scope of end-group functionalisation in the immortal ROP of *rac*-LA using $Y(ON^{Me,Cy})\{N(SiHMe_2)_2\}_2(THF)$ (**16**), $Y(ON^{Me,Cy})_2\{N(SiHMe_2)_2\}$ (**17**), $Y(ON^{Me,NMe2})\{N(SiHMe_2)_2\}_2$ (**18**) and $La(ON^{Me,NMe2})\{N(SiHMe_2)_2\}_2$ (**19**).[a]

Complex	Co-initiator	Conv. (%)[b]	M_n(calcd) (g mol^{-1})[c]	M_n(GPC) (g mol^{-1})[d]	M_w/M_n[d]
16	[e]	94	13,560	16,460	1.93
16	[e]	91[f]	2,620[f]	9,720[g]	1.25[g]
			2,620[f]	3,190[g]	1.11[g]
16	$BnNH_2$	95	2,850	3,330	1.34
16	$C_5H_{10}NH$	96	2,850	2,640	2.60
16	BnOH	98	2,930	4,040	1.38
17	[e]	80[h]	[h]	[h]	[h]
17	[e]	91[i]	13,120	13,170	2.39
17	$BnNH_2$	95	2,850	3,950	1.43
17	$C_5H_{10}NH$	97	2,880	2,360	2.54
17	BnOH	97	2,990	4,230	1.27
18	[e]	97	13,980	14,570	2.17
18	$BnNH_2$	96	2,870	3,560	1.37
18	$C_5H_{10}NH$	95	2,820	3,150	1.86
18	BnOH	98	2,930	3,000	1.67
19	[e]	95	13,690	11,580	1.98
19	$BnNH_2$	95	2,850	3,050	2.05
19	$C_5H_{10}NH$	96	2,850	2,330	2.49
19	BnOH	98	2,930	2,270	2.15

[a] [*rac*-LA]$_0$:[Co-initiator]$_0$:[**1**]$_0$ = 100:5:1, 2 mL THF, [*rac*-LA]$_0$ = 0.69 M, rt, 20 mins. [b] Measured by ^{1}H NMR in $CDCl_3$. [c] M_n(calcd) = (Conv. (%) × [*rac*-LA]$_0$:[Co-initiator]$_0$ × 144.1 + M_R Co-initiator). [d] Measured by GPC against polystyrene standards using the appropriate Mark-Houwink corrections for poly(*rac*-LA) in THF at 30 °C. [e] No Co-initiator added. [f] [*rac*-LA]$_0$:[**16**]$_0$ = 20:1. [g] Bimodal distribution of molecular weights, peak areas were 63 and 37 % respectively. [h] 80% conversion recorded after 20 mins, molecular weight not determined. [i] 91% conversion recorded after 40 mins.

Inclusion of 5 equivs. of $BnNH_2$ or BnOH in polymerisation mixtures led to the expected chain shortening and narrowing of molecular weight distributions but M_n(GPC) were generally higher than that expected for one chain per molar equiv. of co-initiator (Table 5.1). In a representative run with **16**, [*rac*-LA]$_0$:[$BnNH_2$]$_0$:[**16**]$_0$ = 100:5:1, 95% conversion of monomer to poly(*rac*-LA) was recorded after 20 mins and M_n(GPC) = 3,330 g mol^{-1} was higher than expected (M_n(calcd) = 2,850 g mol^{-1}), although a moderately broad distribution of molecular weights formed (PDI = 1.34). With BnOH, the agreement was worse, with M_n(GPC) = 4,040 g mol^{-1} (PDI = 1.38) and M_n(calcd) = 2,930 g mol^{-1} (98% conversion). ^{1}H NMR and MALDI-ToF MS were consistent with the formation of linear poly(*rac*-LA) with HOCH(Me)– and BnNH– or BnO– end-groups. However, the $\Delta(m/z)$ = 72.0 g mol^{-1} between the peak envelopes of the major distribution was consistent with undesired tranesterification products forming. Cyclic polymer products with no apparent end-group were also consistently detected. The MALDI-ToF mass spectrum of the poly(*rac*-LA) isolated from the reaction, [*rac*-LA]$_0$:[$BnNH_2$]$_0$:[**16**]$_0$ = 100:5:1 is shown in Figure 5.7 by way of example.

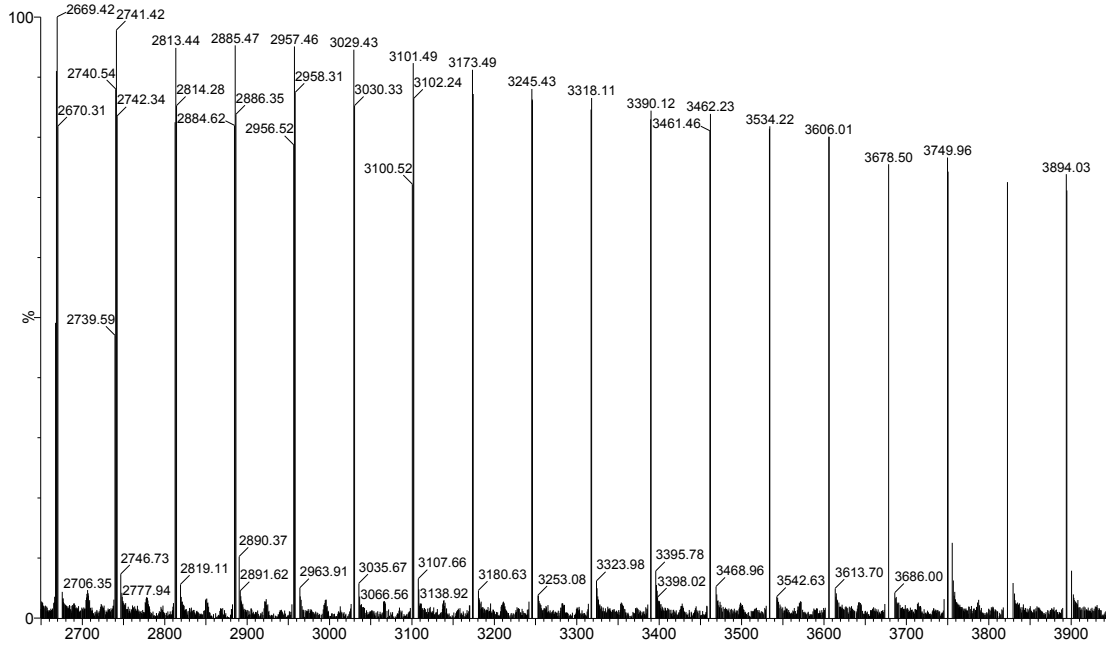

Figure 5.7. Expansion of the MALDI-ToF mass spectrum of crude benzyl amine-capped PLA isolated from the reaction, [*rac*-LA]$_0$:[$BnNH_2$]$_0$:[**16**]$_0$ = 100:5:1. K^+ dopant, $\Delta(m/z)$ = 72.0 g mol^{-1}.

The molecular weight data for co-initiated ROP reactions using **17** and $BnNH_2$ or BnOH were similar to **16** and PDIs were moderately broad (1.43 and 1.27). M_n(GPC) for the runs, [*rac*-LA]$_0$:[$BnNH_2$]$_0$:[**17**]$_0$ = 100:5:1 and [*rac*-LA]$_0$:[BnOH]$_0$:[**17**]$_0$ = 100:5:1 were 3,950 g mol^{-1} and 4,230 g mol^{-1} with M_n(calcd) = 2,850 g mol^{-1} and 2,990 g mol^{-1} (Table 5.1). MALDI-ToF mass spectra were also analogous to poly(*rac*-LA) produced by **16**, showing systematic benzyl amine or benzyl alcohol end-group incorporation. However, poly(*rac*-LA) products showed evidence of extensive transesterification and cyclic polymers were also present.

The molecular weight data for $BnNH_2$ or BnOH co-initiated ROP of *rac*-LA using **16** or **17** were consistent with non-initiating Y–N(SiHMe$_2$)$_2$ moieties. BnOH was added to the pre-catalysts (**16** and **17**) prior to the addition of *rac*-LA and was likely to eliminate HN(SiHMe$_2$)$_2$ from each complex. In an NMR tube scale experiment, two equivs. of ^{i}PrOH were added to **16** in an attempt to prepare a new bis(alkoxide) species. A preparative scale reaction was not performed, but HN(SiHMe$_2$)$_2$ was liberated from **16** and a new bis(alkoxide) species was apparent. Importantly, $ON^{Me,Cy}$ was not eliminated, indicating that the phenolate-amino ligand was robust in the presence of primary alcohols. The *in situ* formed bis(benzyl alkoxide) species when BnOH is used as the co-initiator are likely to initiate *via* a coordination-insertion mechanism with the remaining BnOH acting as a chain transfer agent. $BnNH_2$ co-initiated ROP reactions were likely to initiate *via* an activated-monomer process. The benzyl amine-capped macromonomers were the likely protic sources responsible for the elimination of Y–N(SiHMe$_2$)$_2$ from **16** or **17**, given that an isolated macromonomer (**9**) was shown to liberate HN(SiHMe$_2$)$_2$ from Y(O_2N^{NMe2}){N(SiHMe$_2$)$_2$}(THF) (**1.15**) (Chapter Two, Figure 2.26).

Piperidine-capped poly(*rac*-LA) produced using **16** and **17** as catalysts had molecular weight distributions (PDI = 2.6) that were much broader than BnOH or $BnNH_2$-capped poly(*rac*-LA) (PDI = 1.3–1.4, Table 5.1). M_n(GPC) = 2,640 and 2,360 g mol^{-1} were in good agreement with five chains forming (M_n(calcd) = 2,850 g mol^{-1} (**16**) and 2,880 g mol^{-1} (**17**)) but the broad PDIs were non-ideal for immortal ROP. From the kinetics experiments with **1** and piperidine (Chapter Two, Figure 2.18), a significant induction period was observed for piperidine co-initiated ROP in contrast to $BnNH_2$ or BnOH co-initiated ROP with **1**. In light of this observation, ROP co-initiated by piperidine, with **16** or **17** as the catalyst may also feature a significant induction

period. Initiation pathways involving trace impurities (lactic acid or water) are likely to be competitive with the proposed activated-monomer initiation step and if propagation is also competitive with initiation, then a broad distribution of polymer products is likely to form.

The $BnNH_2$, piperidine or BnOH-capped poly(*rac*-LA) products produced in the presence of **18** had experimental molecular weights and molecular weight distributions that were comparable to poly(*rac*-LA) products prepared using **16** and **17** (Table 5.1). In runs with [*rac*-LA]$_0$:[$BnNH_2$]$_0$:[**18**]$_0$ = 100:5:1 or [*rac*-LA]$_0$:[BnOH]$_0$:[**18**]$_0$ = 100:5:1, 96% and 98% conversions were achieved within 20 mins. M_n(GPC) = 3,560 g mol^{-1} (PDI = 1.37) and M_n(calcd) = 2,870 g mol^{-1} for the $BnNH_2$ run demonstrated the consistently higher than expected experimental molecular weights. Good agreement was seen in the BnOH run, with M_n(GPC) = 3,000 g mol^{-1} and M_n(calcd) = 2,930 g mol^{-1}, but the molecular weight distribution was broader (PDI = 1.67). Piperidine-capped poly(*rac*-LA) produced by **18** had a broader PDI = 1.86 (M_n(GPC) = 3,150 g mol^{-1} and M_n(calcd) = 2,820 g mol^{-1}), again demonstrating the inefficiency of the activated-monomer initiation step when piperidine was employed as the co-initiator. With the lanthanum complex, **19**, agreement between expected and observed molecular weights was good (M_n(calcd) = 2,850 g mol^{-1} and M_n(GPC) = 3,050 g mol^{-1} for the $BnNH_2$ run) but PDIs were consistently broader (2.0–2.5) (Table 5.1). In the initial screening experiments with the zwiterrionic complexes, La(O_2N^{NMe2})(HO_2N^{NMe2}) (**2.4**) and Y(O_2N^{NMe2})(HO_2N^{NMe2}) (**1**) (Chapter Two, Table 2.2), broader PDIs were also seen in $BnNH_2$ co-initiated ROP when **2.4** was employed as the catalyst. These data further demonstrated that whilst the larger metals can be more active, ROP reactions show poorer control.

MALDI-ToF mass spectra of poly(*rac*-LA) samples produced using **18** or **19** in the presence of a co-initiator showed systematic end-group incorporation (Figure 5.8). HOCH(Me)– and BnNH–, $C_5H_{10}N$– or BnO– end-groups were assigned but the $\Delta(m/z)$ = 72.0 g mol^{-1} between peak envelopes was again consistent with extensive transesterification. Cyclic polymer products with no apparent end-group were also present.

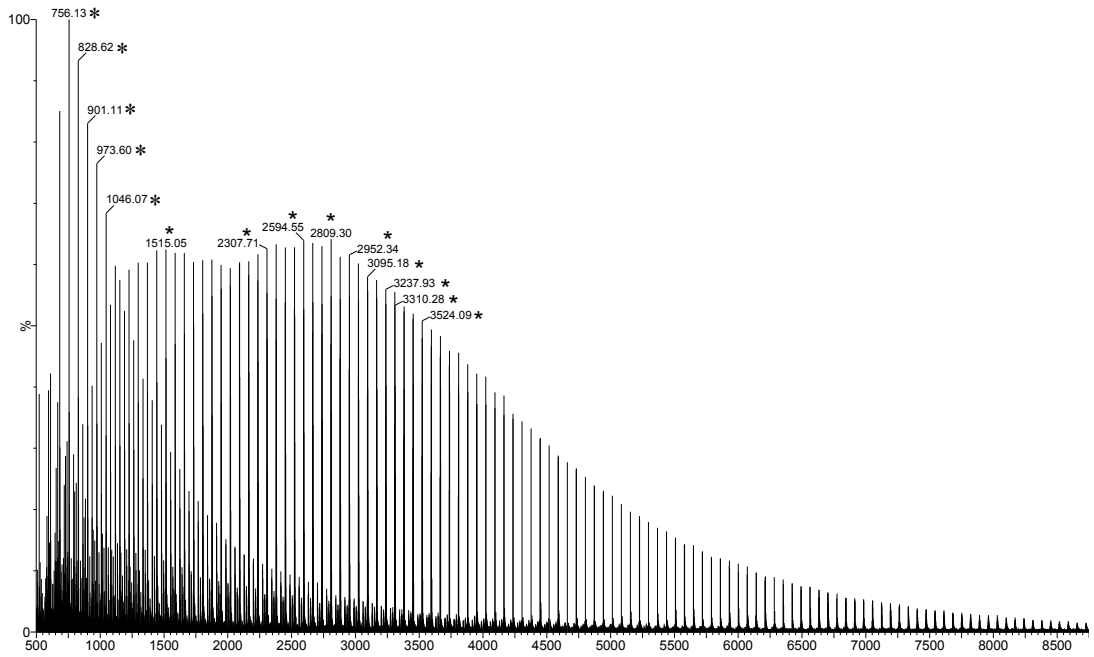

Figure 5.8. Full MALDI-ToF MS of benzyl amine-capped poly(*rac*-LA) (*) ([*rac*-LA]$_0$:[BnNH$_2$]$_0$:[**18**]$_0$ = 100:5:1). K^+ dopant, $\Delta(m/z)$ = 72.0 g mol^{-1}. The distribution of cyclic poly(*rac*-LA) products (*) is centred at m/z = 756 g mol^{-1}.

5.4.1 Loading experiments with 16 and 17

To further demonstrate the suitability of **16–19** as catalysts in the amine-initiated, immortal ROP of *rac*-LA, catalyst loading experiments were undertaken to establish any relationship between M_n and [*rac*-LA]$_0$:[BnNH$_2$]$_0$ and demonstrate catalyst tolerance. The initial screening experiments (Table 5.1) showed that BnNH$_2$ was a more suitable amine than piperidine for amine-initiated, immortal ROP and further studies utilised BnNH$_2$ as the co-initiator.

Beginning with **16** and **17**, [BnNH$_2$]$_0$:[Y]$_0$ was held constant at 5:1 and [*rac*-LA]$_0$ was increased through 100, 200, 500, 800 and 1000 molar equivs. with respect to [Y]$_0$. Each reaction was run to high conversion but conversions greater than 90% were not achieved with the higher loading experiments ([*rac*-LA]$_0$:[Y]$_0$ = 800 or 1000:1) until 60 mins had elapsed (40 mins for the runs, [*rac*-LA]$_0$:[Y]$_0$ = 500:1). Nevertheless, the higher loading runs demonstrated the tolerance of each catalyst to a large excess of monomer. M_n(GPC) for both series of runs were plotted against ([*rac*-LA]$_0$ – [*rac*-LA]$_t$):[BnNH$_2$]$_0$ (Figure 5.9). In general, experimental molecular weights were higher than expected (M_n(calcd) represented by the dashed line in Figure 5.9), which was reflected by the gradients of the lines of least-squares fit through the experimental

M_n(GPC) points. The gradient of the fitted line through the points representing runs with **16** was 163(3) (R^2 = 0.998) g mol^{-1}, which was close to the expected gradient of 144 g mol^{-1} within error. However, the fitted line through the points representing runs with **17** was much greater than expected, with a gradient of 193(5) (R^2 = 0.995) g mol^{-1}. Polydispersity indices were broader for poly(*rac*-LA) produced using **17**, e.g. 1.54 *vs*. 1.33 for the points representing the run, [*rac*-LA]$_0$:[BnNH$_2$]$_0$:[Y]$_0$ = 1000:5:1 (M_n(GPC) = 36,730 g mol^{-1} (**17**) and 32,560 g mol^{-1} (**16**)). Each PDI (Figure 5.9) was representative of moderately broad molecular weight distributions, but the broader distributions for **17** at higher loadings of *rac*-LA may indicate that polymerisation reactions with **17** are less well-controlled and that propagation may be competitive with initiation.

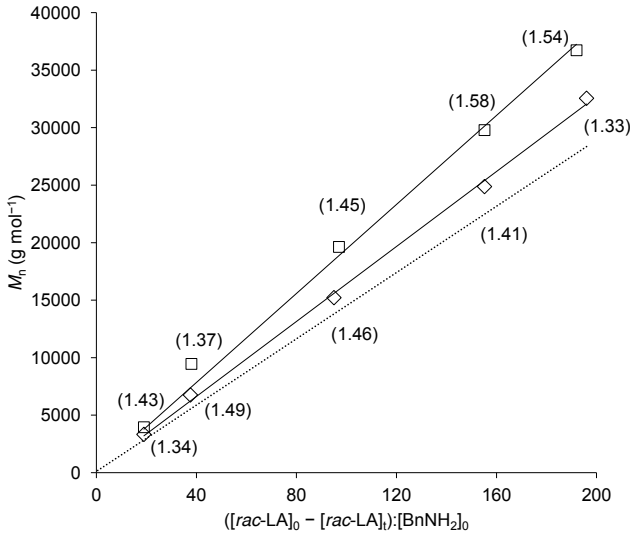

Figure 5.9. M_n(GPC) *vs*. ([*rac*-LA]$_0$ − [*rac*-LA]$_t$):[BnNH$_2$]$_0$ for the polymerisation runs [BnNH$_2$]$_0$:[Y]$_0$ = 5:1, [*rac*-LA]$_0$:[Y]$_0$ = 100, 200, 500, 800 or 1000, using Y(ON^{Me,Cy}){N(SiHMe$_2$)$_2$}$_2$(THF) (**16**) (diamonds) or Y(ON^{Me,Cy})$_2${N(SiHMe$_2$)$_2$} (**17**) (squares) as the catalyst. The dashed line represents M_n(calcd) based on [*rac*-LA]$_0$:[BnNH$_2$]$_0$ = *n*:5 and the PDIs are given in parentheses. The gradients of the fitted lines are 163(3) (R^2 = 0.998) (**16**) and 193(5) (R^2 = 0.995) (**17**) and the vertical-axis intercepts were set to 107.2 g mol^{-1} (M_R BnNH$_2$).

In the polymerisation reactions with no co-initiator, [*rac*-LA]$_0$:[**17**]$_0$ = 100:1 (Table 5.1), a slight heterotactic bias (P_r = 0.65) was calculated from the homonuclear decoupled ^{1}H-{^{1}H} NMR spectrum of isolated poly(*rac*-LA). However, no significant heterotactic bias was detected in PLA produced in these loading experiments. It would seem that the C_2-coordination geometry of **17** is unable to effect selective

enchainment of *D*- and *L*-LA units to produce PLA with a high degree of isotactic or heterotactic enrichment. In solution, fast exchange processes are likely to be operating and a stable, chiral coordination mode is unlikely to form. Both complex enantiomers are also likely to be present in solution. C_2-symmetric complexes that are chiral (as well as achiral complexes) have been shown to selectively polymerise either the *D*- or *L*- enantiomer of *rac*-LA. As described in Chapter One, aluminium salen complexes have been the focus of many of these studies, with the tetradentate salen ligand forming a rigid chelating framework.[20-29] Two distinct kinetic regimes may operate when chiral catalysts are employed. *rac*-LA polymerisation will be fast up to 50% conversion (i.e. when the preferred enantiomer is consumed), but after 50% conversion, the rate will slow dramatically when the opposite enantiomer is enchained and stereoblock PLA forms. Gibson (and others) has shown that achiral, salan (or salen) aluminium complexes can display both isotactic and heterotactic selectivity depending on the choice of phenolate substituents.[30-39]

5.4.2 Loading experiments with 18 and 19

The same loading experiments were performed using **18** and **19** (Figure 5.10). The gradients of the lines of least-squares fit through the experimental M_n(GPC) points were 170(6) (R^2 = 0.994) g mol^{-1} for **18** and 160(5) (R^2 = 0.996) for **19**. Along with the gradient of the fitted line for the comparable runs with **16** (163(3) (R^2 = 0.998) g mol^{-1}), these gradients consistently showed that M_n(GPC) were slightly higher than expected, although close to the expected 144 g mol^{-1} within three standard deviations. However, the PDIs provide a more accurate reflection of polymerisation performance. At higher *rac*-LA loadings, [*rac*-LA]$_0$:[**18**]$_0$ = 500, 800 or 1000:1), the polydispersity indices for PLA produced using **18** were 1.14, 1.13 and 1.11 and were consistent with well-controlled, immortal ROP processes. The corresponding PDIs were moderately broad with **16** (PDI ≈ 1.5) and broader still with **19** (PDI ≈ 1.7). The much broader PDIs for runs with **19** reflected poorly controlled polymerisation with the larger metal catalyst, as was highlighted in the initial screening experiments (Table 5.1). Back-biting transesterification may be more easily facilitated with the larger metal that may lead to a broader distribution of molecular weights, but optimisation of polymerisation runs with **19** may have led to the isolation of PLA with narrower PDI.

Tranesterification products were present in the MALDI-ToF mass spectra of benzyl amine-capped PLA produced using **18**, but the narrow PDIs at higher loadings of

[*rac*-LA]$_0$:[**18**]$_0$, indicated that the inherent control over immortal ROP processes was better with the smaller yttrium centre of **18** *cf.* **19**. Furthermore, a slight heterotactic bias was noted in the PLA products represented by the points, [*rac*-LA]$_0$:[**18**]$_0$ = 500:1 (M_n(GPC) = 15,140 g mol^{-1}), 800:1 (M_n(GPC) = 27,750 g mol^{-1}) and 1000:1 (M_n(GPC) = 31,520 g mol^{-1}), with P_r values of 0.70, 0.65 and 0.68 calculated from homonuclear decoupled ^{1}H-{^{1}H} NMR spectra (the equivalent PLA products produced by **19** were atactic). Although these values were not indicative of a high degree of heterotactic enrichment, they did highlight the correlation between heterotactic enrichment and the inclusion of NMe_2 pendant arm donors in bis(phenolate)-amino and phenolate-amino supporting ligands. Chen was also able to demonstrate heteroselective ROP of *rac*-LA using phenoxy-imine supported zinc alkoxide complexes that incorporated an NMe_2 pendant arm donor.[40]

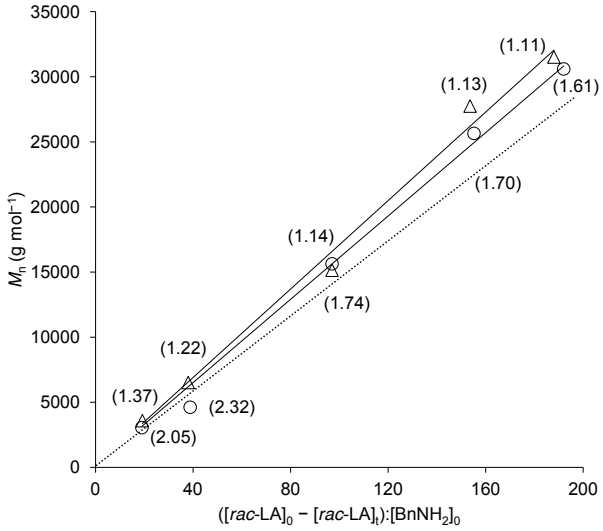

Figure 5.10. M_n(GPC) *vs.* ([*rac*-LA]$_0$ – [*rac*-LA]$_t$):[$BnNH_2$]$_0$ for the polymerisation runs [$BnNH_2$]$_0$:[Ln]$_0$ = 5:1, [*rac*-LA]$_0$:[Ln]$_0$ = 100, 200, 500, 800 or 1000, using Y(ON^{Me,NMe2}){N(SiHMe$_2$)$_2$}$_2$ (**18**) (triangles) or La(ON^{Me,NMe2}){N(SiHMe$_2$)$_2$}$_2$ (**19**) (circles) as the catalyst. The dashed line represents M_n(calcd) based on [*rac*-LA]$_0$:[$BnNH_2$]$_0$ = *n*:5 and the PDIs are given in parentheses. The gradients of the fitted lines are 170(6) (R^2 = 0.994) (**18**) and 160(5) (R^2 = 0.996) (**19**) and the vertical-axis intercepts were set to 107.2 g mol^{-1} (M_R $BnNH_2$).

Y(ON^{Me,Cy}){N(SiHMe$_2$)$_2$}$_2$(THF) (**16**) and Y(ON^{Me,NMe2}){N(SiHMe$_2$)$_2$}$_2$ (**18**) showed the best control over M_n(GPC) and the loading experiments (Figures 5.9 and 5.10) revealed that the narrowest molecular weight distributions were formed when **18** was employed as the catalyst in the amine-initiated, immortal ROP of *rac*-LA. However,

even for ROP polymerisations co-initiated by **18**, propagation was likely to have been competitive with initiation, given the higher than expected M_n(GPC) values that were consistently observed in the loading experiments (Figure 5.10).

5.4.3 NMR tube scale polymerisation reaction with 18

An NMR tube scale reaction was performed with $Y(ON^{Me,NMe2})\{N(SiHMe_2)_2\}_2$ (**18**) to ensure that the $Y–N(SiHMe_2)_2$ amide ligands were eliminated under polymerisation conditions. $BnNH_2$ (2 equivs.) was added to a solution of **18** (C_6D_6) before 10 equivs. of *rac*-LA were added to the mixture. Compound **18** did not react with $BnNH_2$, but ^{1}H NMR analysis of the mixture of *rac*-LA, $BnNH_2$ and **18** showed that the benzyl amine had been consumed and benzyl amine-capped PLA had formed. $HN(SiHMe_2)_2$ (labelled *, Figure 5.11, bottom) was also present and no bound $Y–N(SiHMe_2)_2$ ligands remained.

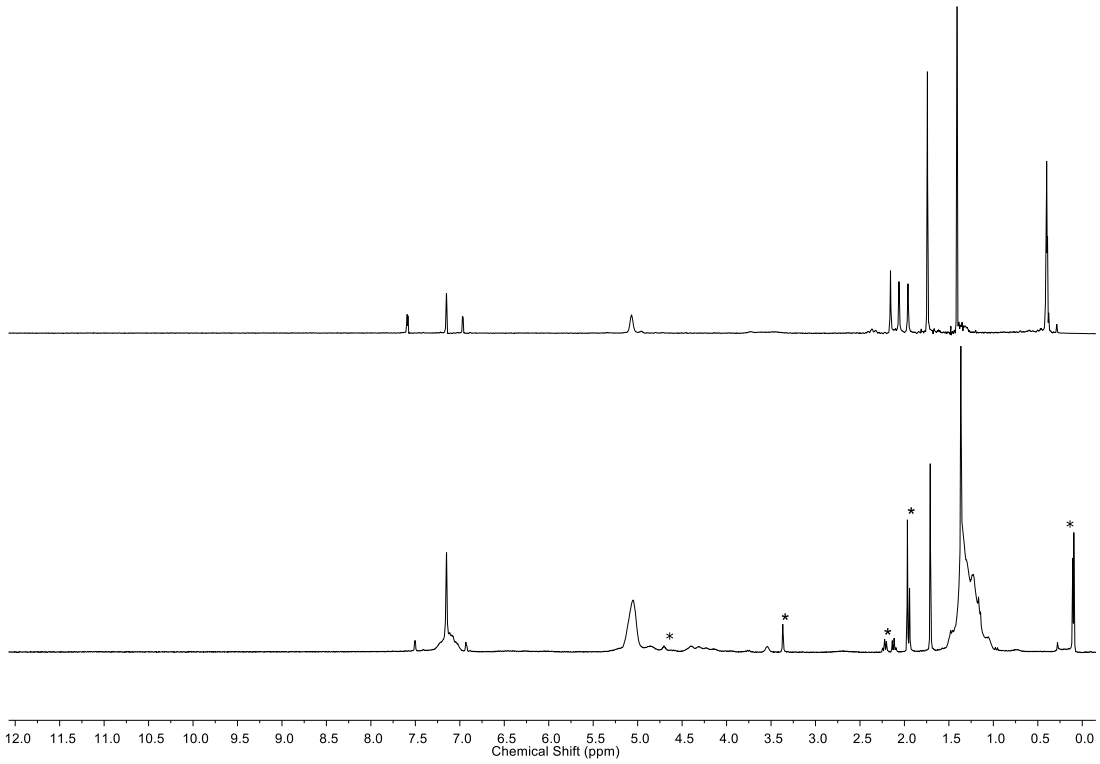

Figure 5.11. ^{1}H NMR spectra (299.9 MHz, C_6D_6, 298 K) of top, $Y(ON^{Me,NMe2})\{N(SiHMe_2)_2\}_2$ (**18**), and bottom, NMR tube scale reaction, $[rac\text{-}LA]_0:[BnNH_2]_0:[\mathbf{18}]_0 = 10:2:1$. * Denotes decomplexed $N^{Me,NMe2}$ environments and * denotes liberated $HN(SiHMe_2)_2$.

However, comparing the ^{1}H NMR spectrum of the reaction mixture (Figure 5.11, bottom) to the ^{1}H NMR spectrum of $Y(ON^{Me,NMe2})\{N(SiHMe_2)_2\}_2$ (**18**) (Figure 5.11,

top), the neutral amino donor (NMe) and pendant arm ($CH_2CH_2NMe_2$) environments (labelled *) resembled those of the protio-ligand. Specifically, a $ArCH_2$ singlet was present at δ = 3.4 ppm and the methylene groups of the $C\underline{H}_2C\underline{H}_2NMe_2$ pendant arm were observed at δ = 2.3 and 2.1 ppm. NMe and NMe_2 singlets were also visible at δ ≈ 2.0 ppm. In the ^{1}H NMR spectrum of **18** (Figure 5.11, top), there were three NMe singlets centred at δ = 2.2 ppm, indicating that the pendant arm was coordinated to the yttrium centre. Importantly, there was no OH singlet at low field in the ^{1}H NMR spectrum of the polymerisation mixture, indicating that the $ON^{Me,NMe2}$ ligand was still bound to the metal centre through the phenolate oxygen atom. In the ^{1}H NMR spectrum of the pure, protio-ligand in C_6D_6, the OH proton appeared as a sharp singlet at δ = 11.1 ppm. Sobota also noted that the neutral amino groups of $M(ON^{Me,Cy})_2$ (M = Mg (**5.4**) or Zn (**5.5**)) decomplexed when each complex was used in representative NMR tube scale reactions.[10, 11]

The loading studies with **18** (and **16**, **17** and **19**) (Figure 5.10) showed that the catalyst was tolerant of a monomer loading up to 1000 equivs. Furthermore, M_n(GPC) = 31,520 g mol^{-1} was in good agreement with M_n(calcd) = 27,200 g mol^{-1} and the PDI = 1.11 was indicative of a well-controlled polymerisation reaction. Compound **18** was a better performing catalyst than **16** (which contained the bidentate $ON^{Me,Cy}$ ligand), based on the PDI of isolated PLA (typically = 1.1 for **18** and 1.3–1.4 for **16**, Figures 5.9 and 5.10). A slight heterotactic bias (P_r = 0.68) was also noted in the PLA produced from the $[rac\text{-LA}]_0$:$[BnNH_2]_0$:[**18**]$_0$ = 1000:5:1 run which was likely to have arisen from a chain-end control mechanism, influenced in part by the coordination-geometry of the $ON^{Me,NMe2}$ ligand.

Multiple polymer chains per metal are generated in immortal ROP. These polymer chains may form competitive chelates, forcing decomplexation of the NMe_2 pendant arm from the yttrium centre. ROP experiments with the zwitterionic bis(phenolate)-amino complexes, **1.24**, **1.25**, **2.2**, **2.4**, **2.6**, **1**, **2** and **3** (Chapter Two, Table 2.2 and 2.3), effectively demonstrated that the pendant arm donor was a crucial component of the bis(phenolate)-amino framework. The lack of a pendant arm donor in $Y(O_2N^{Me})(HO_2N^{Me})$ (**3**) resulted in catalytic inactivity and the optimum control over M_n, PDI and P_r was achieved when O_2N^{NMe2} was employed as the supporting ligand. Furthermore, tranesterification was minimal when $Sm(O_2N^{NMe2})(HO_2N^{NMe2})$ (**1.24**) and $Y(O_2N^{NMe2})(HO_2N^{NMe2})$ (**1**) were used as catalysts for the immortal ROP of *rac*-

LA. The bis(phenolate)-amino ligands also form more rigid chelate structures, which bring the neutral donors into close proximity with the metal centre, and the greater steric bulk of the O_2N^L (L = OMe or NMe_2) ligands may inhibit PLA chelation at the metal centre, ensuring that the pendant arm remains complexed during polymerisation. Delbridge noted that $ON^{Me,NMe2}$ ligands may be labile under polymerisation conditions when rare earth catalysts were used for ROP, and replaced the NMe_2 donor with an anionic alkoxide donor ($ON^{Me,O}$) to ensure that the pendant arm remained coordinated.[14, 18]

5.5 Summary and Conclusions for Chapter Five

This Chapter has described the synthesis and characterisation of four new rare earth amide complexes supported by phenolate-amino ligands. Complexes **16**, **17** and **19** were successfully characterised in the solid state and their molecular structures were presented. $Y(ON^{Me,Cy})\{N(SiHMe_2)_2\}_2(THF)$ (**16**) and $Y(ON^{Me,Cy})_2\{N(SiHMe_2)_2\}$ (**17**) contained a bidentate phenolate-amino ligand and a C_2-symmetric ligand arrangement formed in the bis-substituted complex, **17**. No significant iso- or hetero-tactic bias was detected in the poly(*rac*-LA) products formed when **17** was used as a ROP catalyst, both in the absence and in the presence of co-initiators.

$Ln(ON^{Me,NMe2})\{N(SiHMe_2)_2\}_2$ (Ln = Y (**18**) or La (**19**)) contained a phenolate-amino ligand with a pendant NMe_2 donor and **18** was shown to be the best performing ROP catalyst based on the series of loading experiments (Figures 5.9 and 5.10). Each catalyst was suitable for the amine-initiated, immortal ROP of *rac*-LA. M_n(GPC) were in reasonable agreement with M_n(calcd) for one PLA chain forming per equiv. of $BnNH_2$ and the PDI indicated that narrow to moderately broad molecular weight distributions formed. Furthermore, a slight heterotactic bias was noted in the poly(*rac*-LA) products formed when **18** was used as the catalyst. However, the $\Delta(m/z)$ = 72.0 g mol^{-1} in MALDI-ToF mass spectra showed that undesired transterification processes were operating. Importantly, $HN(SiHMe_2)_2$-capped PLA were not assigned, indicating that the $Ln–N(SiHMe_2)_2$ groups were innocent with respect to fast activated-monomer initiation pathways involving LA, the co-initiator and the metal complex. The protic end-groups of the benzyl amine-capped macromonomers were likely to eliminate $HN(SiHMe_2)_2$ from **16–19** during initiation or in the early phases of propagation, as established by the NMR tube scale experiments with **18** (and $Y(O_2N^{NMe2})\{N(SiHMe_2)_2\}(THF)$ (**1.15**), Chapter Two, Figure 2.26). Unfortunately,

the NMR tube scale experiment also showed that the $N^{Me,NMe2}$ pendant arm may decomplex under immortal ROP conditions.

Whilst initial ROP experiments with **16–19** further established the generality of the amine-initiated, immortal ROP methodology, it was clear that the $ON^{Me,Cy}$ and $ON^{Me,NMe2}$ ligands did not represent an optimal class of ancillary ligand. The bis(phenolate)-amino ligands represented in **1** and **1.15** are a superior ancillary ligand framework that enabled the well-controlled ROP of *rac*-LA and *rac*-BBL with minimal transesterification. The ligands are robust in the presence of multiple PLA chains under immortal ROP conditions and stereoselective polymerisations are enforced *via* chain-end control. Further optimisation of the ligand periphery i.e. steric bulk can lead to improve levels of heterotacticity in PLA or syndiotacticity in PHB. The studies with **16–19** have sought to bridge the development of phenolate ligands between $Y(O\text{-}2,4\text{-}C_6H_3{}^tBu_2)_3(THF)_2$ (**15**) and $Y(O_2N^{NMe2})(HO_2N^{NMe2})$ (**1**) and successfully demonstrated the improvements in polymerisation control when ROP proceeds *via* a coordination-insertion mechanism.

5.6 References for Chapter Five

1. W. J. Evans, R. N. R. Broomhall-Dillard and J. W. Ziller, *Organometallics*, 1996, **15**, 1351.
2. W. J. Evans, R. N. R. Broomhall-Dillard and J. W. Ziller, *J. Organomet. Chem.*, 1998, **569**, 89.
3. J. M. Berg, D. L. Clark, J. C. Huffman, D. E. Morris, A. P. Sattelberger, W. E. Streib, W. G. Van der Sluys and J. G. Watkin, *J. Am. Chem. Soc.*, 1992, **114**, 10811.
4. E. Y. Tshuva, I. Goldberg, M. Kol and Z. Goldschmidt, *Inorg. Chem. Commun.*, 2000, **3**, 611.
5. E. Y. Tshuva, I. Goldberg, M. Kol and Z. Goldschmidt, *Organometallics*, 2001, **20**, 3017.
6. E. Y. Tshuva, I. Goldberg, M. Kol, H. Weitman and Z. Goldschmidt, *Chem. Commun.*, 2000, 379.
7. H. E. Dyer, D.Phil Thesis, University of Oxford, 2009.
8. H. E. Dyer, S. Huijser, N. Susperregui, F. Bonnet, A. D. Schwarz, R. Duchateau, L. Maron and P. Mountford, *Organometallics*, 2010, **29**, 3602.

9. J. Ejfler, M. Kobylka, L. B. Jerzykiewicz and P. Sobota, *Dalton Trans.*, 2005, 2047.
10. J. Ejfler, K. Krauzy-Dziedzic, S. Szafert, L. B. Jerzykiewicz and P. Sobota, *Eur. J. Inorg. Chem.*, **2010**, 3602.
11. J. Ejfler, S. Szafert, K. Mierzwicki, L. B. Jerzykiewicz and P. Sobota, *Dalton Trans.*, 2008, 6556.
12. C. K. Williams, L. E. Breyfogle, S. K. Choi, W. Nam, V. G. Young, M. A. Hillmyer and W. B. Tolman, *J. Am. Chem. Soc.*, 2003, **125**, 11350.
13. I. Westmoreland and J. Arnold, *Dalton Trans.*, 2006, 4155.
14. P. I. Binda, E. E. Delbridge, H. B. Abrahamson and B. W. Skelton, *Dalton Trans.*, 2009, 2777.
15. E. Piedra-Arroni, P. Brignou, A. Amgoune, S. M. Guillaume, J.-F. Carpentier and D. Bourissou, *Chem. Commun.*, 2011, **47**, 9828.
16. A. Pietrangelo, M. A. Hillmyer and W. B. Tolman, *Chem. Commun.*, 2009, 2736.
17. A. Pietrangelo, S. C. Knight, A. K. Gupta, L. J. Yao, M. A. Hillmyer and W. B. Tolman, *J. Am. Chem. Soc.*, 2010, **132**, 11649.
18. P. I. Binda and E. E. Delbridge, *Dalton Trans.*, 2007, 4685.
19. D. A. Fletcher, R. F. McMeeking and D. Parkin, *J. Chem. Inf. Comput. Sci.*, 1996, **36**, 746 (The UK Chemical Database Service: CSD version 5.33 updated November 2011).
20. R. H. Platel, L. M. Hodgson and C. K. Williams, *Polym. Rev.*, 2008, **48**, 11.
21. N. Spassky, M. Wisniewski, C. Pluta and A. Le Borgne, *Macromol. Chem. Phys.*, 1996, **197**, 2627.
22. T. M. Ovitt and G. W. Coates, *J. Am. Chem. Soc.*, 1999, **121**, 4072.
23. T. M. Ovitt and G. W. Coates, *J. Polym. Sci., Part A: Polym. Chem.*, 2000, **38**, 4686.
24. T. M. Ovitt and G. W. Coates, *J. Am. Chem. Soc.*, 2002, **124**, 1316.
25. Z. Zhong, P. J. Dijkstra and J. Feijen, *Angew. Chem. Int. Ed.*, 2002, **41**, 4510.
26. Z. Zhong, P. J. Dijkstra and J. Feijen, *J. Am. Chem. Soc.*, 2003, **125**, 11291.
27. M. H. Chisholm, N. J. Patmore and Z. Zhou, *Chem. Commun.*, 2005, 127.
28. C. P. Radano, G. L. Baker and M. R. Smith, *J. Am. Chem. Soc.*, 2000, **122**, 1552.
29. K. Majerska and A. Duda, *J. Am. Chem. Soc.*, 2004, **126**, 1026.

30. P. A. Cameron, D. Jhurry, V. C. Gibson, A. J. P. White, D. J. Williams and S. Williams, *Macromol. Rapid Commun.*, 1999, **20**, 616.
31. P. Hormnirun, E. L. Marshall, V. C. Gibson, A. J. P. White and D. J. Williams, *J. Am. Chem. Soc.*, 2004, **126**, 2688.
32. N. Nomura, R. Ishii, M. Akakura and K. Aoi, *J. Am. Chem. Soc.*, 2002, **124**, 5938.
33. Z. Tang, X. Chen, X. Pang, Y. Yang, X. Zhang and X. Jing, *Biomacromolecules*, 2004, **5**, 965.
34. Z. Tang, X. Chen, Y. Yang, X. Pang, J. Sun, X. Zhang and X. Jing, *J. Polym. Sci., Part A: Polym. Chem.*, 2004, **42**, 5974.
35. Z. Tang, Y. Yang, X. Pang, J. Hu, X. Chen, N. Hu and X. Jing, *J. Appl. Polym. Sci.*, 2005, **98**, 102.
36. H. Du, X. Pang, H. Yu, X. Zhuang, X. Chen, D. Cui, X. Wang and X. Jing, *Macromolecules*, 2007, **40**, 1904.
37. H. Du, A. H. Velders, P. J. Dijkstra, Z. Zhong, X. Chen and J. Feijen, *Macromolecules*, 2009, **42**, 1058.
38. A. Bhaw-Luximon, D. Jhurry and N. Spassky, *Polym. Bull.*, 2000, **44**, 31.
39. D. Jhurry, A. Bhaw-Luximon and N. Spassky, *Macromol. Symp.*, 2001, **175**, 67.
40. H.-Y. Chen, H.-Y. Tang and C.-C. Lin, *Macromolecules*, 2006, **39**, 3745.

Chapter Six

Experimental details and characterising data

6.1 General methods and instrumentation

All air and moisture sensitive manipulations were carried out using standard dual manifold Schlenk-line and dry-box techniques under an atmosphere of argon or dinitrogen. Toluene and THF were pre-dried over activated 4 Å molecular sieves then heated to reflux over sodium (toluene) or potassium (THF) under a dinitrogen atmosphere and distilled. Pentane or hexanes were degassed by sparging with dinitogen and dried by passing through a column of activated alumina.[1, 2] Dried solvents were stored in glass ampoules fitted with J. Young Teflon stoppers. Deuterated solvents (Goss Scientific) were dried over potassium (C_6D_6 or THF-d_8) or sodium (toluene-d_8) at reflux then distilled under reduced pressure and stored under dinitrogen in glass ampoules fitted with J. Young Teflon stoppers. $CDCl_3$ (Sigma-Aldrich) was used as received for non-sensitive samples.

Solution NMR samples were prepared under a dinitrogen atmosphere in a dry-box in 5 mm Wilmad NMR 507-PP tubes fitted with J. Young Teflon valves. ^{1}H, ^{1}H-{^{1}H} and ^{13}C-{^{1}H} NMR spectra were recorded on Varian Mercury-VX 300, Varian Unity Plus 500 or Bruker AVII 500 (with a ^{13}C cryoprobe (27 and 32)) spectrometers at ambient temperature unless stated otherwise. ^{1}H and ^{13}C-{^{1}H} spectra were referenced internally to residual protio-solvent (^{1}H) or solvent (^{13}C) resonances, and are reported relative to tetramethylsilane (δ = 0 ppm). ^{1}H and ^{13}C assignments were assisted by the use of two-dimensional ^{1}H-^{1}H and ^{1}H-^{13}C correlation experiments. IR spectra were recorded on a Nicolet Magna 560 E.S.P FTIR spectrometer. Samples were prepared in a dry-box as Nujol mulls between NaCl plates. IR data are quoted as wavenumbers within the range 4000–400 cm^{-1}. Mass spectra were recorded by the departmental service, and elemental analyses were carried out by the Elemental Analysis Service at London Metropolitan University.

MALDI-ToF MS analysis was performed on a Waters MALDI micro equipped with a 337 nm nitrogen laser and an accelerating voltage of 25 kV was applied. The polymer samples were dissolved in THF at a concentration of 1.0 mg mL^{-1}. The cationisation agent used was potassium trifluoroacetate (Fluka, > 99%) dissolved in THF at a concentration of 5.0 mg mL^{-1}. The matrix used was *trans*-2-[3-(4-*tert*-butylphenyl)-2-methyl-2-propenylidene]malononitrile (DCTB) (Fluka) and was dissolved in THF at a concentration of 40 mg mL^{-1}. Solutions of matrix, salt and polymer were mixed in a volume ratio of 4:1:4, respectively. The mixed solution was hand spotted on a

stainless steel MALDI target and left to dry. The spectra were recorded in the reflectron mode.

Polymer molecular weights (M_w, M_n and PDI) were determined by GPC using a Polymer Laboratories PL-GPC50 Plus instrument equipped with a Polymer Laboratories Plgel Mixed-D column (300 mm length, 7.5 mm diameter) and a refractive index (RI) detector. Samples were dissolved in THF (Fisher, HPLC grade, stabilised with BHT, 2.5 ppm) at a concentration of 2.0 mg mL^{-1} and filtered prior to injection. THF (Fisher, HPLC grade, stabilised with BHT, 2.5 ppm) was used as the eluent at 30 °C and the flow rate was set to 1.0 mL min^{-1}. Linear polystyrenes (Polymer Laboratories) were used as the primary calibration standards and the appropriate Mark-Houwink corrections for poly(*rac*-LA) and poly(ε-CL) in THF at 30 °C were used to calculate the experimental molecular weights.[3, 4] Poly(*rac*-BBL) was treated as a polystyrene and experimental molecular weight values were not corrected.

6.2 Literature preparations and reagent purification

$ScCl_3(THF)_3$,[5] $LiCH_2SiMe_3$,[6] $Sc(CH_2SiMe_3)_3(THF)_2$,[7] $Y\{N(SiMe_3)_2\}_3$,[8] $Ln\{N(SiHMe_2)_2\}_3(THF)_2$ (Ln = Y or La),[9] $HO_2^{R2}N^L$ (R = ^{t}Bu or Me; L = NMe_2, OMe, py or Me),[10-14] $HON^{Me,Cy}$ [15], $HON^{Me,NMe2}$ [16] and $Y(O_2N^{NMe2})\{N(SiHMe_2)_2\}(THF)$ (**1.15**)[17] were synthesised according to or adapted from published procedures. ε-CL and *rac*-BBL were dried over freshly ground CaH_2 for at least three days and distilled under reduced pressure. The process was repeated for *rac*-BBL and purified liquid monomers were stored under dinitrogen in ampoules fitted with J. Young Teflon stoppers. *L*- and *rac*-LA were recrystallised twice from hot toluene solutions and dried *in vacuo*. The recrystallised products were then sublimed twice under reduced pressure with gradual heating in 10 °C increments from 50 °C to 90 °C. Crushed ice was used as the coolant and purified LA was stored in a dry-box and used within three weeks of being sublimed. $BnNH_2$, piperidine, $^nPrNH_2$, ^{i}PrOH, $Me_2NCH_2CH_2NH_2$ and tren were dried over freshly ground CaH_2 for at least three days and distilled under reduced pressure. BnOH (anhydrous, Sigma-Aldrich) was degassed prior to use. All liquid co-initiators were stored under dinitrogen in glass ampoules fitted with J. Young Teflon stoppers.

6.3 Experimental details and characterising data for Chapter Two

6.3.1 Synthesis

$Y(O_2N^{NMe2})(HO_2N^{NMe2})$ (1) originally prepared by Dr. Hellen E. Dyer. A solution of $H_2O_2N^{NMe2}$ (0.37 g, 0.70 mmol) in pentane (15 mL) was added dropwise to a stirring solution of $Y\{N(SiMe_3)_2\}_3$ (0.20 g, 0.35 mmol) in pentane (15 mL) at room temperature. The yellow reaction mixture was stirred for 16 h before the volatiles were removed under reduced pressure. The crude, yellow solids were dissolved in pentane (10 mL) and the solution was filtered. The filtrate was concentrated under reduced pressure and the title compound crystallised after refrigeration at −30 °C. The white, crystalline solids were isolated by filtration, washed with pentane (3 × 5 mL) then dried *in vacuo*. Yield = 0.26 g, 64%. $Y\{N(SiHMe_2)_2\}_3(THF)_2$ is also a suitable metal precursor. ^{1}H NMR (299.9 MHz, C_6D_6, 298 K) (*Superscript a or b denotes resonances corresponding to each phenolate side arm of the bidentate (phenolate)-amino ligand, whilst superscript c or d denote resonances corresponding to each phenolate side arm of the tetradentate bis(phenolate)-amino ligand.*): 8.74 (1H, br s, NH), 7.67 (1H, d, 3-$C_6\underline{H}_2{}^tBu_2{}^d$, ^4J = 3.0 Hz), 7.66 (1H, d, 3-$C_6\underline{H}_2{}^tBu_2{}^c$, ^4J = 3.0 Hz), 7.53 (1H, d, 3-$C_6\underline{H}_2{}^tBu_2{}^b$, ^4J = 3.0 Hz), 7.46 (1H, d, 3-$C_6\underline{H}_2{}^tBu_2{}^a$, ^4J = 3.0 Hz), 7.10 (1H, d, 5-$C_6\underline{H}_2{}^tBu_2{}^c$, ^4J = 3.0 Hz), 7.10 (1H, overlapping m, $ArCH_2{}^b$), 7.05 (1H, d, 5-$C_6\underline{H}_2{}^tBu_2{}^d$, ^4J = 3.0 Hz), 6.98 (1H, d, 5-$C_6\underline{H}_2{}^tBu_2{}^b$, ^4J = 3.0 Hz), 6.72 (1H, d, 5-$C_6\underline{H}_2{}^tBu_2{}^a$, ^4J = 3.0 Hz), 6.64 (1H, d, $ArCH_2{}^a$, ^2J = 12.0 Hz), 4.63 (1H, d, $ArCH_2{}^c$, ^2J = 12.0 Hz), 4.32 (1H, d, $ArCH_2{}^d$, ^2J = 12.0 Hz), 3.28 (2 × 1H, overlapping m, $ArCH_2{}^b$ and $CH_2C\underline{H}_2N(CH_3)_2{}^{cd}$), 3.02 (1H, d, $ArCH_2{}^c$, ^2J = 12.0 Hz), 2.95 (1H, overlapping m, $ArCH_2{}^a$), 2.85 (1H, d, $ArCH_2{}^d$, ^2J = 12.0 Hz), 2.77 (1H, overlapping m, $C\underline{H}_2CH_2N(CH_3)_2$), 2.29 (2 × 3H, br s, $N(CH_3)_2{}^{cd}$), 2.01 (2 × 3H, br s, $N(CH_3)_2{}^{ab}$), 1.89 (9H, s, 2-$C_6H_2{}^t\underline{Bu}_2{}^c$), 1.77 (9H, s, 2-$C_6H_2{}^t\underline{Bu}_2{}^b$), 1.68 (9H, s, 2-$C_6H_2{}^t\underline{Bu}_2{}^d$), 1.53 (9H, s, 2-$C_6H_2{}^t\underline{Bu}_2{}^a$), 1.47 (9H, s, 4-$C_6H_2{}^t\underline{Bu}_2{}^d$), 1.45 (9H, s, 4-$C_6H_2{}^t\underline{Bu}_2{}^c$), 1.36 (9H, s, 4-$C_6H_2{}^t\underline{Bu}_2{}^b$), 1.31 (9H, s, 4-$C_6H_2{}^t\underline{Bu}_2{}^a$) ppm. Remaining $C\underline{H}_2C\underline{H}_2N(CH_3)_2$ resonances could not be assigned. ^{13}C-{^{1}H} NMR (C_6D_6, 75.4 MHz, 298 K) (*Superscript a or b denotes resonances corresponding to each phenolate side arm of the bidentate (phenolate)-amino ligand, whilst superscript c or d denote resonances corresponding to each phenolate side arm of the tetradentate bis(phenolate)-amino ligand.*): 163.7 (q, d, 1-$\underline{C}_6H_2{}^tBu_2{}^c$, $^2J_{Y\text{-}C}$ = 2.9 Hz), 162.8 (q, d, 1-$\underline{C}_6H_2{}^tBu_2{}^b$, $^2J_{Y\text{-}C}$ = 4.6 Hz), 162.6 (q, d, 1-$\underline{C}_6H_2{}^tBu_2{}^d$, $^2J_{Y\text{-}C}$ = 1.5 Hz), 162.4 (q, d, 1-$\underline{C}_6H_2{}^tBu_2{}^a$, $^2J_{Y\text{-}C}$ = 4.6 Hz), 140.5 (q, 2-

$\underline{C}_6H_2{}^tBu_2{}^a$), 139.4 (q, 2-$\underline{C}_6H_2{}^tBu_2{}^b$), 138.8 (q, 4-$\underline{C}_6H_2{}^tBu_2{}^a$), 137.0 (q, 4-$\underline{C}_6H_2{}^tBu_2{}^b$), 136.6 (q, 2-$\underline{C}_6H_2{}^tBu_2{}^c$), 136.5 (q, 4-$\underline{C}_6H_2{}^tBu_2{}^d$), 136.2 (q, 4-$\underline{C}_6H_2{}^tBu_2{}^c$), 135.9 (q, 2-$\underline{C}_6H_2{}^tBu_2{}^d$), 127.2 (5-$\underline{C}_6H_2{}^tBu_2{}^d$), 126.2 (3-$\underline{C}_6H_2{}^tBu_2{}^a$), 125.6 (3-$\underline{C}_6H_2{}^tBu_2{}^b$), 125.3 (5-$\underline{C}_6H_2{}^tBu_2{}^c$), 125.2 (q, 6-$\underline{C}_6H_2{}^tBu_2{}^d$), 125.0 (5-$\underline{C}_6H_2{}^tBu_2{}^b$), 124.9 (q, 6-$\underline{C}_6H_2{}^tBu_2{}^c$), 124.8 (3-$\underline{C}_6H_2{}^tBu_2{}^d$), 124.4 (5-$\underline{C}_6H_2{}^tBu_2{}^a$), 123.6 (3-$\underline{C}_6H_2{}^tBu_2{}^c$), 122.3 (q, 6-$\underline{C}_6H_2{}^tBu_2{}^a$), 120.7 (q, 6-$\underline{C}_6H_2{}^tBu_2{}^b$), 66.0 ($CH_2\underline{C}H_2N(CH_3)_2{}^{cd}$), 64.7 ($CH_2\underline{C}H_2N(CH_3)_2{}^{ab}$), 63.2 ($ArCH_2{}^c$), 62.7 ($ArCH_2{}^d$), 60.8 ($ArCH_2{}^b$), 60.6 ($N(CH_3)_2{}^{cd}$), 60.4 ($ArCH_2{}^a$), 56.7 ($N(CH_3)_2{}^{cd}$), 55.7 ($N(CH_3)_2{}^{ab}$), 55.5 ($N(CH_3)_2{}^{ab}$), 51.4 ($\underline{C}H_2CH_2N(CH_3)_2{}^{ab}$), 48.0 ($\underline{C}H_2CH_2N(CH_3)_2{}^{cd}$), 36.2 (q, 2-$\underline{C}(CH_3)_3{}^c$), 35.9 (q, 2-$\underline{C}(CH_3)_3{}^b$), 35.8 (q, 2-$\underline{C}(CH_3)_3{}^a$), 35.4 (q, 2-$\underline{C}(CH_3)_3{}^d$), 34.3 (q, 4-$\underline{C}(CH_3)_3{}^d$), 34.1 (q, 4-$\underline{C}(CH_3)_3{}^{a\text{ and }c}$), 34.0 (q, 4-$\underline{C}(CH_3)_3{}^b$), 32.3 (4-C($\underline{C}H_3)_3{}^{c\text{ and }d}$), 32.2 (4-C($\underline{C}H_3)_3{}^b$), 31.9 (4-C($\underline{C}H_3)_3{}^a$), 31.7 (2-C($\underline{C}H_3)_3{}^d$), 31.2 (2-C($\underline{C}H_3)_3{}^c$), 31.0 (2-C($\underline{C}H_3)_3{}^b$), 30.0 (2-C($\underline{C}H_3)_3{}^a$) ppm. IR (NaCl plates, Nujol mull): 1606(w), 1413(s), 1362(s), 1327(w), 1299(s), 1239(m), 1206(w), 1206(w), 1173(w), 1136(w), 1116(w), 1043(w), 1026(w), 876(w), 834(m), 776 (w), 665(m) cm^{-1}. EI-MS *m/z*: 612 (40%, $[M - C_{34}H_{55}N_2O_2]^+$). Anal. found (Calcd. for $C_{68}H_{109}N_4O_4Y$): C, 72.00 (71.93); H, 4.89 (4.93); N, 9.70 (9.67) %. Single crystals suitable for X-ray diffraction were grown from a saturated pentane solution at −30 °C.

$Y(O_2N^{OMe})(HO_2N^{OMe})$ (2) originally prepared by Dr. Hellen E. Dyer. A solution of $H_2O_2N^{OMe}$ (0.36 g, 0.70 mmol) in pentane (15 mL) was added dropwise to a stirring solution of $Y\{N(SiMe_3)_2\}_3$ (0.20 g, 0.35 mmol) in pentane (15 mL) at room temperature. The yellow reaction mixture was stirred for 16 h before the volatiles were removed under reduced pressure. The crude yellow solids were dissolved in pentane (10 mL) and the solution filtered. The filtrate was concentrated under reduced pressure and the title compound crystallised after refrigeration at –30 °C. The white, crystalline solids were isolated by filtration, washed with pentane (3 × 5 mL) then dried *in vacuo*. Yield = 0.30 g, 76%. $Y\{N(SiHMe_2)_2\}_3(THF)_2$ is also a suitable metal precursor. ^{1}H NMR (499.9 MHz, toluene-d_8, 248 K) (*Superscript a or b denotes resonances corresponding to each phenolate side arm of the bidentate (phenolate)-amino ligand, whilst superscript c or d denote resonances corresponding to each phenolate side arm of the tetradentate bis(phenolate)-amino ligand.*): 9.07 (1H, br s, NH), 7.70 (1H, d, 3-$C_6\underline{H}_2{}^tBu_2{}^d$, ^4J = 5.0 Hz), 7.68 (1H, d, 3-$C_6\underline{H}_2{}^tBu_2{}^c$, ^4J = 5.0 Hz), 7.57 (1H, d, 3-$C_6\underline{H}_2{}^tBu_2{}^b$, ^4J = 5.0 Hz), 7.45 (1H, d, 3-$C_6\underline{H}_2{}^tBu_2{}^a$, ^4J = 5.0 Hz), 7.16

(1H, overlapping m, 5-$C_6\underline{H}_2{}^tBu_2{}^c$), 7.10 (1H, d, 5-$C_6\underline{H}_2{}^tBu_2{}^d$, ^4J = 5.0 Hz), 6.99 (1H, d, 5-$C_6\underline{H}_2{}^tBu_2{}^b$, ^4J = 5.0 Hz), 6.84 (1H, d, $ArCH_2{}^b$, ^2J = 10.0 Hz), 6.80 (1H, d, 5-$C_6\underline{H}_2{}^tBu_2{}^a$, ^4J = 5.0 Hz), 6.34 (1H, d, $ArCH_2{}^a$, ^2J = 10.0 Hz), 4.72 (1H, d, $ArCH_2{}^c$, ^2J = 15.0 Hz), 4.22 (1H, d, $ArCH_2{}^d$, ^2J = 15.0 Hz), 3.54 (1H, ddd, $CH_2C\underline{H}_2OCH_3{}^{cd}$, ^2J = 10.0 Hz, ^3J = 5.0 Hz, ^3J = 5.0 Hz), 3.22 (1H, d, $ArCH_2{}^b$, ^2J = 10.0 Hz), 3.01 (1H, d, $ArCH_2{}^c$, ^2J = 15.0 Hz), 2.96 (1H, d, $ArCH_2{}^a$, ^2J = 10.0 Hz), 2.80 (1H, d, $ArCH_2{}^d$, ^2J = 15.0 Hz), 2.74 (1H, overlapping m, $C\underline{H}_2CH_2OCH_3$), 2.73 (3H, s, $OCH_3{}^{cd}$), 2.46 (3H, s, $OCH_3{}^{ab}$), 2.26 (1H, overlapping m, $C\underline{H}_2CH_2OCH_3{}^{ab}$), 2.26 (1H, overlapping m, $CH_2C\underline{H}_2OCH_3{}^{ab}$), 2.17 (1H, ddd, $C\underline{H}_2CH_2OCH_3{}^{cd}$, ^2J = 10.0 Hz, ^3J = 5.0 Hz, ^3J = 5.0 Hz), 2.09 (1H, overlapping m, $C\underline{H}_2CH_2OCH_3{}^{ab}$), 2.06 (1H, overlapping m, $CH_2C\underline{H}_2OCH_3{}^{ab}$), 2.02 (1H, ddd, $CH_2C\underline{H}_2OCH_3{}^{cd}$, ^2J = 10.0 Hz, ^3J = 5.0 Hz, ^3J = 5.0 Hz), 1.93 (9H, s, 2-$C_6H_2{}^t\underline{Bu}_2{}^c$), 1.79 (9H, s, 2-$C_6H_2{}^t\underline{Bu}_2{}^b$), 1.67 (9H, s, 2-$C_6H_2{}^t\underline{Bu}_2{}^d$), 1.55 (9H, s, 2-$C_6H_2{}^t\underline{Bu}_2{}^a$), 1.51 (9H, s, 4-$C_6H_2{}^t\underline{Bu}_2{}^d$), 1.48 (9H, s, 4-$C_6H_2{}^t\underline{Bu}_2{}^c$), 1.37 (9H, s, 4-$C_6H_2{}^t\underline{Bu}_2{}^b$), 1.37 (9H, s, 4-$C_6H_2{}^t\underline{Bu}_2{}^a$) ppm. ^{13}C-{^1H} NMR (125.7 MHz, toluene-d_8, 248 K) (*Superscript a or b denotes resonances corresponding to each phenolate side arm of the bidentate (phenolate)-amino ligand, whilst superscript c or d denote resonances corresponding to each phenolate side arm of the tetradentate bis(phenolate)-amino ligand.*): 162.8 (q, d, 1-$\underline{C}_6H_2{}^tBu_2{}^c$, $^2J_{Y\text{-}C}$ = 2.9 Hz), 162.5 (q, d, 1-$\underline{C}_6H_2{}^tBu_2{}^b$, $^2J_{Y\text{-}C}$ = 4.6 Hz), 162.4 (q, d, 1-$\underline{C}_6H_2{}^tBu_2{}^d$, $^2J_{Y\text{-}C}$ = 1.5 Hz), 162.2 (q, d, 1-$\underline{C}_6H_2{}^tBu_2{}^a$, $^2J_{Y\text{-}C}$ = 4.6 Hz), 139.4 (q, 2-$\underline{C}_6H_2{}^tBu_2{}^a$), 138.6 (q, 2-$\underline{C}_6H_2{}^tBu_2{}^b$), 136.8 (q, 4-$\underline{C}_6H_2{}^tBu_2{}^a$), 136.5 (q, 4-$\underline{C}_6H_2{}^tBu_2{}^b$), 136.0 (q, 2-$\underline{C}_6H_2{}^tBu_2{}^c$), 135.8 (q, 4-$\underline{C}_6H_2{}^tBu_2{}^d$), 135.4 (q, 4-$\underline{C}_6H_2{}^tBu_2{}^c$), 135.3 (q, 2-$\underline{C}_6H_2{}^tBu_2{}^d$), 127.2 (5-$\underline{C}_6H_2{}^tBu_2{}^d$), 125.8 (3-$\underline{C}_6H_2{}^tBu_2{}^a$), 125.6 (3-$\underline{C}_6H_2{}^tBu_2{}^b$), 125.6 (5-$\underline{C}_6H_2{}^tBu_2{}^c$), 125.4 (q, 6-$\underline{C}_6H_2{}^tBu_2{}^d$), 124.9 (5-$\underline{C}_6H_2{}^tBu_2{}^b$), 124.6 (q, 6-$\underline{C}_6H_2{}^tBu_2{}^c$), 124.5 (3-$\underline{C}_6H_2{}^tBu_2{}^d$), 124.3 (5-$\underline{C}_6H_2{}^tBu_2{}^a$), 123.8 (3-$\underline{C}_6H_2{}^tBu_2{}^c$), 120.2 (q, 6-$\underline{C}_6H_2{}^tBu_2{}^a$), 120.2 (q, 6-$\underline{C}_6H_2{}^tBu_2{}^b$), 73.4 ($CH_2\underline{C}H_2OCH_3{}^{cd}$), 66.0 ($CH_2\underline{C}H_2OCH_3{}^{ab}$), 65.8 ($ArCH_2{}^c$), 64.3 ($ArCH_2{}^d$), 63.2 ($ArCH_2{}^b$), 62.2 ($ArCH_2{}^a$), 60.7 ($OCH_3{}^{cd}$), 58.0 ($OCH_3{}^{ab}$), 51.5 ($\underline{C}H_2CH_2OCH_3{}^{ab}$), 48.1 ($\underline{C}H_2CH_2OCH_3{}^{cd}$), 36.0 (q, 2-$\underline{C}(CH_3)_3{}^c$), 35.8 (q, 2-$\underline{C}(CH_3)_3{}^b$), 35.6 (q, 2-$\underline{C}(CH_3)_3{}^a$), 35.6 (q, 2-$\underline{C}(CH_3)_3{}^d$), 34.1 (q, 4-$\underline{C}(CH_3)_3{}^d$), 34.1 (q, 4-$\underline{C}(CH_3)_3{}^c$), 34.0 (q, 4-$\underline{C}(CH_3)_3{}^a$), 34.0 (q, 4-$\underline{C}(CH_3)_3{}^b$), 32.2 (4-$C(\underline{C}H_3)_3{}^c$), 32.2 (4-$C(\underline{C}H_3)_3{}^d$), 31.9 (4-$C(\underline{C}H_3)_3{}^b$), 31.9 (4-$C(\underline{C}H_3)_3{}^a$), 31.5 (2-$C(\underline{C}H_3)_3{}^d$), 30.9 (2-$C(\underline{C}H_3)_3{}^c$), 30.8 (2-$C(\underline{C}H_3)_3{}^b$), 30.6 (2-$C(\underline{C}H_3)_3{}^a$) ppm. IR (NaCl plates, Nujol mull): 1606(m), 1413(s), 1361(s), 1325(s), 1205(s), 1185(m), 1165(s), 1136(s), 1121(m), 1026(m), 1001(w), 912(m), 873(s), 835(s), 744(s), 665(w), 644(s) cm^{-1}. EI-MS *m/z*: 612 (5%, $[M - C_{33}H_{52}NO_3]^+$). Anal.

found (Calcd. for $C_{66}H_{103}N_2O_6Y$): C, 71.42 (71.45); H, 9.45 (9.36); N, 2.60 (2.52) %. Single crystals suitable for X-ray diffraction were grown from a saturated pentane solution at −30 °C.

$Y(O_2N^{Me})(HO_2N^{Me})$ (3). A solution of HO_2N^{Me} (0.63 g, 1.27 mmol) in pentane (10 mL) was added dropwise to a stirring solution of $Y\{N(SiHMe_2)_2\}_3(THF)_2$ (0.40 g, 0.63 mmol) in pentane (10 mL) at room temperature. After stirring for 16 h the volatiles were removed under reduced pressure. The crude solids were dissolved in pentane (10 mL) and the solution was filtered before being concentrated under reduced pressure. The solution was refrigerated (4 °C) and the title compound crystallised as a white solid, which was isolated by filtration, washed with pentane (2 × 5 mL) and dried *in vacuo*. Yield = 0.35 g, 51%. ^{1}H NMR (500.3 MHz, C_6D_6, 298 K): 9.48 (1H, br s, NH), 7.58 (1H, d, 3- or 5-$C_6\underline{H}_2{}^tBu_2$, ^4J = 5.0 Hz), 7.57 (1H, d, 3- or 5-$C_6\underline{H}_2{}^tBu_2$, ^4J = 5.0 Hz), 7.54 (1H, d, 3- or 5-$C_6\underline{H}_2{}^tBu_2$, ^4J = 5.0 Hz), 7.45 (1H, d, 3- or 5-$C_6\underline{H}_2{}^tBu_2$, ^4J = 5.0 Hz), 7.23 (1H, d, 5-$C_6\underline{H}_2{}^tBu_2$, ^4J = 5.0 Hz), 6.92 (1H, d, 3- or 5-$C_6\underline{H}_2{}^tBu_2$, ^4J = 5.0 Hz), 6.82 (1H, d, 3- or 5-$C_6\underline{H}_2{}^tBu_2$, ^4J = 5.0 Hz), 6.74 (1H, d, 3- or 5-$C_6\underline{H}_2{}^tBu_2$, ^4J = 5.0 Hz), 5.03 (1H, br s, $ArCH_2{}^a$), 4.04 (1H, br s, $ArCH_2{}^b$), 3.72 (1H, br s, $ArCH_2{}^b$), 3.16 (1H, br s, $ArCH_2{}^d$), 3.07 (1H, app t, $ArCH_2{}^c$, ^3J = 5.0 Hz), 2.92 (1H, app t, $ArCH_2{}^a$, ^3J = 5.0 Hz, two remaining $ArCH_2$ obscured), 2.58 (2H, br s, $C\underline{H}_2CH_2CH_3{}^a$), 2.09 (2H, br s, $C\underline{H}_2CH_2CH_3{}^b$), 1.83 (9H, s, $C_6H_2{}^t\underline{Bu}_2$), 1.77 (9H, s, $C_6H_2{}^t\underline{Bu}_2$), 1.49 (9H, s, $C_6H_2{}^t\underline{Bu}_2$), 1.48 (9H, s, $C_6H_2{}^t\underline{Bu}_2$), 1.42 (9H, s, $C_6H_2{}^t\underline{Bu}_2$), 1.38 (9H, s, $C_6H_2{}^t\underline{Bu}_2$), 1.35 (9H, s, $C_6H_2{}^t\underline{Bu}_2$), 1.28 (9H, s, $C_6H_2{}^t\underline{Bu}_2$), 1.26 (2H, overlapping, $CH_2C\underline{H}_2CH_3{}^b$), 0.59 (2H, br s, $CH_2C\underline{H}_2CH_3{}^a$), 0.41 (3H, t, $CH_2CH_2C\underline{H}_3{}^b$, ^3J = 5.0 Hz), 0.11 (3H, t, $CH_2CH_2C\underline{H}_3{}^a$, ^3J = 5.0 Hz) ppm. ^{13}C-{^{1}H} NMR (125.8 MHz, C_6D_6, 298 K): 162.3 (q, d, 1-$\underline{C}_6H_2{}^tBu_2$, $^2J_{Y\text{-}C}$ = 2.5 Hz), 161.6 (q, d, 1-$\underline{C}_6H_2{}^tBu_2$, $^2J_{Y\text{-}C}$ = 2.5 Hz), 161.4 (q, 1-$\underline{C}_6H_2{}^tBu_2$), 160.9 (q, 1-$\underline{C}_6H_2{}^tBu_2$), 138.6 (q, 2- or 4-$\underline{C}_6H_2{}^tBu_2$), 138.3 (q, 2- or 4-$\underline{C}_6H_2{}^tBu_2$), 138.2 (q, 2- or 4-$\underline{C}_6H_2{}^tBu_2$), 137.8 (q, 2- or 4-$\underline{C}_6H_2{}^tBu_2$), 137.4 (q, 2- or 4-$\underline{C}_6H_2{}^tBu_2$), 137.1 (q, 2- or 4-$\underline{C}_6H_2{}^tBu_2$), 136.4 (q, 2- or 4-$\underline{C}_6H_2{}^tBu_2$), 135.9 (q, 2- or 4-$\underline{C}_6H_2{}^tBu_2$), 126.3 (two overlapping, 3- or 5-$\underline{C}_6H_2{}^tBu_2$, couples to ^{1}H 3- or 5-$\underline{C}_6H_2{}^tBu_2$ at 7.45 and 6.92 ppm), 125.8 (3- or 5-$\underline{C}_6H_2{}^tBu_2$, couples to ^{1}H at 7.23 ppm), 125.6 (3- or 5-$\underline{C}_6H_2{}^tBu_2$, couples to ^{1}H at 7.57 ppm), 124.6 (two overlapping, 3- or 5-$\underline{C}_6H_2{}^tBu_2$, couples to ^{1}H at 6.82 and 6.74 ppm), 124.4 (q, 6-$\underline{C}_6H_2{}^tBu_2$), 124.3 (3- or 5-$\underline{C}_6H_2{}^tBu_2$, couples to ^{1}H at 7.58 ppm), 124.2 (q, 6-$\underline{C}_6H_2{}^tBu_2$), 123.5 (3- or 5-$\underline{C}_6H_2{}^tBu_2$, couples to ^{1}H at 7.54 ppm), 119.1 (q, 6-

$\underline{C}_6H_2{}^tBu_2$) and 118.8 (q, 6-$\underline{C}_6H_2{}^tBu_2$) ppm. 3- and 5-$\underline{C}_6H_2{}^tBu_2$ ^{1}H and ^{13}C aryl resonances are paired, with arbitrary aryl ring assignment as follows. Aryl ring 1: ^{1}H 7.23 ppm and ^{13}C 125.8 ppm with ^{1}H 7.59 ppm and ^{13}C 124.3 ppm. Aryl ring 2: ^{1}H 7.54 ppm and ^{13}C 123.5 ppm with ^{1}H 6.92 ppm and ^{13}C 126.3 ppm. Aryl ring 3: ^{1}H 7.57 ppm and ^{13}C 125.6 ppm with ^{1}H 6.82 ppm and ^{13}C 124.6 ppm. Aryl ring 4: ^{1}H 7.45 ppm and ^{13}C 126.3 ppm with ^{1}H 6.74 ppm and ^{13}C 124.6 ppm. 62.0 ($ArCH_2{}^c$), 61.2 ($ArCH_2{}^a$), 59.2 ($ArCH_2{}^b$, remaining $ArCH_2{}^d$ obscured), 56.5 ($\underline{C}H_2CH_2CH_3{}^b$), 54.0 ($\underline{C}H_2CH_2CH_3{}^a$), 35.8 ($\underline{C}(CH_3)_3$), 35.7 ($\underline{C}(CH_3)_3$), 35.1 ($\underline{C}(CH_3)_3$), 34.2 ($\underline{C}(CH_3)_3$), 34.2 ($\underline{C}(CH_3)_3$), 34.1 ($\underline{C}(CH_3)_3$, couples to ^{1}H at 6.82 ppm), 34.1 ($\underline{C}(CH_3)_3$, couples to ^{1}H at 6.74 ppm), 32.2 ($C(\underline{C}H_3)_3$), 32.1 (($C(\underline{C}H_3)_3$), couples to ^{1}H at 1.42 ppm), 32.0 (($C(\underline{C}H_3)_3$), couples to ^{1}H at 1.35 ppm), 31.8 (($C(\underline{C}H_3)_3$), couples to ^{1}H at 1.28 ppm), 31.2 ($C(\underline{C}H_3)_3$), 31.1 ($C(\underline{C}H_3)_3$), 30.6 ($C(\underline{C}H_3)_3$), 30.5 ($C(\underline{C}H_3)_3$), 18.5 ($CH_2\underline{C}H_2CH_3{}^a$), 13.6 ($CH_2\underline{C}H_2CH_3{}^b$), 11.6 ($CH_2CH_2\underline{C}H_3{}^b$), 10.4 ($CH_2CH_2\underline{C}H_3{}^a$) ppm. IR (NaCl plates, Nujol mull): 1604(m), 1299(s), 1273(s), 1237(s), 1203(s), 1167(m), 1133(m), 1026(m), 911(m), 878(m), 837(s), 779(s) cm^{-1}. EI-MS *m/z*: 207 (50%, $[C_{14}H_{22}O]^+$). Anal. found (Calcd. for $C_{66}H_{103}N_2O_4Y$): C, 73.36 (73.57); H, 9.64 (9.69); N, 2.60 (2.48) %. Single crystals suitable for X-ray analysis were grown from a saturated pentane solution at 4 °C.

Sc(O_2N^{py})(HO_2N^{py}) (4). A solution of $H_2O_2N^{py}$ (0.73 g, 1.33 mmol) in THF (15 mL) at −78 °C was added dropwise to a stirring solution of $Sc(CH_2SiMe_3)_3(THF)_2$ (0.30 g, 0.67 mmol) in THF (15 mL) at −78 °C. The reaction mixture was allowed to warm to room temperature and stirred for 16 h, after which time the solvent volume was reduced to a minimum (1 mL) under reduced pressure. Pentane (15 mL) was added and the title compound precipitated as a white solid. The solids were isolated by filtration, washed with pentane (3 × 5 mL) then dried *in vacuo*. Yield = 0.32 g, 43%. ^{1}H NMR (299.9 MHz, C_6D_6, 298 K): 10.9 (1H, br s, NH), 8.55 (1H, d, 6-C_5H_4N, ^3J = 3.0 Hz), 8.08 (1H, d, 6-C_5H_4N, ^3J = 3.0 Hz), 7.74 (1H, d, 3- or 5-$C_6\underline{H}_2{}^tBu_2$, ^4J = 3.0 Hz), 7.66 (1H, d, 3- or 5-$C_6\underline{H}_2{}^tBu_2$, ^4J = 3.0 Hz), 7.59 (1H, d, 3- or 5-$C_6\underline{H}_2{}^tBu_2$, ^4J = 3.0 Hz), 7.55 (1H, d, 3- or 5-$C_6\underline{H}_2{}^tBu_2$, ^4J = 3.0 Hz), 7.43 (1H, d, 3- or 5-$C_6\underline{H}_2{}^tBu_2$, ^4J = 3.0 Hz), 7.38 (1H, d, 3- or 5-$C_6\underline{H}_2{}^tBu_2$, ^4J = 3.0 Hz), 6.90 (1H, t, 4-C_5H_4N, ^3J = 6.0 Hz), 6.90 (1H, t, 4-C_5H_4N, ^3J = 6.0 Hz), 6.67 (1H, d, 3- or 5-$C_6\underline{H}_2{}^tBu_2$, ^4J = 3.0 Hz), 6.63 (1H, app t, 5-C_5H_4N, ^3J = 6.0 Hz), 6.58 (1H, d, 3- or 5-$C_6\underline{H}_2{}^tBu_2$, ^4J = 3.0 Hz), 6.54 (1H, d, 3-C_5H_4N, ^3J = 9.0 Hz), 6.30 (1H, app t, 5-C_5H_4N, ^3J = 6.0 Hz), 6.17 (1H,

d, 3-C_5H_4N, ^3J = 9.0 Hz), 5.50 (1H, d, $ArCH_2^a$, ^2J = 12.0 Hz), 5.38 (1H, d, $ArCH_2^b$, ^2J = 12.0 Hz), 5.24 (1H, d, $ArCH_2^c$, ^2J = 12.0 Hz), 4.88 (1H, d, $ArCH_2^a$, ^2J = 12.0 Hz), 4.79 (1H, d, $C\underline{H}_2^dC_5H_4N$, ^2J = 15.0 Hz), 4.69 (1H, d, $ArCH_2^e$, ^2J = 15.0 Hz), 4.48 (1H, d, $C\underline{H}_2^dC_5H_4N$, ^2J = 15.0 Hz), 4.34 (1H, d, $C\underline{H}_2^fC_5H_4N$, ^2J = 12.0 Hz), 3.85 (1H, d, $ArCH_2^b$, ^2J = 12.0 Hz), 3.81 (1H, d, $ArCH_2^c$, ^2J = 12.0 Hz), 3.77 (1H, d, $C\underline{H}_2^fC_5H_4N$, ^2J = 12.0 Hz), 3.64 (1H, d, $ArCH_2^e$, ^2J = 15.0 Hz), 1.61 (9H, s, $C_6H_2{}^t\underline{Bu}_2$), 1.58 (9H, s, $C_6H_2{}^t\underline{Bu}_2$), 1.53 (9H, s, $C_6H_2{}^t\underline{Bu}_2$), 1.44 (9H, s, $C_6H_2{}^t\underline{Bu}_2$), 1.40 (9H, s, $C_6H_2{}^t\underline{Bu}_2$), 1.35 (9H, s, $C_6H_2{}^t\underline{Bu}_2$), 1.26 (9H, s, $C_6H_2{}^t\underline{Bu}_2$), 1.20 (9H, s, $C_6H_2{}^t\underline{Bu}_2$) ppm. ^{13}C-{^1H} NMR (75.4 MHz, C_6D_6, 298 K): 161.8 (q, 1-$\underline{C}_6H_2{}^tBu_2$), 161.3 (q, 1-$\underline{C}_6H_2{}^tBu_2$), 161.2 (q, 1-$\underline{C}_6H_2{}^tBu_2$), 157.5 (q, 2-$C_5H_4N$), 157.0 (q, 2-$C_5H_4N$), 148.8 (6-$C_5H_4N$), 148.6 (6-$C_5H_4N$), 141.7 (q, 2- or 4-$\underline{C}_6H_2{}^tBu_2$), 138.7 (q, 2- or 4-$\underline{C}_6H_2{}^tBu_2$), 138.1 (4-$C_5H_4N$), 137.8 (4-$C_5H_4N$), 136.7 (q, 2- or 4-$\underline{C}_6H_2{}^tBu_2$), 136.5 (q, 2- or 4-$\underline{C}_6H_2{}^tBu_2$), 136.4 (q, 2- or 4-$\underline{C}_6H_2{}^tBu_2$), 135.1 (q, 2- or 4-$\underline{C}_6H_2{}^tBu_2$), 134.4 (q, 2- or 4-$\underline{C}_6H_2{}^tBu_2$), 127.5 (3- or 5-$\underline{C}_6H_2{}^tBu_2$), 127.1 (3- or 5-$\underline{C}_6H_2{}^tBu_2$), 125.8 (3-$C_5H_4N$), 125.5 (5-$C_5H_4N$), 125.3 (3- or 5-$\underline{C}_6H_2{}^tBu_2$), 125.1 (3-$C_5H_4N$), 124.6 (3- or 5-$\underline{C}_6H_2{}^tBu_2$), 124.4 (3- or 5-$\underline{C}_6H_2{}^tBu_2$), 123.6 (3- or 5-$\underline{C}_6H_2{}^tBu_2$), 123.5 (q, 6-$\underline{C}_6H_2{}^tBu_2$), 123.3 (q, 6-$\underline{C}_6H_2{}^tBu_2$), 122.7 (3- or 5-$\underline{C}_6H_2{}^tBu_2$), 121.8 (3- or 5-$\underline{C}_6H_2{}^tBu_2$), 121.6 (5-$C_5H_4N$), 117.7 (q, 6-$\underline{C}_6H_2{}^tBu_2$), 60.8 ($ArCH_2^c$), 60.1 ($ArCH_2^a$), 59.2 ($ArCH_2^b$), 58.2 ($ArCH_2^e$), 50.7 ($\underline{C}H_2^fC_5H_4N$), 46.3 ($\underline{C}H_2^dC_5H_4N$), 35.5 (2-$\underline{C}(CH_3)_3$), 35.4 (2-$\underline{C}(CH_3)_3$), 35.3 (2-$\underline{C}(CH_3)_3$), 35.2 (2-$\underline{C}(CH_3)_3$), 34.6 (4-$\underline{C}(CH_3)_3$), 34.5 (4-$\underline{C}(CH_3)_3$), 34.4 (4-$\underline{C}(CH_3)_3$), 34.0 (4-$\underline{C}(CH_3)_3$), 32.2 (4-C($\underline{C}H_3)_3$), 32.1 (4-C($\underline{C}H_3)_3$), 32.0 (4-C($\underline{C}H_3)_3$), 31.9 (4-C($\underline{C}H_3)_3$), 30.3 (2-C($\underline{C}H_3)_3$), 30.1 (2-C($\underline{C}H_3)_3$), 30.0 (2-C($\underline{C}H_3)_3$), 29.9 (2-C($\underline{C}H_3)_3$) ppm. Remaining quaternary (q, 1-$C_6H_2{}^tBu_2$ and q, 6-$C_6H_2{}^tBu_2$) were not observed or are overlapping. IR (NaCl plates, Nujol mull): 1606(w), 1309(s), 1277(s), 1239(m), 1203(m), 1186(m), 1168(m), 1134(m), 1021(m), 973(w), 883(m), 748(s) cm^{-1}. EI-MS *m/z*: 693 (100%, $[M - C_{30}H_{45}O_2]^+$). Anal. found (Calcd. for $C_{72}H_{101}N_4O_4Sc$): C, 76.43 (76.42); H, 8.88 (9.00); N, 4.96 (4.95) %.

$Sc(O_2{}^{Me2}N^{py})(HO_2{}^{Me2}N^{py})$ (5). A solution of $H_2O_2{}^{Me2}N^{py}$ (0.50 g, 1.33 mmol) in THF (15 mL) at −78 °C was added dropwise to a stirring solution of $Sc(CH_2SiMe_3)_3(THF)_2$ (0.30 g, 0.67 mmol) in THF (15 mL) at −78 °C. The reaction mixture was allowed to warm to room temperature and stirred for 16 h, after which time the solvent volume was reduced to a minimum (1 mL) under reduced pressure. Pentane (15 mL) was added and the title compound precipitated as a white solid. The solids were isolated

by filtration, washed with pentane (3 × 5 mL) then dried *in vacuo*. Yield = 0.21 g, 40%. ^{1}H NMR (500.3 MHz, C_6D_6, 298 K): 11.2 (1H, br s, NH), 8.37 (1H, s, 6-C_5H_4N), 8.24 (1H, s, 6-C_5H_4N), 7.17 (1H, s, 3-$C_6\underline{H}_2Me_2$), 7.06 (1H, s, 3-$C_6\underline{H}_2Me_2$), 6.95 (1H, s, 3-$C_6\underline{H}_2Me_2$), 6.90 (1H, s, 5-$C_6\underline{H}_2Me_2$), 6.78 (1H, m, 4-C_5H_4N), 6.68 (1H, s, 5-$C_6\underline{H}_2Me_2$), 6.57 (1H, s, 3-$C_6\underline{H}_2Me_2$), 6.51 (1H, s, 5-$C_6\underline{H}_2Me_2$), 6.47 (1H, s, 5-C_5H_4N), 6.41 (1H, m, 4-C_5H_4N), 6.34 (1H, s, 5-$C_6\underline{H}_2Me_2$), 6.23 (1H, d, 3-C_5H_4N, ^{3}J = 5.0 Hz), 6.09 (1H, m, $ArCH_2^{a}$, ^{2}J = 10.0 Hz), 6.05 (1H, overlapping m, $ArCH_2^{b}$), 6.03 (1H, s, 5-C_5H_4N), 5.72 (1H, d, 3-C_5H_4N, ^{3}J = 5.0 Hz), 5.25 (1H, d, $ArCH_2^{c}$, ^{2}J = 10.0 Hz), 4.43 (1H, d, $ArCH_2^{d}$, ^{2}J = 10.0 Hz), 4.26 (1H, app t, $ArCH_2^{a}$, ^{2}J = 10.0 Hz), 4.15 (1H, d, $C\underline{H}_2^{e}C_5H_4N$, ^{2}J = 15.0 Hz), 3.73 (1H, app t, $ArCH_2^{b}$, ^{2}J = 10.0 Hz), 3.34 (1H, d, $C\underline{H}_2^{f}C_5H_4N$, ^{2}J = 10.0 Hz), 3.22 (1H, d, $C\underline{H}_2^{f}C_5H_4N$, ^{2}J = 10.0 Hz), 3.22 (1H, d, $ArCH_2^{c}$, ^{2}J = 10.0 Hz), 2.89 (3H, s, 2-$C_6H_2\underline{Me}_2$), 2.76 (1H, d, $ArCH_2^{d}$, ^{2}J = 10.0 Hz), 2.66 (1H, d, $C\underline{H}_2^{e}C_5H_4N$, ^{2}J = 15.0 Hz), 2.61 (3H, s, 2-$C_6H_2\underline{Me}_2$), 2.53 (3H, s, 2-$C_6H_2\underline{Me}_2$), 2.40 (3H, s, 4-$C_6H_2\underline{Me}_2$), 2.21 (3H, s, 4-$C_6H_2\underline{Me}_2$), 2.18 (3H, s, 4-$C_6H_2\underline{Me}_2$), 2.13 (3H, s, 4-$C_6H_2\underline{Me}_2$), 1.99 (3H, s, 2-$C_6H_2\underline{Me}_2$) ppm. ^{13}C-{^{1}H} NMR (125.8 MHz, C_6D_6, 298 K): 162.8 (q, 1-$\underline{C}_6H_2Me_2$, two overlapping), 162.2 (q, 1-$\underline{C}_6H_2Me_2$), 161.6 (q, 1-$\underline{C}_6H_2Me_2$), 158.1 (q, 2-C_5H_4N), 151.6 (q, 2-C_5H_4N), 136.8 (4-C_5H_4N), 136.0 (4-C_5H_4N), 133.3 (3-$\underline{C}_6H_2Me_2$, two overlapping), 131.9 (3-$\underline{C}_6H_2Me_2$), 131.3 (5-$\underline{C}_6H_2Me_2$), 128.8 (3- and 5-$\underline{C}_6H_2Me_2$, four overlapping), 128.5 (q, 6-$\underline{C}_6H_2Me_2$, two overlapping), 126.3 (q, 2-$\underline{C}_6H_2Me_2$), 125.3 (3-C_5H_4N), 124.2 (q, 2-$\underline{C}_6H_2Me_2$), 124.1 (q, 2-$\underline{C}_6H_2Me_2$), 123.4 (q, 4-$\underline{C}_6H_2Me_2$), 123.2 (q, 2-$\underline{C}_6H_2Me_2$), 123.0 (5-C_5H_4N), 122.4 (q, 4-$\underline{C}_6H_2Me_2$), 122.2 (q, 6-$\underline{C}_6H_2Me_2$), 121.5 (q, 4-$\underline{C}_6H_2Me_2$), 121.1 (q, 4-$\underline{C}_6H_2Me_2$), 120.8 (q, 6-$\underline{C}_6H_2Me_2$), 119.3 (5-C_5H_4N), 118.9 (3-C_5H_4N), 64.2 ($ArCH_2^{d}$), 63.8 ($ArCH_2^{c}$), 58.0 ($ArCH_2^{b}$), 57.7 ($ArCH_2^{a}$), 57.6 ($\underline{C}H_2^{e}C_5H_4N$), 49.5 ($\underline{C}H_2^{f}C_5H_4N$), 21.0 (4-$CH_3$), 20.7 (4-$CH_3$), 20.7 (4-$CH_3$), 20.6 (4-$CH_3$), 18.1 (2-$CH_3$), 17.9 (2-$CH_3$), 17.3 (2-$CH_3$), 17.2 (2-$CH_3$) ppm. IR (NaCl plates, Nujol mull): 1606(s), 1591(m), 1571(m), 1314(s), 1275(s), 1179(m), 1161(s), 1101(m), 1017(m), 959(m), 856(s), 821(s) cm^{-1}. EI-MS *m/z*: 419 (5%, $[M - C_{24}H_{27}N_2O_2]^+$). Anal. found (Calcd. for $C_{48}H_{53}N_4O_4Sc$): C, 72.40 (72.53); H, 6.85 (6.72); N, 6.89 (7.05) %. Single crystals suitable for X-ray analysis were grown from a dilute THF/pentane solution at room temperature.

Sc($O_2^{Me2}N^{NMe2}$)($HO_2^{Me2}N^{NMe2}$) (6). A solution of $H_2O_2^{Me2}N^{NMe2}$ (0.32 g, 0.89 mmol) in THF (15 mL) at −78 °C was added dropwise to a stirring solution of

$Sc(CH_2SiMe_3)_3(THF)_2$ (0.20 g, 0.44 mmol) in THF (15 mL) at −78 °C. The reaction mixture was allowed to warm to room temperature and stirred for 16 h, after which time the solvent volume was reduced to a minimum (1 mL) under reduced pressure. Pentane (15 mL) was added and the title compound precipitated as a white solid. The solids were isolated by filtration, washed with pentane (3 × 5 mL) then dried *in vacuo*. Yield = 0.16 g, 48%. ^{1}H NMR (500.3 MHz, C_6D_6, 298 K) (*Superscript a, b, c and d denote resonances corresponding to each phenolate side arm of the (phenolate)-amino ligand. a and b resonances are on the same phenolate ligand, with the remaining c and d resonances on the second bis(phenolate)–amino ligand.*): 9.70 (1H, br s, NH), 7.11 (2 × 1H, s, 3-$C_6\underline{H}_2Me_2$), 7.03 (1H, s, 5-$C_6\underline{H}_2Me_2$), 6.84 (2 × 1H, s, 3-$C_6\underline{H}_2Me_2$), 6.72 (1H, s, 5-$C_6\underline{H}_2Me_2$), 6.54 (1H, s, 3-$C_6\underline{H}_2Me_2$), 6.46 (1H, d, $ArCH_2^a$, ^2J = 15.0 Hz), 6.30 (1H, s, 3-$C_6\underline{H}_2Me_2$), 5.83 (1H, d, $ArCH_2^b$, ^2J = 15.0 Hz), 4.93 (1H, d, $ArCH_2^c$, ^2J = 15.0 Hz), 4.46 (1H, d, $ArCH_2^d$, ^2J = 15.0 Hz), 2.98 (1H, d, $ArCH_2^b$, ^2J = 15.0 Hz), 2.95 (1H, d, $ArCH_2^a$, ^2J = 15.0 Hz), 2.79 (1H, d, $ArCH_2^d$, ^2J = 15.0 Hz), 2.72 (1H, overlapping m, $ArCH_2^b$), 2.72 (1H, overlapping m, $C\underline{H}_2CH_2N(CH_3)_2^{cd}$), 2.64 (3H, s, 2-$C_6H_2\underline{Me}_2$), 2.54 (3H, s, 2-$C_6H_2\underline{Me}_2$), 2.41 (3H, s, 2-$C_6H_2\underline{Me}_2$), 2.37 (3H, s, 4-$C_6H_2\underline{Me}_2$), 2.35 (3H, s, 2-$C_6H_2\underline{Me}_2$), 2.32 (3H, s, 4-$C_6H_2\underline{Me}_2$), 2.23 (3H, s, 4-$C_6H_2\underline{Me}_2$), 2.21 (1H, overlapping m, $CH_2C\underline{H}_2N(CH_3)_2$, coordinated to Sc), 2.21 (1H, overlapping m, $C\underline{H}_2CH_2N(CH_3)_2^{ab}$), 2.15 (3H, s, 4-$C_6H_2\underline{Me}_2$), 2.03 (3H, s, $N(CH_3)_2$, coordinated to Sc), 1.98 (3H, s, $N(CH_3)_2$, coordinated to Sc), 1.96 (1H, overlapping m, $C\underline{H}_2CH_2N(CH_3)_2^{cd}$), 1.56 (6H, s, $N(CH_3)_2$, uncoordinated to Sc), 1.42 (2H, m, $CH_2C\underline{H}_2N(CH_3)_2$, uncoordinated to Sc), 1.20 (1H, m, $CH_2C\underline{H}_2N(CH_3)_2$, coordinated to Sc) ppm. Remaining resonance ($C\underline{H}_2CH_2N(CH_3)_2^{ab}$) could not be assigned. ^{13}C-{^{1}H} NMR (125.8 MHz, C_6D_6, 298 K) (*Superscript a, b, c and d denote resonances corresponding to each phenolate side arm of the bis(phenolate)-amino ligand. a and b resonances are on the same phenolate ligand, with the remaining c and d resonances on the second bis(phenolate)–amino ligand.*): 162.2 (q, 1-$\underline{C}_6H_2Me_2$), 162.2 (q, 1-$\underline{C}_6H_2Me_2$), 162.1 (q, 1-$\underline{C}_6H_2Me_2$), 162.0 (q, 1-$\underline{C}_6H_2Me_2$), 133.4 (5-$\underline{C}_6H_2Me_2$), 133.3 (3-$\underline{C}_6H_2Me_2$), 132.1 (3-$\underline{C}_6H_2Me_2$), 131.9 (3-$\underline{C}_6H_2Me_2$), 129.6 (5-$\underline{C}_6H_2Me_2$), 129.4 (3-$\underline{C}_6H_2Me_2$), 128.5 (q, 6-$\underline{C}_6H_2Me_2^{c\ or\ d}$), 128.3 (5-$\underline{C}_6H_2Me_2$), 127.8 (5-$\underline{C}_6H_2Me_2$), 127.5 (q, 6-$\underline{C}_6H_2Me_2^{c\ or\ d}$), 125.8 (q, 2-$\underline{C}_6H_2Me_2$), 124.5 (q, 2-$\underline{C}_6H_2Me_2$), 123.6 (q, 2-$\underline{C}_6H_2Me_2$), 123.3 (q, 2-$\underline{C}_6H_2Me_2$), 123.2 (q, 4-$\underline{C}_6H_2Me_2$), 122.8 (q, 4-$\underline{C}_6H_2Me_2$), 122.3 (q, 4-$\underline{C}_6H_2Me_2$), 122.2 (q, 4-$\underline{C}_6H_2Me_2$), 119.8 (q, 6-$\underline{C}_6H_2Me_2^a$), 119.4 (q, 6-$\underline{C}_6H_2Me_2^b$), 65.1 ($ArCH_2^c$), 64.9 ($ArCH_2^d$), 61.4 ($ArCH_2^b$), 60.9 ($ArCH_2^a$),

59.5 ($CH_2\underline{C}H_2N(CH_3)_2$, coordinated to Sc), 54.3 ($CH_2\underline{C}H_2N(CH_3)_2$, uncoordinated to Sc), 50.2 ($\underline{C}H_2CH_2N(CH_3)_2$[ab]), 49.2 ($\underline{C}H_2CH_2N(CH_3)_2$[cd]), 48.3 ($N(CH_3)_2$, coordinated to Sc), 45.4 ($N(CH_3)_2$, coordinated to Sc), 44.3 ($N(CH_3)_2$, uncoordinated to Sc), 21.0 (4-CH_3), 20.8 (4-CH_3), 20.6 (4-CH_3), 20.5 (4-CH_3), 18.4 (2-CH_3), 17.6 (2-CH_3), 17.3 (2-CH_3), 17.1 (2-CH_3) ppm. IR (NaCl plates, Nujol mull): 1610(m), 1314(s), 1275 (s), 1176(w), 1161(m), 1107(w), 1036(m), 1016(m), 971(w), 865(s), 827(s), 773(m) cm^{-1}. EI-MS *m/z*: 754 (85%, $[M]^+$). Anal. found (Calcd. for $C_{44}H_{61}N_4O_4Sc$): C, 69.76 (70.00); H, 8.25 (8.14); N, 7.29 (7.42) %.

Sc($O_2^{Me2}N^{OMe}$)($HO_2^{Me2}N^{OMe}$) (7). A solution of $H_2O_2^{Me2}N^{OMe}$ (0.31 g, 0.91 mmol) in THF (15 mL) at −78 °C was added dropwise to a stirring solution of $Sc(CH_2SiMe_3)_3(THF)_2$ (0.21 g, 0.45 mmol) in THF (15 mL) at −78 °C. The reaction mixture was allowed to warm to room temperature and stirred for 16 h, after which time the solvent volume was reduced to a minimum (1 mL) under reduced pressure. Pentane (15 mL) was added and the title compound precipitated as a white solid. The solids were isolated by filtration, washed with pentane (3 × 5 mL) then dried *in vacuo*. Yield = 0.13 g, 39%. ^{1}H NMR (500.3 MHz, C_6D_6, 298 K) (*Superscript a, b, c and d denote resonances corresponding to each phenolate side arm of the bis(phenolate)-amino ligand. a and b resonances are on the same phenolate ligand, with the remaining c and d resonances on the second bis(phenolate)-amino ligand.*): 10.5 (1H, br s, NH), 7.10 (1H, s, 3-$C_6\underline{H}_2Me_2$), 7.08 (1H, s, 3-$C_6\underline{H}_2Me_2$), 7.07 (1H, s, 3-$C_6\underline{H}_2Me_2$), 6.91 (1H, s, 3-$C_6\underline{H}_2Me_2$), 6.82 (1H, s, 5-$C_6\underline{H}_2Me_2$[c]), 6.67 (1H, s, 5-$C_6\underline{H}_2Me_2$[d]), 6.61 (1H, s, 5-$C_6\underline{H}_2Me_2$[a]), 6.40 (1H, s, 5-$C_6\underline{H}_2Me_2$[b]), 6.02 (1H, d, $ArCH_2$[a], ^2J = 15.0 Hz), 5.73 (1H, d, $ArCH_2$[b], ^2J = 15.0 Hz), 4.98 (1H, d, $ArCH_2$[c], ^2J = 15.0 Hz), 4.42 (1H, d, $ArCH_2$[d], ^2J = 15.0 Hz), 3.52 (1H, m, $ArCH_2$[a], ^2J = 10.0 Hz), 3.17 (1H, m, $ArCH_2$[b], ^2J = 10.0 Hz), 3.02 (1H, d, $ArCH_2$[c], ^2J = 15.0 Hz), 2.84 (3H, s, OCH_3), 2.81 (1H, d, $ArCH_2$[d], ^2J = 15.0 Hz), 2.75 (3H, s, 2-$C_6H_2\underline{Me}_2$), 2.76 (1H, overlapping m, $CH_2C\underline{H}_2OCH_3$), 2.72 (3H, s, OCH_3), 2.58 (3H, s, 2-$C_6H_2\underline{Me}_2$), 2.53 (2 × 1H, overlapping m, $C\underline{H}_2CH_2OCH_3$[cd] and $CH_2C\underline{H}_2OCH_3$), 2.46 (1H, overlapping m, $CH_2C\underline{H}_2OCH_3$), 2.44 (3H, s, 2-$C_6H_2\underline{Me}_2$), 2.36 (3H, s, 4-$C_6H_2\underline{Me}_2$), 2.36 (3H, s, 2-$C_6H_2\underline{Me}_2$), 2.33 (3H, s, 4-$C_6H_2\underline{Me}_2$), 2.32 (1H, overlapping m, $CH_2C\underline{H}_2OCH_3$), 2.30 (1H, overlapping m, $C\underline{H}_2CH_2OCH_3$[ab]), 2.24 (3H, s, 4-$C_6H_2\underline{Me}_2$), 2.19 (2 × 1H, overlapping m, $C\underline{H}_2CH_2OCH_3$[cd] and $C\underline{H}_2CH_2OCH_3$[ab]), 2.17 (3H, s, 4-$C_6H_2\underline{Me}_2$) ppm. ^{13}C-{^{1}H} NMR (125.8 MHz, C_6D_6, 298 K) (*Superscript a, b, c and d denotes*

resonances corresponding to each phenolate side arm of the bis(phenolate)-amino ligand. a and b resonances are on the same phenolate ligand, with the remaining c and d resonances on the second bis(phenolate)–amino ligand.): 162.1 (q, 1-$\underline{C}_6H_2Me_2$, two overlapping), 161.9 (q, 1-$\underline{C}_6H_2Me_2$), 161.3 (q, 1-$\underline{C}_6H_2Me_2$), 133.4 (3-$\underline{C}_6H_2Me_2$), 133.1 (3-$\underline{C}_6H_2Me_2$), 132.0 (3-$\underline{C}_6H_2Me_2$), 131.9 (3-$\underline{C}_6H_2Me_2$), 129.4 (5-$\underline{C}_6H_2Me_2^{d}$), 128.6 (5-$\underline{C}_6H_2Me_2^{c}$), 128.3 (5-$\underline{C}_6H_2Me_2^{b}$), 128.1 (5-$\underline{C}_6H_2Me_2^{a}$), 125.8 (q, 2-$\underline{C}_6H_2Me_2$), 124.4 (q, 2-$\underline{C}_6H_2Me_2$), 124.1 (q, 2-$\underline{C}_6H_2Me_2$), 123.8 (q, 4-$\underline{C}_6H_2Me_2$), 123.5 (q, 4-$\underline{C}_6H_2Me_2$), 122.8 (q, 4-$\underline{C}_6H_2Me_2$), 122.2 (q, 4-$\underline{C}_6H_2Me_2$), 118.8 (q, 6-$\underline{C}_6H_2Me_2^{a\ or\ b}$), 118.8 (q, 6-$\underline{C}_6H_2Me_2^{a\ or\ b}$), 72.8 ($CH_2\underline{C}H_2OCH_3$), 65.9 ($CH_2\underline{C}H_2OCH_3$), 65.0 ($ArCH_2^{c}$), 64.2 ($ArCH_2^{d}$), 59.8 ($OCH_3$), 58.9 ($ArCH_2^{a}$), 58.8 ($ArCH_2^{b}$), 58.5 ($OCH_3$), 50.0 ($\underline{C}H_2CH_2OCH_3^{cd}$), 46.6 ($\underline{C}H_2CH_2OCH_3^{ab}$), 20.9 (4-$CH_3$), 20.8 (4-$CH_3$), 20.7 (4-$CH_3$), 20.6 (4-$CH_3$), 18.4 (2-$CH_3$), 17.7 (2-$CH_3$), 17.3 (2-$CH_3$), 18.9 (2-$CH_3$) ppm. (2 × q, 6-$\underline{C}_6H_2Me_2^{cd}$) and (1 × q, 2-$\underline{C}_6H_2Me_2$) obscured. IR (NaCl plates, Nujol mull): 1611(s), 1311(s), 1274(s), 1181(m), 1161(s), 1136(s), 1110(m), 1072(s), 1027(s), 973(m), 947(w), 860(s), 843(s), 750(w) cm^{-1}. EI-MS *m/z*: 386 (40%, $[M - C_{21}H_{28}NO_3]^+$). Anal. found (Calcd. for $C_{42}H_{55}N_2O_6Sc$): C, 69.20 (69.21); H, 7.48 (7.61); N, 3.78 (3.84) %.

NMR tube scale synthesis of Y(O_2N^{NMe2})(OBn) (8). BnOH (1.0 μg, 1.0 μL, 9.4 μmol) was added to a solution of Y(O_2N^{NMe2})(HO_2N^{NMe2}) (10.6 mg, 9.4 μmol) (**1**) in THF-d_8 at room temperature. ^{1}H NMR (300.1 MHz, THF-d_8, 298 K): 7.41 (2H, d, Ph, ^3J = 6.0 Hz), 7.26 (2H, m, Ph, ^3J = 6.0 Hz), 7.18 (2H, d, 3-$C_6\underline{H}_2{}^tBu_2$, ^4J = 3.0 Hz), 7.11 (1H, m, Ph, ^3J = 6.0 Hz), 6.91 (2H, d, 5-$C_6\underline{H}_2{}^tBu_2$, ^4J = 3.0 Hz), 4.87 (2H, s, Ph$C\underline{H}_2$), 4.10 (1H, d, $ArCH_2$, ^2J = 12.0 Hz), 3.14 (1H, d, $ArCH_2$, ^2J = 12.0 Hz), 1.98 (3H, s, N(CH_3)), 1.92 (1H, t, CH_2CH_2, ^3J = 3.0 Hz), 1.50 (9H, s, 2-$C_6H_2{}^t\underline{Bu}_2$), 1.26 (9H, s, 4-$C_6H_2{}^t\underline{Bu}_2$) ppm.

6.3.2 Polymerisation procedures

Representative procedure for room temperature *rac*-LA (and ε-CL) polymerisations without a co-initiator. In a dry-box, *rac*-LA (0.20 g, 1.39 mmol, 100 equivs.) was weighed into a vial and dissolved in THF (1.5 mL). The monomer solution was added quickly in one portion to a stirring solution of a zwitterionic complex (**1**−**7**) ([*rac*-LA]$_0$:[ZI]$_0$ = 100:1) in THF (0.5 mL). The vial was sealed and the reaction mixture stirred for 20 minutes, before immediate quenching outside the dry-box by addition of THF (as supplied, ≈ 0.5 mL). Four aliquots (≈ 0.2 mL) were

taken and dried *in vacuo*. These samples were used for ^{1}H NMR ($CDCl_3$), MALDI-ToF MS and GPC analysis.

Representative procedure for room temperature *rac*-LA (and ε-CL) polymerisations with co-initiators, and synthesis of 9. In a dry-box, *rac*-LA (0.20 g, 1.39 mmol, 100 equivs.) was weighed into a vial and dissolved in THF (1.5 mL). The monomer solution was added quickly in one portion to a stirring mixture of a zwitterionic complex (**1**−**7**) ([*rac*-LA]$_0$:[ZI]$_0$ = 100:1) and co-initiator ([Co-initiator]$_0$:[ZI]$_0$ = 5:1) in THF (0.5 mL). An appropriate volume of $BnNH_2$, BnOH, $C_5H_{10}NH$, $^nPrNH_2$, ^{i}PrOH or $^t BuNH_2$ was measured using a microlitre syringe (Hamilton 10 μL). The vial was sealed and the reaction mixture stirred for 20 minutes before immediate quenching outside the dry-box by addition of THF (as supplied, ≈ 0.5 mL). Four aliquots (≈ 0.2 mL) were taken and dried *in vacuo*. These samples were used for ^{1}H NMR ($CDCl_3$), MALDI-ToF MS and GPC analysis. In cases where the polymer was purified, the remaining liquor was concentrated under reduced pressure and ethanol (20 mL) was added. The solution was then refrigerated (–30 °C) to aid precipitation of the polymer. The white solids were isolated by filtration, then washed with ethanol, then hexanes as required, before drying *in vacuo*.

BnNH-[PLA]-H (representative of 9). Yield = 0.10 g, 52%. ^{1}H NMR (300.1 MHz, $CDCl_3$, 298 K): 7.27 (5H, overlapping m, Ph), 6.57 (1H, t, NH, ^3J = 6.0 Hz), 5.16 (overlapping q, C<u>H</u>(Me), ^3J = 6.0 Hz), 4.44 (2H, dd, PhC<u>H</u>$_2$NH, ^2J = 6.0 Hz, ^3J = 3.0 Hz), 4.33 (1H, m, C<u>H</u>(Me)OH, ^3J = 6.0 Hz), 2.70 (1H, d, OH, ^3J = 6.0 Hz), 1.53 (overlapping d, CH(<u>Me</u>), ^3J = 6.0 Hz) ppm. ^{13}C-{^{1}H} NMR (75.4 MHz, $CDCl_3$, 298 K): 169.3 and 169.1 (CO), 128.6, 127.5, 124.8 and 123.3 (Ph), 69.2 and 69.0 (<u>C</u>H(Me)), 16.7 and 16.7 (CH(<u>Me</u>)) ppm.

BnO-[PLA]-H. Yield = 0.11 g, 59%. ^{1}H NMR (300.1 MHz, $CDCl_3$, 298 K): 7.35 (5H, overlapping m, Ph), 5.16 (overlapping q, C<u>H</u>(Me), ^3J = 6.0 Hz), 4.33 (1H, m, C<u>H</u>(Me)OH, ^3J = 6.0 Hz), 2.70 (1H, d, OH, ^3J = 6.0 Hz), 1.53 (overlapping d, CH(<u>Me</u>), ^3J = 6.0 Hz) ppm. ^{13}C-{^{1}H} NMR (75.4 MHz, $CDCl_3$, 298 K): 169.3 and 169.1 (CO), 69.2 and 69.0 (<u>C</u>H(Me)), 16.7 and 16.7 (CH(<u>Me</u>)) ppm. No BnO– ^{13}C signals were assignable.

C_5H_{10}N-[PLA]-H. Yield = 0.11 g, 57%. ^{1}H NMR (300.1 MHz, $CDCl_3$, 298 K): 5.39 (1H, q, $C_5H_{10}NC(O)C$<u>H</u>(Me), ^3J = 6.0 Hz), 5.16 (overlapping q, C<u>H</u>(Me), ^3J = 6.0

Hz), 4.33 (1H, m, C<u>H</u>(Me)OH, ^{3}J = 6.0 Hz), 3.46 (br s, $C_5H_{10}N$), 3.34 (br s, $C_5H_{10}N$), 2.70 (1H, d, OH, ^{3}J = 6.0 Hz), 1.53 (overlapping d, CH(<u>Me</u>), ^{3}J = 6.0 Hz) ppm. ^{13}C-{^{1}H} NMR (75.4 MHz, $CDCl_3$, 298 K) 169.3 and 169.1 (CO), 69.2 and 69.0 (<u>C</u>H(Me), 16.7 and 16.7 (CH(<u>Me</u>)) ppm. No <u>C</u>$_5$H$_{10}$N– ^{13}C signals were assignable.

^{n}PrNH-[PLA]-H. Yield = 0.08 g, 45%. ^{1}H NMR (300.1 MHz, $CDCl_3$, 298 K): 6.18 (1H, br s, NH), 5.16 (overlapping q, C<u>H</u>(Me), ^{3}J = 6.0 Hz), 4.33 (1H, m, C<u>H</u>(Me)OH, ^{3}J = 6.0 Hz), 3.22 (1H, m, NHC<u>H$_2$</u>CH$_2$CH$_3$, ^{2}J = 6.0 Hz), 3.12 (1H, m, NHC<u>H$_2$</u>CH$_2$CH$_3$, ^{2}J = 6.0 Hz), 2.72 (1H, d, OH, ^{3}J = 6.0 Hz), 1.53 (overlapping d, CH(<u>Me</u>), ^{3}J = 6.0 Hz), 1.53 (2H, overlapping, NHCH$_2$C<u>H$_2$</u>CH$_3$), 0.87 (3H, m, NHCH$_2$CH$_2$C<u>H$_3$</u>, ^{3}J = 9.0 Hz) ppm. ^{13}C-{^{1}H} NMR (75.4 MHz, $CDCl_3$, 298 K) 169.3 and 169.1 (CO), 69.2 and 69.0 (<u>C</u>H(Me), 16.7 and 16.7 (CH(<u>Me</u>)) ppm. No ^{n}PrNH– ^{13}C signals were assignable.

Representative room temperature kinetics procedures using 1 or 1.15 as the catalyst. In a dry-box, *rac*-LA (0.40 g, 2.78 mmol, [*rac*-LA]$_0$:[Y]$_0$ = 200:1, 200:2, 200:3 or 200:4) was weighed into a vial and dissolved in THF (3.5 mL). The monomer solution was added quickly in one portion to a stirring mixture of catalyst ([*rac*-LA]$_0$:[Y]$_0$ = 200:1, 200:2, 200:3 or 200:4) and co-initiator ([Co-initiator]$_0$:[Y]$_0$ = 2:1, 3:1, 4:1 or 6:1) in THF (0.5 mL). An appropriate mass or volume of macromonomer (**9**), $PhCH_2NH_2$, $PhCH_2OH$, or $C_5H_{10}NH$ was weighed into a vial or measured using a microlitre syringe (Hamilton 10 μL). Aliqouts (≈ 0.1 mL) were taken at the appropriate time interval and were quenched inside the dry-box with degassed but not dried THF (6 drops). The volatiles were removed from the aliquots under reduced pressure and dried *in vacuo*. The crude aliquots were dissolved in $CDCl_3$ for determination of the monomer to polymer conversion by ^{1}H NMR analysis. The conversion was measured by integration of the C<u>H</u>(Me) resonances of PLA and unreacted *rac*-LA. Aliquots were then recovered for GPC and MALDI-ToF MS analysis.

6.4 Polymerisation procedures and characterising data for Chapter Three

6.4.1 Polymerisation procedures

Representative procedure for room temperature *rac*-LA polymerisations with co-initiators. In a dry-box, *rac*-LA (0.20 g, 1.39 mmol, 100 equivs.) was weighed into a vial and dissolved in THF (1.5 mL). The monomer solution was added quickly

in one portion to a stirring mixture of **1** ([*rac*-LA]$_0$:[**1**]$_0$ = 100:1) and co-initiator ([Co-initiator]$_0$:[**1**]$_0$ = 5:1) in THF (0.5 mL). An appropriate volume of tren or $Me_2NCH_2CH_2NH_2$ was measured using a microlitre syringe (Hamilton 10 μL). The vial was sealed and the reaction mixture stirred for 20 minutes before immediate quenching outside the dry-box by addition of THF (as supplied, ≈ 0.5 mL). Four aliquots (≈ 0.2 mL) were taken and dried *in vacuo*. These samples were used for ^{1}H NMR ($CDCl_3$), MALDI-ToF MS and GPC analysis. In cases where the polymer was purified, the remaining liquor was concentrated under reduced pressure and ethanol (20 mL) was added. The solution was then refrigerated (–30 °C) to aid precipitation of the polymer. The white solids were isolated by filtration, then washed with ethanol, then hexanes as required, before drying *in vacuo*.

N(CH$_2$CH$_2$NH-[PLA]-H)$_3$. Yield = 0.15 g, 77 %. ^{1}H NMR (300.1 MHz, $CDCl_3$, 298 K): 6.89 (3H, br s, NH), 5.16 (overlapping q, C<u>H</u>(Me), ^3J = 6.0 Hz), 4.33 (3H, m, C<u>H</u>(Me)OH, ^3J = 6.0 Hz), 2.73 (3H, d, OH, ^3J = 6.0 Hz), 2.50 (br s, CH_2CH_2), 1.53 (overlapping d, CH(<u>Me</u>), ^3J = 6.0 Hz) ppm. ^{13}C-{^{1}H} NMR (75.4 MHz, $CDCl_3$, 298 K) analogous to BnNH-[PLA]-H, no tren-core ^{13}C signals were assignable.

Me$_2$NCH$_2$CH$_2$NH-[PLA]-H. Yield = 0.13 g, 68 %. ^{1}H NMR (300.1 MHz, $CDCl_3$, 298 K): 5.16 (overlapping q, C<u>H</u>(Me), ^3J = 6.0 Hz), 4.33 (1H, m, C<u>H</u>(Me)OH, ^3J = 6.0 Hz), 2.59 (1H, m, OH), 2.33 (6H, s, $N(CH_3)_2$), 1.78 (br s, CH_2CH_2), 1.53 (overlapping d, CH(<u>Me</u>), ^3J = 6.0 Hz) ppm. ^{13}C-{^{1}H} NMR (75.4 MHz, $CDCl_3$, 298 K) analogous to BnNH-[PLA]-H, no $Me_2NCH_2CH_2NH$– ^{13}C signals were assignable.

Representative room temperature kinetics procedures for *rac*-LA polymerisations using 1 as the catalyst. In a dry-box, *rac*-LA (0.40 g, 2.78 mmol, [*rac*-LA]$_0$:[**1**]$_0$ = 200:1) was weighed into a vial and dissolved in THF (3.5 mL). The monomer solution was added quickly in one portion to a stirring mixture of **1** ([*rac*-LA]$_0$:[**1**]$_0$ = 200:1) and co-initiator ([tren]$_0$:[**1**]$_0$ = 1:1, 2:1 or 3:1; [$Me_2NCH_2CH_2NH_2$]$_0$:[**1**]$_0$ = 3:1, 6:1 or 9:1) in THF (0.5 mL). An appropriate volume of tren or $Me_2CH_2CH_2NH_2$ was measured using a microlitre syringe (Hamilton 10 μL). Aliqouts (≈ 0.1 mL) were taken at the appropriate time interval and were quenched inside the dry-box with degassed but not dried THF (6 drops). The volatiles were removed from the aliquots under reduced pressure and dried *in vacuo*. The crude aliquots were dissolved in $CDCl_3$ for determination of the monomer to polymer conversion by ^{1}H NMR analysis. The conversion was measured by integration of the

C<u>H</u>(Me) resonances of PLA and unreacted *rac*-LA. Aliquots were then recovered for GPC and MALDI-ToF MS analysis.

Representative procedure for room temperature *rac*-BBL polymerisations without a co-initiator. In a dry-box, *rac*-BBL (0.20 g, 2.32 mmol, 100 equivs.) was weighed into a vial and dissolved in toluene (1.5 mL). The monomer solution was added quickly in one portion to a stirring solution of **1** ($[rac\text{-BBL}]_0$:$[\mathbf{1}]_0$ = 100:1) in toluene (0.5 mL). The vial was sealed and the reaction mixture stirred for 5 minutes, before immediate quenching outside the dry-box by addition of THF (as supplied, ≈ 0.5 mL). Four aliquots (≈ 0.2 mL) were taken and dried *in vacuo*. These samples were used for ^{1}H NMR ($CDCl_3$), MALDI-ToF MS and GPC analysis.

Representative procedure for room temperature *rac*-BBL polymerisations with co-initiators. In a dry-box, *rac*-BBL (0.20 g, 2.32 mmol, 100 equivs.) was weighed into a vial and dissolved in toluene (1.5 mL). The monomer solution was added quickly in one portion to a stirring mixture of **1** ($[rac\text{-BBL}]_0$:$[\mathbf{1}]_0$ = 100:1) and co-initiator ($[\text{Co-initiator}]_0$:$[\mathbf{1}]_0$ = 5:1) in toluene (0.5 mL). An appropriate volume of $BnNH_2$, BnOH, $C_5H_{10}NH$, $^nPrNH_2$ or $^tBuNH_2$ was measured using a microlitre syringe (Hamilton 10 μL). The vial was sealed and the reaction mixture stirred for 5 minutes before immediate quenching outside the dry-box by addition of THF (as supplied, ≈ 0.5 mL). Four aliquots (≈ 0.2 mL) were taken and dried *in vacuo*. These samples were used for ^{1}H NMR ($CDCl_3$), MALDI-ToF MS and GPC analysis. In cases where the polymer was purified, hexanes (20 mL) were added to the remaining liquor and the polymer products precipitated. The white solids were isolated by filtration, then washed with hexanes and pentane as required, before drying *in vacuo*.

BnNH-[PHB]-H. Yield = 0.16 g, 76%. ^{1}H NMR (300.1 MHz, $CDCl_3$, 298 K): 7.28 (5H, m, Ph), 6.28 (1H, br s, NH), 5.22 (m, C<u>H</u>(Me), ^3J = 6.0 Hz), 4.43 (2H, m, PhC<u>H</u>$_2$NH), 4.17 (1H, m, C<u>H</u>(Me)OH), 3.12 (1H, d, OH, ^3J = 3.0 Hz), 2.62 – 2.38 (m, CH_2), 1.26 (d, CH(<u>Me</u>), ^3J = 9.0 Hz) ppm. ^{13}C-{^{1}H} NMR (125.8 MHz, $CDCl_3$, 298 K): 169.2 and 169.1 (CO), 67.6 (C<u>H</u>(Me)), 40.8, 40.7, 40.7 and 40.6 (CH_2), 19.8 and 19.7 (CH(<u>Me</u>)) ppm. No BnNH– ^{13}C signals were assignable.

BnO-[PHB]-H. Yield = 0.13 g, 62%. ^{1}H NMR (300.1 MHz, $CDCl_3$, 298 K): 7.53 (5H, m, Ph), 5.22 (m, C<u>H</u>(Me), ^3J = 9.0 Hz), 5.01 (2H, d, PhC<u>H</u>$_2$O, ^3J = 3.0 Hz), 4.17 (1H, m, C<u>H</u>(Me)OH), 3.11 (1H, d, OH, ^3J = 3.0 Hz), 2.62 – 2.40 (m, CH_2), 1.26 (d,

CH(C<u>H</u>$_3$), ^3J = 6.0 Hz) ppm. ^{13}C-{^{1}H} NMR (75.4 MHz, $CDCl_3$, 298 K): 169.2 and 169.1 (CO), 67.6 (C<u>H</u>(Me)), 40.8, 40.7, 40.7 and 40.6 (CH_2), 19.8 and 19.7 (CH(<u>Me</u>)) ppm. No BnO– ^{13}C signals were assignable.

C_5H_{10}N-[PHB]-H. Yield = 0.14 g, 67%. ^{1}H NMR (300.1 MHz, $CDCl_3$, 298 K): 5.22 (m, C<u>H</u>(Me), ^3J = 6.0 Hz), 4.17 (1H, m, C<u>H</u>(Me)OH), 3.49 (2H, t, NCH_2, ^3J = 6.0 Hz), 3.39 (2H, t, NCH_2, ^3J = 6.0 Hz), 3.11 (1H, d, OH, ^3J = 6.0 Hz), 2.62 – 2.40 (m, CH_2), 1.54 (6H, br s, $C_5H_{10}N$), 1.26 (d, CH(<u>Me</u>), ^3J = 6.0 Hz) ppm. ^{13}C-{^{1}H} NMR (75.4 MHz, $CDCl_3$, 298 K): 169.2 and 169.1 (CO), 67.6 (C<u>H</u>(Me)), 40.8, 40.7, 40.7 and 40.6 (CH_2), 19.8 and 19.7 (CH(<u>Me</u>)) ppm. No $C_5H_{10}NH$– ^{13}C signals were assignable.

N(CH_2CH_2NH-[PHB]-H)$_3$. Yield = 0.12 g, 57%. ^{1}H NMR (300.1 MHz, $CDCl_3$, 298 K): 6.82 (3H, br s, NH), 5.22 (m, C<u>H</u>(Me), ^3J = 6.0 Hz), 4.17 (1H, m, C<u>H</u>(Me)OH), 3.22 (br m, CH_2CH_2), 3.11 (1H, d, OH, ^3J = 6.0 Hz), 2.62 – 2.40 (m, CH_2), 1.26 (d, CH(<u>Me</u>), ^3J = 6.0 Hz) ppm. ^{13}C-{^{1}H} NMR (75.4 MHz, $CDCl_3$, 298 K): 169.2 and 169.1 (CO), 67.6 (C<u>H</u>(Me)), 40.8, 40.7, 40.7 and 40.6 (CH_2), 19.8 and 19.7 (CH(<u>Me</u>)) ppm. No tren-core ^{13}C signals were assignable.

Representative room temperature kinetics procedures for *rac*-BBL polymerisations using 1 as the catalyst. In a dry-box, *rac*-BBL (0.40 g, 4.65 mmol, [*rac*-LA]$_0$:[**1**]$_0$ = 200:1, 200:2 or 200:3) was weighed into a vial and dissolved in toluene (7.0 mL). The monomer solution was added quickly in one portion to a stirred mixture of **1** ([*rac*-BBL]$_0$:[**1**]$_0$ = 200:1) and $BnNH_2$ ([$BnNH_2$]$_0$:[**1**]$_0$ = 3:1, 5:1, 7.5:1, 10:1, 12.5:1 or 15:1) in toluene (1.0 mL). An appropriate volume of $BnNH_2$ was measured using a microlitre syringe (Hamilton 10 μL). Aliqouts (≈ 0.1 mL) were taken at the appropriate time interval and were quenched inside the dry-box with degassed but not dried THF (6 drops). The volatiles were removed from the aliquots under reduced pressure and dried *in vacuo*. The crude aliquots were dissolved in $CDCl_3$ for determination of the monomer to polymer conversion by ^{1}H NMR analysis. The conversion was measured by integration of the C<u>H</u>(Me) resonances of PHB and unreacted *rac*-BBL. Aliquots were then recovered for GPC and MALDI-ToF MS analysis.

6.5 Experimental details and characterising data for Chapter Four

6.5.1 Synthesis

Y(O-2,4-$C_6H_3{}^tBu_2)_3(THF)_2$ (15). A solution of 2,4-di-*tert*-butylphenol (0.53 g, 2.54 mmol) in THF (10 mL) was added dropwise to a stirring solution of $Y\{N(SiHMe_2)_2\}_3(THF)_2$ (0.53 g, 0.85 mmol) in THF (10 mL) at room temperature. The reaction mixture was stirred for 16 h, during which time the solution colour changed from colourless to yellow but remained clear. The volatiles were removed under reduced pressure and the crude solids were dissolved in THF (10 mL). The solution was filtered and then concentrated under reduced pressure. Hexanes were added (10 mL) and the title compound precipitated as a white solid, which was isolated by filtration and dried *in vacuo* at 0 °C. Yield = 0.40 g, 56%. ^{1}H NMR (500.3 MHz, C_6D_6, 298 K): 7.60 (3H, d, 3-$C_6\underline{H}_2{}^tBu_2$, ^4J = 5.0 Hz), 7.35 (3H, dd, 5-$C_6\underline{H}_2{}^tBu_2$, ^3J = 15.0 Hz, ^4J = 5.0 Hz), 7.13 (3H, d, 6-$C_6\underline{H}_2{}^tBu_2$, ^3J = 15.0 Hz), 3.73 (8H, br s, $OC\underline{H}_2CH_2$), 1.76 (27H, s, 2-$C_6H_2{}^t\underline{Bu}_2$), 1.38 (27H, s, 4-$C_6H_2{}^t\underline{Bu}_2$), 1.06 (8H, br s, $OCH_2C\underline{H}_2$) ppm. ^{13}C-{^{1}H} NMR (125.8 MHz, C_6D_6, 298 K): 161.3 (q, 1-$\underline{C}_6H_2{}^tBu_2$), 138.2 (q, 2-$\underline{C}_6H_2{}^tBu_2$), 135.9 (q, 4-$\underline{C}_6H_2{}^tBu_2$), 123.9 (3-$\underline{C}_6H_2{}^tBu_2$), 123.4 (5-$\underline{C}_6H_2{}^tBu_2$), 121.8 (6-$\underline{C}_6H_2{}^tBu_2$), 68.0 ($O\underline{C}H_2CH_2$), 35.5 (q, 2-$\underline{C}(CH_3)_3$), 34.3 (q, 4-$\underline{C}(CH_3)_3$), 32.1 (4-C($\underline{C}H_3)_3$), 30.5 (2-C($\underline{C}H_3)_3$), 25.7 ($OCH_2\underline{C}H_2$) ppm. IR (NaCl plates, Nujol mull): 1602(w), 1485(s), 1419(m), 1361(s), 1219(m), 1203(m), 1153(w), 1086(m), 1018(m), 827(s), 742(m) cm^{-1}. EI-MS *m/z*: 921 (1%, $[M + C_4H_8O]^+$), 206 (80%, $[C_{14}H_{22}O]^+$). Anal. found (Calcd. For $C_{50}H_{79}O_5Y$): C, 70.56 (70.73); H, 9.29 (9.38) %.

6.5.2 Polymerisation procedures

Representative procedure for room temperature *rac*-LA polymerisations without a co-initiator. In a dry-box, *rac*-LA (0.20 g, 1.39 mmol, 100 equivs.) was weighed into a vial and dissolved in THF (1.5 mL). The monomer solution was added quickly in one portion to a stirring solution of Nd(O-2,4-$C_6H_3{}^tBu_2)_3(THF)_3$ (**10**), Gd(O-2,4-$C_6H_3{}^tBu_2)_3(THF)_3$ (**11**), Ca_2(O-2,4-$C_6H_3{}^tBu_2)_4(DME)_5$ (**12**), Sr_2(O-2,4-$C_6H_3{}^tBu_2)_4(DME)_3$ (**13**), Sr_3(O-2,4-$C_6H_3{}^tBu_2)_6(THF)_6$ (**14**) or Y(O-2,4-$C_6H_3{}^tBu_2)_3(THF)_2$ (**15**) ([*rac*-LA]$_0$:[Complex]$_0$ = 100:1) in THF (0.5 mL). The vial was sealed and the reaction mixture stirred until high conversion was recorded, before immediate quenching outside the dry-box by addition of THF (as supplied, ≈ 0.5 mL).

Four aliquots (≈ 0.2 mL) were taken and dried *in vacuo*. These samples were used for ^{1}H NMR ($CDCl_3$), MALDI-ToF MS and GPC analysis.

Representative procedure for room temperature *rac*-LA polymerisations with co-initiators. In a dry-box, *rac*-LA (0.20 g, 1.39 mmol, 100 equivs.) was weighed into a vial and dissolved in THF (1.5 mL). The monomer solution was added quickly in one portion to a stirred mixture of Nd(O-2,4-$C_6H_3{}^tBu_2)_3(THF)_3$ (**10**), Gd(O-2,4-$C_6H_3{}^tBu_2)_3(THF)_3$ (**11**), Ca_2(O-2,4-$C_6H_3{}^tBu_2)_4(DME)_5$ (**12**), Sr_2(O-2,4-$C_6H_3{}^tBu_2)_4(DME)_3$ (**13**), Sr_3(O-2,4-$C_6H_3{}^tBu_2)_6(THF)_6$ (**14**) or Y(O-2,4-$C_6H_3{}^tBu_2)_3(THF)_2$ (**15**) ([*rac*-LA]$_0$:[Complex]$_0$ = 100:1) and co-initiator ([Co-initiator]$_0$:[Complex]$_0$ = 5:1 in THF (0.5 mL). An appropriate volume of $BnNH_2$ or BnOH was measured using a microlitre syringe (Hamilton 10 μL). The vial was sealed and the reaction mixture stirred for 30 minutes before immediate quenching outside the dry-box by addition of THF (as supplied, ≈ 0.5 mL). Four aliquots (≈ 0.2 mL) were taken and dried *in vacuo*. These samples were used for ^{1}H NMR ($CDCl_3$), MALDI-ToF MS and GPC analysis.

Representative kinetics procedures for room temperature *rac*-LA polymerisations using 12 or 13 as the catalyst. In a dry-box, *rac*-LA (0.80 g, 2.78 mmol, [*rac*-LA]$_0$:[Complex]$_0$ = 400:1.0–5.0) was weighed into a vial and dissolved in THF (7.5 mL). The monomer solution was added quickly in one portion to a stirred mixture of **12** or **13** ([*rac*-LA]$_0$:[Complex]$_0$ = 400:1.0–5.0) and co-initiator ([$BnNH_2$]$_0$:[Complex]$_0$ = 12.5:1, 10.0:1, 7.5:1, 6.0:1, 5.0:1, 4.0:1 or 2.5:1 in THF (0.5 mL). An appropriate volume of $BnNH_2$ was measured using a microlitre syringe (Hamilton 10 μL). Aliqouts (≈ 0.1 mL) were taken at the appropriate time interval and were quenched inside the dry-box with degassed but not dried THF (6 drops). The volatiles were removed from the aliquots under reduced pressure and dried *in vacuo*. The crude aliquots were dissolved in $CDCl_3$ for determination of the monomer to polymer conversion by ^{1}H NMR analysis. The conversion was measured by integration of the C<u>H</u>(Me) resonances of PLA and unreacted *rac*-LA. Aliquots were then recovered for GPC and MALDI-ToF MS analysis.

6.6 Experimental details and characterising data for Chapter Five

6.6.1 Synthesis

$Y(ON^{Me,Cy})\{N(SiHMe_2)_2\}_2(THF)$ (16). A solution of $HON^{Me,Cy}$ (0.33 g, 1.0 mmol) in pentane (10 mL) was added dropwise to a stirring solution of $Y\{N(SiHMe_2)_2\}_3(THF)_2$ (0.62 g, 1.0 mmol) in pentane (10 mL) at room temperature. After stirring for 16 hours, the volatiles were removed under reduced pressure. The crude solids were dissolved in pentane (10 mL) and the solution was filtered before being concentrated under reduced pressure. The title compound crystallised as clear and colourless blocks at room temperature. The supernatant liquids were decanted and the crystals were washed with pentane (3 × 5 mL), before drying *in vacuo* to afford the title compound as a white crystalline solid. Yield = 0.42 g, 57%. ^{1}H NMR (300.1 MHz, C_6D_6, 298 K): 7.58 (1H, d, 3-$C_6\underline{H}_2{}^tBu_2$, ^4J = 3.0 Hz), 7.05 (1H, d, 5-$C_6\underline{H}_2{}^tBu_2$, ^4J = 3.0 Hz), 5.07 (4H, sept, Si$\underline{H}(CH_3)_2$, ^3J = 3.0 Hz), 4.12 (4H, t, OC$\underline{H}_2CH_2$, ^3J = 3.0 Hz), 2.19 (3H, s, NCH_3), 1.69 (9H, s, 2-$C_6H_2{}^t\underline{Bu}_2$), 1.46 (4H, t, $OCH_2C\underline{H}_2$, ^3J = 3.0 Hz), 1.41 (9H, s, 4-$C_6H_2{}^t\underline{Bu}_2$), 0.33 (24H, d, SiH(C$\underline{H}_3)_2$, ^3J = 3.0 Hz) ppm. ^{1}H NMR (499.9 MHz, toluene-d_8, 363 K): 7.46 (1H, d, 3-$C_6\underline{H}_2{}^tBu_2$, ^4J = 5.0 Hz), 6.93 (1H, d, 5-$C_6\underline{H}_2{}^tBu_2$, ^4J = 5.0 Hz), 4.98 (4H, sept, Si$\underline{H}(CH_3)_2$, ^3J = 5.0 Hz), 3.86 (4H, t, OC$\underline{H}_2CH_2$, ^3J = 5.0 Hz), 3.72 (2H, s, $ArCH_2$), 2.65 (1H, m, 1-C_5H_{11}), 2.24 (3H, s, NCH_3), 1.87 (1H, br d, C_5H_{11}, ^3J = 10.0 Hz), 1.60 (9H, s, 2-$C_6H_2{}^t\underline{Bu}_2$), 1.54 (4H, t, $OCH_2C\underline{H}_2$, ^3J = 5.0 Hz), 1.41 (br m, C_5H_{11}), 1.32 (9H, s, 4-$C_6H_2{}^t\underline{Bu}_2$), 1.03 (br m, C_5H_{11}), 0.33 (24H, d, SiH(C$\underline{H}_3)_2$, ^3J = 5.0 Hz) ppm. ^{13}C-{^{1}H} NMR (75.4 MHz, C_6D_6, 298 K): 161.1 (q, d, 1-$\underline{C}_6H_2{}^tBu_2$, $^2J_{Y\text{-}C}$ = 3.0 Hz), 137.6 (q, 4-$\underline{C}_6H_2{}^tBu_2$), 135.7 (q, 2-$\underline{C}_6H_2{}^tBu_2$), 126.3 (5-$\underline{C}_6H_2{}^tBu_2$), 124.4 (q, 6-$\underline{C}_6H_2{}^tBu_2$), 124.1 (3-$\underline{C}_6H_2{}^tBu_2$), 71.4 (O$\underline{C}H_2CH_2$), 62.3 (1-$C_6H_{11}$), 57.8 (Ar$\underline{C}H_2$), 37.8 ($NCH_3$), 35.4 (q, 2-$\underline{C}(CH_3)_3$), 34.2 (q, 4-$\underline{C}(CH_3)_3$), 32.2 (4-C($\underline{C}H_3)_3$), 32.1 ($C_6H_{11}$), 30.8 ($C_6H_{11}$) 30.4 (2-C($\underline{C}H_3)_3$), 29.7 ($C_6H_{11}$), 26.3 ($C_6H_{11}$), 26.1 ($C_6H_{11}$), 25.3 ($OCH_2\underline{C}H_2$), 3.42 (SiH$(CH_3)_2$) ppm. IR (NaCl plates, Nujol mull): 2049(s) (Si−H), 1418(m), 1384(m), 1360(w), 1325(w), 1282(s), 1303(s), 1241(s), 1167(w), 1029(s), 937(s), 886(s), 833(s), 770(s), 761(s), 679(m), 617(m) cm^{-1}. EI-MS *m/z*: 749 (Recombined fragment 100%, $[Y(ON^{Me,Cy})_2]^+$), 331 (10%, $[HON^{Me,Cy}]^+$). Anal. found (Calcd. For $C_{34}H_{72}N_3O_2Y$): C, 53.62 (54.00); N, 9.50 (9.60); N, 5.37 (5.56) %. Single crystals suitable for X-ray diffraction were grown from a concentrated pentane solution at room temperature.

$Y(ON^{Me,Cy})_2\{N(SiHMe_2)_2\}$ (17). A solution of $HON^{Me,Cy}$ (0.62 g, 1.87 mmol) in hexanes (10 mL) was added to a stirring solution of $Y\{N(SiHMe_2)_2\}_3(THF)_2$ (0.59 g, 0.94 mmol) in hexanes (10 mL) at room temperature. After complete addition, the reaction mixture developed a yellow colour and was stirred for 16 h before the volatiles were removed under reduced pressure. The crude solids were dissolved in pentane (10 mL) and filtered. The filtered solution was concentrated under reduced pressure then refrigerated (4 °C). The title compound crystallised as clear, colourless blocks that were isolated by filtration, washed with pentane (2 × 5 mL) and dried *in vacuo*, affording a white, crystalline powder. Yield = 0.46 g, 55%. ^{1}H NMR (500.3 MHz, C_6D_6, 298 K): 7.57 (1H, br m, 3-$C_6\underline{H}_2{}^tBu_2$), 7.55 (1H, d, 3-$C_6\underline{H}_2{}^tBu_2$, ^4J = 5.0 Hz), 6.96 (1H, br s, 5-$C_6\underline{H}_2{}^tBu_2$), 6.82 (1H, br s, 5-$C_6\underline{H}_2{}^tBu_2$), 5.27 (1.5H, br m, Si$\underline{H}(CH_3)_2$ major isomer), 5.13 (0.5H, br s, Si$\underline{H}(CH_3)_2$ minor isomer), 4.02 (1H, d, $ArCH_2$, ^2J = 15.0 Hz), 2.54 (6H, br s, NCH_3 overlapping), 2.30 (1H, d, $ArCH_2$, ^2J = 15.0 Hz), 1.73 (18H, s, 2-$C_6H_2{}^t\underline{Bu}_2$), 1.39 (18H, s, 4-$C_6H_2{}^t\underline{Bu}_2$), 1.13 (br m, C_6H_{11}), 0.79 (br m, C_6H_{11}), 0.37 (7H, br m, $SiH(C\underline{H}_3)_2$ major isomer), 0.26 (5H, br m, $SiH(C\underline{H}_3)_2$ minor isomer) ppm. ^{1}H NMR (299.9 MHz, toluene-d_8, 343 K): 7.51 (2H, d, 3-$C_6\underline{H}_2{}^tBu_2$), 6.91 (2H, br s, 5-$C_6\underline{H}_2{}^tBu_2$), 5.21 (2H, br s, (Si$\underline{H}(CH_3)_2$), 4.08 (1H, br s, $ArCH_2$), 2.59 (6H, br s, NCH_3 overlapping), 1.69 (18H, br s, 2-$C_6H_2{}^t\underline{Bu}_2$), 1.37 (18H, br s, 4-$C_6H_2{}^t\underline{Bu}_2$), 0.85 (6H, br m, C_6H_{11}), 0.29 (12H, br s, $SiH(C\underline{H}_3)_2$) ppm. ^{1}H NMR (299.9 MHz, toluene-d_8, 233 K): 7.66 (1H, br m, 3-$C_6\underline{H}_2{}^tBu_2$, couples to ^{1}H at 6.91 ppm), 7.56 (1H, br m, 3-$C_6\underline{H}_2{}^tBu_2$, couples to ^{1}H at 6.78 ppm), 6.91 (1H, br m, 5-$C_6\underline{H}_2{}^tBu_2$, couples to ^{1}H at 7.66 ppm), 6.78 (1H, br m, 5-$C_6\underline{H}_2{}^tBu_2$, couples to ^{1}H at 7.56 ppm), 5.30 (1H, br m, Si$\underline{H}(CH_3)_2$), 5.16 (1H, br m, Si$\underline{H}(CH_3)_2$), 4.59 (1H, d, $ArCH_2{}^a$, ^2J = 12.0 Hz), 3.84 (1H, d, $ArCH_2{}^b$, ^2J = 15.0 Hz), 3.39 (1H, d, $ArCH_2{}^a$, ^2J = 12.0 Hz), 2.74 (1H, app t, 1-C_6H_{11}, ^3J = 6.0 Hz), 2.67 (1H, d, $ArCH_2{}^b$, ^2J = 15.0 Hz), 2.41 (6H, s, NMe overlapping), 2.29 (1H, m, 1-C_6H_{11}), 1.81 (18H, s, 2-$C_6H_2{}^t\underline{Bu}_2$), 1.65 (br m, C_6H_{11}), 1.52 (6H, s, 4-$C_6H_2{}^t\underline{Bu}_2$ minor isomer), 1.43 (12H, s, 4-$C_6H_2{}^t\underline{Bu}_2$ major isomer), 1.22 (br m, C_6H_{11}), 0.81 (br m, C_6H_{11}), 0.60 (br m, C_6H_{11}), 0.41 (3H, d, $SiH(C\underline{H}_3)_2$, ^3J = 5.0 Hz), 0.37 (3H, d, $SiH(C\underline{H}_3)_2$, ^3J = 5.0 Hz), 0.29 (6H, app t, $SiH(C\underline{H}_3)_2$, ^3J = 5.0 Hz) ppm. ^{13}C-{^{1}H} (125.8 MHz, C_6D_6, 298 K): 161.3 (q, 1-$\underline{C}_6H_2{}^tBu_2$), 161.1 (q, d, 1-$\underline{C}_6H_2{}^tBu_2$, $^2J_{Y\text{-}C}$ = 2.5 Hz), 137.7 (q, 4-$\underline{C}_6H_2{}^tBu_2$), 137.5 (q, 4-$\underline{C}_6H_2{}^tBu_2$), 136.0 (q, 2-$\underline{C}_6H_2{}^tBu_2$), 135.9 (q, 2-$\underline{C}_6H_2{}^tBu_2$), 126.6 (5-$\underline{C}_6H_2{}^tBu_2$), 126.3 (5-$\underline{C}_6H_2{}^tBu_2$), 125.1 (q, 6-$\underline{C}_6H_2{}^tBu_2$), 124.5 (q, 6-$\underline{C}_6H_2{}^tBu_2$), 123.8 (3-$\underline{C}_6H_2{}^tBu_2$),

123.7 (3-$\underline{C}_6H_2{}^tBu_2$), 60.8 ($ArCH_2$), 58.4 ($ArCH_2$), 38.7 ($N(CH_3)$), 38.0 ($N(CH_3)$), 35.4 (2-$\underline{C}(CH_3)_3$), 34.2 (4-$\underline{C}(CH_3)_3$), 32.1 (4-C($\underline{C}H_3)_3$), 32.1 ($C_6H_{11}$), 31.7 ($C_6H_{11}$), 30.8 (2-C($\underline{C}H_3)_3$), 30.6 ($C_6H_{11}$), 30.5 ($C_6H_{11}$), 26.6 ($C_6H_{11}$), 26.3 ($C_6H_{11}$), 26.3 ($C_6H_{11}$), 26.2 ($C_6H_{11}$), 25.8 ($C_6H_{11}$), 25.8 ($C_6H_{11}$), 25.6 ($C_6H_{11}$), 24.2 ($C_6H_{11}$), 3.7 ($SiH(CH_3)_2$), 3.4 ($SiH(CH_3)_2$), 3.1 ($SiH(CH_3)_2$), 2.9 ($SiH(CH_3)_2$) ppm. IR (NaCl plates, Nujol mull): 2037(m) (Si–H), 1362(m), 1293(s), 1276(m), 1244(m), 1167(m), 1129(w), 1028(m), 894(s), 773(s), 746(w) cm^{-1}. EI-MS *m/z*: 749 (10%, $[M - N(SiHMe_2)_2]^+$), 666 (100%, $[M - N(SiHMe_2)_2 - C_6H_{11}]^+$). Anal. Found (Calcd. For $C_{48}H_{86}N_3O_2Si_2Y$): C, 65.34 (65.48); H, 9.74 (9.82); N, 4.61 (4.76) %. Single crystals suitable for X-ray analysis were grown from a saturated pentane solution at 4 °C.

$Y(ON^{Me,NMe2})\{N(SiHMe_2)_2\}_2$ (18). A solution of $HON^{Me,NMe2}$ (0.27 g, 0.84 mmol) in pentane (10 mL) was added dropwise to a stirring solution of $Y\{N(SiHMe_2)_2\}_3(THF)_2$ (0.53 g, 0.84 mmol) in pentane (10 mL) at room temperature. After stirring for 16 h the volatiles were removed under reduced pressure and the white product was dried *in vacuo*. Yield = 0.37 g, 65%. ^1H NMR (500.3 MHz, C_6D_6, 298 K): 7.58 (1H, d, 3-$C_6\underline{H}_2{}^tBu_2$, ^4J = 5.0 Hz), 6.96 (1H, d, 5-$C_6\underline{H}_2{}^tBu_2$, ^4J = 5.0 Hz), 5.07 (4H, br m $Si\underline{H}(CH_3)_2$), 3.74 (2H, br s, $ArCH_2$), 2.37 (1H, app t, $C\underline{H}_2CH_2NMe_2$, ^2J = 15.0 Hz), 2.16 (3H, s, $N(CH_3)_2$), 2.16 (1H, $CH_2C\underline{H}_2NMe_2$, overlapping with $N(CH_3)_2$), 2.06 (3H, s, $N(CH_3)$), 1.96 (3H, s, $N(CH_3)_2$), 1.74 (9H, s, 2-$C_6H_2{}^t\underline{Bu}_2$), 1.41 (9H, s, 4-$C_6H_2{}^t\underline{Bu}_2$), 1.36 (1H, br m, $CH_2C\underline{H}_2NMe_2$, and 1H, br m $C\underline{H}_2CH_2NMe_2$), 0.40 (24H, overlapping d, $SiH(C\underline{H}_3)_2$, ^3J = 5.0 Hz) ppm. ^1H NMR (499.9 MHz, toluene-d_8, 363 K): 7.49 (1H, d, 3-$C_6\underline{H}_2{}^tBu_2$, ^4J = 5.0 Hz), 6.90 (1H, d, 5-$C_6\underline{H}_2{}^tBu_2$, ^4J = 5.0 Hz), 5.00 (4H, m $Si\underline{H}(CH_3)_2$, ^3J = 5.0 Hz), 3.68 (1H, d, $ArCH_2$, ^2J = 15.0 Hz), 3.51 (1H, d, $ArCH_2$, ^2J = 15.0 Hz), 2.50 (1H, app t, $C\underline{H}_2CH_2NMe_2$, ^2J = 10.0 Hz), 2.27 (1H, app t, $CH_2C\underline{H}_2NMe_2$, ^2J = 10.0 Hz), 2.23 (6H, s, $N(CH_3)_2$), 2.17 (3H, s, $N(CH_3)$), 1.74 (1H, d, $C\underline{H}_2CH_2NMe_2$, ^2J = 10.0 Hz), 1.72 (1H, d, $CH_2C\underline{H}_2NMe_2$, ^2J = 10.0 Hz), 1.63 (9H, s, 2-$C_6H_2{}^t\underline{Bu}_2$), 1.33 (9H, s, 4-$C_6H_2{}^t\underline{Bu}_2$), 0.29 (24H, d, $SiH(C\underline{H}_3)_2$, ^3J = 5.0 Hz) ppm. ^{13}C-{^1H} NMR (125.8 MHz, C_6D_6, 298 K): 161.5 (q, 1-$\underline{C}_6H_2{}^tBu_2$), 137.4 (q, 2-$\underline{C}_6H_2{}^tBu_2$), 136.8 (q, 4-$\underline{C}_6H_2{}^tBu_2$), 125.3 (5-$\underline{C}_6H_2{}^tBu_2$), 124.6 (3-$\underline{C}_6H_2{}^tBu_2$), 123.1 (q, 6-$\underline{C}_6H_2{}^tBu_2$), 65.2 ($ArCH_2$), 58.1 ($CH_2\underline{C}H_2NMe_2$), 53.7 ($\underline{C}H_2CH_2NMe_2$), 48.1 ($N(CH_3)_2$, couples to ^1H 2.16 (3H, s, $N(CH_3)_2$)), 45.7 ($N(CH_3)_2$, couples to ^1H 1.96 (3H, s, $N(CH_3)_2$)), 44.2 ($N(CH_3)$, 35.6 (q, 2-$\underline{C}(CH_3)_3$), 34.2 (q, 4-$\underline{C}(CH_3)_3$), 32.2 (4-C($\underline{C}H_3$)), 30.6 (2-C($\underline{C}H_3$)), 3.8 ($SiH(CH_3)_2$) ppm. IR (NaCl plates, Nujol mull):

2067(m) (Si−H), 1310(s), 1282(m), 1244(s), 1033(s), 975(s), 898(s), 838(s), 791(m), 778(m), 762(m) cm^{-1}. EI-MS *m/z*: 540 (70%, $[M - N(SiHMe_2)_2]^+$). Anal. found (Calcd. For $C_{28}H_{63}N_4OSi_4Y$): C, 49.65 (49.96); H, 9.51 (9.43); N, 8.24 (8.32) %.

$La(ON^{Me,NMe2})\{N(SiHMe_2)_2\}_2$ (19). A solution of $HON^{Me,NMe2}$ (0.09 g, 0.28 mmol) in pentane (10 mL) was added dropwise to a stirring solution of $La\{N(SiHMe_2)_2\}_3(THF)_2$ (0.19 g, 0.28 mmol) in pentane (10 mL) at room temperature. After stirring for 16 h the volatiles were removed under reduced pressure and the white product dried *in vacuo*. Yield = 0.09 g, 45%. ^{1}H NMR (500.3 MHz, C_6D_6, 298 K): 7.58 (1H, d, 3-$C_6\underline{H}_2{}^tBu_2$, ^4J = 5.0 Hz), 6.98 (1H, d, 5-$C_6\underline{H}_2{}^tBu_2$, ^4J = 5.0 Hz), 5.04 (4H, sept, $Si\underline{H}(CH_3)_2$, ^3J = 5.0 Hz), 3.79 (1H, d, $ArCH_2$, ^2J = 15.0 Hz), 3.08 (1H, d, $ArCH_2$, ^2J = 15.0 Hz), 2.32 (1H, dt, $C\underline{H}_2CH_2NMe_2$, ^3J = 5.0 Hz, ^2J = 15.0 Hz), 2.18 (1H, dt, $CH_2C\underline{H}_2NMe_2$, ^3J = 5.0 Hz, ^2J = 15.0 Hz), 2.05 (3H, s, $N(CH_3)_2$), 1.90 (3H, s, $N(CH_3)_2$), 1.90 (3H, s, $N(CH_3)$), 1.76 (9H, s, 2-$C_6H_2{}^t\underline{Bu}_2$), 1.45 (1H, m, $C\underline{H}_2CH_2NMe_2$, ^3J = 5.0 Hz, ^2J = 15.0 Hz), 1.42 (9H, s, 4-$C_6H_2{}^t\underline{Bu}_2$), 1.36 (1H, m, $CH_2C\underline{H}_2NMe_2$, ^3J = 5.0 Hz, ^2J = 15.0 Hz), 0.38 (24H, d, $SiH(C\underline{H}_3)_2$, ^3J = 5.0 Hz) ppm. ^{13}C-{^{1}H} NMR (125.8 MHz, C_6D_6, 298 K): 161.6 (q, 1-$\underline{C}_6H_2{}^tBu_2$), 137.2 (q, 2-$\underline{C}_6H_2{}^tBu_2$), 136.6 (q, 4-$\underline{C}_6H_2{}^tBu_2$), 125.6 (5-$\underline{C}_6H_2{}^tBu_2$), 124.5 (3-$\underline{C}_6H_2{}^tBu_2$), 123.1 (q, 6-$\underline{C}_6H_2{}^tBu_2$), 64.8 ($ArCH_2$), 57.2 ($CH_2\underline{C}H_2NMe_2$), 55.1 ($\underline{C}H_2CH_2NMe_2$), 46.8 ($N(CH_3)_2$, couples to ^{1}H 2.05 (3H, s, $N(CH_3)_2$)), 44.3 ($N(CH_3)_2$, couples to ^{1}H 1.90 (3H, s, $N(CH_3)_2$)), 41.2 ($N(CH_3)$, 35.6 (q, 2-$\underline{C}(CH_3)_3$), 34.2 (q, 4-$\underline{C}(CH_3)_3$), 32.2 (4-$C(\underline{C}H_3)$), 30.5 (2-$C(\underline{C}H_3)$), 3.2 ($SiH(CH_3)_2$) ppm. IR (NaCl plates, Nujol mull): 2045(m) (Si−H), 1308(m), 1281(m), 1243(s), 937(m), 900(s), 836(s), 762(m), 745(w), 682(w) cm^{-1}. EI-MS *m/z*: 589 (50%, $[M - N(SiHMe_2)_2]^+$). Anal. found (Calcd. for $C_{28}H_{63}N_4OSi_4La$): C, 46.44 (46.51); H, 8.91 (8.78); N, 7.54 (7.75) %. Single crystals suitable for X-ray diffraction were grown from a saturated hexane solution at room temperature.

6.6.2 Polymerisation procedures

Representative procedure for room temperature *rac*-LA polymerisations without a co-initiator. In a dry-box, *rac*-LA (0.20 g, 1.39 mmol, 100 equivs.) was weighed into a vial and dissolved in THF (1.5 mL). The monomer solution was added quickly in one portion to a stirred solution of **16**, **17**, **18** or **19** ($[rac\text{-LA}]_0$:$[Ln]_0$ = 100:1) in THF (0.5 mL). The vial was sealed and the reaction mixture stirred for 20 minutes,

before immediate quenching outside the dry-box by addition of THF (as supplied, ≈ 0.5 mL). Four aliquots (≈ 0.2 mL) were taken and dried *in vacuo*. These samples were used for ^{1}H NMR ($CDCl_3$), MALDI-ToF MS and GPC analysis.

Representative procedure for room temperature *rac*-LA polymerisations with co-initiators. In a dry-box, *rac*-LA (0.20 g, 1.39 mmol, 100 equivs.) was weighed into a vial and dissolved in THF (1.5 mL). The monomer solution was added quickly in one portion to a stirred mixture of **16**, **17**, **18** or **19** ([*rac*-LA]$_0$:[Ln]$_0$ = 100:1) and co-initiator ([Co-initiator]$_0$:[Ln]$_0$ = 5:1) in THF (0.5 mL). An appropriate volume of $BnNH_2$, BnOH or $C_5H_{10}NH$ was measured using a microlitre syringe (Hamilton 10 μL). The vial was sealed and the reaction mixture stirred for 20 minutes before immediate quenching outside the dry-box by addition of THF (as supplied, ≈ 0.5 mL). Four aliquots (≈ 0.2 mL) were taken and dried *in vacuo*. These samples were used for ^{1}H NMR ($CDCl_3$), MALDI-ToF MS and GPC analysis.

6.7 X-ray data collection and processing parameters

Crystal data collection and processing parameters are given in Table 6.1 (Compounds **3** and **5**) and Table 6.2 (Compounds **16**, **17** and **19**). Crystals were mounted on glass fibres using perfluoropolyether oil and cooled rapidly in a stream of dinitrogen gas (150 K) from an Oxford Cryostreams unit. Diffraction data were measured using an Enraf-Nonius KappaCCD diffractometer. As appropriate, absorption and decay corrections were applied to the data and equivalent reflections merged.[18] The structures were solved with SIR92[19] and further refinements and all other crystallographic calculations were performed using the CRYSTALS program suite.[20] Other details of structure solutions and refinements (CIF data) are provided in the CD Appendix.

Table 6.1. X-ray data collection and processing parameters.

compound		$Y(O_2N^{Me})(HO_2N^{Me})$ (**3**)•0.25(C_5H_{12})	$Sc(O_2{}^{Me2}N^{py})(HO_2{}^{Me2}N^{py})$ (**5**)
empirical formula		$C_{66}H_{103}N_2O_4Y$•0.25(C_5H_{12})	$C_{48}H_{53}N_4O_4Sc$
fw		1095.50	794.93
temp / K		150	150
wavelength / Å		0.71073	0.71073
space group		$P\,2_1/c$	$P\,\bar{1}$
a / Å		16.3010(3)	13.8302(2)
b / Å		30.0912(5)	16.1478(2)
c / Å		14.9654(12)	21.3184(3)
α / deg		90	69.4872(4)
β / deg		106.268(6)	73.4982(4)
γ / deg		90	87.9328(5)
V / Å^3		7046.9(3)	4264.75(10)
Z		4	4
d (calcd) Mg m^{-3}		1.033	1.238
abs coeff / mm^{-1}		0.869	0.221
R indices:[a]	R_1 =	0.0704	0.0477
	R_w =	0.0614	0.0460

[a] $R_1 = \Sigma||F_o|-|F_c|| \,/\, \Sigma|F_o|$; $R_w = \sqrt{\{\Sigma w\,(|F_o|-|F_c|)^2 \,/\, \Sigma w|F_o|^2\}}$ for data with $I > 3\sigma(I)$.

Table 6.2. X-ray data collection and processing parameters.

compound		$Y(ON^{Me,Cy})\{N(SiHMe_2)_2\}(THF)$ (**16**)	$Y(ON^{Me,Cy})_2\{N(SiHMe_2)_2\}$ (**17**)	$La(ON^{Me,NMe2})\{N(SiHMe_2)_2\}_2$ (**19**)
empirical formula		$C_{34}H_{72}N_3O_2Si_4Y$	$C_{48}H_{86}N_3O_2Si_2Y$	$C_{28}H_{63}N_4O_1Si_4La$
fw		756.21	882.31	723.08
temp / K		150	150	150
wavelength / Å		0.71073	0.71073	0.71073
space group		$P\,2_1/n$	$C\,2/c$	$P\,2_1/n$
a / Å		12.83910(10)	29.14240(40)	19.4516(2)
b / Å		10.95880(10)	10.42630(10)	9.86730(10)
c / Å		31.1823(3)	16.93110(29)	20.6867(2)
α / deg		90	90	90
β / deg		101.752(3)	92.2257(6)	100.2868(4)
γ / deg		90	90	90
V / Å^3		4295.42(3)	5140.590(125)	3906.68(7)
Z		4	4	4
d (calcd) Mg m^{-3}		1.169	1.140	1.229
abs coeff / mm^{-1}		1.499	1.218	1.240
R indices:[a]	R_1 =	0.0611	0.0528	0.0845
	R_w =	0.0536	0.0521	0.0822

[a] $R_1 = \Sigma||F_o|-|F_c|| / \Sigma|F_o|$; $R_w = \sqrt{\{\Sigma w\,(|F_o|-|F_c|)^2 / \Sigma w|F_o|^2\}}$ for data with $I > 3\sigma(I)$.

6.8 References for Chapter Six

1. P. J. Alaimo, D. W. Peters, J. Arnold and R. G. Bergman, *J. Chem. Ed.*, 2001, **78**, 64.
2. A. B. Pangborn, M. A. Giardello, R. H. Grubbs, R. K. Rosen and F. J. Timmers, *Organometallics*, 1996, **15**, 1518.
3. A. Rudin and H. L. W. Hoegy, *J. Polym. Sci., Part A: Polym. Chem.*, 1972, **10**, 217.
4. J. R. Dorgan, J. Janzen, D. M. Knauss, S. B. Hait, B. R. Limoges and M. H. Hutchinson, *J. Polym. Sci., Part B: Polym. Phys.*, 2005, **43**, 3100.
5. E. L. Manzer, *Inorg. Synth.*, 1982, **21**, 135.
6. C. Tessier-Youngs, O. T. Beachley, J. P. Oliver and K. Butcher, *Inorg. Synth.*, 2007, **24**, 95.
7. M. F. Lappert and R. Pearce, *J. Chem. Soc., Chem. Commun.*, 1973, 126.
8. D. C. Bradley, J. S. Ghotra and F. A. Hart, *J. Chem. Soc., Dalton Trans.*, 1973, 1021.
9. R. Anwander, O. Runte, J. Eppinger, G. Gerstberger, E. Herdtweck and M. Spiegler, *J. Chem. Soc., Dalton Trans.*, 1998, 847.
10. E. Y. Tshuva, I. Goldberg, M. Kol, H. Weitman and Z. Goldschmidt, *Chem. Commun.*, 2000, 379.
11. E. Y. Tshuva, I. Goldberg, M. Kol and Z. Goldschmidt, *Organometallics*, 2001, **20**, 3017.
12. E. Y. Tshuva, I. Goldberg, M. Kol and Z. Goldschmidt, *Inorg. Chem.*, 2001, **40**, 4263.
13. E. Y. Tshuva, S. Groysman, I. Goldberg, M. Kol and Z. Goldschmidt, *Organometallics*, 2002, **21**, 662.
14. T. Toupance, S. R. Dubberley, N. H. Rees, B. R. Tyrrell and P. Mountford, *Organometallics*, 2002, **21**, 1367.
15. J. Ejfler, M. Kobylka, L. B. Jerzykiewicz and P. Sobota, *Dalton Trans.*, 2005, 2047.

16. C. K. Williams, L. E. Breyfogle, S. K. Choi, W. Nam, V. G. Young, M. A. Hillmyer and W. B. Tolman, *J. Am. Chem. Soc.*, 2003, **125**, 11350.

17. A. Amgoune, C. M. Thomas, T. Roisnel and J.-F. Carpentier, *Chem. Eur. J.*, 2006, **12**, 169.

18. Z. Otwinowski and W. Minor, *Processing of X-ray Diffraction Data Collected in Oscillation Mode*, Academic Press: New York, 1997.

19. A. Altomare, G. Cascarano, G. Giacovazzo, A. Guagliardi, M. C. Burla, G. Polidori and M. Camalli, *J. Appl. Crystallogr.*, 1994, **27**, 435.

20. P. W. Betteridge, J. R. Cooper, R. I. Cooper, K. Prout and D. J. Watkin, *J. Appl. Crystallogr.*, 2003, **36**, 1487.